Activity 12: Atmospheric Dispersion Modelling

Activity 12.8: Dispersion modelling for year 2023 - Ezamokuhle

Document by:

ARM
AIR RESOURCE MANAGEMENT

Final Report

5th November 2024

Document Title

Client		Eskom
Title		Activity 12.8: Baseline dispersion modelling for year 2023 – Ezamokuhle
Our Reference		ESKPMV-2023-ACTV-12-BMEZA
Issued to Client		05/11/2024
Classification		Company Confidential

Document Change Record

Revision Number	Date	Description of Revision
00A	3rd October 2023	Creation of Document
00B	23rd August 2024	Peer Review of Document
00C	2nd September 2024	Draft Document submitted to Eskom
01	5th November 2024	Final Report submitted to Eskom

Document Approval

	Name	Date
Prepared by	Anesu Shamu	3rd October 2023
Reviewed by	Dr G Fourie	3rd November 2024
Approved by	Mr F Goede	5th November 2024

CONTENTS

LIST OF TABLES

LIST OF FIGURES

EXECUTIVE SUMMARY

1. STUDY OBJECTIVE

Aligned to the terms of reference for *Activity 12: Atmospheric Dispersion Modelling*, Air Resource Management (Pty) Ltd (ARM) must compile emission inventories of all sources affecting air quality in the three communities. ARM shall then develop and run appropriate dispersion model(s) to predict ambient PM, SO_2 and NO_X levels in the selected settlements. ARM is required to run the dispersion models on an annual basis to determine the impact of the interventions on ambient air quality, and the baseline in the absence of an offsets roll-out. The focus of this study is on the baseline atmospheric dispersion modelling for Ezamokuhle for the year 2023.

2. STUDY METHODOLOGY

Atmospheric dispersion models utilise mathematical equations that simulate the physics and chemistry that control the transport and transformation of pollutants in the atmosphere. They provide a means of estimating air pollutant concentrations and particle deposition in the ambient environment based on information on emissions and the prevailing meteorology.

All air quality modelling systems comprise of three major components: an emission inventory; a meteorological model and an air quality model. For this study a comprehensive emission inventory was created for Ezamokuhle which included emissions for the following source categories: power generation; residential fuel burning; waste burning, biomass burning and vehicle emissions from both paved & unpaved roads. The air quality impact of these emission sources is strongly influenced by meteorology which covers an array of atmospheric processes that determines the evolution of emissions, chemical species, aerosols and particulate matter. The integrated 3-dimensional mesoscale prognostic TAPM meteorological model was used to provide site-specific and representative meteorological data for the dispersion model. TAPM has been extensively verified both locally (DFFE, 2011; DFFE, 2014; Raghunandan et al, 2009) and internationally (Hurley et al., 2003) where the meteorological results show that TAPM performs well in a variety of regions (e.g., coastal, inland and generally complex terrain for sub-tropical to mid-latitude conditions). The output of the TAPM meteorological model was utilised an input into the dispersion modelling system.

In this study, the US-EPA approved Californian Puff (CALPUFF) dispersion modelling suite was used herein. The modelling approach for this activity is aligned to the prescribed requirements of the Code of Practice for Air Dispersion Modelling in Air Quality Management in South Africa (Gazette No 37804, 2014).

The CALPUFF suite of models was used to predict the dispersion of the following pollutants: SO_2, SO_4, NO_X, HNO_3, NO_3, PM_{10}, $PM_{2.5}$ and TPM (to calculate particulate/dust deposition rates) using

the MESOPUFF II Scheme chemical transformation method. The MESOPUFF II Scheme is a pseudo-first-order chemical reaction mechanism for conversion of SO_2 to SO_4 and total NO_X to NO_3. This baseline modelling study has taken a conservative approach (Scire, 2014) whereby the total concentrations of particulate matter (PM_{10} or $PM_{2.5}$) was computed as the sum of primary particulate matter concentrations (PM_{10} or $PM_{2.5}$) plus the contribution of concentrations from secondary particulate matter, including ammonium nitrate and ammonium sulphate. Results of the modelling were evaluated against the applicable National Ambient Air Quality Standard (NAAQS) for SO_2, NO_X as NO_2, PM_{10}, $PM_{2.5}$ and National Dustfall Standard for dustfall rates. Two modelling domains were utilised in the study. The primary modelling domain is referred to as the Greater Ezamokuhle Airshed. This is a large coarse grid domain which caters for a range of emission source categories within a 30 km radius around Ezamokuhle. The secondary modelling domain is referred to as the Ezamokuhle Airshed. This is a smaller, finer grid domain within the primary grid, which is used to accurately capture the dispersion characteristics and ambient concentrations for Ezamokuhle at a higher resolution.

3. STUDY RESULTS

In this study, the US-EPA approved Californian Puff (CALPUFF) modelling suite was used for this Level 3 tier modelling assessment. The dispersion of the pollutants were simulated for the prevailing meteorological conditions for the period 1 January 2020 to 31 December 2022. TAPM was used to model the hourly surface and upper air meteorology for the study area. In this study, the emission source categories include power generation, residential fuel burning, waste burning, biomass burning, vehicles travelling on paved roads and vehicles travelling on unpaved roads. The emission inventory is presented in Table i.

Table i: Emission Inventory for the Ezamokuhle Study

	Emission rate (tonnes/annum)				
Emission Source Category	**SO_2**	**NO_X**	**PM_{10}**	**$PM_{2.5}$**	**TPM**
Power Generation	182 926.0	109 677.0	14 693.3	5 962.0	
Residential Fuel Burning	48.1	20.1	109.2	109.2	
Waste Burning	1.1	2.7	8.2	7.8	
Biomass Burning	59.5	11.9	487.1	483.4	
Vehicles – Paved Roads	1.3	178.6	3.3	3.3	
Vehicles – Unpaved Roads	0.1	23.6	1 247.2	125.1	4 374.1
All Sources	183 036.0	109 914.1	16 548.4	6 690.8	4 374.1

The results of the model simulations for the Ezamokuhle airshed are as follows:

3.1 NAAQS Compliance

The model predicted concentrations were evaluated against the applicable NAAQS.

3.1.1 Greater Ezamokuhle airshed

- Model predicted 1-hour, 24-hour and annual SO_2 ambient concentrations do not exceed the respective NAAQS within the modelling domain
- Both the model predicted 1-hour and annual NO_2 ambient concentrations do not exceed the NAAQS
- The particulate matter (PM_{10} and $PM_{2.5}$) exceed both the 24-hour and annual respective NAAQS in the Greater Ezamokuhle airshed

3.1.2 Ezamokuhle airshed

- For the Ezamokuhle airshed, there are no model predicted exceedances of the NAAQS for either SO_2 or NO_2
- However, for particulate matter (PM_{10} and $PM_{2.5}$), both the daily and annual NAAQS were exceeded in the Ezamokuhle airshed

3.2 Source Contribution Analysis

As each emission source category was simulated independently in the dispersion model, ARM was able to differentiate the air quality impact of these individual source categories in relation to the cumulative modelled impact.

3.2.1 SO_2

As illustrated (Figure i), the source contribution analysis indicates that residential fuel burning, and power generation were the main contributors to ambient SO_2 levels in the Ezamokuhle airshed. It's however noted that other large industries (petrochemical, metallurgical, etc.) were excluded from the modelling simulation due to data policy privacy issues. However, an analysis of the ambient air quality monitoring data indicates that SO_2 displays a typical industrial signature with increased SO_2 concentrations just around midday due to the break-up of an elevated inversion layer, in addition to the development of daytime convective conditions causing the plume to be brought down to ground level and relatively close to the point of release from tall stacks. This confirms the additional impact of other tall stack sources in the Ezamokuhle airshed.

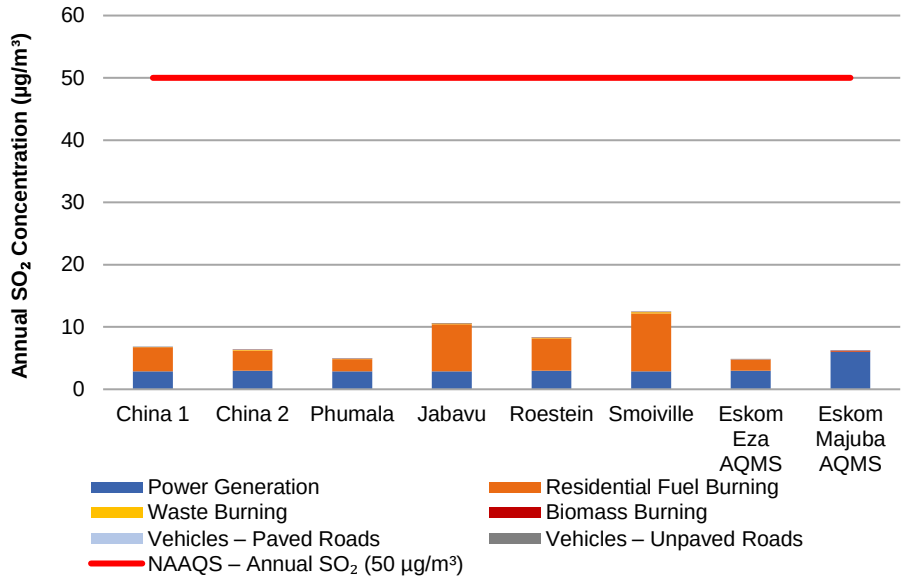

Figure i: Stacked bar graph representing model predicted annual SO_2 ambient concentrations in µg/m³ at discrete receptors for the seven emission source categories

3.2.2 NO_2

The source contribution analysis indicates that power generation, residential burning, vehicles travelling on paved & unpaved roads (Figure ii) are the main contributors to ambient NO_2 levels in the Ezamokuhle airshed. This is further supported by the analysis of the ambient data which clearly shows that elevated NO_2 levels are conditioned by both rush-hour traffic and the contribution of residential fuel burning in winter.

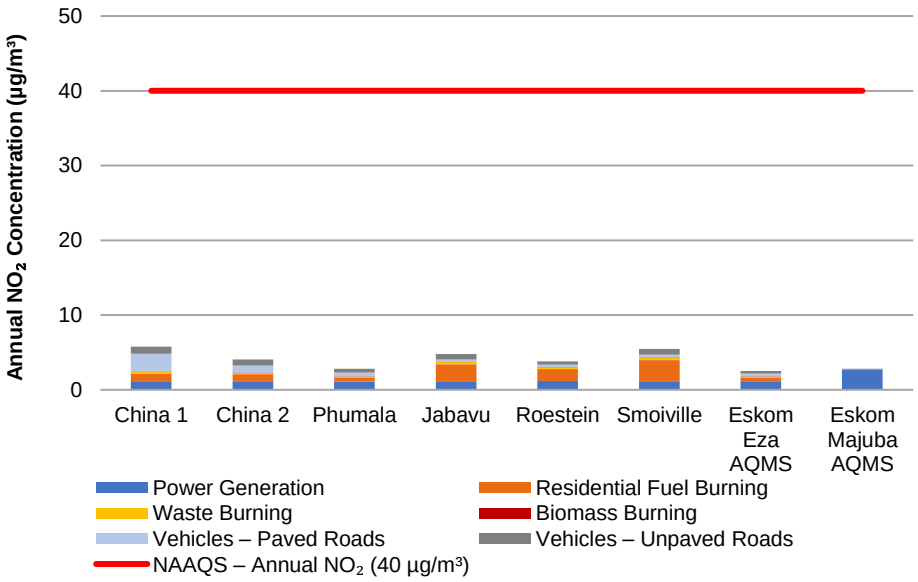

Figure ii: Stacked bar graph representing model predicted annual NO_2 ambient concentrations in µg/m³ at discrete receptors for the seven emission source categories

3.2.3 PM (PM_{10} and $PM_{2.5}$)

The source contribution analysis indicates that residential fuel burning and vehicles travelling on unpaved road surfaces (Figure iii and Figure iv) are the dominant contributors to ambient PM_{10} & $PM_{2.5}$ levels in Ezamokuhle.

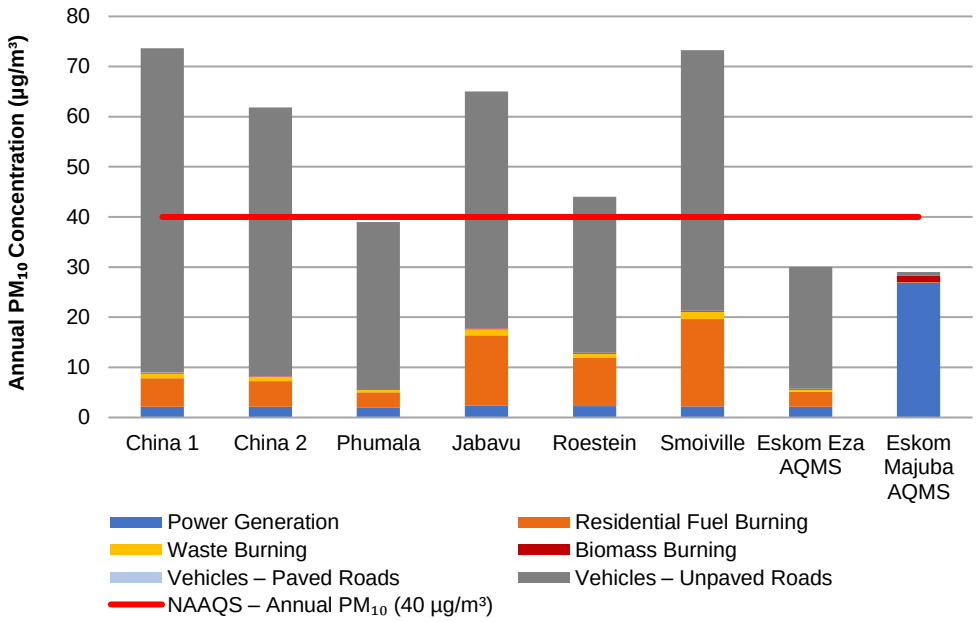

Figure iii: Stacked bar graph representing model predicted annual PM_{10} ambient concentrations in µg/m³ at discrete receptors for the seven emission source categories

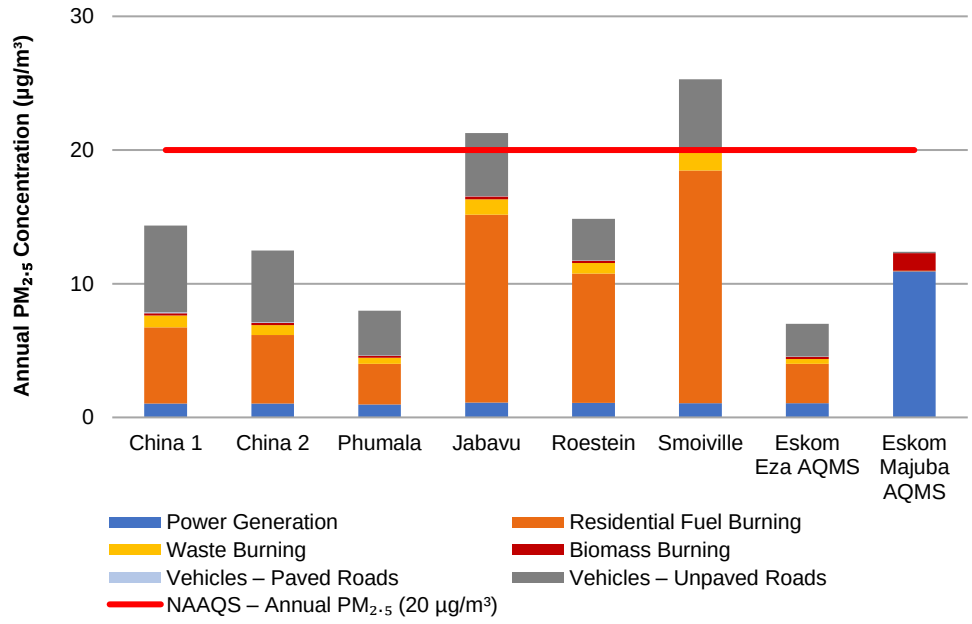

Figure iv: Stacked bar graph representing model predicted annual $PM_{2.5}$ ambient concentrations in µg/m³ at discrete receptors for the seven emission source categories

3.3 DUSTFALL RATES

3.3.1 Ezamokuhle airshed

- The model predicted 24-hour dustfall rates are below the National Dustfall Standard for non-residential areas of 1 200 mg/m^2/day, throughout the modelling domain.
- The model predicted 24-hour dustfall rates exceed the National Dustfall Standard for residential areas of 600 mg/m^2/day in Ezamokuhle.
- Dustfall rates are lowest at the Eskom Ezamokuhle AQMS but are generally much higher in the township. This is expected as the unpaved road networks within the township have a higher rate of vehicle activity which results in mechanical turbulence and entrainment of dust.

4. DISCUSSION

The model simulated results indicate that there are only exceedances of the NAAQS for particulate matter (PM_{10} or $PM_{2.5}$) in the Ezamokuhle airshed. A comparison of the model predicted PM results showed a very good correlation between to measured values at the AQMS (Figure v). It's noted the model under-predicted both SO_2 and NO_2. The extent to which a user has reliable information on emissions data, meteorological data and the correct model physics set-up will influence the accuracy of the model predicted concentrations.

An analysis of the modelled source contribution analysis indicates that the emission sources that have the most significant particulate matter air quality impact in Ezamokuhle include inter alia unpaved roads, residential fuel burning, coal fired power stations and waste burnings (Figure vi). These outcomes align closely with the past source apportionment studies (ARM, 2024), reinforcing the validity of the modelled patterns.

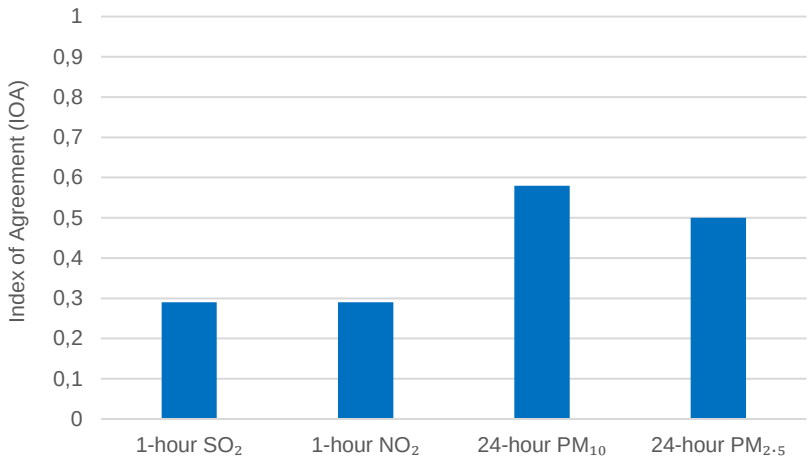

Figure v: Comparative IOA statistics between monitored data and model predictions

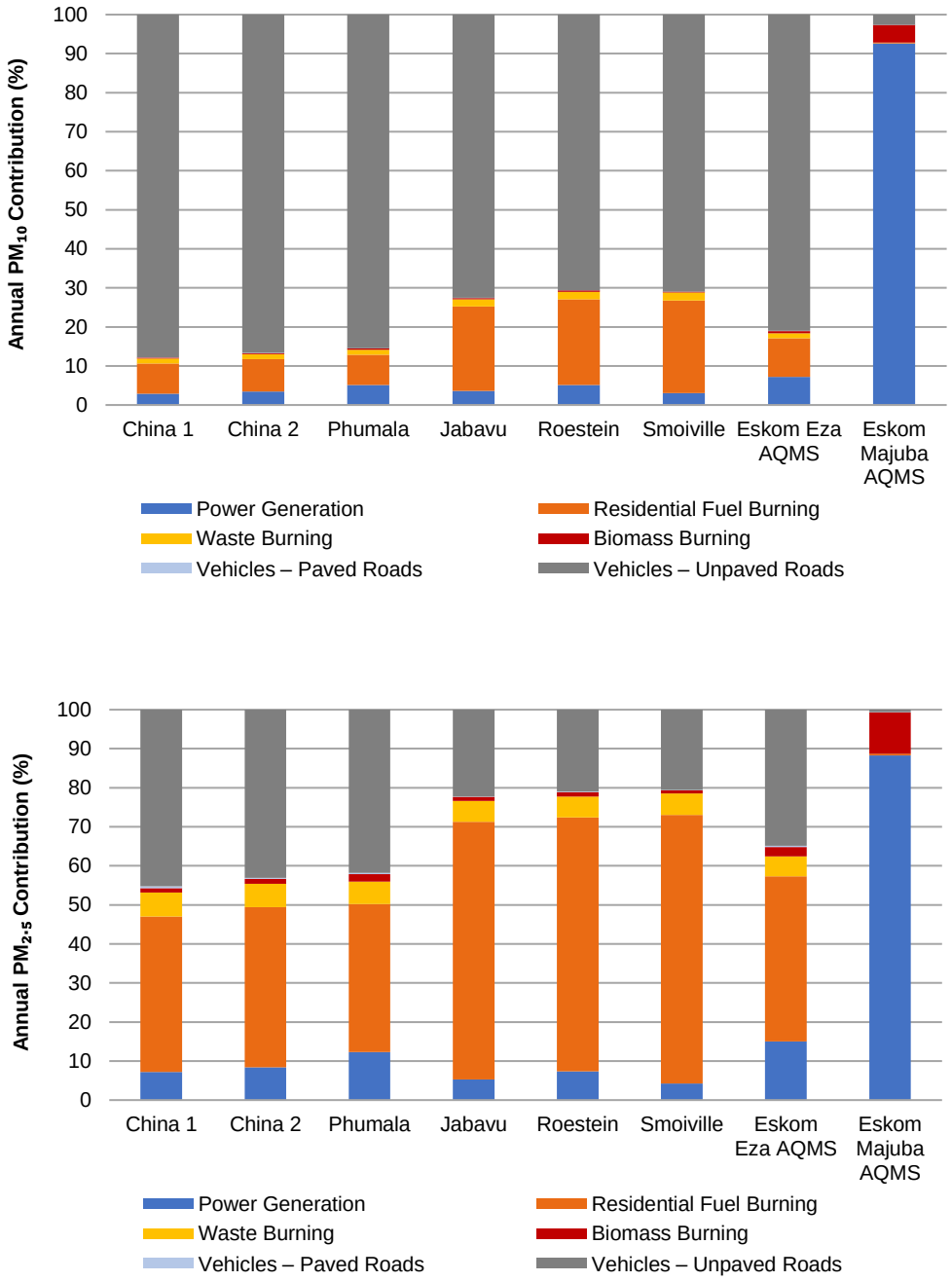

Figure vi: Stacked bar graph representing the percent contribution of PM_{10} (top) and $PM_{2.5}$ (bottom) ambient concentrations at discrete receptors in Ezamokuhle

In summary, this study has evaluated compliance with the applicable National Ambient Air Quality Standard (NAAQS) for SO_2, NO_X as NO_2, PM_{10}, $PM_{2.5}$ and National Dustfall Standard for dustfall rates. The study has demonstrated the exceedances of the NAAQS PM_{10} and $PM_{2.5}$ at Ezamokuhle and highlighted the significant contribution of residential fuel burning and unpaved road surfaces. This is aligned Eskom's AQO intervention for Ezamokuhle which is focussing on reducing the air quality impact of residential fuel burning sources.

1. INTRODUCTION

1.1 Air Quality Offsets Guideline

An environmental offset is an action(s), designed to compensate for a negative environmental impact of resource use, a discharge, emission, or other activity. The Department of Environment, Forestry & Fisheries (DEFF) defines air emission offsets as an intervention, or interventions, specifically implemented to counterbalance the adverse and residual environmental impact of atmospheric emissions in order to deliver a net ambient air quality benefit within, but not limited to, the affected airshed where ambient air quality standards are being or have the potential to be exceeded and whereby opportunities and need for offsetting exist (Notice 333 of 2016).

1.2 ESKOM'S Approach to Air Quality Offsets

DEFF's Air Quality Offset Guideline has shaped and informed Eskom's Air Quality Offsets Implementation Plan. This Plan has been based on a scientific process of feasibility studies, testing and demonstration, and on consultation with key stakeholders. Figure 1-1 illustrates the concept schedule for the phased implementation of Eskom's air quality offsets.

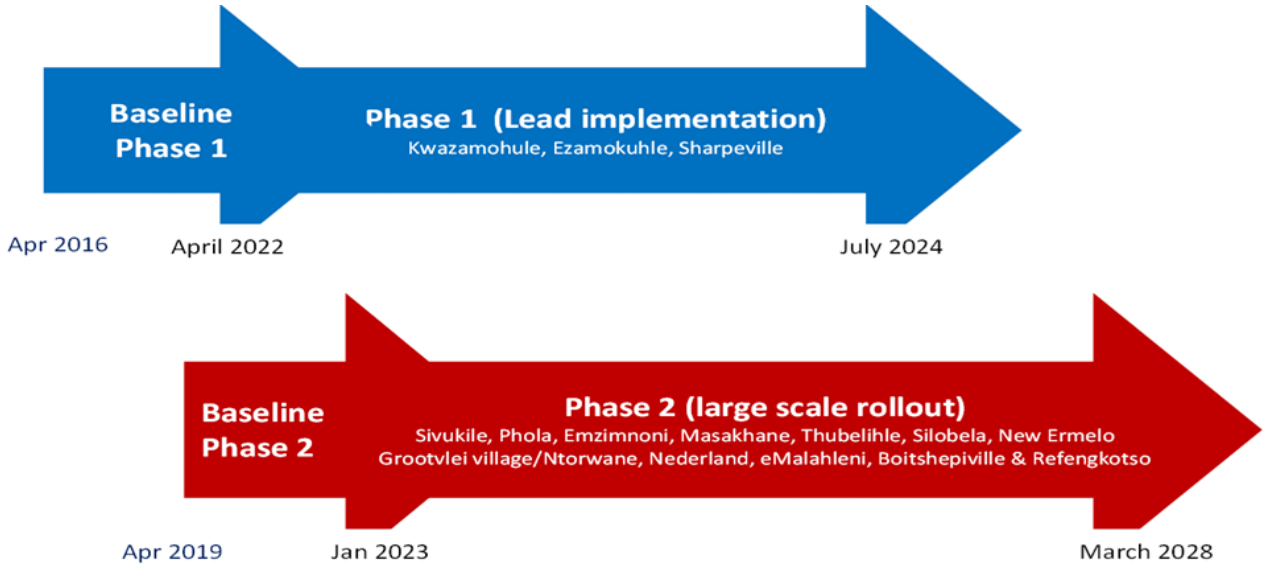

Figure 1-1: Concept Schedule for the implementation of Eskom's air quality offsets (Matimolane, 2023)

Eskom has adopted the phased approach (Figure 1-2) herein to increase the probability of success and to ensure that learnings from early phases are incorporated into the large-scale roll-out. (Matimolane, 2020).

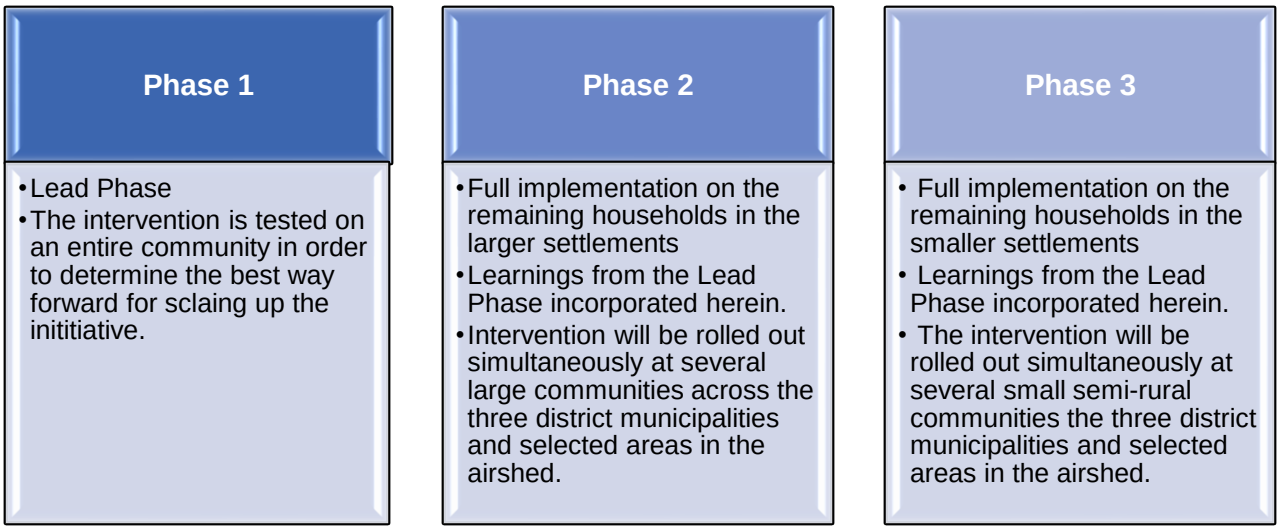

Figure 1-2: Eskom's Phased approach to the rollout of air quality offset interventions (Matimolane, 2020)

Eskom's air quality offsets programme is designed to reduce human exposure to harmful levels of air pollution by reducing emissions from local sources, like domestic coal burning and waste burning. Thus, air quality offsets can improve ambient air quality in low-income communities in the vicinity of Eskom's power stations. Eskom has developed air quality offset (AQO) implementation plans for Majuba Power Station (Ezamokuhle township), Hendrina Power Station (KwaZamokuhle township) and Lethabo Power station (Sharpeville).

1.3 ESKOM'S PLANNING, MONITORING AND VERIFICATION (PMV) PROJECT

For Eskom's PMV Project, interventions to reduce household emissions from domestic coal/wood burning will be rolled out in KwaZamokuhle and Ezamokuhle in the Mpumalanga Highveld. For formal dwellings the intervention will be a thermal insulation retrofit and an electricity starter pack and installation. The intervention for informal dwellings still needs to be selected and tested. Interventions also need to be identified and implemented to improve air quality in Sharpeville, Gauteng. Since domestic coal burning is less prevalent in Sharpeville, it is expected that a community-scale intervention, like reducing waste burning, will be more suitable there.

Air Resource Management (ARM) (Pty) Ltd has been appointed by Eskom to support the PMV services in support of the *Phase 1: Lead implementation* at: KwaZamokuhle; Ezamokuhle and Sharpeville. It's ARM (Pty) Ltd understanding that the overall objective *Lead Implementation Phase* is to benefit the specific local communities, minimize implementation risk, increase practical and scientific knowledge, and develop and refine monitoring, reporting and verifications processes. To achieve this, Eskom has included sixteen targeted work package Activities (Table 1-1) for these respective communities. This report focuses on *Activity 12.8: Dispersion Modelling for the year 2023 for Ezamokuhle.*

Table 1-1: Eskom PMV Activity Schedule (Eskom PMV NEC Contract, 27082020)

Activities	Kwazamokuhle	Ezamokuhle	Sharpeville
Activity 1: Preliminary air quality assessment		✓	
Activity 2: Gather Area intelligence		✓	
Activity 3: Rapid in situ assessment		✓	
Activity 4: Obtain ethical clearance		✓	
Activity 5: Census	✓	✓	✓
Activity 6: Community source survey		✓	
Activity 7: Fuel source survey		✓	
Activity 8: Household surveys		✓	
Activity 9: Annual (household/community) surveys and monitoring of project effectiveness	✓	✓	✓
Activity 10: Ambient air quality monitoring	✓	✓	✓
Activity 11: Conduct indoor air quality monitoring	✓	✓	
Activity 12: Atmospheric Dispersion Model	✓	✓	✓
Activity 13: Design of Intervention		✓	✓
Activity 14: Development of Database Reporting	✓	✓	✓
Activity 15: Strategic Assistance and offsets methodology	✓	✓	✓
Activity 16: Research and Development	✓	✓	✓

1.4 Scope of Work

In accordance with the scope of work, for *Activity 12: Atmospheric Dispersion Modelling*, ARM must compile emission inventories of all sources affecting air quality in the three communities. ARM shall then develop and run appropriate dispersion model(s) to predict ambient SO_2, NO_2 and particulate matter (PM_{10} and $PM_{2.5}$) levels in the selected settlements to an acceptable level of accuracy. ARM will run the dispersion models on an annual basis to determine the impact of the interventions on ambient air quality, and the baseline in the absence of an offsets roll-out. The focus of this study is on the baseline atmospheric dispersion modelling for Ezamokuhle (Figure 1-3).

Figure 1-3: Locality Map for Ezamokuhle

1.5 STUDY OBJECTIVE

The main objective of this study is to use results of the dispersion modelling to inform Eskom's Air Quality Offsets Implementation Plan. This is done by firstly compiling a comprehensive emission inventory for a number of emission source categories which include power generation, residential fuel burning, waste burning, biomass burning, vehicles travelling on paved roads, vehicles travelling on unpaved roads, and then assessing the contribution of each emission source to the ambient concentrations in the study area, with a strong focus on PM.

The second objective of this study is to assess the modelled ambient concentrations of SO_2, NO_2 and particulate matter (PM_{10} and $PM_{2.5}$) against the respective National Ambient Air Quality Standards NAAQS (Table 1-2). Additionally, an assessment of the modelled dustfall rates are evaluated against the National Dustfall Standard. The National Dust Control Regulations were published on 1 November 2013 (DEA, 2013b). It lists guidance on the requirements for monitoring dust fallout and provides limit values for acceptable dustfall rates for residential and non-residential areas (Table 1-3).

Table 1-2: NAAQS in µg/m³ for SO_2, NO_2, PM_{10} (DEA, 2009) and $PM_{2.5}$ (DEA, 2012)

Pollutant	Averaging Period	Limit value (µg/m³)	Permitted frequency of exceedance	Compliance Date
Sulphur Dioxide (SO_2)	10 minutes	500	526	Immediate
	1 hour	350	88	Immediate
	24 hour	125	4	Immediate
	1 year	50	0	Immediate
Nitrogen Dioxide (NO_2)	1 hour	200	88	Immediate
	1 year	40	0	Immediate
Inhalable particulate matter less than 10 µm in diameter (PM_{10})	24 hour	75	4	Immediate
	1 year	40	0	Immediate
Inhalable particulate matter less than 2.5 µm in diameter ($PM_{2.5}$)	24 hour	40	4	Immediate
	24 hour	25	4	1 January 2030
	1 year	20	0	Immediate
	1 year	15	0	1 January 2030

Table 1-3: National limit values for dustfall rates in mg/m²/day as a 30-day average (DEA, 2013b)

Area	Dustfall rate (D)	Permitted frequency of exceedance
Residential	D < 600	Two within a year, not in sequential months
Non-residential	600 < D < 1 200	Two within a year, not in sequential months

2. GENERAL DESCRIPTION OF AREA

2.1 LOCATION

The township of Ezamokuhle lies adjacent to the town of Amersfoort within the Pixley Ka Seme Local Municipality in the Mpumalanga Province, South Africa (Figure 1). According to the Census 2011 data, Ezamokuhle has an area of 6.21 km^2 with a population of 10,293 (1,657.64 per km^2) and has 2,956 households (476.05 per km^2) (StatsSA, 2012).

2.2 TOPOGRAPHY AND LAND USE

2.2.1 TOPOGRAPHY

The Australian CSIRO Atmospheric Research Division, The Air Pollution Model (TAPM) was used to determine the topographical terrain map for the study area (Figure 2-1). The global terrain height and land use datasets are sourced from the US Geological Survey (USGS), Earth Resources Observation Systems (EROS) Data Center Distributed Active Archive Center (EDC DAAC). The topography of the area is relatively flat with a generally uniform terrain.

2.2.2 LAND USE

For atmospheric dispersion modelling an understanding of the land use information is critical. Based on this information, appropriate chemical transformation mechanisms, dispersion coefficients, albedo, surface moisture and surface roughness are selected for the modelling assessment. The classification of a site as urban or rural is based on the Auer method specified in the United States Environmental Protection Agency (USEPA) guideline on air dispersion models (USEPA, 2005). The classification scheme is based on activities within a 3 km radius of the emitting source.

From the Auer's method, areas typically defined as rural include residences with grass lawns and trees, large estates, metropolitan parks and golf courses, agricultural areas, undeveloped land and water surfaces. An area is defined as urban if it has less than 35% vegetation coverage or the area falls into one of the land use types in Table 2-1.

A land cover map of the study area is presented in Figure 2-2. Based on the Auer's assessment method detailed above, the study area is classified as rural as the emitting sources are located throughout the modelling domain.

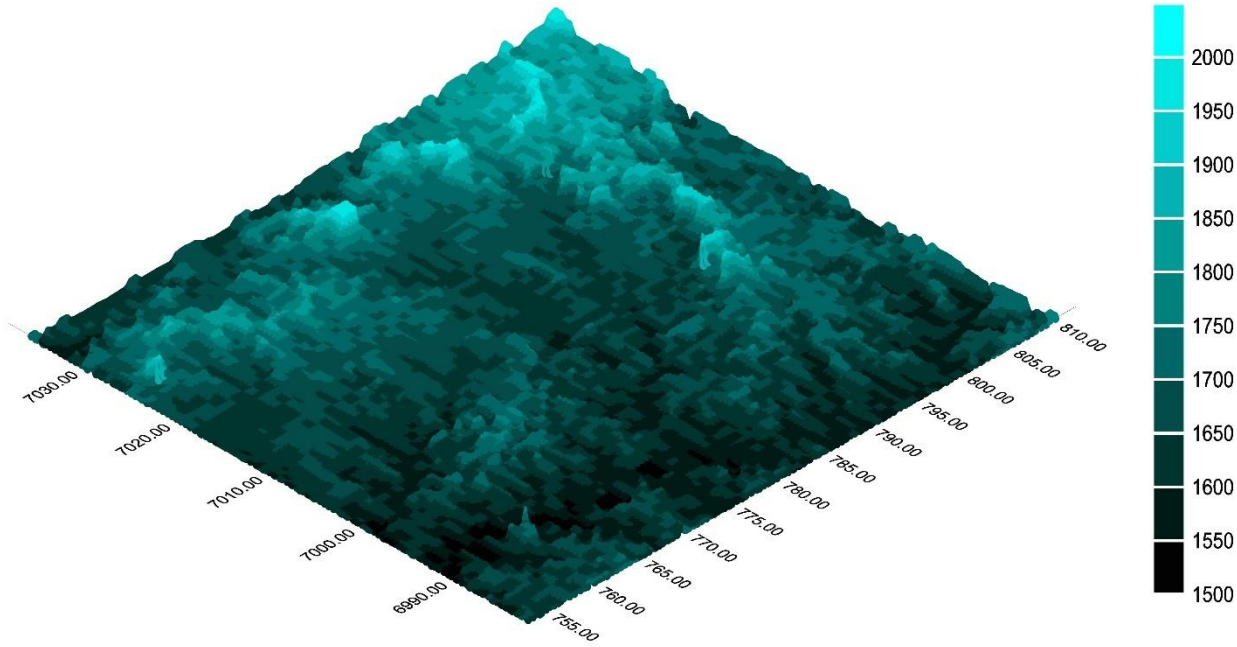

Figure 2-1: Topography of the Study Area

Table 2-1: Land types, use and structures and vegetation cover

Urban Land Use		
Type	**Land Use and Structures**	**Vegetation**
I1	Heavy industrial	Less than 5 %
I2	Light/moderate industrial	Less than 5 %
C1	Commercial	Less than 15 %
R2	Dense single / multi-family	Less than 30 %
R3	Multi-family, two-story	Less than 35 %

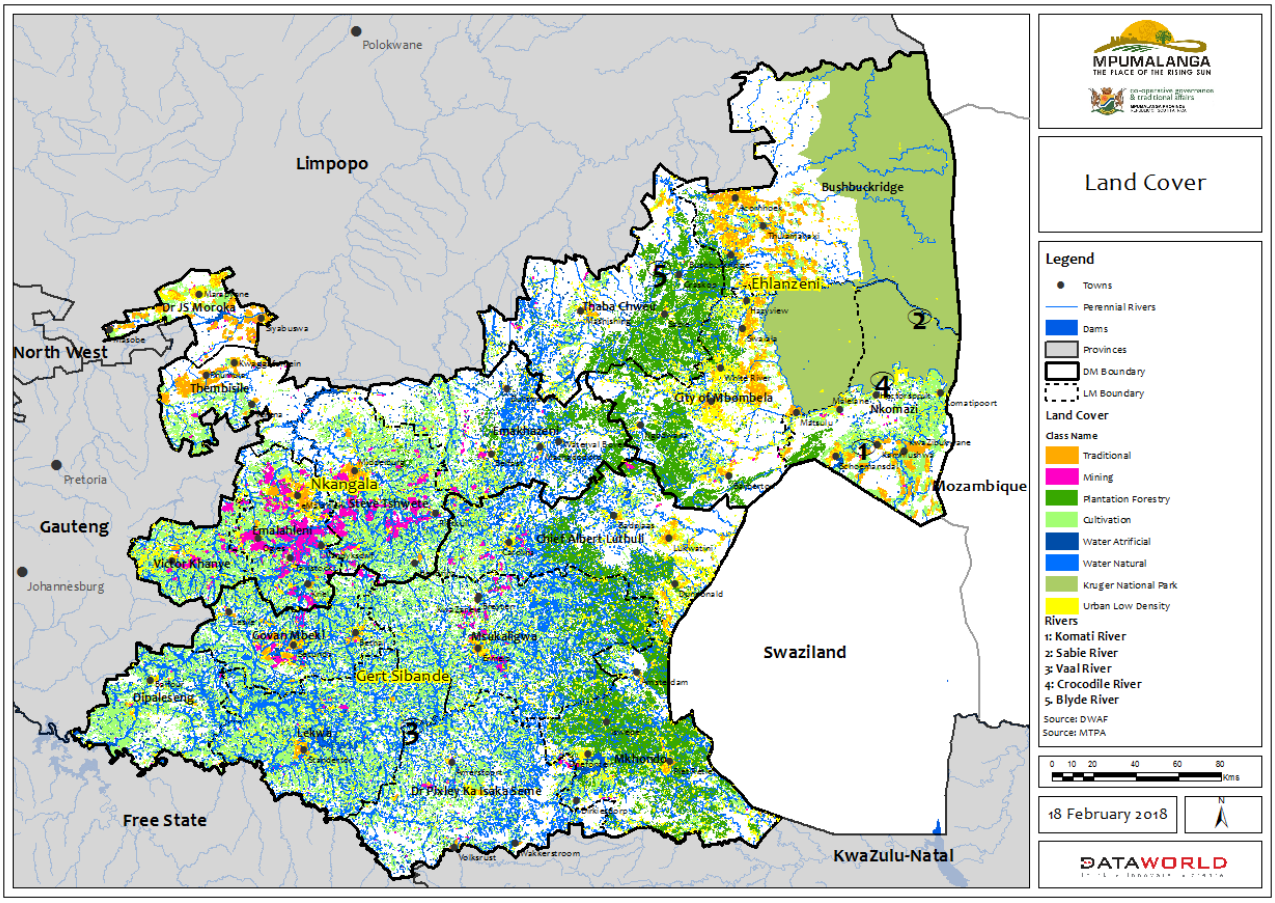

Figure 2-2: Land cover for Mpumalanga (Source: Mpumalanga Spatial Development Framework, 2019)

2.3 Climate and Meteorology

The Highveld experiences a temperate climate with dry winters according to the Köppen Climate Classification system (Köppen, 1884). The winters are mild and dry, but cold at night. Rainfall occurs in summer. The rain is largely due to the development of low-pressure troughs over the central plateau in summer whilst the dry winters are due to the dominant subtropical high pressure system. The temperate temperatures are attributed to the relatively high altitude (DEFF, 2010).

2.3.1 Rainfall and Temperature

The mean monthly rainfall totals recorded at the Eskom Ezamokuhle Air Quality Monitoring Station (AQMS) for the period 2020 to 2022 is presented in Figure 2-3. It is noted that rainfall occurs predominantly from October to April, with the maximum in summer (December). The region received a mean annual rainfall of ~79 mm for the period 2020 to 2022. Average temperatures for the area are mild throughout the year with slightly cooler temperatures in winter. The long-term average (2020-2022) maximum temperature is 31°C in summer and 24.1°C in winter, with extreme maxima of 31.1°C in summer and 26°C in winter. The long-term minimum, maximum and mean temperatures observed at the Eskom Ezamokuhle AQMS station is presented in Figure 2-3.

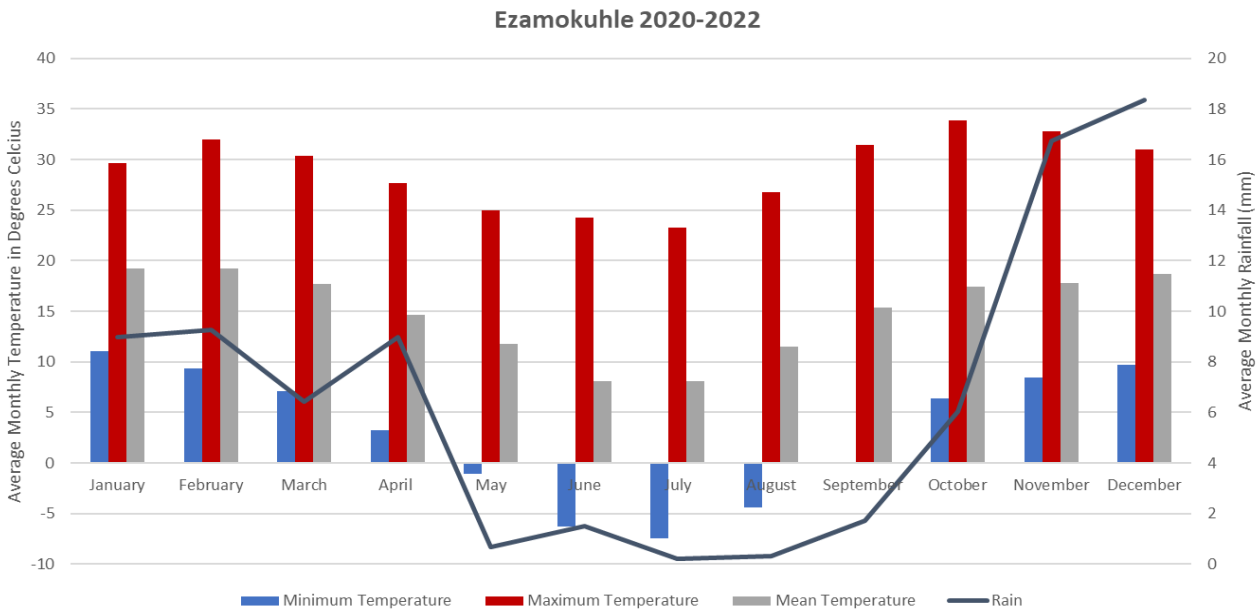

Figure 2-3: Average monthly maximum, minimum and mean temperatures and average monthly rainfall recorded at the Eskom Ezamokuhle AQMS

2.3.2 Surface and Near-Surface Winds

Air quality is strongly influenced by meteorology. Meteorological mechanisms govern the dispersion, transformation, and eventual removal of pollutants from the atmosphere (Seaman, 2000). The analysis of hourly average meteorological data is necessary to facilitate a comprehensive understanding of the dispersion potential of the site. The horizontal dispersion of pollution is largely a function of the wind field. The wind speed determines both the distance of downward transport and rate of pollutant dilution. The wind rose is a useful way of showing how wind speed and wind direction conditions vary by year.

Wind Direction

At the Eskom Ezamokuhle AQMS, the average wind speed for the period 2020-2022 was recorded at 1.96 m/s with calm condition at 0% (Figure 2-4). Calm condition means that wind speed is recorded at 0 m/s (Carlaw, 2015). The predominant wind directions were both easterly (~15% frequency of occurrence) and westerly (~15% frequency of occurrence) with maximum wind speeds of 8-11 m/s. The wind speed and direction data for the period 2020-2022 also demonstrates a seasonal signal at the Eskom Ezamokuhle AQMS (Figure 2-5). For the spring and summer months, the average wind speed was recorded at ~3.1 m/s, with a predominant wind direction of easterly winds (~15-20% frequency of occurrence). For the autumn and winter months, the average wind speed was recorded at ~2.5 m/s with a predominant wind direction of westerly winds (~19% frequency of occurrence).

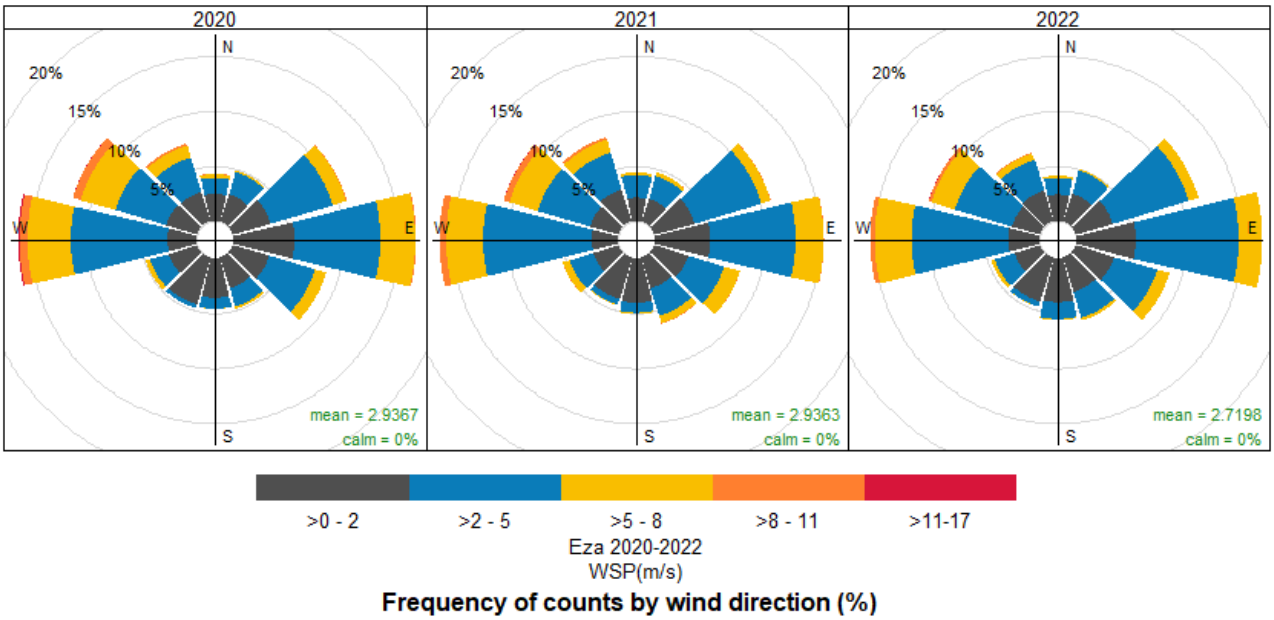

Figure 2-4: Annual wind rose for the Eskom Ezamokuhle AQMS for the period 2020 to 2022

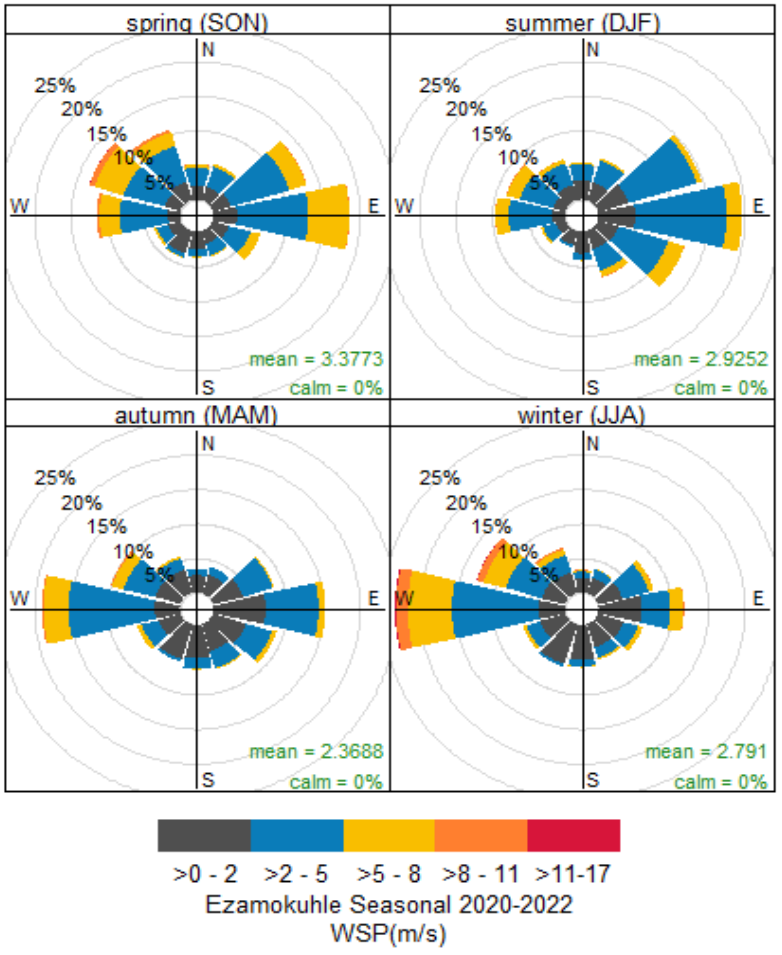

Figure 2-5: Seasonal wind rose for the Eskom Ezamokuhle AQMS for the period 2020 to 2022

WIND SPEED

Wind drives the atmospheric transport and strongly affects vertical mixing and thus the ventilation of the urban air (Grundstrom et al., 2015). Stagnant atmospheric conditions with calm, clear weather often leads to stable atmospheric stratification which then leads to poor air quality (Delaney and Dowding, 1998; Janhall et al., 2006; Olofson et al., 2009). Low wind speeds leads to restricted air ventilation and may cause ambient air quality to deteriorate particularly when pollutants are emitted near ground level (Jones et al., 2010). In contrast, high wind speeds are associated with increased dispersion and mixing of atmospheric pollutants which may result in low ambient pollution concentrations.

Monthly wind speed averages for the Eskom Ezamokuhle AQMS is presented in Figure 2-6. For the period January to May, the wind speed pattern shows a general decrease in values with low averages recorded until July. This is associated with less mixing and dispersion of pollutants which may result in elevated ambient concentrations particularly during winter (Liebenberg, 1999). Conversely, there is an increase in wind speeds from August to November. This is associated with increased dispersion and mixing of atmospheric pollutants which may result in lower ambient pollution concentrations during this period.

Diurnal wind speed averages for the Eskom Ezamokuhle AQMS is presented in Figure 2-7. Lower wind speeds are logged from 19h00 to 05h00. This is associated with elevated atmospheric pollution concentrations due to less mixing and dispersion. The wind speeds then increase from 05h00 to 13h00. This is associated with lower pollution concentrations influenced by an increase in the mixing and dispersion of atmospheric pollutants (Liebenberg, 1999).

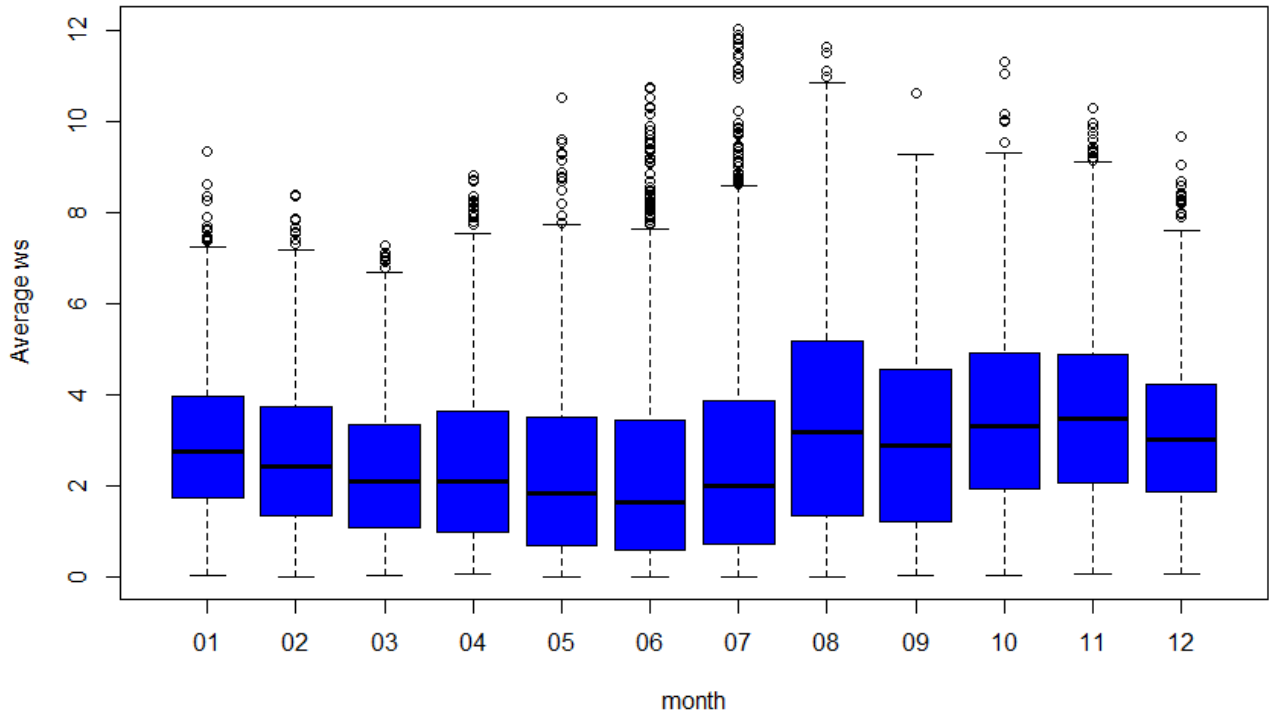

Figure 2-6: Monthly wind speed averages for the Eskom Ezamokuhle AQMS (box and whisker plot indicates interquartile range, diamond indicate outliers and bars indicate the min and max value)

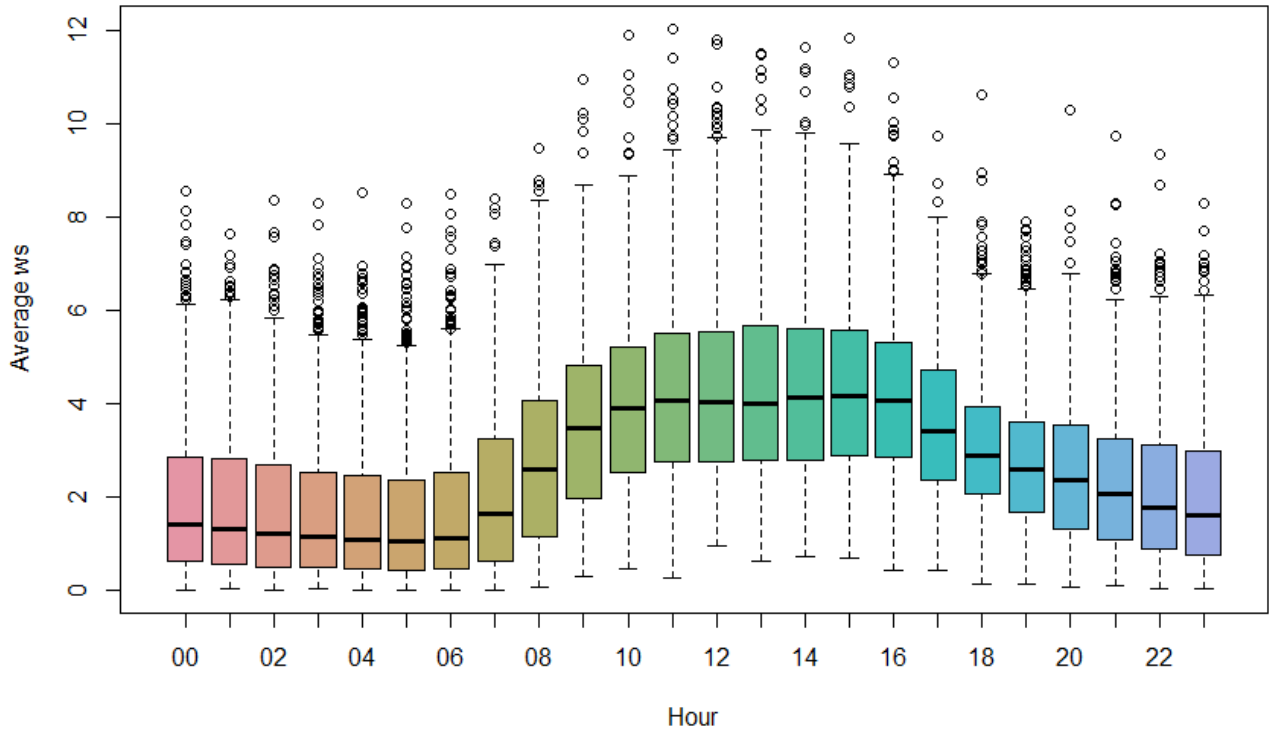

Figure 2-7: Diurnal wind speed averages for the Eskom Ezamokuhle AQMS (box and whisker plot indicates interquartile range, diamond indicate outliers and the bars indicate the min and max value)

2.3.3 DISPERSION POTENTIAL

The extent to which synoptic systems and weather disturbances impact on the dispersion potential of the atmosphere depends on the height and persistence of elevated temperature inversions. Elevated inversions reduce the height at which pollutants are able to mix, and consequently results in the accumulation of pollutants between the surface and the base of the inversion layers. These inversions therefore play a key role in the recirculation of pollutants as well as controlling long-range transport.

The southern African subcontinent is under the influence of a semi-permanent sub-tropical anticyclone. They are dominant in mid-winter with a frequency of occurrence of 80% as opposed to 20% in summer (Garstang et al., 1996). These high pressure systems are associated with large-scale subsidence inversions which has a considerable influence on the accumulation of trace gases and aerosols in the troposphere (Garstang et al., 1996; Swap and Tyson, 1999). The presence of subsidence induced semi-permanent absolutely-stable layers at altitudes of approximately 700 hPa (~3 km), 500 hPa (~5 km) and 300 hPa (~7 km) (Figure 2-8), were identified over southern Africa by Cosijn and Tyson (1996) and Freiman and Tyson (2000). The horizontal and vertical transport of aerosols between the surface and the tropopause is controlled by these stable layers (Garstang et al, 1996). The lower level elevated subsidence inversion is significant in that it represents a persistent cap impeding the upward mixing of air pollutants (DEFF, 2007).

Convective activity hinders the formation of inversions. Whilst cyclonic disturbances are usually associated with the dissipation of inversions, pre-frontal conditions tend to lower the base of the elevated inversion, thus reducing the mixing depth. After the passage of a cold front, there is a gradual increase in the mixing depth (Scott and Diab, 2000).

For Ezamokuhle, the dispersion potential is anticipated to be better during the day due to higher daytime temperatures and a higher frequency of moderate wind speeds. In addition, summer months will have a better dispersion potential than the winter months due to a higher frequency of stronger winds, higher rainfall, stronger thermal mixing, weaker and less persistent night-time temperature inversions.

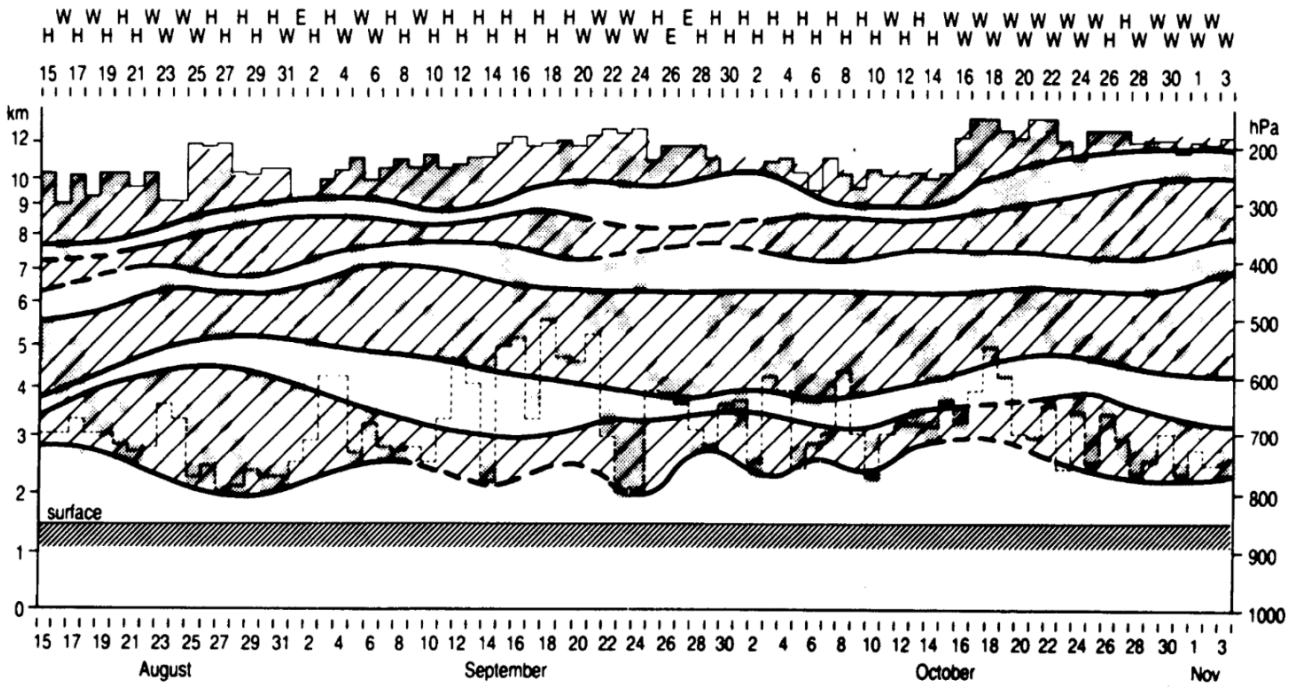

Figure 2-8: Daily variation of absolutely stable layers over Pretoria (southern Africa) during SAFARI-92. Stippled boxes indicate the height and depth of stable layers. Envelopes of continuous and discontinuous stable layers are indicated by cross-hatched regions enclosed by solid and dashed lines respectively. Light dashed lines depict the height of the 1200UT mixing depth. Circulation class for each day is shown by H (continental high), W (westerly disturbance) and E (easterly disturbance) (Source: Garstang et al., 1996: p 23724)

2.4 AMBIENT AIR QUALITY MONITORING ANALYSIS

The Openair air quality model was used to statistically analyse the semi-empirical mathematical relationships between air pollutant concentration and meteorological factors for the Eskom Ezamokuhle AQMS for the period 1 January 2020 to 31 December 2022.

2.4.1 TREND ANALYSIS PLOT

The trend analysis (mean with 95% confidence interval) of ambient pollutant concentrations measured at the Eskom Ezamokuhle AQMS show the variation of these pollutants over daily, weekly and annual cycles for the period 2020-2022.

Mean pollutant concentrations for the Eskom Ezamokuhle AQMS for the hourly mean during weekdays, a single day, monthly and daily mean for the period 2020-2022 is presented in Figure 2-9 for SO_2 and NO_2; and in Figure 2-10 for particulate matter (PM_{10} and $PM_{2.5}$).

SO_2 displays a typical industrial signature with increased SO_2 concentrations just around midday due to the break-up of an elevated inversion layer, in addition to the development of daytime convective conditions causing the plume to be brought down to ground level and relatively close to the point of release from tall stacks. The elevated SO_2 levels in winter (June, July and August)

indicates the contribution of residential fuel burning at the Eskom Ezamokuhle AQMS. It is also evident that there is a second less pronounced peak (compared to the midday values), that occurs at 18h00 in winter (peaking in the months of June and July) which indicates the impact of residential fuel burning.

The variability of NO_2 clearly shows that it is highly influenced by vehicle emissions. Daily and weekly variation corresponds to the cyclical nature of traffic volumes with marked peaks in concentration on weekdays around the early-morning and late-afternoon rush-hour. NO_2 concentrations plotted by time-of-day shows a clear rise in concentrations corresponding to the peak of the morning rush-hour at around 06h00 and a second more marked rise with the evening rush-hour, peaking at around 18h00. The elevated NO_2 levels in winter (June, July and August) indicates the contribution of residential fuel burning at the Eskom Ezamokuhle AQMS.

The particulate matter morning peak occurs at 06h00 while the evening peak occurs at 18h00. This is a typical profile for residential fuel burning. The morning peak reduces towards midday as the inversion layer rises and improves the mixing height of the planetary boundary layer. It is evident that there is a third less pronounced peak that occurs at midday due to the break-up of an elevated inversion layer, in addition to the development of daytime convective conditions causing the plume from tall stacks to be brought down to ground level. Monthly variation of particulate matter shows elevated concentrations during early winter months to early spring (May to September) due to the greater contribution from residential fuel burning, dust from uncovered soil and the lack of the settling influence of rainfall.

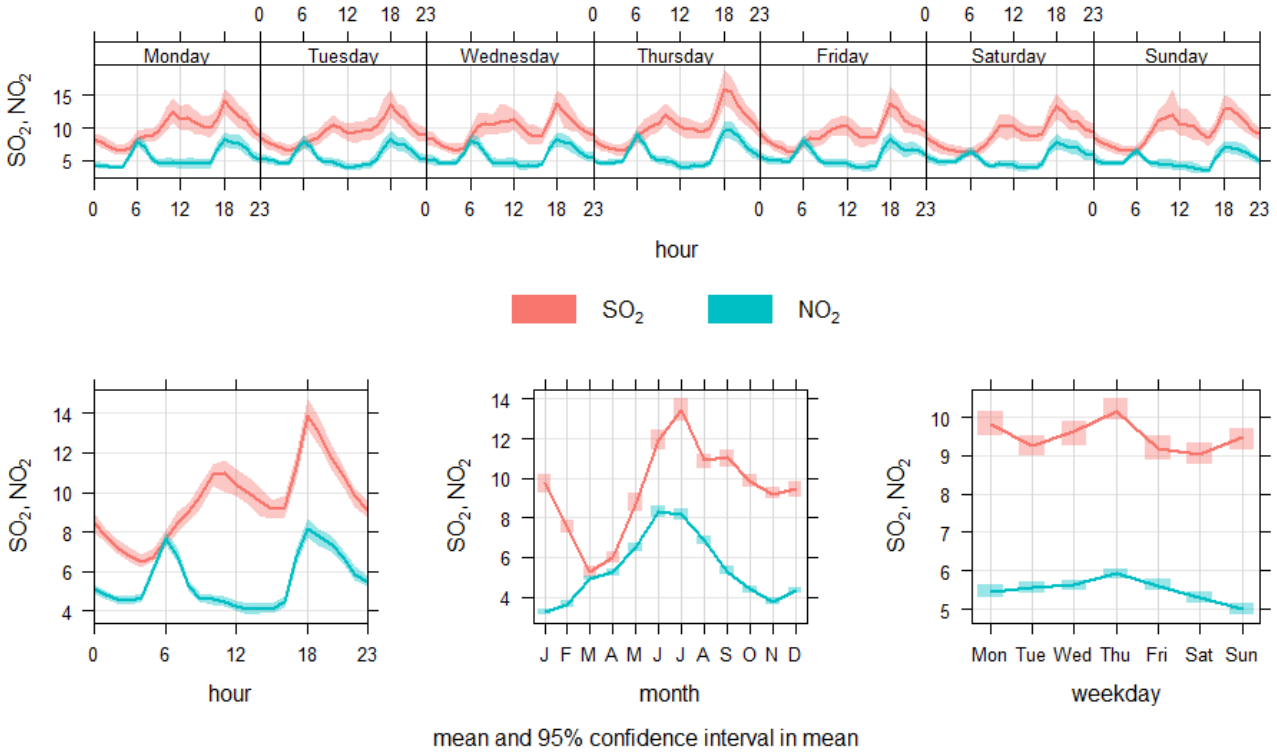

Figure 2-9: Mean pollutant concentrations in ppb for the Eskom Ezamokuhle AQMS for the hourly mean during weekdays, a single day, monthly and daily mean for the period 2020-2022 for SO_2 and NO_2

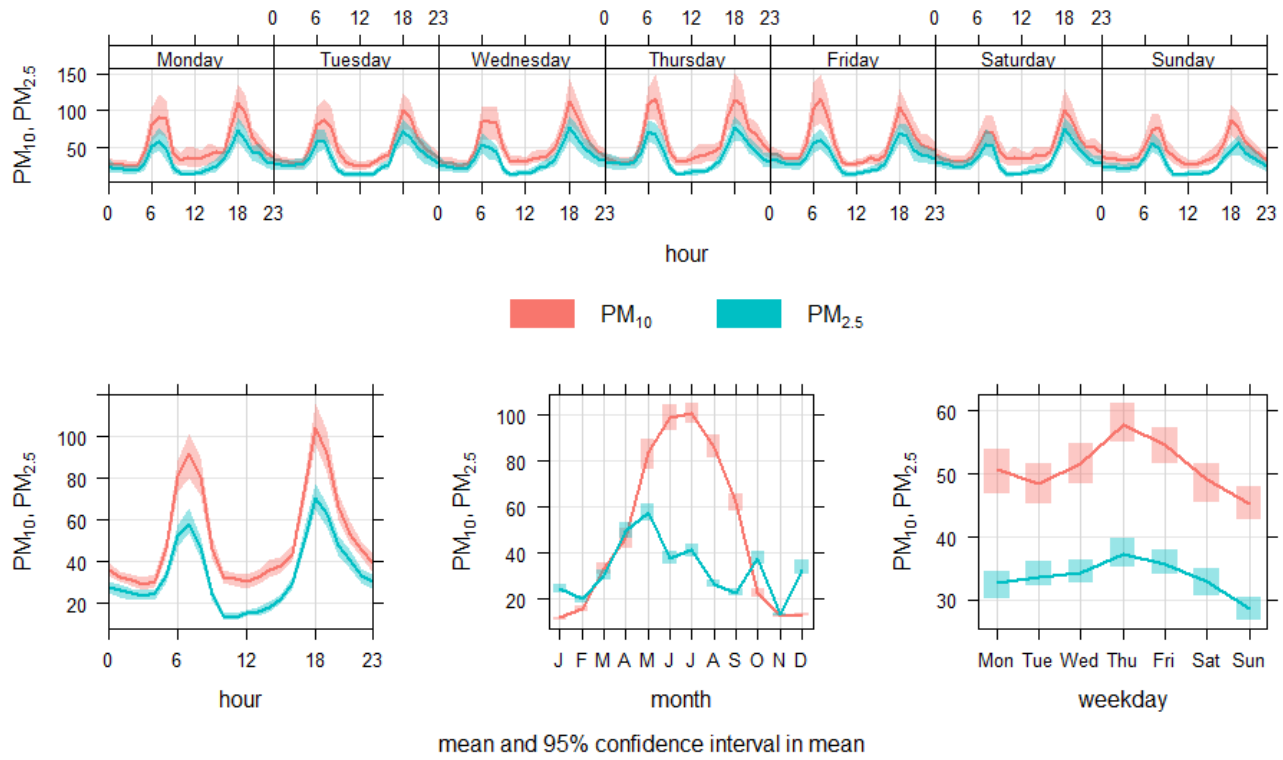

Figure 2-10: Mean pollutant concentrations in µg/m^3 for the Eskom Ezamokuhle AQMS for the hourly mean during weekdays, a single day, monthly and daily mean for the period 2020-2022 for $PM_{2.5}$

2.4.2 TIME SERIES ANALYSIS

A summary of ambient data measured at the Eskom Ezamokuhle AQMS for the period 2020-2022 is presented in Table 2-2.

Table 2-2: Summary of ambient air quality measurements at the Eskom Ezamokuhle AQMS

Station	Year	Maximum Measured Pollutant Measurement			
		SO_2 (ppb)		NO_2 (ppb)	$PM_{2.5}$ (µg/m^3)
		Hourly	Daily	Hourly	Daily
Eskom Ezamokuhle AQMS	2020	131	20.2	61.7	152
	2021	158	15.1	46.6	218
	2022	116	28.2	42.4	80.4

Time-series graphs for measured concentrations at the Eskom Ezamokuhle AQMS for the period 2020 to 2022 is presented in Figure 2-11 and Figure 2-12 for hourly and daily SO_2 concentrations respectively, in Figure 2-13 for hourly NO_2 concentrations, and in Figure 2-14 for daily $PM_{2.5}$ concentrations.

The hourly 99th percentiles for SO_2 were above the limit value of 134 ppb for two occasions during the 2020 to 2022 period. These exceedances occur in the months of August and December just around 10h00 and in the evening at 18h00. Additionally, the hourly SO_2 polar plot for the Eskom Ezamokuhle AQMS (Figure 2-15) further shows a typical industrial signature with increased SO_2 concentrations just before midday due to the break-up of an elevated inversion layer, in addition to the development of daytime convective conditions causing the plume to be brought down to ground level relatively close to the point of release from tall stacks. Thus, these exceedances are likely due to the impact of an elevated emission source. It is evident that daily SO_2 concentrations were below the NAAQS limit value of 48 ppb during the entire period.

Similarly, hourly NO_2 concentrations clearly indicate that there were no recorded exceedances of the NAAQS standard of 106 ppb.

The NAAQS for the daily $PM_{2.5}$ limit (40 µg/m^3) was exceeded on numerous occasions during the 2020-2022 period, indicating the impact of a residential fuel burning source. The NAAQS for daily $PM_{2.5}$ was exceeded mainly in the winter months, with morning peak concentrations occurring at 08h00 and evening peaks occurring at 18h00, which is a typical profile for residential fuel burning.

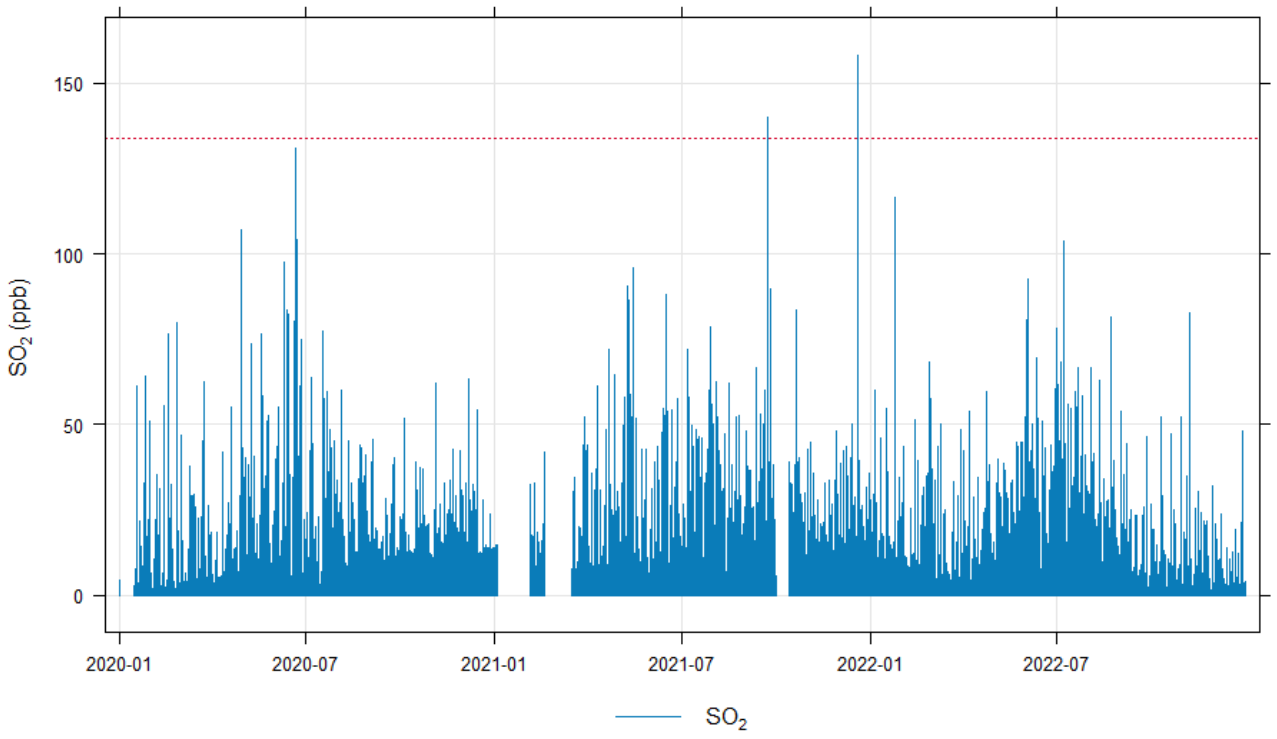

Figure 2-11: Time series for hourly SO_2 ground level concentrations measured at the Eskom Ezamokuhle AQMS (2020-2022)

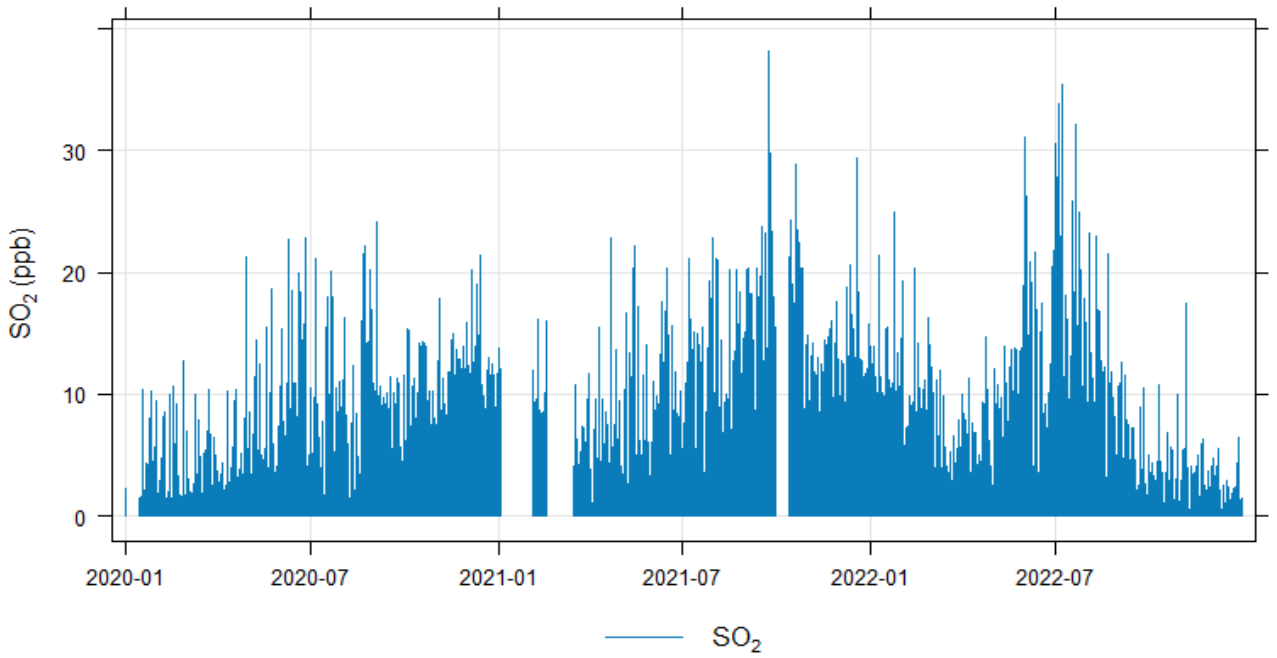

Figure 2-12: Time series for daily SO_2 ground level concentrations measured at the Eskom Ezamokuhle AQMS (2020-2022)

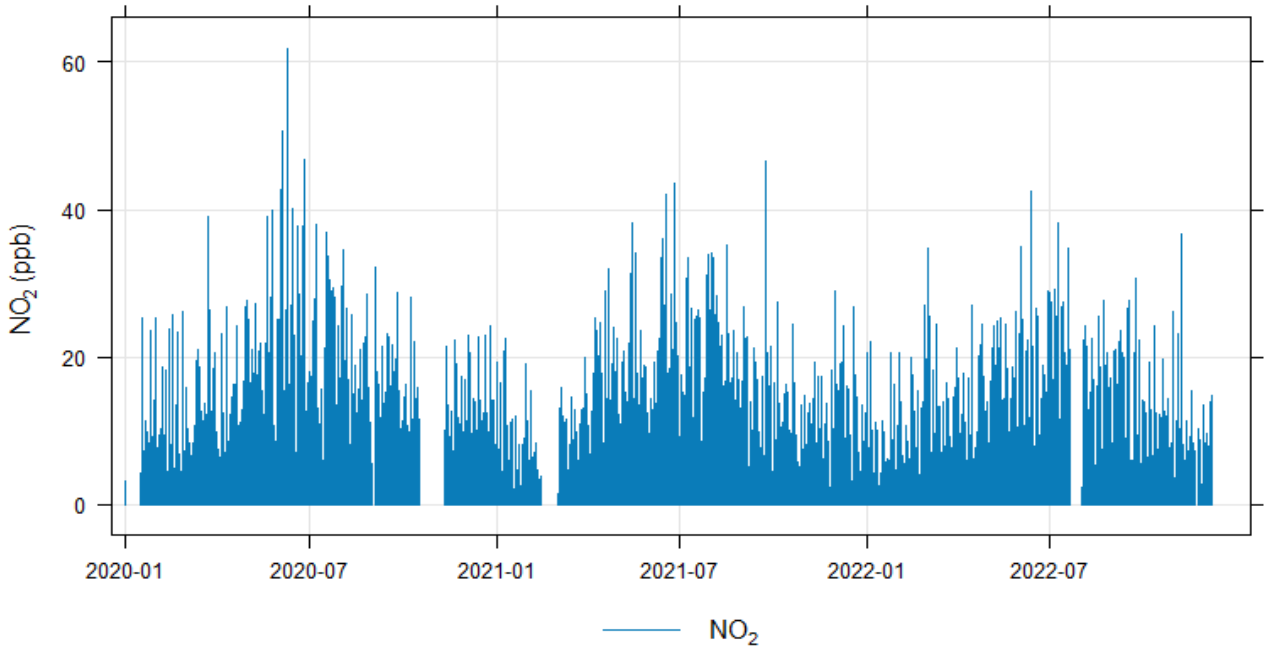

Figure 2-13: Time series for hourly NO_2 ground level concentrations measured at the Eskom Ezamokuhle AQMS (2020-2022)

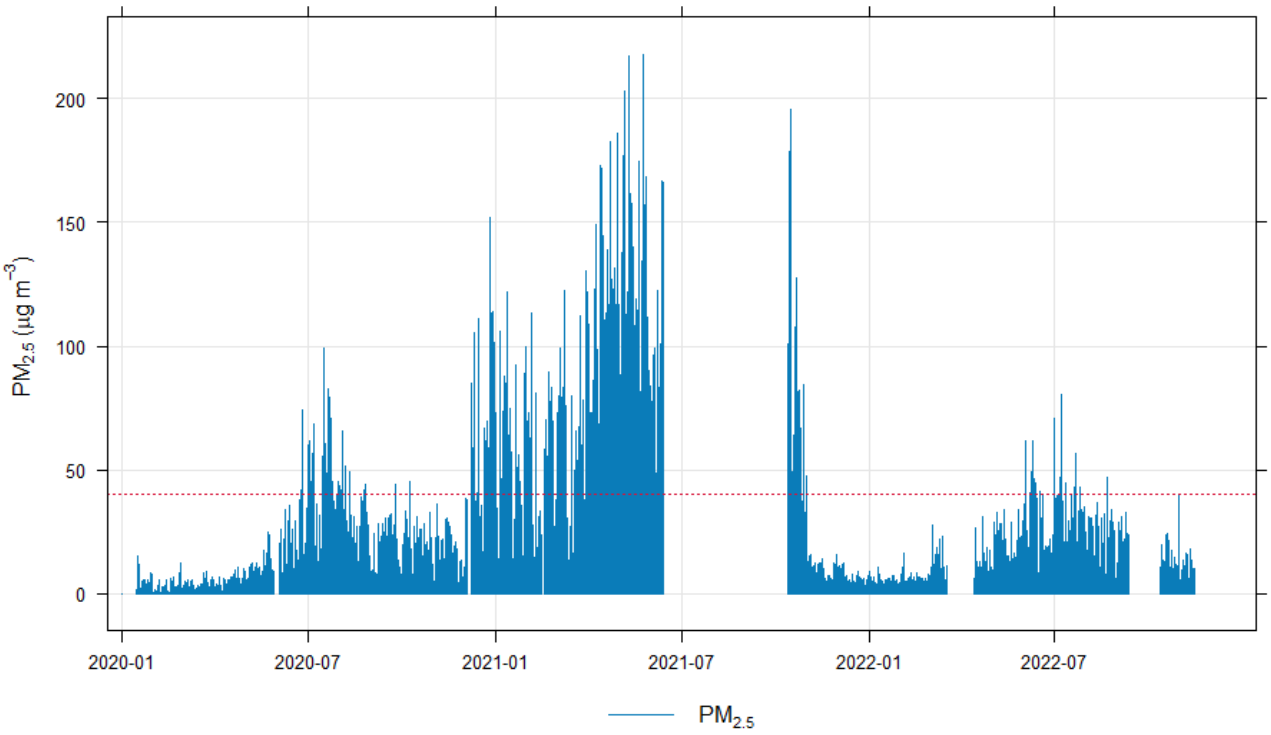

Figure 2-14: Time series for daily $PM_{2.5}$ ground level concentrations measured at the Eskom Ezamokuhle AQMS (2020-2022)

2.4.3 EMISSION SOURCE CONTRIBUTION

Source-specific information can be extracted if analyses are performed using a subset of data that has been "conditionally-selected" to exclude superimposed impacts from non-relevant sources (Malby et al., 2013). A common method for source characterisation is the use of bivariate polar plots (Carslaw et al., 2006; Westmoreland et al., 2007; Carslaw and Beevers, 2013; Uria Tellaetxe and Carslaw, 2014). Bivariate polar plots for the Eskom Ezamokuhle AQMS conditioned for the mean pollutant concentration of hourly SO_2, NO_2, PM_{10} and $PM_{2.5}$ is presented in Figure 2-15.

According to the SO_2 bivariate plot, SO_2 concentrations measured at the Eskom Ezamokuhle AQMS show a distinct source from the southwest and northwest. High concentrations present at high wind speeds are indicative of emissions from stacks rather than non-buoyant ground-level sources. Hence the higher SO_2 concentrations associated with the southwesterly winds are most likely due to emissions from the Eskom Majuba Power Station. Similarly, SO_2 concentrations from the northwest indicate distinct tall stack emission sources located in Secunda.

According to the NO_2 bivariate polar plot, the highest NO_2 concentrations occur under very low wind speed conditions from the southwest. These high concentrations occur under stable atmospheric conditions when non-buoyant ground-level sources are important, such as road transport emissions. The bivariate polar plot confirms that these NO_2 concentrations are the likely impact of vehicle emissions. The bivariate polar plot also shows an area of high concentration to the northwest that occurs at high wind speeds, possibly corresponding to the activities of tall stack emission sources located in Secunda.

According to the particulate bivariate polar plot, elevated particulate concentrations at the Eskom Ezamokuhle AQMS show contributions from the northeast and southwest at low wind speeds. The generally symmetrical plots shows a localised contribution, most likely the result of residential fuel burning.

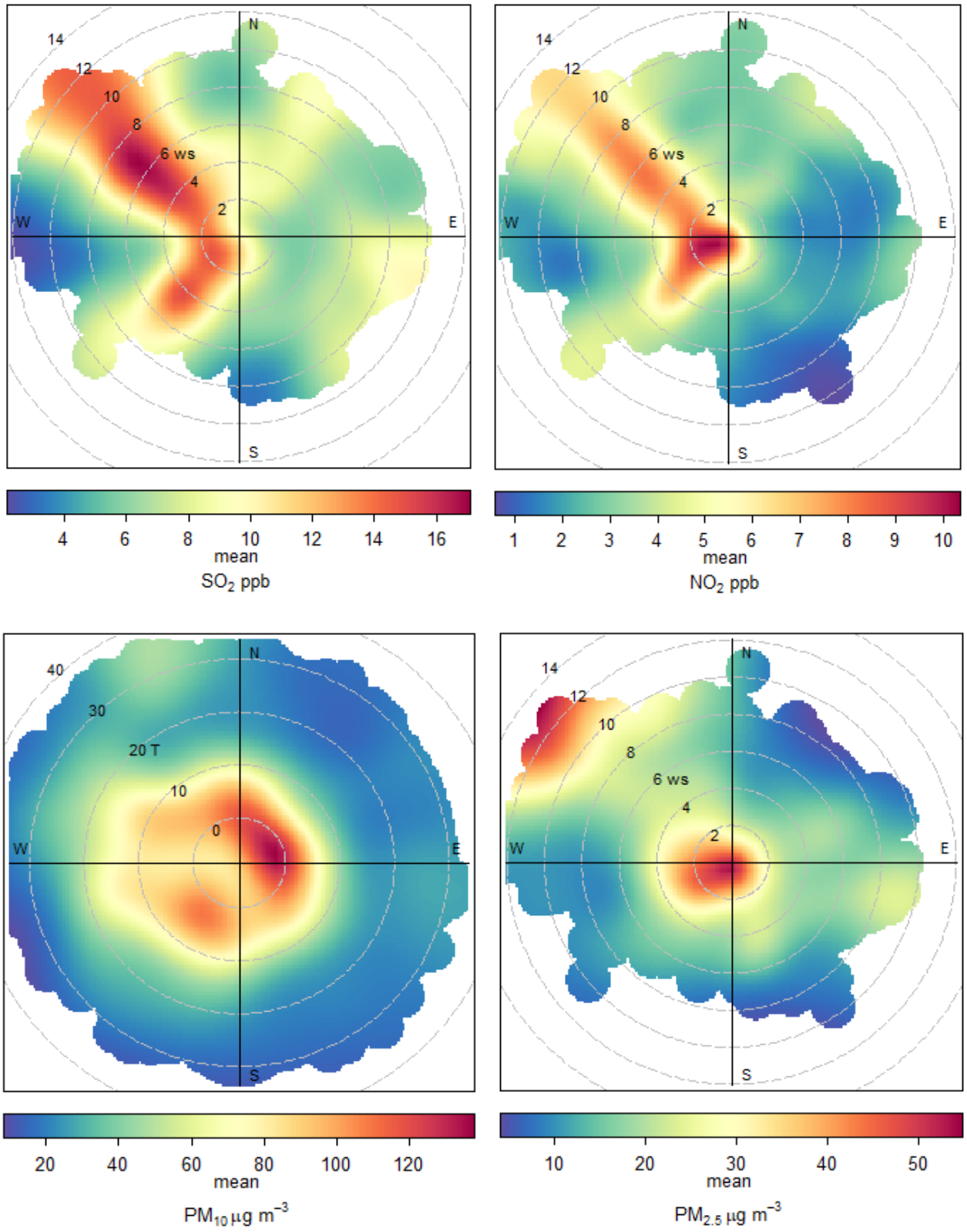

Figure 2-15: Bivariate polar plot of hourly mean SO_2, NO_2, PM_{10} and $PM_{2.5}$, concentrations at the Eskom Ezamokuhle AQMS for 2020 to 2022

3. MODELLING PROCEDURE

3.1 BACKGROUND

Models have been used for decades to approximate physical systems and make estimates about the nature of a system under study (USEPA, 2004). Graedel and Crutzen (1997) have shown that it has become common practice in the environmental science field to describe complex systems of interacting physical, chemical and biological processes through the design of numerical models. For example, mathematical models are often used for assessing air pollution impacts in order to gain a better insight into this multidimensional (Denzer, 2004) and multidisciplinary (Wang, 2005) challenge.

Atmospheric dispersion models use mathematical equations that simulate the physics (Briggs, 1975; Gifford, 1960; Pasquill, 1983; Turner, 1970) and chemistry (Seinfeld and Pandis, 1998) that control the transport and transformation of pollutants in the atmosphere. They provide a means of estimating air pollutant concentrations and particle deposition in the ambient environment based on information on emissions and the prevailing meteorology (Chen et al., 2001; NSW, 2004).

3.2 ASSESSMENT LEVEL PROPOSED AND JUSTIFICATION

A number of dispersion models are used for regulatory applications in South Africa. The suitability of a particular model for an air quality assessment will vary depending on the complexity and scope of the study; the objectives of the modelling; technical factors and the level of risk associated with the project. According to the Regulations Regarding Air Dispersion Modelling (Gazette No 37804, 2014), a tiered approach in the selection of a suitable air dispersion model is recommended. According to the regulations, it is recommended that simple screening models (Level 1) are considered first before the application of more advanced models (Level 2 and 3).

In this study, a detailed understanding of the air quality impacts (time and space variation of the concentrations) is required. Additionally this modelling study must be able to account for causality effects, calms, non-linear plume trajectories, spatial variations in turbulent mixing, multiple source types and chemical transformations. In light of the above, and in accordance with recommendations provided in the Regulations, a Level 3 modelling assessment was regarded as most appropriate for application in this study.

3.3 MODELS USED IN STUDY

3.3.1 METEOROLOGICAL MODEL

Air quality is strongly influenced by meteorology which covers an array of atmospheric processes that determines the evolution of emissions, chemical species, aerosols and particulate matter (Seaman, 2000). The performance of atmospheric dispersion models depends critically on the meteorological

data to simulate the fate and transport of air pollution (Busillo et al., 2005; Davakis et al., 2007; Pielke and Uliasz, 1998). The representativeness of meteorological data is a key factor in accurately modelling the dispersion of these pollutants since meteorological conditions are not uniform over larger distances or in complex terrain, coastal environments, or in urban areas (Alapaty, 1994; Moschandreas et al., 2002).

South Africa is constrained by the lack of an adequate network of surface and upper air meteorological stations that are representative of the atmospheric boundary layer near the surface or at higher levels (Zunckel, 2007). Further, spatially and temporally representative wind flow statistics are not widely available for South Africa (Raghunandan et al., 2008). In this study, no upper air meteorological data is recorded within the modelling domain and the nearest upper air station is located at Irene in Pretoria. Due to the scarcity of surface and upper air meteorological stations available for the study area, TAPM was used to provide site-specific and representative meteorological data for the dispersion model.

TAPM

TAPM, developed by the Australian CSIRO Atmospheric Research Division, is an integrated 3-dimensional mesoscale prognostic meteorological and air pollution regulatory model that is controlled by a graphical user interface (Hurley et al., 2005a; Hurley, 2005b; Luhar and Hurley, 2004; Zawar-Reza et al., 2005).

The meteorological component of TAPM is an incompressible, optionally non-hydrostatic, primitive equation model which uses a terrain-following vertical coordinate system for 3-dimensional simulations (Zawar-Reza and Sturman, 2008). It includes comprehensive parameterisations for cloud/rain micro-physical processes, urban/vegetative canopy and soil, turbulence closure and radiative fluxes (Katzfey and Ryan, 1997; Lai and Chang, 2009; Mahrer and Pielke, 1977).

TAPM predicts local-scale flows, for instance sea breezes and terrain-induced circulations, by using meteorological fields obtained from larger scale synoptic analyses (Luhar and Hurley, 2004). TAPM is able to make use of fundamental fluid dynamics and scalar transport equations to predict the underlying meteorology of an area (Hurley, 2005c). It solves momentum equations to determine the mean horizontal wind components, the incompressible continuity equation for vertical velocity, and scalar equations for potential virtual temperature and moisture (Luhar and Hurley, 2004). The model allows for the option of observed wind data to be assimilated into the momentum equations as nudging terms (Luhar and Hurley, 2003; Raghunandan et al., 2008). Potential virtual temperature is determined from an equation combining the conservation of heat and water vapour. Pressure is determined by the application of a Poisson equation to the nonhydrostatic component (Luhar and Hurley, 2003; Hurley 2005b). A detailed description of the equations and parameterisations,

including the numerical methods used to solve the model equations, used in the present study is given by Hurley et al. (2005a) and Hurley (2005c).

TAPM uses databases of global terrain height, land use, sea-surface temperature and synoptic meteorological analyses as input. The global terrain height and land use datasets are available at a grid space resolution of approximately 1 km and sea surface temperature and synoptic scale meteorological datasets are available at a 100 km resolution. The global terrain height and land use datasets are sourced from the US Geological Survey (USGS), Earth Resources Observation Systems (EROS) and the Data Center Distributed Active Archive Center (EDC DAAC) data (Hurley, 2005b). Global long-term monthly mean sea surface temperatures are derived from the US National Center for Atmospheric Research (NCAR) and the synoptic scale analyses are obtained from the Australian Bureau of Meteorology.

TAPM has been verified for a number of Australian and international datasets, and results from these studies have shown good model performance for both meteorology and air pollution predictions, particularly for the study of annual extreme (high) concentrations important for environmental impact assessments. The meteorological results show that TAPM performs well in a variety of regions (e.g., coastal, inland and generally complex terrain for sub-tropical to mid-latitude conditions). The pollution results show that TAPM performs well for a range of important phenomena (e.g. nocturnal inversion break-up fumigation; stable, neutral, convective and building wake dispersion; shoreline fumigation; and general dispersion in complex rural and urban conditions). In particular, TAPM performs very well for the prediction of extreme pollution statistics, important for environmental impact assessments, for both non-reactive (tracer) and reactive (nitrogen dioxide, ozone and particulate) pollutants for a variety of sources (e.g. industrial stacks and/or general surface or urban emissions (Hurley et al., 2008).

TAPM has also been used extensively in South Africa for many dispersion modelling studies for AQMPs, Air Quality Impact Assessments, Atmospheric Impact Reports and Offsetting Projects. Some of the important AQMP studies include the first-generation Highveld Priority Area Air Quality Management Plan (DEA, 2011) and the Waterberg-Bojanala Priority Area Air Quality Management Plan: Baseline Characterisation (DEA, 2014). A TAPM verification study has also been conducted in South Africa at two coastal sites (Alexander Bay and Richards Bay) (Raghunandan et al., 2008). In this study, TAPM model output was compared with meteorological data measured at South African Weather Service (SAWS) meteorological stations at these locations. It was concluded that the TAPM model performed exceptionally well.

3.3.2 DISPERSION MODEL

In this study, the US-EPA approved Californian Puff (CALPUFF) modelling suite was used for this Level 3 tier modelling assessment.

CALPUFF MODELLING SUITE

The CALPUFF model is an integrated modelling system which can simulate the effects of time- and space-varying meteorological conditions for pollutant dispersion, transformation and deposition (USEPA, 2005; Zhou et al., 2006). The CALPUFF modelling suite comprises of three main components: CALMET, CALPUFF and CALPOST (Figure 3-1). CALMET is a diagnostic meteorological model that generates hourly surface wind fields and micrometeorological variables on a three-dimensional gridded domain for CALPUFF (Elbir, 2006; Hao et al., 2007; Lopez et al., 2005; Song et al., 2006; Zhou et al., 2003). CALPUFF is a non-steady-state Gaussian based transport and dispersion model. It uses three-dimensional meteorological fields developed by CALMET and a series of overlapping puffs to represent the spatial and temporal distribution of emissions from a source (Scire et al., 2000b; Song et al., 2006). The CALPOST program is a powerful postprocessor used to average and report results based on data in the CALPUFF model output files. (Wang, 2006). A brief overview of the CALMET and CALPUFF models is presented in the sections below.

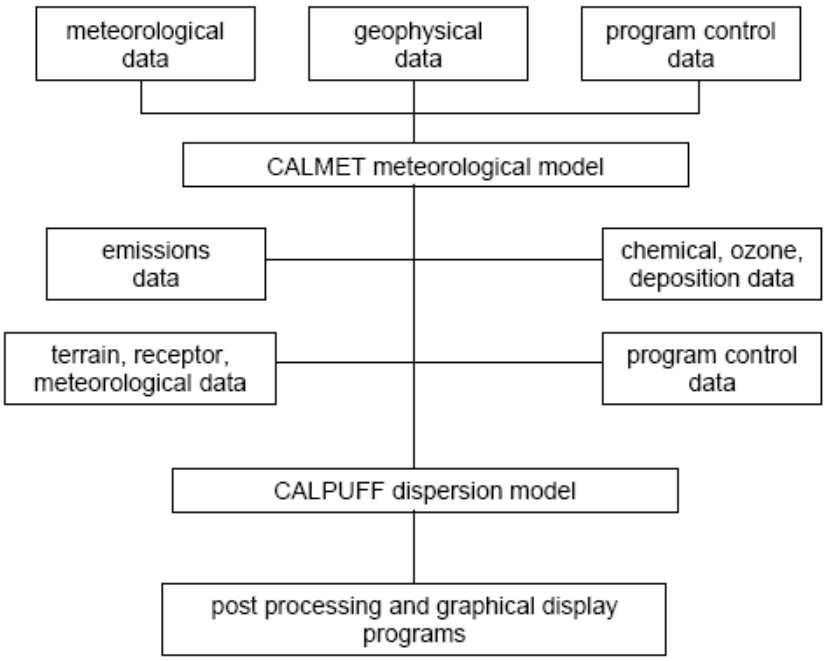

Figure 3-1: CALPUFF modelling system (Source: SRC, 2008)

CALMET

A three-dimensional wind field is computed by the CALMET meteorological model (USEPA, 2005). CALMET requires both geophysical data (terrain elevations and land use categories) and hourly meteorological data (wind speed, wind direction, temperature, cloud cover, ceiling height, surface pressure, relative humidity, precipitation and upper air sounding data) (USEPA, 2005; Scire and Robe, 2004).

CALMET consists of an advanced diagnostic wind field generator as well as a micrometeorological module for overwater and overland boundary layers. An initial guess wind field is modified to take account of kinematic effects of terrain, slope flows, valley flows and terrain blocking effects to create a Step 1 wind field. Observational data are then combined with this Step 1 wind field through an objective analysis procedure to generate the final Step 2 wind field (USEPA 2005; Scire 1999a; Scire 2000a). CALPUFF advects and disperses along these wind vectors created by CALMET (Allwine et al., 1998).

CALPUFF

CALPUFF is a non-steady-state, time-and space-dependent Gaussian puff model which is designed to simulate the transport, dispersion, chemical reactions and deposition of gases and particles in the atmosphere (Ainslie and Jackson, 2009; Scire et al., 2000b). CALPUFF treats emissions as a series of continuous puffs. Each puff is allowed to move with the ambient wind flow (Moschandreas et al., 2006). As the wind flow changes from hour to hour, the path of each puff is displaced in a Lagrangian fashion while undergoing Gaussian dispersion. The model predicted concentrations are calculated based on the contributions of each puff as it passes near or over a discrete receptor point in the modelling domain (Scire et al., 2000b).

CALPUFF is able to model four different source types: point, line, volume and area sources within a single modelling domain. The model makes use of similarity theory to estimate the horizontal and vertical plume dispersion coefficients and contains comprehensive algorithms for both near-source stack and building effects (such as building downwash, partial penetration, plume rise) and long-range effects (chemical transformation, deposition, plume fumigation) (Ainslie and Jackson, 2009; Holmes and Morawska, 2006; USEPA, 2005).

The non-steady state approach of the CALPUFF model makes use of a full three-dimensional meteorological field which can account for spatial and temporal variability in the wind field and atmospheric stability (Scire and Robe, 2004). CALPUFF is able to take account of complex terrain effects, wind reversals, wind stagnation, and causality effects over large spatial scales (Beychok, 2005; Hao et al., 2007; Paradiz et al., 2008). These provide a more realistic simulation for dispersion

and transport as opposed to steady-state Gaussian plume models (Elbir, 2003; Moschandreas et al., 2006).

3.4 MODELLING DOMAINS AND GRID RESOLUTION

3.4.1 METEOROLOGICAL MODELLING DOMAINS

TAPM

TAPM was used to model the hourly surface and upper air meteorology for the study area, for the period 2020 to 2022. TAPM was set-up in a nested configuration of three domains. The outer domain is 600 km by 600 km at a 24 km grid resolution, the middle domain is 300 km by 300 km at a 12 km grid resolution and the inner domain is 75 km by 75 km at a 3 km grid resolution (Figure 3-2). The larger outer domains are used to initialise the inner fine-resolution modelling domains. The nesting configuration also ensures that topographical effects on meteorology are captured and that meteorology is well resolved and characterised across the boundaries of the inner domain. These simulations use default databases of global terrain height data, land use and synoptic scale meteorological analyses data as model input, as discussed in Section 3.3.

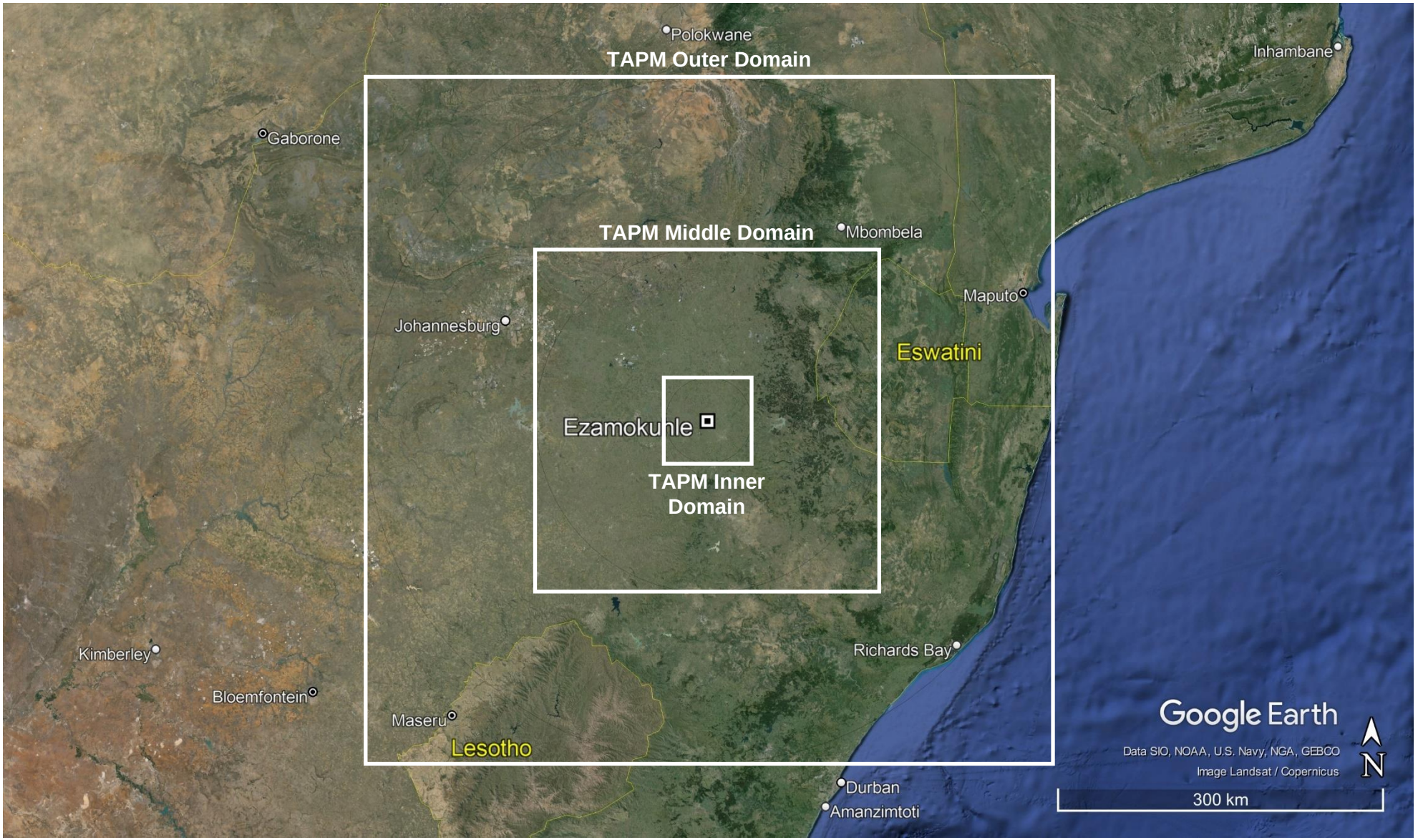

Figure 3-2: Nested grid domains used in the TAPM simulation

CALMET

The CALMET modelling domain for the study area has an extent of 65 km by 65 km with a uniformly spaced horizontal grid resolution of 1 km (Figure 3-3). The top of the domain was set at 5 km with 12 vertical levels.

3.4.2 Dispersion Modelling Domain

CALPUFF

A primary (coarse resolution) grid and a secondary (fine resolution) grid was used in the CALPUFF simulations (Figure 3-3). The grid specifications for each modelling domain is specified in Table 3-1.

Table 3-1: CALPUFF modelling domain grid specifications

Variable	Primary Grid	Secondary Grid
Spatial Area (km^2)	3 721	64
Grid Distance (km) in x and y direction	61 x 61	8 x 8
Horizontal Grid resolution (m)	1 000	200
Number of grid cells in x and y direction	61 x 61	40 x 40
Total number of gridded receptors in domain	3 721	1 600

Primary Modelling Grid: Greater Ezamokuhle Airshed

The domain extends 61 km (west-east) by 61 km (north-south) for a CALPUFF modelling domain of 3 721 km^2. It consists of a uniformly spaced Cartesian receptor grid with 1 000 m spacing, giving 3 721 grid cells (61 x 61 grid cells). This modelling domain caters for a range of emission source categories within a 30 km radius around Ezamokuhle.

Secondary Modelling Grid: Ezamokuhle Airshed

The domain extends 8 km (west-east) by 8 km (north-south) for a CALPUFF modelling domain of 64 km^2. It consists of a uniformly spaced Cartesian receptor grid with 200 m spacing, giving 1 600 grid cells (40 x 40 grid cells). This fine grid resolution ensures that dispersion characteristics and ambient concentrations are accurately captured within and in the immediate vicinity of Ezamokuhle.

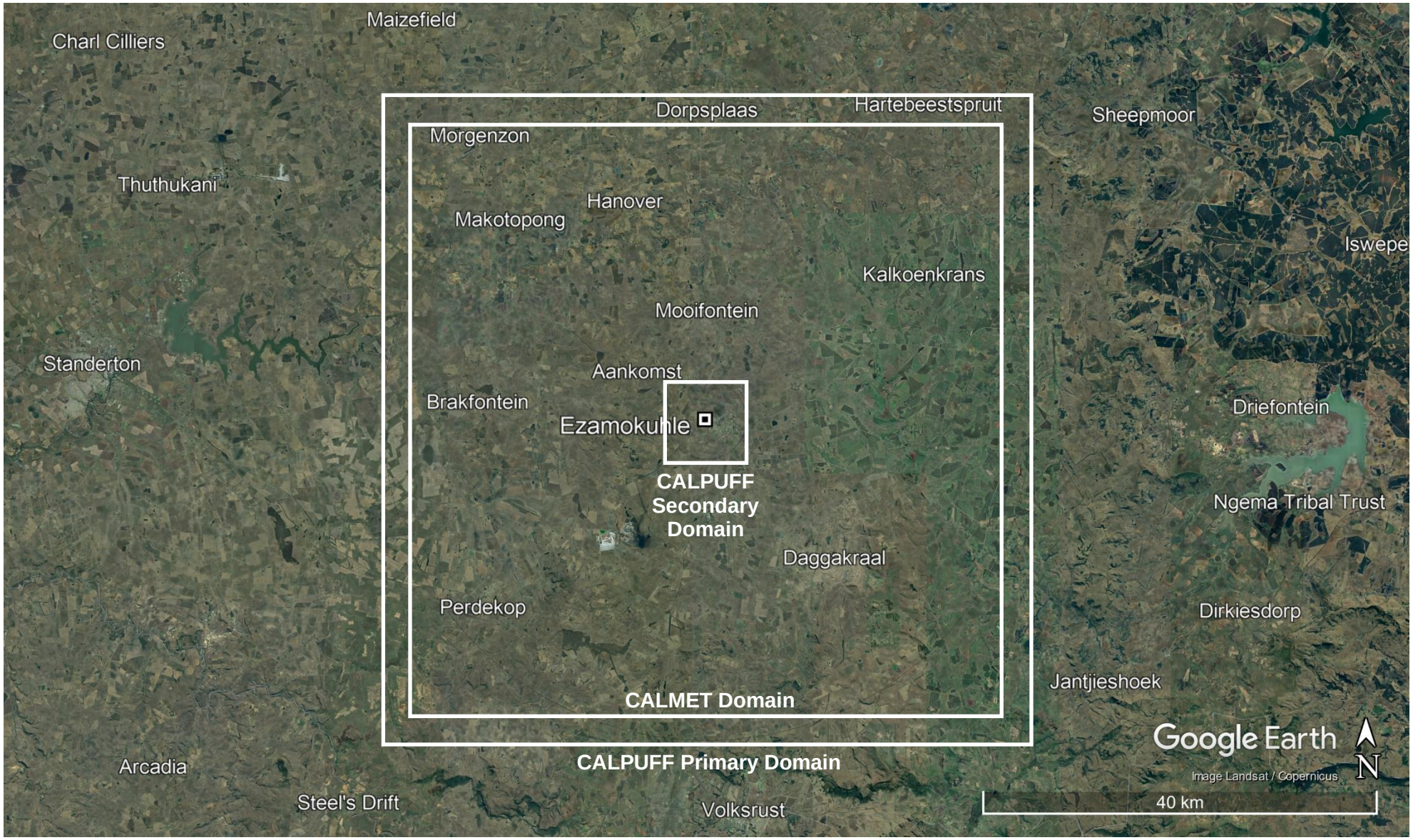

Figure 3-3: CALMET and CALPUFF Modelling Domains

3.5 MODEL SETTINGS

A summary of model control options for CALMET and CALPUFF is presented in Table 3-2 and Table 3-3, respectively.

Table 3-2: Parameterization of key variables for CALMET

Parameter	Model value
12 vertical cell face heights (m)	0, 20, 40, 80, 160, 320, 640, 1000, 1500, 2000, 2500, 3000, 4000
Coriolis parameter (per second)	0.0001
Empirical constants for mixing height equation	Neutral, mechanical: 1.41 Convective: 0.15 Stable: 2400 Overwater, mechanical: 0.12
Minimum potential temperature lapse rate (K/m)	0.001
Depth of layer above convective mixing height through which lapse rate is computed (m)	200
Wind field model	Diagnostic wind module
Surface wind extrapolation	Similarity theory
Restrictions on extrapolation of surface data	No extrapolation as modelled upper air data field is used
Radius of influence of terrain features (km)	5
Radius of influence of surface stations (km)	Not applicable as continuous surface data field is used

Table 3-3: Parameterization of key variables for CALPUFF

Parameter	Model value
Chemical transformation	Default NO_2 conversion factor is applied
Wind speed profile	Rural
Calm conditions	Wind speed < 0.5 m/s
Plume rise	Transitional plume rise, stack tip downwash, and partial plume penetration is modelled
Dispersion	CALPUFF used in PUFF mode
Dispersion option	Pasquill-Gifford coefficients are used for rural and McElroy-Pooler coefficients are used for urban
Terrain adjustment method	Partial plume path adjustment

3.6 POLLUTANTS SIMULATED

The CALPUFF suite of models was used to predict the dispersion of the following pollutants: SO_2, SO_4, NO_X, HNO_3, NO_3, PM_{10}, $PM_{2.5}$ and TPM (to calculate particulate/dust deposition rates) using the MESOPUFF II Scheme chemical transformation method. The MESOPUFF II Scheme is a pseudo-first-order chemical reaction mechanism for conversion of SO_2 to SO_4 and total NO_X to NO_3. Results of the modelling are presented for SO_2, NO_X as NO_2, PM_{10}, $PM_{2.5}$ and dustfall rates.

The dispersion of the pollutants were simulated for the prevailing meteorological conditions for the period 1 January 2020 to 31 December 2022.

3.7 TOTAL PARTICULATE CALCULATION

Ambient particulate matter is a complex mixture of inorganic and organic compounds. The NAAQS regulates particulate matter for different size fractions (PM_{10} and $PM_{2.5}$) which are based on epidemiological evidence for mortality and cardiorespiratory health effects.

Sulphate and nitrate constitute a significant portion of the particle mass in the atmosphere. According to Reis *et. al* (2007) few epidemiological studies have included the sulphate content of particulate matter as a specific variable in health effect analyses. There is considerably less data for nitrates.

Reis *et. al* (2007) however demonstrated that epidemiologic and toxicological evidence provide little or no support for a causal association of particulate sulphate and health risk at ambient concentrations. Further, for nitrate-containing particulate matter, there is no epidemiological data and the toxicological evidence does not support a causal association between particulate nitrate compounds and excess health risks. There is insufficient evidence to include or exclude secondary organic processes for sulphates and nitrates as being potentially important to particulate matter associated health risk. (Reis *et. al*, 2007).

This baseline modelling study has taken a conservative approach (Scire, 2014) whereby the total concentrations of particulate matter (PM_{10} or $PM_{2.5}$) was computed as the sum of primary particulate matter concentrations (PM_{10} or $PM_{2.5}$) plus the contribution of concentrations from secondary particulate matter, including ammonium nitrate (NH_4NO_3) and ammonium sulphate ($(NH_4)_2SO_4$) as shown in the equation below:

Total PM_{10} or $PM_{2.5}$ = sum of (PM_{10} or $PM_{2.5}$) + $(NH_4)_2SO_4$ + NH_4NO_3

In this study, the total concentration of particulate matter (either PM_{10} or $PM_{2.5}$) was then compared to the applicable PM_{10} or $PM_{2.5}$ NAAQS (Table 1-2).

3.8 EMISSION SCENARIOS

In this study, the following emission scenarios were modelled:

- Power Generation
- Residential Fuel Burning
- Waste Burning
- Biomass Burning
- Vehicles – Paved Roads
- Vehicles – Unpaved Roads
- All Sources

A comprehensive emissions inventory for each of these scenarios is presented in Section 4.

3.9 DISCRETE RECEPTORS

The location of discrete receptors that were selected for the Ezamokuhle modelling domain is presented in Figure 3-4.

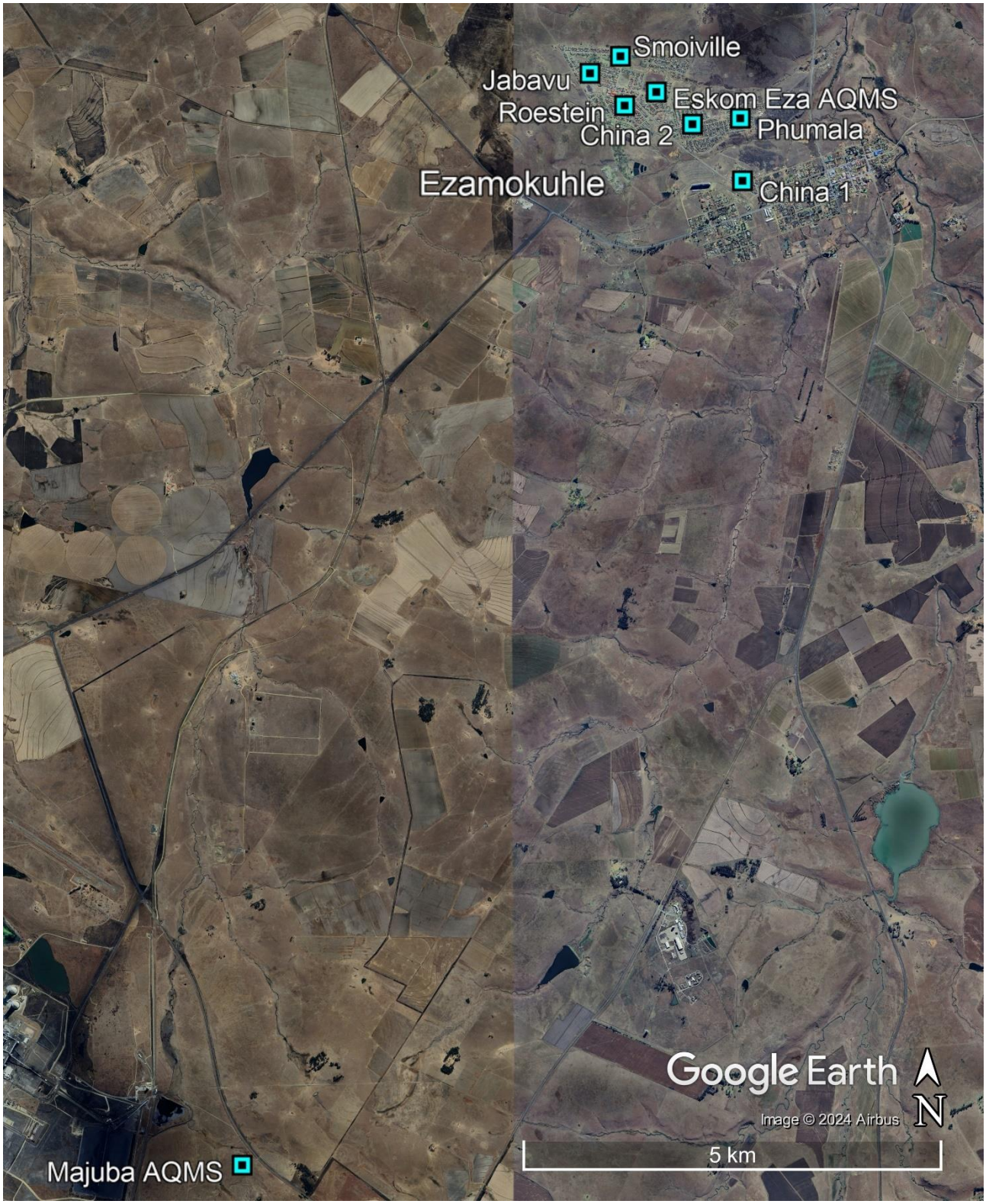

Figure 3-4: Location of discrete receptors for the modelling domain

4. EMISSION INVENTORY USED IN MODELLING

The identification of existing sources of emission in the modelling domain and the characterisation of existing ambient pollutant concentrations is fundamental to the assessment of the potential for cumulative impacts and synergistic effects given the existing operations and their associated emissions. In order to identify possible effects of reduction measures in an area it is necessary to prepare a representative emission inventory. In this study, an emission inventory was compiled for a number of source categories within the modelling domain, which includes:

- Power Generation
- Residential Fuel Burning
- Waste Burning
- Biomass Burning
- Vehicles – Paved Roads
- Vehicles – Unpaved Roads
- All Sources

4.1 POWER GENERATION

4.1.1 INTRODUCTION

Coal has traditionally dominated the energy supply sector in South Africa. Presently, about 80 percent of South Africa's primary energy needs are provided by coal. Through 2032, South Africa is projected to continue generating the majority of its electricity from traditional thermal power sources, primarily coal-fired generation. Approximately 95% of the electricity used in South Africa and 45% of the electricity used in Africa is produced by Eskom (ITA, 2024).

4.1.2 EMISSION INVENTORY

For the study, emissions from Eskom's Majuba Power Station was included. The emission inventory for the power station which accounts for stack, ash dump and coal yard emissions is compiled using data provided by Eskom (*pers com*, Mhlarhi, 2023). The emission inventory for the Eskom Majuba Power Station is presented in Table 4-1 and Table 4-2.

Table 4-1: Stack parameters and emission rates for Eskom Majuba Power Station Stacks

Source	Height (m)	Diameter (m)	Exit Temp (K)	Exit Velocity (m/s)	SO_2 (t/a)	NO_2 (t/a)	PM_{10} (t/a)	$PM_{2.5}$ (t/a)
Stack 1	250	12.3	398	35.4	91 463	54 839	424	212
Stack 2	250	12.3	398	35.4	91 463	54 839	424	212
TOTAL					182 926	109 677	849	424

Table 4-2: Emission rates for the Eskom Majuba Power Station Ash Dump and Coal Yard

Source	Emission Basis	PM_{10} (t/a)	$PM_{2.5}$ (t/a)
Ash Dump	Materials Handling (quantity-based)	0.10	0.01
	Wind Erosion (surface area-based)	13 678.99	5 471.60
Coal Yard	Materials Handling (quantity-based)	0.58	0.09
	Wind Erosion (surface area-based)	164.96	65.98
	TOTAL	13 844.62	5 537.68

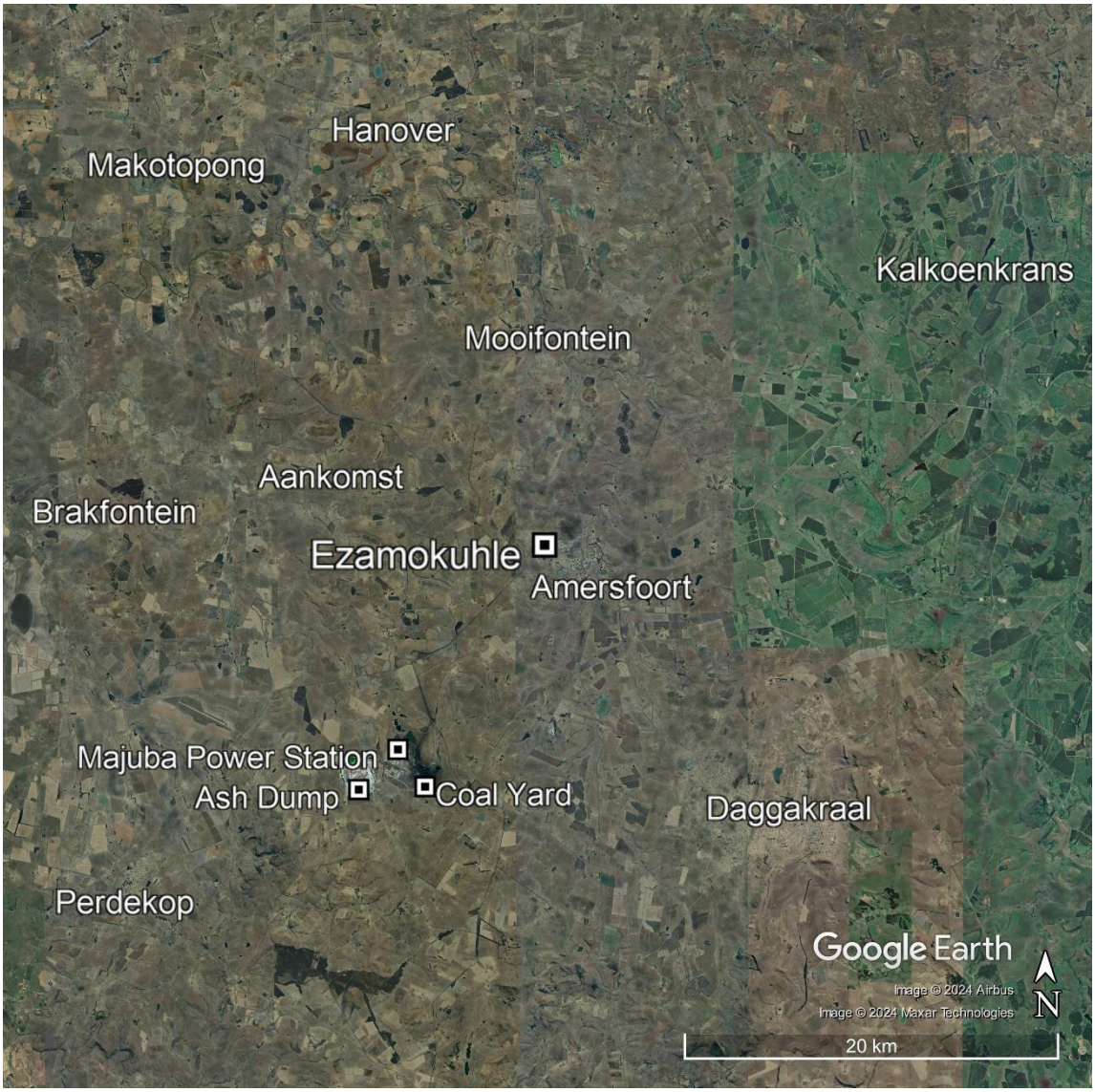

Figure 4-1: Location of the Eskom Majuba Power Station, Ash Dump and Coal Yard relative to Ezamokuhle

4.2 RESIDENTIAL FUEL BURNING

4.2.1 INTRODUCTION

The spatial variability and different pollutant contributions (both primarily driven by variability in fuel use by type) need to be captured in detail to estimate a gridded representation of emissions from residential fuel burning. Approaches to derive an emission inventory for residential fuel use generally rely on activity data from a national census.

The data from the South African Census i.e., Stats SA 2016 Community Survey is based on questions around the type of fuel used for cooking, heating, and lighting. This represents, at a spatial level of Census geographic units, the number of households using a specific type of fuel.

Top-down approaches, that use a regional fuel consumption estimate, disaggregate the regional sum down to these geographic units. Bottom-up approaches, that use a fuel consumption estimate per household, scale up fuel use by number of households within each geographic unit.

4.2.2 METHODOLOGY

The emission inventory development process for the Residential Fuel Burning emission inventory employed both a top-down and bottom-up approach. A top-down approach for gas, paraffin, and coal was used for the residential fuel use emissions in this study; and the spatial aspect was refined using a dwelling inventory. Naturally, the top-down approaches have inherent uncertainties since it relies on a national fuel consumption estimate, which is subject to uncertainty in assumptions on the aggregated national level. On the other hand, while wood burning is a well-known fuel used for residential purposes i.e., cooking, heating and lighting, the data from the South African Census i.e., Stats SA 2016 Community Survey does not have questions around wood as the type of fuel used in residential areas. As such, it is difficult to obtain the spatial variability for wood burning captured in detail to estimate a finer resolution representation of emissions from residential fuel burning.

BOTTOM-UP

A useful feature of the Stats SA 2016 Community Survey is that is provides information on the number of households in each Local Municipality using a specific fossil fuel for residential fuel burning activities. The provincial fossil fuel consumption is aggregated by the number of households using residential fuel burning to obtain a household fossil fuel consumption figure. This value is then used to estimate the fossil fuel consumption per household at the Local Municipality level which is then cascaded down to ward level (Figure 4-2). With respect to the modelling, the ward level emissions were applied only over areas which corresponded specifically to residential areas (Figure 4-3).

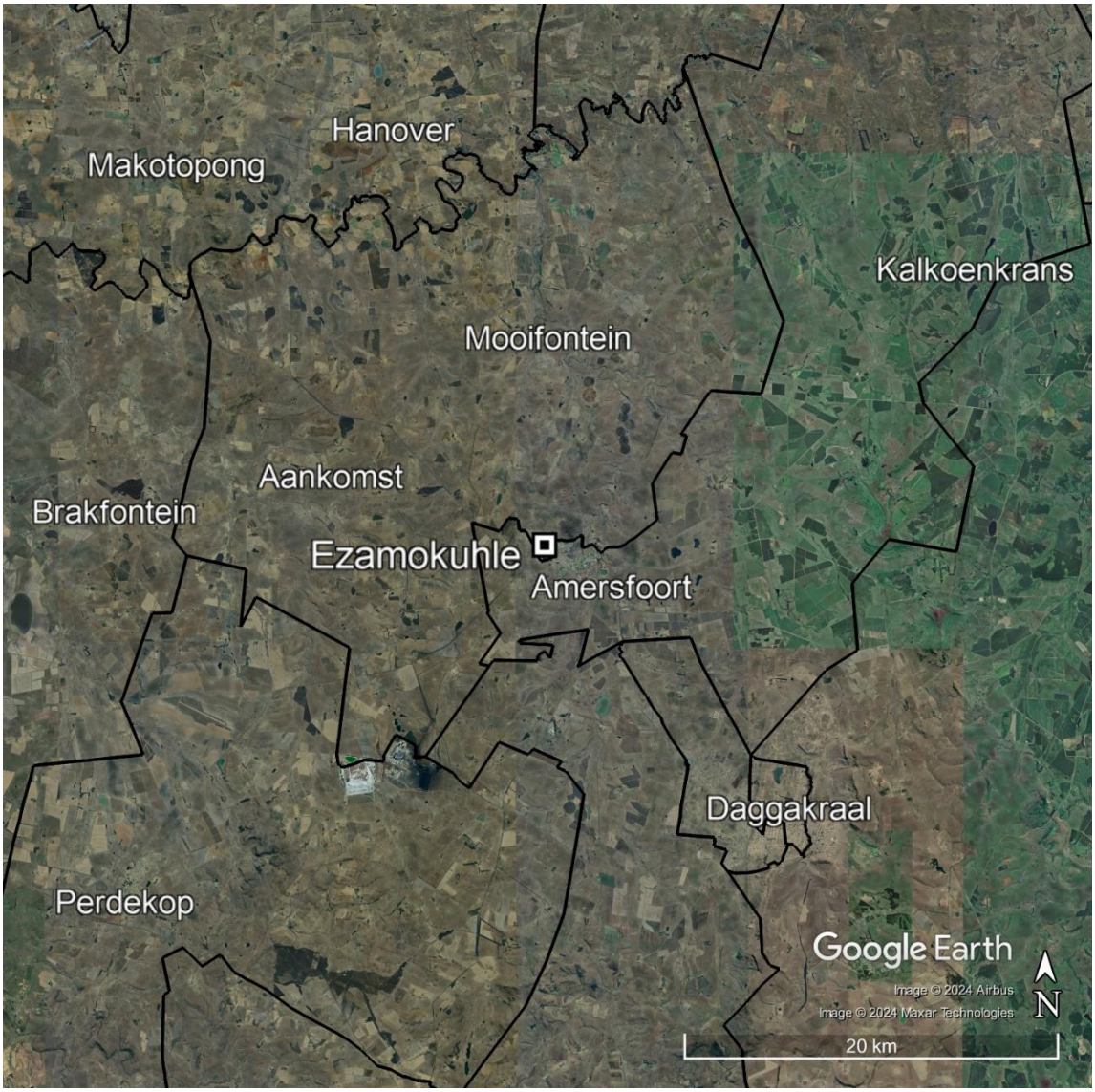

Figure 4-2: Wards within Ezamokuhle modelling domain for which Residential Fuel Burning emissions were estimated

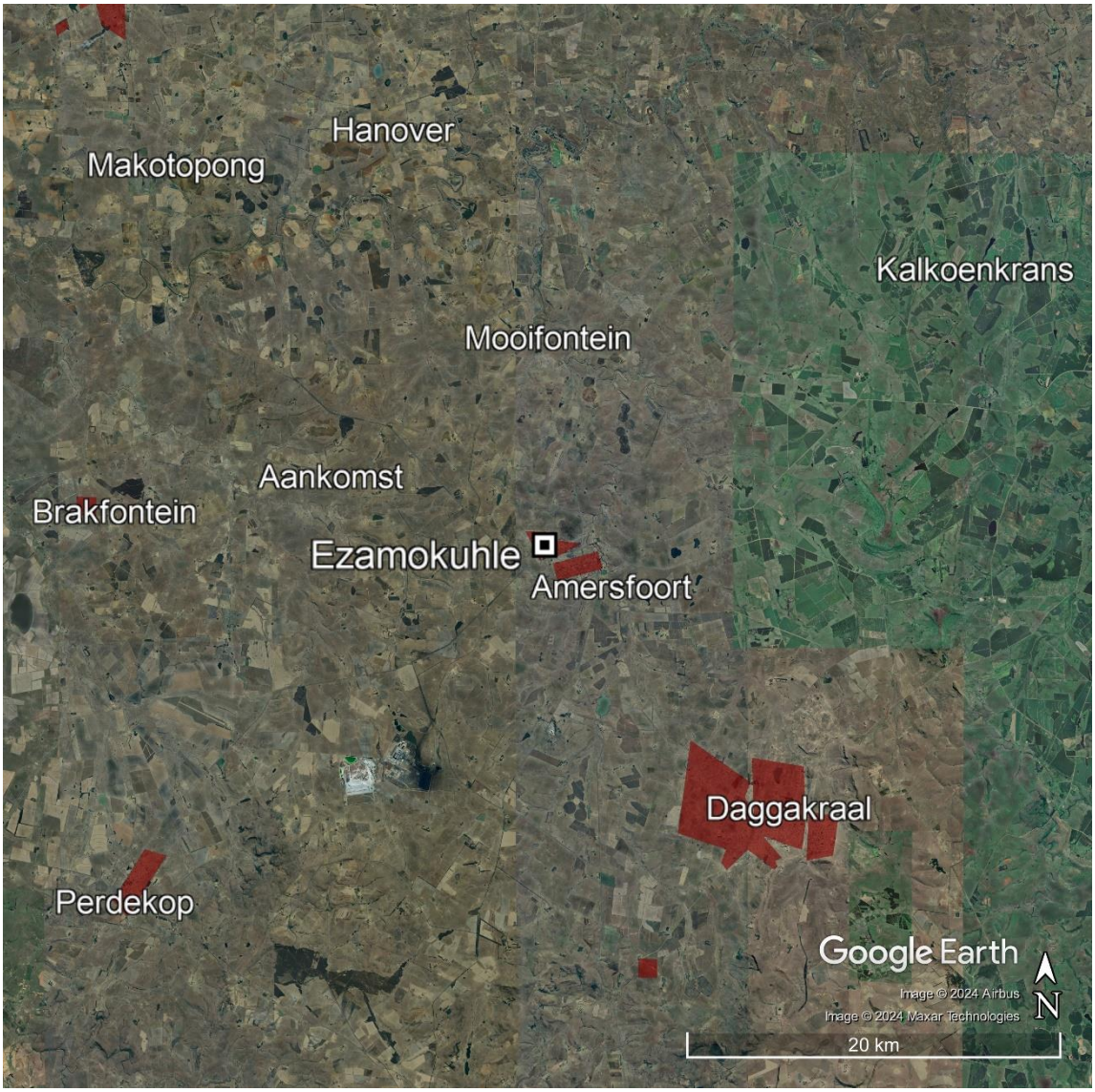

Figure 4-3: Location of residential areas within Ezamokuhle modelling domain for which Residential Fuel Burning emissions were applied

While this method is scientifically sound, it does present some challenges with an underestimation of fossil fuel use, which may not necessarily align with ground-truth surveys. In order to overcome this, literature values are used as a substitute where the national total for residential bituminous coal combustion is noted to significantly underestimate residential coal combustion at the household level e.g., 46.44 kg/ household level in Mpumalanga where domestic coal use is thought to be significantly greater. Consequently, literature values are used as a substitute with the value of 2.4 tonnes of coal assumed to be burned at the household level also informed by the Highveld Priority Area Health Study (HPAHS) (CSIR, 2017). Additionally, while residential wood combustion is a component of residential fuel burning, this data is not detailed in the DMRE National Commodity Flows Commerce and Public Services (2018). In order to overcome this, literature values are used as a substitute with the value of 3 tonnes of wood being assumed to be burned at the household level as informed by the HPAHS published by the CSIR and SAMRC (2019).

TOP-DOWN

The bottom-up approach detailed above has effectively provided the estimated fossil fuel combustion at the household level which must then be applied to the number of households at a more local level which, in this case, is at the ward level. The Stats SA 2016 Community Survey details the number of households at the Local Municipality level with associated intercensal growth rates which estimates population growth between two census campaigns as a percentage. This percentage is applied to Ward Level populations data obtained from Stats SA (2011) as to estimate ward populations in 2022 where household level fossil fuel literature values are applied to 2022 ward level population estimates. Fuel specific emission factors are then applied to the total volume of fuel burned for the various wards in question. The selected emissions factors are detailed below.

4.2.3 EMISSION FACTORS

A comparison of emission factors was done, considering those from the FRIDGE study (Scorgie et al., 2004), the USEPA AP-42 dataset, the GAINS United States and Australia model (Amann et al., 2011), Ballard-Tremeer (1997), Britton (1998), Scorgie (2012) and Makonese et al. (2015). Many of the South African studies focused on coal. A hybrid selection from these studies is considered in this household fuel combustion emissions methodology and are presented in Table 4-3.

Table 4-3: Emission factors used for residential fuel combustion

Pollutant	LPG		Paraffin		Coal		Wood	
	Emission Factor (g/kg)	Source	Emission Factor (g/kg)	Source	Emission Factor (g/kg)	Source	Emission Factor (g/kg)	Source
SO_2	0.01	FRIDGE	0.851	FRIDGE	11.6	Scorgie, 2012	0.123	Ballard-Tremeer, 1997
NO_X	1.4	FRIDGE	1.5	FRIDGE	3.95	Makonese et al., 2015	1.224	AP-42
PM_{10} (a)	0	NA	0	NA	0	Makonese et al., 2015	1.035	AP-42
$PM_{2.5}$	0.068	AP-42	0.359	AP-42	16.146	Makonese et al., 2015	13.745	AP-42

Note: (a) PM_{10} represents only the coarse fraction (i.e., PM with a diameter 2.5 µm to 10 µm).

4.2.4 Emission Inventory

As indicated in the sections above, it is important to understand the type of fossil fuel being burned, for which purpose, and in which area, to ensure the development of appropriate air pollution interventions. As a results, household fuel consumption estimates are presented per household to account for the fact that some areas will have a higher consumption due purely to a higher number of households. In addition, fuel type and application are also presented per household to allow for a comparison against non-electrical cooking and space heating in the Ezamokuhle modelling domain. This is to gain insight into the relationship between electrification and residential fuel burning practices as well as fossil fuel consumption at the ward level. Emission estimates were calculated by multiplying the total fuel use (obtained via top-down and bottom-up approach) by emission factors in Table 4-3.

The residential fuel burning emission quantification from a variety of fuels inherently introduces significant variability. As a result, understanding the total pollutant emission contribution from each fuel type is key to this type of assessment. Table 4-4 summarises the pollution contribution of each residential fuel burning fuel type to the total residential fuel burning emission estimated for the Ezamokuhle modelling domain.

Table 4-4: Pollution contribution summary for each residential fuel burning fuel type to the total residential fuel burning emission estimated for the Ezamokuhle modelling domain

Fuel Type	SO_2	NO_X	PM_{10}	$PM_{2.5}$
Coal	47.7	16.2	66.3	66.3
LPG	0.0	0.0	0.0	0.0
Paraffin	0.06	0.11	0.03	0.03
Wood	0.4	3.8	42.8	42.8
Total	48.1	20.1	109.2	109.2

Table 4-4 indicates that the highest emissions in terms of residential fuel burning are PM_{10} and $PM_{2.5}$, followed by SO_2 and NO_X. It is also clear that coal and wood fuels release the most emissions into the atmosphere compared to LPG and Paraffin which are noted to be cleaner fuels.

4.3 WASTE BURNING

4.3.1 INTRODUCTION

In South Africa, open burning of waste typically occurs in low-income settlements where municipal collection of waste is infrequent and waste generation is high due to the high population density in these areas. In the absence of municipal waste collection, residents are forced to find alternative means of disposal other than through formal landfills. Disposal can be done either through open burning or burial of waste. Open burning of waste has a negative impact on ambient air quality.

4.3.2 METHODOLOGY

In this study, the approach used to estimate domestic waste burning emissions is based on Wiedinmyer et al. (2014), which follow IPCC methods (IPCC, 2006). Based on Equation 1, the emission of pollutant i (Ei) are estimated as the product of the emission factor of the waste (EFi) and the amount of waste burned (WB). The generalized equation to estimate waste burned is shown in Equation 2.

$$E_i = W_B \times EF_i \quad \text{Equation 1}$$

Where:

- E_i: The emission of pollutant i
- W_B: The amount of waste burned
- EF_i: Emission factor of the waste

$$W_B = P \times P_{frac} \times MSW_P \times B_{frac} \quad \text{Equation 2}$$

Where:

- W_B: The amount of waste burned
- P: Population
- P_{frac}: The fraction of the population accounts whose waste is not collected i.e., assumed to burn their waste
- MSW_p: The mass of annual per capita waste production
- B_{frac}: The fraction that is available to be burned that is actually burned

In this study, waste burning emissions are based on local data relating to waste accumulated per person and per composition i.e., waste generated per person per capita. According to the 2018 Sasol Waste Collection Interventions (WCI) Study (Mamadi and Co., 2018), waste generated per capita was estimated at 0.612 tonne/person/annum. This rate (waste generated per capita) is assumed to be representative of the Ezamokuhle study area.

Equation 2 takes into account that some of the waste is not combustible. For example, glass and metals will not readily burn, thus a burn fraction is required. The IPCC recommended fraction of 0.6 is used i.e., 60% of the waste generated by people that do not have waste removal services is burned. According to Equation 2, population is another variable required to estimate the amount of waste burned. The Stats SA 2016 Community Survey data was therefore used; and an intercensal growth rate was applied to estimate the population in the Ezamokuhle modelling domain for 2022. The Stats SA 2016 Community Survey data was also used to determine the number of people not receiving waste services. By multiplying the waste generated per capita with the number of people not receiving waste services, an estimate of the amount of waste generated (that may likely be burned) is calculated.

In this study, emissions from waste burning is calculated at ward level (Figure 4-4). With respect to the modelling, the ward level emissions were applied only over areas which corresponded specifically to residential areas (Figure 4-5).

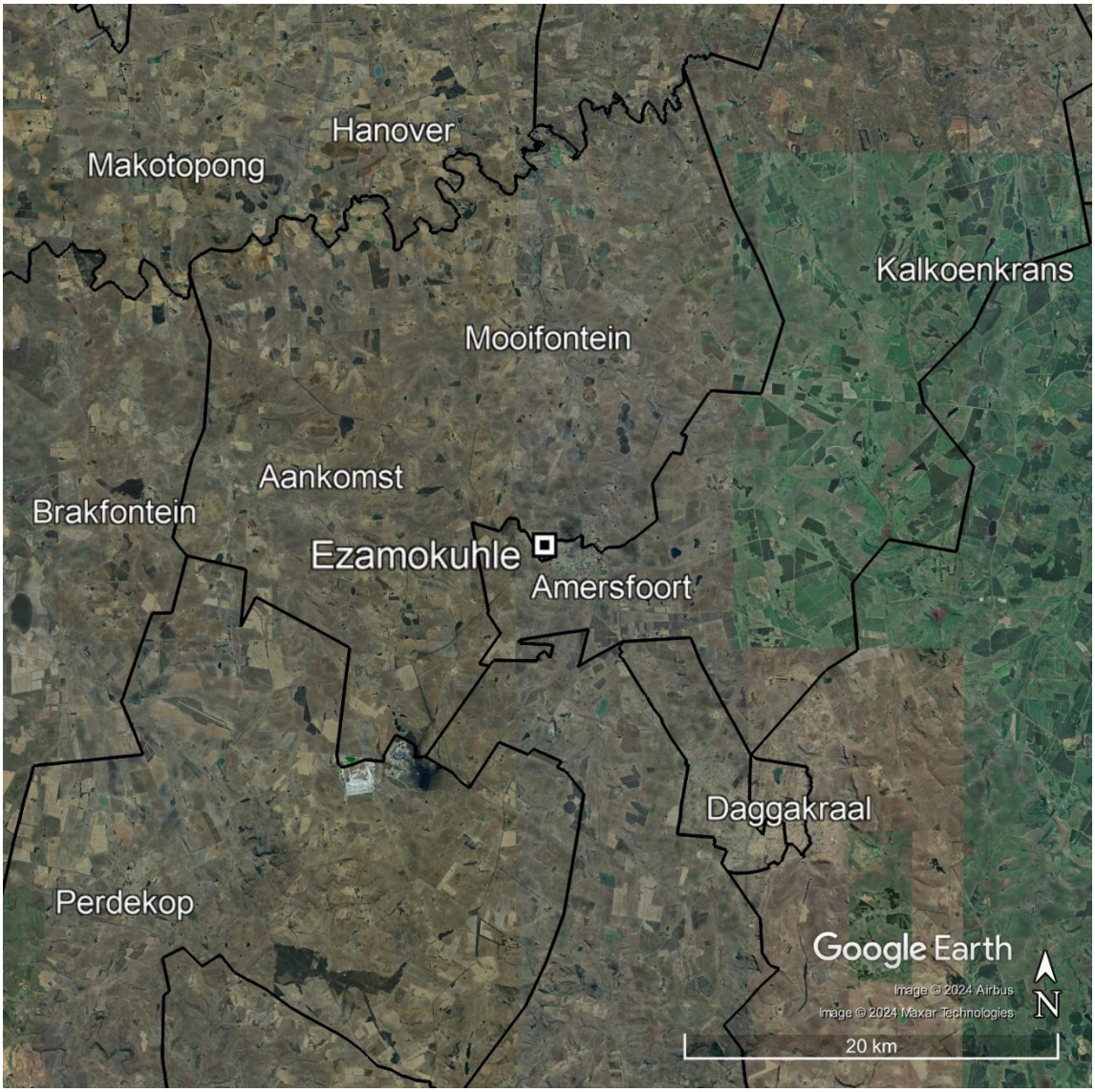

Figure 4-4: Wards within Ezamokuhle modelling domain for which Waste Burning emissions were estimated

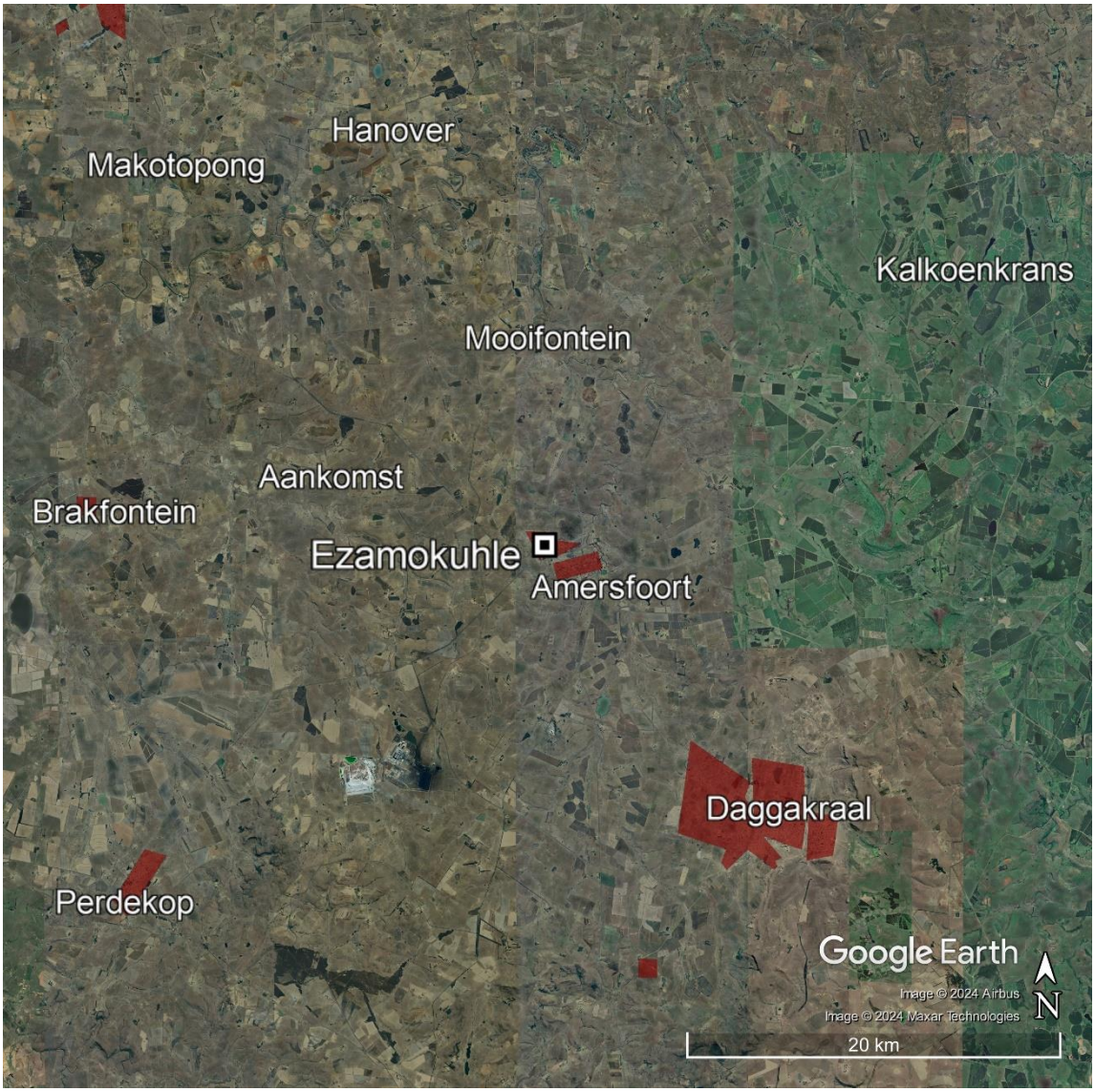

Figure 4-5: Location of residential areas within the Ezamokuhle modelling domain for which Waste Burning emissions were applied

4.3.3 EMISSION FACTORS

The most recent compilation of waste emission factors for a South African context are presented in the Sasol South Africa Emission Factors for Criteria Pollutants from Solid Waste Material Combustion Report (Mamadi & Co., 2018). In this report, several categories of materials are identified that are commonly found in waste burned in South African townships. A weight distribution for the composition of waste materials collected by the Sasol WCI program is presented in Figure 4-6. The major waste components identified in this program were paper, leather/rubber, textile, plastic bottles and bags, ceramic, metal, and glass. Emission factors used for estimating SO_2, NO_X, PM_{10} and $PM_{2.5}$ due to waste burning emissions is presented in Table 4-5.

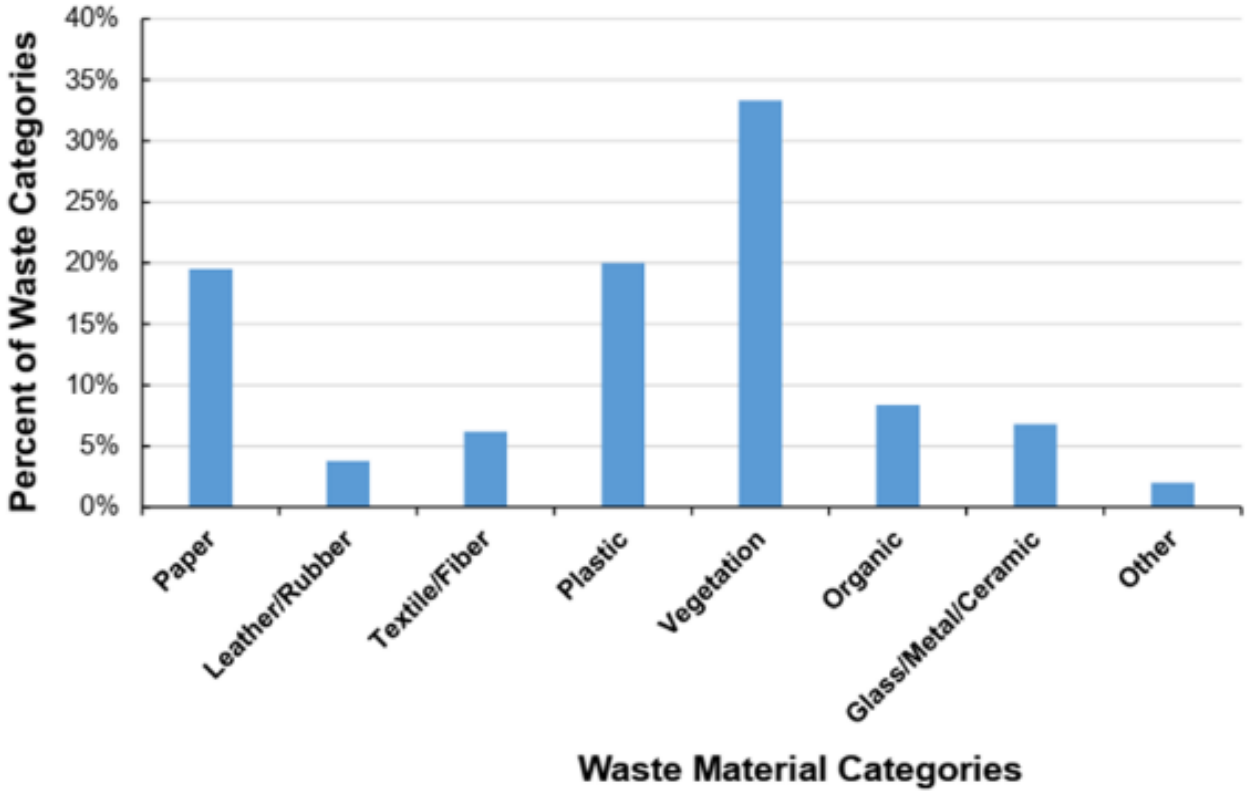

Figure 4-6: Weight fraction of municipal solid waste categories collected by Sasol (data provided by Mr Warren Carter, Sasol Technology)

Table 4-5: South African specific waste burning emission factors

Emission Factors (g/kg fuel)			
SO_2	**NO_X**	**PM_{10}**	**$PM_{2.5}$**
0.95	2.41	7.26	6.86

4.3.4 Emission Inventory

Emissions of SO_2, NO_X, PM_{10} and $PM_{2.5}$ for the Ezamokuhle study area due to waste burning is presented in Table 4-6. Compared to SO_2 and NO_X, it is evident that PM_{10} and $PM_{2.5}$ have the highest emission loading in the area.

Table 4-6: Emission inventory for waste burning emissions estimated for the Ezamokuhle modelling domain

Pollutant	SO_2	NO_X	PM_{10}	$PM_{2.5}$
Emission Rate (tonnes/annum)	1.1	2.7	8.2	7.8

4.4 Biomass Burning

4.4.1 Introduction

Biomass burning refers to the large scale burning of vegetation, which includes savanna, forests and grasslands, domestic fuels and agricultural wastes (Andreae, 1991; Crutzen and Andreae, 1990). Open fires, such as wildfires, prescribed burns, agricultural fires, and land-clearing fires, are sources of atmospheric pollutants. Fire activity contributes to local, regional, and global emissions of greenhouse gases including carbon dioxide (CO_2) and methane (CH_4), reactive gases such as non-methane organic gases (NMOGs) and nitrogen oxides (NO_X) that form ozone, dioxins and other air toxics, and particulate matter (PM).

Fire emissions and their transport change the atmospheric composition, which cause impacts at many scales, with implications for air quality, regional and global climate, visibility and human health outcomes. Many factors contribute to the spatial and temporal patterns and severity of fires and their emissions, including agricultural, forest, and waste management practices, land use change, climatic factors such as temperature, rainfall, and drought conditions, and ecosystem diversity and health.

Accurate estimates of fire emissions are required to understand chemistry and climate, to assess ambient pollutant concentrations and population exposure, and to evaluate the effectiveness of emissions control programs for air quality planning and management.

In southern Africa, biomass burning occurs predominantly during the dry season corresponding to the period from May to October (Cahoon et al., 1996; Scholes et al., 1996a, 1996b; Scholes and Andreae, 2000; Swap et al., 1996). The majority of fires on the Highveld are thought to be anthropogenic in nature and include veld fires, burning of grazing land and crop-residue (DEFF, 2010). The biomes of South Africa (Figure 4-7) which are categorised as high to extreme risk include the following: fynbos, savanna and grassland. Mpumalanga is predominantly a grassland biome, thus an area at high to extreme risk of veld fires.

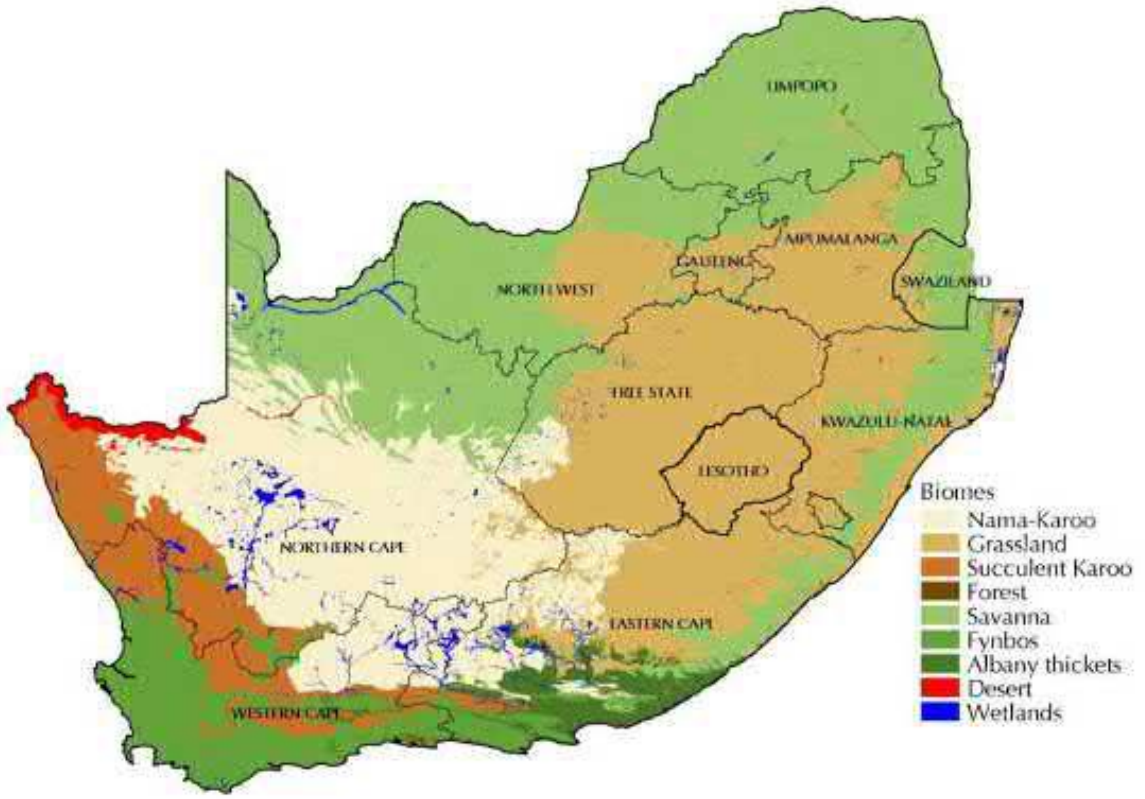

Figure 4-7: South African Biomes (SANBI, 2004)

4.4.2 METHODOLOGY

THE FIRE INVENTORY FROM NCAR VERSION 2.5: AN UPDATED GLOBAL FIRE EMISSIONS MODEL FOR CLIMATE AND CHEMISTRY APPLICATIONS

The FINN (Fire INventory from the National Center for Atmospheric Research (NCAR)) inventory (Wiedinmyer et al., 2011) was developed more than a decade ago to provide daily global estimates of pollutant emissions from open fires with a high spatial and temporal resolution for use in air quality, atmospheric composition, and climate modelling applications. The National Center for Atmospheric Research (NCAR) has served as the central repository for FINN global emissions files spanning from 2002–2020. FINN emission estimates have been applied in regions of the world that experience high fire activity to evaluate the influences on air quality and public health to assess emissions trends, to examine the effects of changing climate and development patterns on wildfire emissions and in comparisons with surface, aircraft, and satellite-based observations. Real-time emissions estimates from FINN version 1 (FINNv1) are currently used in the NCAR Whole Atmosphere Community Climate Model (WACCM) chemistry and aerosol forecasts.

The Fire INventory from NCAR version 2.5 (FINNv2.5) is an updated global fire emissions model that provides publicly available emissions of trace gases and aerosols for various applications,

including use in global and regional atmospheric chemistry modelling. FINNv2.5 is an updated version of the FINN version 1 framework, with many updates to better represent burned area, vegetation burned, and chemicals emitted.

Some of the major updates include:

- The use of active fire detections from the Visible Infrared Imaging Radiometer Suite (VIIRS) at 375 m spatial resolution, which allows smaller fires to be included in the emissions processing.
- The calculation of burned area has been updated to improve aggregate fire detections, which better accounts for larger fires and enables using multiple satellite products simultaneously for emissions estimates.
- Fuel characterization and emissions factors have also been updated in FINNv2.5.

The FINNv1 model is based on a bottom-up approach to estimate the emissions described by Wiedinmyer et al. (2011). In FINNv1, global observations from the Moderate Resolution Imaging Spectroradiometer (MODIS) sensors on board the National Aeronautics and Space Administration's (NASA) Terra and Aqua satellites are used to detect fire activity, beginning with the MODIS Rapid Response (MRR) system or the MODIS Adaptive Processing System (MODAPS) Collection 5 (Davies et al., 2009).

Fuel characterization in FINNv1 is based on the Collection 5 MODIS Land Cover Type (LCT) product for 2005 (Friedl et al., 2010), with land cover classifications defined by the International Geosphere–Biosphere Programme (IGBP) and the Collection 3 MODIS Vegetation Continuous Fields (VCF) product for 2001 (Carroll et al., 2011). Fuel loadings are assigned from Hoelzemann (2004) or Akagi et al. (2011). Estimates of fuel burned use the approach of Ito and Penner (2004). Emissions factors by land cover classification for trace gases and particulate air pollutants in FINNv1 are based on the published literature (Akagi et al., 2011; Andreae and Merlet, 2001; Andreae and Rosenfeld, 2008; McMeeking, 2008).

FINN version 2.5 (FINNv2.5) has extensive updates to the input data and processing used for the detection of fire activity, characterization of annual land use and/or land cover and vegetation density, determination of area burned, and the application of fuel loadings by global region compared to the FINNv1 configuration. FINNv2.5 also includes revisions to emissions factors based on the current literature.

METHODS USED FOR THE DEVELOPMENT OF FINNV2.5

FINNv2.5 was released in 2022. A global emissions database for the period 2002 to 2021 has been created for public use, for incorporation in emission inventories, chemical modelling and climate modelling applications. FINNv2.5 uses the same FINNv1 bottom-up methodology (Wiedinmyer et al., 2011) as defined by the following overall equation:

$$E_i = A(x,t) \times B(x) \times FB \times EF_i$$

where the emissions (*E*; mass of pollutant *i*) is the product of the area burned at location *x* and time *t* [*A*(*x*,*t*)], the biomass at location *x* [*B*(*x*)], the fraction of biomass that is burned (FB), and an emissions factor (EF_i; mass of pollutant *i* per biomass burned).

The FINNv2.5 model framework has the following three components:

- Burned area and land cover determination
- Fuel consumption and emissions calculation
- Speciation of the non-methane organic gases.

FIRE LOCATION AND TIMING

FINNv2.5 first determines the burned area from daily satellite detections of active fires. FINNv2.5 uses MODIS detections at a 1 km^2 resolution (as in FINNv1), and adds an option to use active fire detections at 375 m resolution from the Visible Infrared Imaging Radiometer Suite (VIIRS), which is on board the Suomi National Polar-orbiting Partnership (Suomi-NPP) satellite, in isolation or together with MODIS active fire data. The use of VIIRS 375 m detections is regarded as a major advancement from the use of MODIS-only fire detections, as this product is able to capture small fires better.

The MODIS Collection 6 (MCD14DL) and VIIRS active fire products are obtained from NASA's Fire Information for Resource Management System (FIRMS) data portal. The MODIS product provides the location, overpass time (Coordinated Universal Time, UTC), and confidence of daily fire detections. Data confidence in the MODIS product is specified by a numerical scale of 0 % to 100 %. Detections with a confidence specification that is less than 20 % are eliminated from calculations in FINNv2.5, as implemented in earlier versions of FINN.

With its improved spatial resolution of 375 m, the VIIRS product provides a more sensitive detection of the fires of relatively small areas, fully global coverage, improved mapping of large fire perimeters, and improved nighttime performance relative to MODIS fire detections (Schroeder et al., 2014). Detection confidence is provided by the VIIRS product and is specified by three categories, i.e. low, nominal, and high. In the FINNv2.5 preprocessor, detections with a confidence specification

identified as low are eliminated from the analysis. Only data attributed to thermal anomalies from vegetation fires are included in the analysis. Thermal anomalies associated with active volcanos or static land sources are eliminated from the analysis.

The processing of the two simultaneous fire products in FINNv2.5 does not lead to double-counting of the fires; the FINNv2.5 method determines the spatial union of all adjacent detections for a given day as the daily burned area of a fire. The identity of the sensor is not relevant for the determination of the burned area, as long as the pixel size for each detection is correctly represented (i.e., 0.14 km^2 for VIIRS and 1 km^2 for MODIS).

BURNED AREA

FINNv1 estimates burned area for each fire pixel identified individually, and the nominal pixel size for the MODIS fire detections of 1 km^2 is assumed per detection. Spatially overlapping detections are eliminated from further analysis. It was recognized that for large fires in forested regions, an array of multiple discrete detections is typically reported, and an estimate of a contiguous area that represents the total area burned by a fire is needed.

In FINNv2, a new approach is adopted where the burned area estimate is improved to better represent the area associated with each fire. In the new approach used in FINNv2.5, each reported active fire detection is assigned a square area of 0.14 km^2 from VIIRS or 1 km^2 from MODIS, based on the nominal horizontal resolution of the data. Detections determined to be in proximity with one another are aggregated by two different approaches, depending on the land cover type and forest cover. Initially, it is assumed that multiple detections by adjacent pixels in a satellite sensor array are part of a larger fire, and these detections are merged. The scan and track sizes of the satellite pixel are provided by the fire detection product and define the actual resolution of the fire detection. The scan and track sizes for each fire detection are used for identifying groups of records that represent adjoining or overlapping detections. A rectangle with easterly and northerly sizes equal to 110 % of the scan and track sizes is established for each detection, with the objective of identifying adjacent neighbouring detections but not for direct application to the burned area estimation. Fire detections are identified as being from one larger fire when any of the satellite detection rectangles overlap. To minimize an overestimation of the burned area, a convex hull is generated between corresponding pairs of detection rectangles that directly intersect. The union of pairwise convex hulls from a cluster forms an extended fire polygon that represents the tentative estimated burned area for a single fire event or group of nearby fires for the day. This approach effectively fills any gap between instrument resolution squares (Wiedinmyer and Emmons, 2023).

For each of the extended polygons, the MOD44B v006 MODIS/Terra VCF annual product is overlaid, and the average tree cover fraction is determined. For forested areas with tree cover ≥50 %,

as determined by the VCF product, the merged polygons are accepted as the final burned area estimate. Otherwise, the merging is not used, and instead, an alternative, more conservative, approach is applied to determine the burned area for the region. This alternative approach is used to prevent overestimation of emissions in regions with many small fires, as in the savanna fires in sub-Saharan Africa. The alternative polygon aggregation is achieved by aggregating nearby detections only when the instrument pixels themselves are intersecting and therefore not with the extended detection footprints. The result is an aggregation algorithm that is repeated with a smaller set of detections to determine the alternative conservative set of polygons (denoted as the conservative fire polygon). The final burned area polygons is ultimately a composite of polygons based on these two different aggregation approaches (Wiedinmyer and Emmons, 2023).

Subsequently, the final burned area polygons are subdivided using a Voronoi tessellation algorithm in order to develop emissions estimates by land cover classification. Each of the undivided final burned area polygons are assigned a unique fire ID to enable users to group emission estimates from a presumed single fire event (Wiedinmyer and Emmons, 2023).

FUEL LOADING AND VEGETATION INPUTS

The NASA MODIS VCF product provides estimates of the percentage of bare surface, herbaceous, and forested cover at a horizontal resolution of 250 m. For each fire area, the subdivided polygons are overlaid on the vegetation cover data from the MOD44B v006 MODIS/Terra VCF annual product. The VCF data for the prior year are chosen, so that the VCF before any land cover changes due to fire are used in the emissions estimation process. The VCF raster is clipped to the geometry of the fire polygon, and the averages of the VCF tree, herbaceous, and bare cover are calculated for each fire polygon (Wiedinmyer and Emmons, 2023).

FINNv2.5 uses the Terra and Aqua combined MODIS LCT MCD12Q1 Version 6 data product with the International Geosphere–Biosphere Programme (IGBP) classification scheme as its default land cover information. Use of the LCT and VCF products in FINNv2.5 is an improvement on FINNv1. FINNv1 used one static map of LCT and VCF (from 2002) for any year processed. FINNv2.5 employs year-specific MODIS LCT and VCF maps that change annually. Furthermore, the specific vegetation assignments for each subdivided polygon enable different vegetation types and coverage to be represented across larger fires. These input data and processes enable better representation of the vegetation that is burned. All fire polygons are assigned to 1 of 13 global regions (Wiedinmyer et al., 2011) used to assign fuel loadings. This completes the first component of the FINNv2.5 modelling framework and results in a file of daily burned areas and associated land cover information (Wiedinmyer and Emmons, 2023).

EMISSION CALCULATION

The next step of the model framework is the emissions calculation. In this step, the daily burned area and associated vegetation information (described above) are assigned associated fuel loadings. Using the same process described by Wiedinmyer et al. (2011), where the biomass burned is assigned based on land cover type and global region (B), the fraction of the biomass that is burned (FB) is assigned as a function of tree and herbaceous cover, emissions factors (EFs) are determined based on land cover, and daily pollutant emissions estimates are calculated following Eq. (1). Overall, the emissions calculation process follows this framework, as described by Wiedinmyer et al. (2011).

Similar to earlier FINN versions (Wiedinmyer et al., 2011), the 16 IGBP land cover classifications of the LCT product are mapped to consolidated vegetation types, depending on the land cover class and latitude that distinguish tropical, temperate, and boreal forests (Table 4-7). The consolidated vegetation types used in FINNv2.5 are grassland and savanna, woody savanna or shrubs, tropical forest, temperate forest, boreal forest, temperate evergreen forest, and crops.

The fuel loading, or the potential maximum amount of biomass available to be burned ($B(x)$ in Eq. 1), is assigned by generic vegetation type and global region (Table 4-8). Selected values were updated for FINNv2.5 from earlier versions of FINN, based on van Leeuwen et al. (2014). The fuel loading for crops was updated to 902 g m^{-2}, based on an average from the literature (Akagi et al., 2011; van Leeuwen et al., 2014; Pouliot et al., 2017). Emissions factors are then assigned based on the generic vegetation type (Table 4-9).

Table 4-7: LCT IGBP and generic vegetation type descriptions

IGBP LCT description	LCT value	Generic vegetation type	Generic vegetation value
Evergreen needleleaf forests	1	If latitude >50, then boreal forest; otherwise, temperate evergreen forest	5,6
Evergreen broadleaf forests	2	If latitude >-23.5 and	3, 4
Deciduous needleleaf forests	3	If latitude >50, then boreal forest; otherwise, temperate forest	5,4
Deciduous broadleaf forests	4	Temperate forest	4
Mixed forests	5	If latitude >5, then boreal forest; if latitude >-23.5 and	5, 3, 4
Closed shrublands	6	Woody savanna or shrubs	2
Open shrublands	7	Woody savanna or shrubs	2
Woody savannas	8	Woody savanna or shrubs	2
Savannas	9	Grassland and savanna	1
Grasslands	10	Grassland and savanna	1
Permanent wetlands	11	Grassland and savanna	1
Croplands	12	Croplands	9
Urban and built-up lands	13	If tree cover 40 and 60, then assign based on latitude	**
Cropland/natural vegetation mosaics	14	Grassland and savanna	1
Permanent snow and ice	15	Remove	
Barren	16	Grassland and savanna	1
Waterbodies	17	Remove	
Unclassified	255	Remove	

** if latitude > 50, then Boreal Forest; if latitude > -30 and < 30, then Tropical Forest; Else, Temperate Forest

Table 4-8: Fuel loadings (g/m2) assigned by generic land cover type and global region as described by Wiedinmyer et al. (2011), unless noted otherwise (values in bold indicate those updated for FINNv2.5, based on van Leeuwen et al. (2014))

Global region	Tropical forest	Temperate forest	Boreal forest	Woody savanna/ shrublands	Savanna and grasslands[e]
North America	28 076[a]	**10 661[c]**	**17 875[c]**	4762	976
Central America	**26 500[c]**	11 000		2224	418
South America	**26 755[c]**	7400		3077	**624[c]**
Northern Africa	25 366	3497		2501	**382[c]**
Southern Africa	25 295	6100		2483	**411[c]**
Western Europe	28 076[a]	7120	6228	4523	1321
Eastern Europe	28 076[a]	11 386	8146	7752	1612
North central Asia	6181[b]	20 807	**14 925[c]**	11 009	2170
Near East	6181[b]	10 316		2946	655
East Asia	**14 941[c]**	7865		4292	722
Southern Asia	**26 546[c]**	14 629		5028	1445
Oceania	16 376	**13 535[c]**		**2483[d]**	**552[c]**

[a] Tropical forest class added for North America and Europe (in LCT). [b] All of Asia is assigned equal tropical forest values. [c] Taken from van Leeuwen et al. (2014). [d] Taken as the same for African woody savanna from van Leeuwen et al. (2014). [e] Croplands are assigned the same fuel loading as grasslands.

Table 4-9: Emissions factors (g/kg) for FINNv2.5

Chemical species	Generic vegetation index and type						
	1	2	3	4	5	6	9
	Savanna grasslands[a]	Woody savanna/ shrubs	Tropical forest	Temperate forest[b]	Boreal[c]	Temperate evergreen forest[b]	Crops[d]
Carbon dioxide (CO_2)	1686	1681	1643	1510	1565	1623	1444
Carbon monoxide (CO)	63	67	93	122	111	112	91
Methane (CH_4)	2	3	5.1	5.61	6	3.4	5.82
Non-methane organic gases (NMOGs)[e]	28.2	24.8	51.9	56	48.5	49.3	51.4
Hydrogen (H_2)	1.7	0.97	3.4	2.03	2.3	2	2.59
Nitrogen oxides (NO_X as NO)	3.9	3.65	2.6	1.04	0.95	1.96	2.43
Sulfur dioxide (SO_2)	0.9	0.68	0.4	1.1	1	1.1	0.4
Particulate matter with diameters less than 2.5 µm ($PM_{2.5}$)	7.17	7.1	9.9	15	18.4	17.9	6.43
Total particulate matter (TPM)	8.3	15.4	18.5	18	18.4	18	13
Total particulate carbon (TPC)	3	7.1	5.2	9.7	8.3	9.7	4
Particulate organic carbon (OC)	2.6	3.7	4.7	7.6	7.8	7.6	2.66
Particulate black carbon (BC)	0.37	1.31	0.52	0.56	0.2	0.56	0.51
Ammonia (NH_3)	0.56	1.2	1.3	2.47	1.8	1.17	2.12
Nitrogen oxide (NO)	2.16	0.77	0.9	0.95	0.83	0.95	1.18
Nitrogen dioxide (NO_2)	3.22	2.58	3.6	2.34	0.63	2.34	2.99
Non-methane hydrocarbons (NMHCs)	3.4	3.4	1.7	5.7	5.7	5.7	7
Particulate matter with diameters less than 10 µm (PM_{10})	7.2	11.4	18.5	16.97	18.4	18.4	7.02

[a] Emissions factors for tropical forests, savannah/grasslands, and woody savannah/shrubs are updated to the average values from Akagi et al. (2011; updated in February 2015). [b] Emissions factors for temperate forest and temperate evergreen forests are the average values from Akagi et al. (2011; updated February 2015), and the results are from Liu et al. (2017), Paton-Walsh et al. (2014), and Urbanski (2014). For temperate evergreen forest, only the results from evergreen forests are included. [c] Boreal forest emissions factors are the average of Akagi et al. (2011), with the emissions factors from boreal forest taken from Urbanski (2014). [d] Crop emissions factors are updated with the average values from Akagi et al. (2011) and results from Fang et al. (2017), Liu et al. (2016), Santiago-De La Rosa et al. (2018), and Stockwell et al. (2015; Table S3). [e] NMOG emissions factors now include identified and unidentified compounds.

4.4.3 EMISSION INVENTORY

The FINNv2.5 model was run in two ways to produce emissions for evaluation and assessment, namely (1) for comparison with the previous version of FINN (FINNv1.5) using MODIS-only fire detections and calculated starting in 2002 (FINNv2.5(MODIS)) and (2) by using both MODIS and VIIRS fire detections and calculated starting in 2012 (FINNv2.5(MODIS + VIIRS) (Wiedinmyer and Emmons, 2023).

For all emitted species, FINNv2.5(MODIS + VIIRS) global emissions are higher than, and approximately double, those predicted by FINNv1.5. This is the case, even when only MODIS fire detections are considered. The increase in emissions from previous versions is primarily due to the new processing of the area burned. In previous versions, the fire area was determined from a satellite detection pixel only; the updated version here also includes the composite of many detections into larger areas of fire activity. The inclusion of VIIRS into the FINNv2.5(MODIS + VIIRS) inventory globally adds approximately 25 % above the FINNv2.5(MODIS) processing for all emitted species. Further, emissions of NMOGs and the individual species that make up NMOGs (e.g., CH_2O and C_2H_6) are increased significantly due to the use of updated emissions factors from recent field campaigns. Previous studies have shown low biases in FINN regional and species-specific estimates. The updated version is expected to correct some of these prior biases (Wiedinmyer and Emmons, 2023).

FINNv2.5(MODIS + VIIRS) emissions estimates are overall at the higher end of the range of annual global total emissions compared to other commonly used emission inventories, likely due to a combination of the aggregated burned areas and the fact that FINNv2.5(MODIS + VIIRS) includes fire information from VIIRS, which captures more small fires. Globally, fire emissions peak in August–September, with the largest emissions in Southern Hemisphere Africa and Southern Hemisphere South America (Wiedinmyer and Emmons, 2023).

The biomass emissions used in the study has been extracted using the extents of the modelling domain. The FINNv2.5 biomass burning emissions are calculated over a period spanning from 2002–2021. Biomass burning emissions are not available for 2022. An average of the 2020 and 2021 period have therefore been averaged to provide an annual average emission rate for biomass burning emissions. The annual average biomass burning emissions for the modelling domain is presented in Table 4-10. The location of biomass burning fires for the 2020 and 2021 period is presented in Figure 4-8.

Table 4-10: Estimated biomass burning emissions

Pollutant	SO_2	NO_X	PM_{10}	$PM_{2.5}$
Emission Rate (tonnes/annum)	59.5	11.9	487.1	483.4

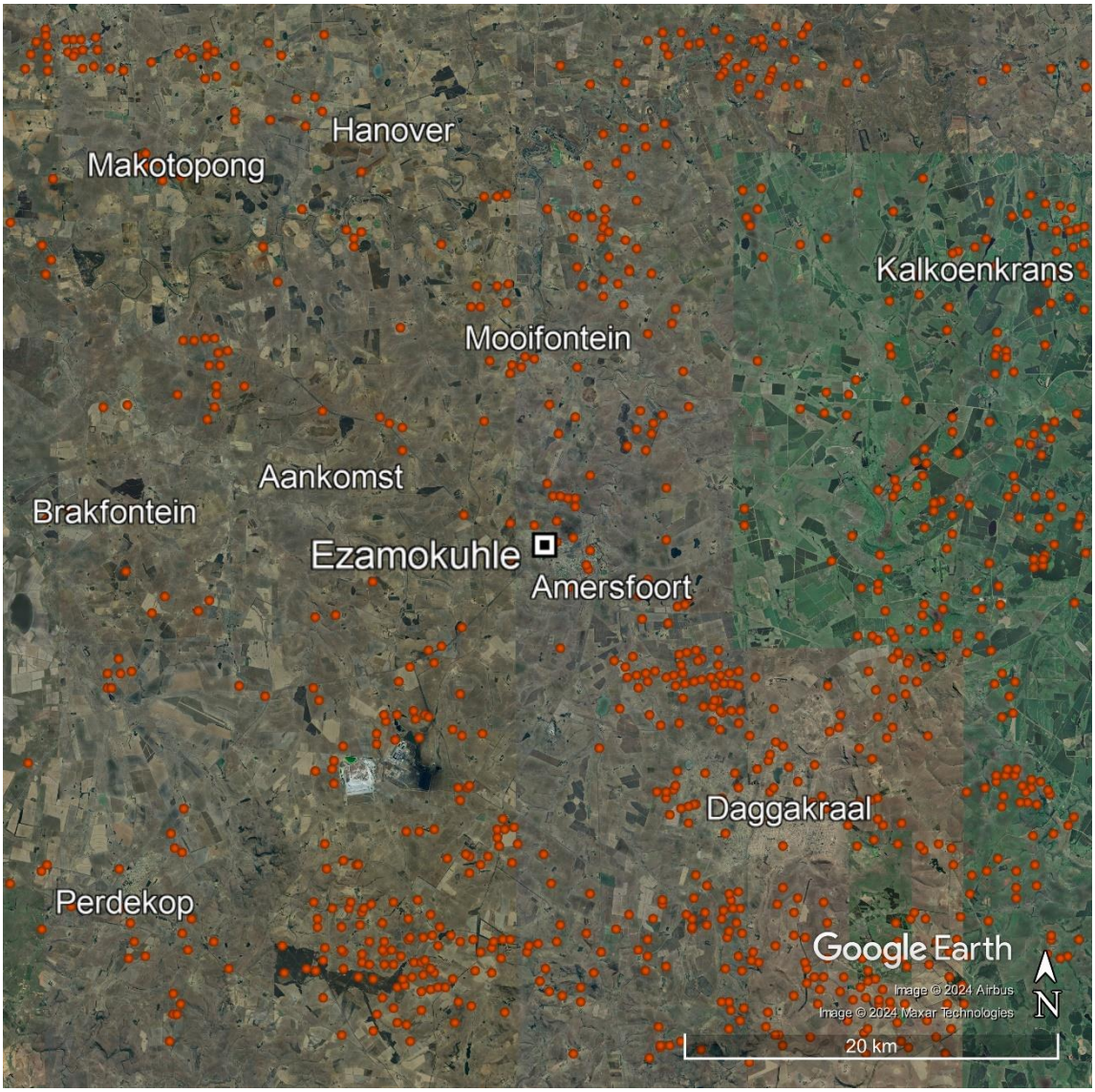

Figure 4-8: Location of biomass burning fires (indicated by orange dots)

4.5 VEHICLES – PAVED ROADS

4.5.1 INTRODUCTION

A paved road is defined as any road that has a semi-permanent surface placed on it (for example, asphalt or concrete). In this section, emissions are calculated for exhaust emissions, brake, tyre and road wear for vehicles travelling on paved roads.

Emissions from vehicles arise during the different cycles of driving from start-up, during driving, evaporation from the engine and fuel line, and during re-fueling (DEFF, 2010). Particulate matter is also emitted from brake, tyre and road wear (DEFF, 2013). Other pollutants associated with vehicle emissions include SO_2, NO_2, carbon monoxide, benzene and lead. In this study, only SO_2, NO_X, and particulates (PM_{10} and $PM_{2.5}$) will be considered. The emission rates are co-dependent on various factors relating to vehicle parc (vehicle class, model, speed and maintenance); fuel specifications

and environmental factors (Samaras *et al*., 1999). Considering the complexity of vehicle emission inventory development, this study has opted to use the COPERT vehicle emission estimation model which is regarded as the EU standard vehicle emissions calculator and has been used in other regulatory strategic documents such as the Second Generation Vaal Triangle Airshed Priority Area (VTAPA) Air Quality Management Plan (DEFF, 2020). COPERT stands for COmputer Programme to calculate Emissions from Road Transport. It uses vehicle population, mileage, speed and other data such as ambient temperature and calculates emissions and energy consumption for a specific country or region. As an initial input basis of the emission estimates, a detailed road network of the region in question is required for which the associated vehicle population, mileage, speed and other data are estimated. The road network within the Greater Ezamokuhle Airshed is presented in Figure 4-9.

The network shown in Figure 4-9 is sourced from the World Bank data CatLog for South African roads delineated by the Word Bank (https://datacatalog.worldbank.org/dataset/south-africa-roads) and based on the South African national roads network.

The dataset classifies roads into three basic classes i.e., Primary, Secondary and Tertiary with road traffic apportioned according to these classifications with “Primary” carrying high volumes of traffic and “Tertiary” carrying less traffic. Thus, two factors play a role in emission intensity when considering these three types of roads. Primary roads may carry more vehicle volume and lead to higher emissions, together with congestion (therefore lowering speed and travel time) can also increase emissions. In general, factors that impact vehicle emissions estimates are:

- Fuel type
- Fuel specifications
- Engine technology
- Engine capacity
- Vehicle speed
- Vehicle age
- Engine/exhaust temperature
- Number of kilometres travelled.

Other, more detailed factors requiring information that is generally not available (particularly on such a large scale) are gearing, driving style, tyre friction and road grading, and are generally not available in a South African context.

Figure 4-9: Road Network within the Greater Ezamokuhle Airshed modelling domain

The basis of deriving vehicle emissions is an estimate of Vehicle Kilometres Travelled (VKT). This data represents an activity to which emission factors are applied. The emission factors are dependent on all other factors noted above and are accounted for in the COPERT model. Thus, any approach to generate a vehicle emission inventory includes an estimation of VKT and use of appropriate emission factors generated via COPERT. The level of detail included in each factor varies depending on available information which is required at the grid cell level for the most accurate estimation results. This is not necessarily possible for all the above-listed factors because many (for example, fuel type) are not tracked at a fine scale.

Thus, assumptions are made using spatial surrogates to generate a finer resolution emission inventory that is spatially representative. There are instances when very detailed information is available (such as traffic count data); however, these are then often spatially limited. Assumptions are then used to extrapolate this data to the larger spatial scale – this is termed a bottom-up approach

– more detail on this approach is provided in section below. When larger scale, but more generalised data exists e.g., Provincial or District Municipality Level Fuel Sales, assumptions are made to create a finer scale variation based on surrogates – this is termed a top-down approach. Both these approaches are viable when estimating vehicle emissions, but largely depend on the data available.

4.5.2 METHODOLOGY

As detailed above, estimation of the on-road vehicle emission inventory in this study has employed both a top-down and bottom-up approach. This is possible due to road count data being available from various sources which is also inherently contained in the road network data set i.e. Primary, Secondary and Tertiary classified roads. For both the top-down and bottom-up methodologies, the common underlying spatial units are the World Bank data CatLog for South African roads road links (Figure 4-9).

Table 4-11: Vehicle classes for which emissions are estimated

eNaTIS Classification	ADDT Light
Motor Cars and Station Wagons	Car Diesel
	Car Petrol
	SUV Diesel
	SUV Petrol
Motorcycles, Quads and Tricycles	MotoBike Petrol
LDV'S, Panel Vans etc	LCV Diesel
	LCV Petrol
eNaTIS Classification	**ADDT Heavy**
Trucks	HCV1 Petrol
	HCV1 Diesel
	HCV2 Diesel
	HCV3 Diesel
eNaTIS Classification	**AADT Very Heavy**
Trucks	HCV4 Diesel
	HCV5 Diesel
	HCV6 Diesel
	HCV7 Diesel
	HCV8 Diesel
eNaTIS Classification	**ADDT Bus**
Buses, bus trains, minibuses	Bus
Taxi	Minibus Taxis

It is important to note that various vehicles may be travelling on a particular piece of road at any given moment which requires a comprehensive vehicle typology or parc to be developed for which emissions will be estimated. Considering this, emissions for the classes listed in Table 4-11 are estimated which follow the electronic National Traffic Information System (eNaTIS) broad classifications as reported in the provincial statistics. This is then used to calibrate the COPERT

model. A top-down approach uses fuel sales to estimate VKT and allocates this to roads by their type; however, the bottom-up approach serves as a starting point of the emission inventory.

BOTTOM-UP

Road count data is used to estimate VKT for each count station by applying the count to the immediate road link and this data is contained within the World Bank data CatLog for South African roads delineated by the Word Bank. The extents are limited in this way because there is no other methodology to describe traffic flow in other links around the station, except using a full-scale network flow model. These links are then removed from the full road network together with estimated fuel consumption for that link by converting VKT to fuel-use using fuel efficiency data that is also generated by the COPERT model. This ensures there is no double counting of both VKT and spatial features. All VKT are converted into fuel consumption using the efficiency data extracted from the COPERT model (see "Emission Factors" section below). This fuel consumption is subtracted from the provincial fuel sales, together with the road links associated with counts, going into the top-down methodology. The SANRAL count data is also useful in that average vehicle speeds are given. Using this information, it was possible to assign typical speeds for different World Bank data CatLog Road types. These speeds are necessary for selecting appropriate emission factors further in the process. Figure 4-10 shows the average speeds for light, heavy and overall classes for each World Bank data CatLog Road class. After all bottom-up estimations are done, the remaining road network is used for the top-down approach.

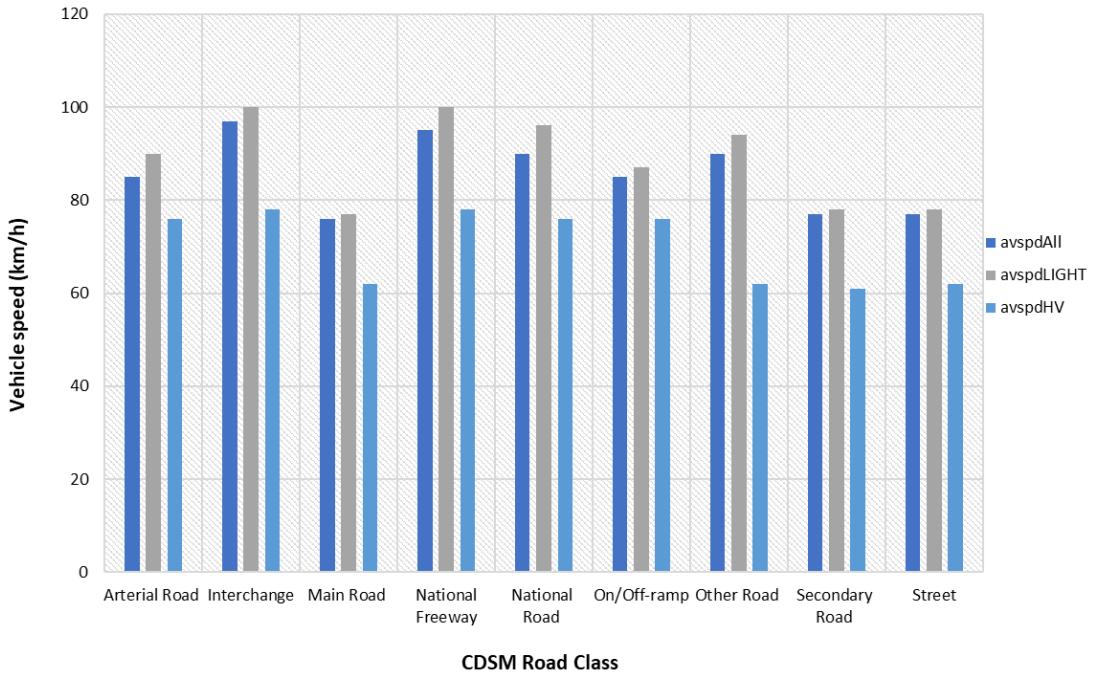

Figure 4-10: Average vehicle speeds for all light and heavy duty vehicles for each CDSM road class (derived from SANRAL count data)

TOP-DOWN

The top-down approach uses provincial fuel sales and fuel efficiency data (from COPERT; see "emission factors" section) to estimate VKT. A key assumption is that fuel sales equate to fuel consumption. This is the case for total national volume, however, the possibility of fuel sales being consumed elsewhere is likely when looking at regional fuel sales. Therefore, Magisterial District sales are used rather than provincial sales (also available from the Department of Energy (DoE)) to minimize this effect. DoE obtained fuel sale data is classified into "Travel Analysis Zone" (TAZ) which comprises of various towns to which fuel/VKT is associated to specific road links.

Once fuel sales are allocated to TAZ, it is necessary to disaggregate further down to road level. This is accomplished by using data from the South African Road Classification and Access Manual (SARCAM) (SANRAL, 2012). Tables B and C of the manual provide typical average annual daily traffic (AADT) for different road classes. These typical road AADTs were used to proportionally distribute fuel to different World Bank data CatLog for South African roads classes.The result of this process is unique road classes, to which typical AADT from the SARCAM can be assigned. Fuel within each TAZ is then distributed by the typical AADT proportion amongst classes.

The final level of disaggregation is achieved by then allocating fuel proportionally within classes based on link length. The result is a fuel consumption estimate on each of the remaining (after removals from the bottom-up processing) World Bank data CatLog for South African roads. This fuel consumption is converted to VKT using the COPERT-derived fuel efficiency data.

4.5.3 EMISSION FACTORS

In this study, "hot running" (thermally stabilized engine and exhaust treatment) emission factors were derived from the COPERT 5 (version 5.0.1145) model. The model is developed by EMISIA SA and supported by the European Environment Agency (EEA). The methodological approach (and thus formulae) for COPERT 5 is identical to the Tier 3 methodology laid out in the EMEP/EEA air pollutant emission inventory guidebook 2013 (European Environment Agency, 2013) for "Exhaust emissions from road transport" (Part B, Section 1.A.3.b.i-iv).

The COPERT approach was chosen since all other locally derived emissions factors (e.g., Stone, 2000; Wong, 1999; Wong and Dutkiewicz, 1998) provided an emission factor at a generalized single speed; while what is required for this emission inventory is a speed-based estimate since emission factors are sensitive to vehicle speed that are effectively linked to the World Bank data CatLog for South African roads and vehicle speeds. Additionally, locally derived emission factors represent a much older vehicle fleet; typically, pre-EURO2. Emission factors were modelled for EURO 1-6 stage vehicles from the classes specified in Table 4-12. An approximate manufacture years for each EURO stage is also listed in Table 4-12.

Table 4-12: Vehicle EURO stage and corresponding manufacture years

EURO Stage	Vehicle Model Year
EURO 1	1992 – 1995
EURO 2	1996 – 1999
EURO 3	2000 – 2004
EURO 4	2005 – 2009
EURO 5	2010 – 2014
EURO 6	2015 – current

Emission factors for SO_2, NO_X, and particulates were estimated in COPERT for speeds from 20 to 120 km/hr (in 20 km/hr increments). COPERT also estimated fuel consumption (i.e., efficiency in l/km) for each speed. Note that in practice the closest speed emission factor is matched to the specific speeds for vehicles travelling on that road. The full emission factor/fuel consumption dataset thus comprised 4 536 factors (6 EURO classes by 6 speeds by 18 vehicle classes by 7 pollutants).

Since there is no indication of vehicle age or technology within the activity data used (both counts for the bottom-up and fuel sales for the top-down) it is necessary to aggregate the emission factors by EURO stage. To simply take an average would not be accurate since that would assume all vehicle ages exist at an equal proportion in the vehicle parc. This is not true as newer vehicles enter the parc, older ones leave, resulting in a shift towards newer vehicles.

The spread of vehicle age in a parc can be determined through scrapping curves. A weighted average of emission factors between EURO stages can then be obtained to derive a single emission factor per vehicle class and pollutant (still at the different speeds). The scrapping curve used in this study is based on Merven et al., (2012) eNaTIS calibrated (year 2010). Weibull cumulative distribution functions show probability of vehicle survival as a function of age. These functions are then applied to the time periods relevant to this study. The scrapping curves used for each class is presented in Figure 4-11 (after Merven et al., 2012). These curves were used for deriving an age proportion weighted average emission factor for each speed and pollutant per vehicle class. The diesel NO_X emission factors derived from COPERT is presented in Figure 4-12 illustrates the importance of vehicle speed.

The emission factors were then applied to the VKT per vehicle class and road type to derive an annual emission estimate per road link for all pollutants of concern. For verification, the VKT and fuel consumption estimates derived from the COPERT model are adjusted to ensure a +/- 10% agreement with petrol and diesel fuel sales determined for each TAZ, ensuring accurate estimation of emissions in each area. Total fuel sales considered as part of this study are presented in Table 4-13.

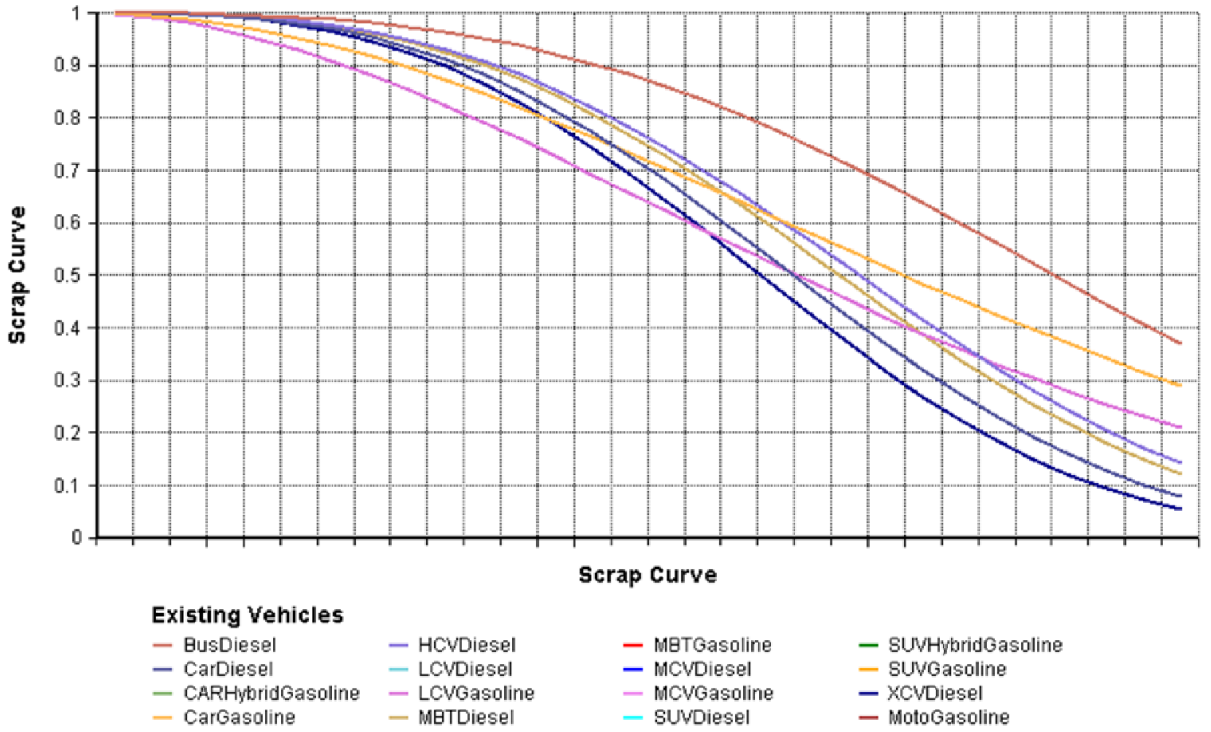

Figure 4-11: Base year scrapping curves for the vehicle technology types in the vehicle parc model (After Merven et al., 2012)

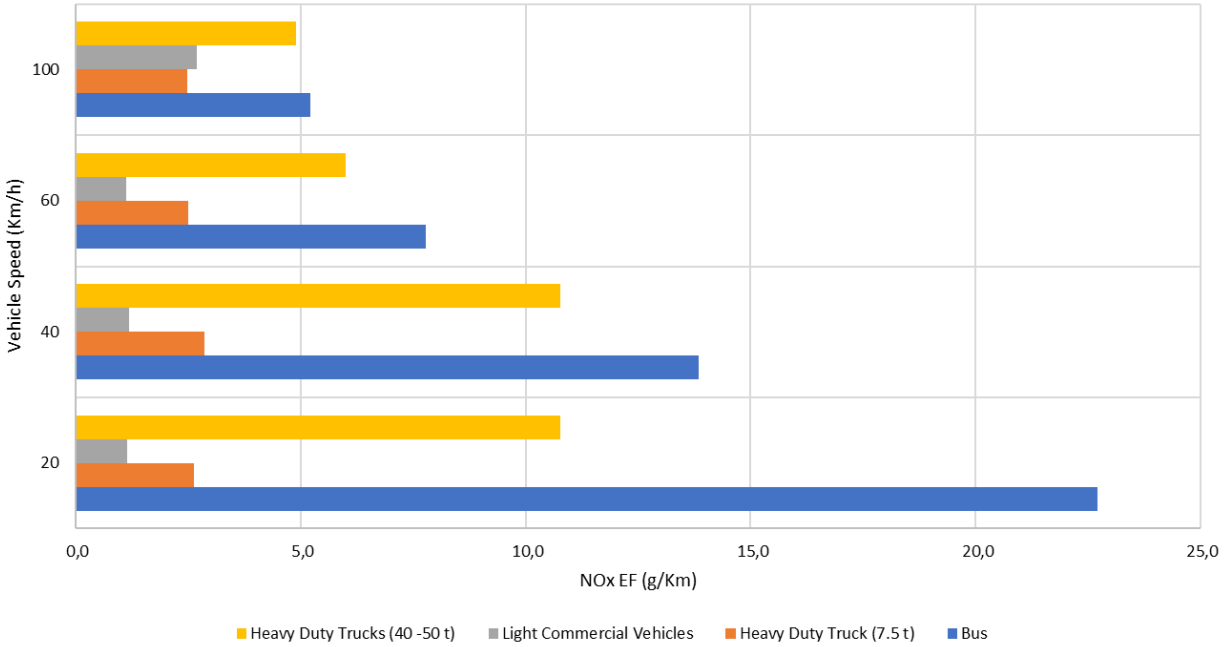

Figure 4-12: NO_X emission factors for diesel classes

Table 4-13: Regional fuels sales used within the Ezamokuhle modelling domain

TAZ	Diesel (million litres)	Petrol (million litres)	Total Fuel Sales (million litres)
Standerton	17.7	3.11	20.8
Volksrust	20.1	2.9	23.0
Piet Retief	11.4	4.5	15.9
Total	49.2	10.5	59.7

4.5.4 Emission Inventory

Expectedly, higher on-road vehicle emissions are observed in areas with greater fuel sales with Standerton and Volrust having the greatest volume of daily traffic and fuel sales subsequently resulting in the greatest emission from on-road vehicles in the region. Table 4-14 presents the total tonnage of estimated annual tonnage of estimated on-road vehicle emissions within the Ezamokuhle modelling domain.

Table 4-14: Estimated on-road vehicle emissions (tonnes/annum) within the Ezamokuhle modelling domain

Pollutant	SO_2	NO_X	PM_{10}	$PM_{2.5}$
Emission rate (tonnes/annum)	1.3	178.6	3.3	3.3

4.6 Vehicles – Unpaved Roads

4.6.1 Introduction

An unpaved road is a road which has a surface that does not meet the definition of a paved road. The road surface may be dirt, rock, gravel, or other non-solidified material and may have a dust palliative applied (*dust palliatives* are substances applied to roads or ground surfaces to reduce airborne dust and its health impacts). Unpaved roads often contribute a significant amount of atmospheric dust formed due to re-suspension of road material by vehicles and observed as a dust cloud behind the driving vehicle. If a dust suppressant is applied to an unpaved road, this segment of road is still considered to be an unpaved road surface.

Most of the roads in South African are classified as gravel roads. A gravel road is a type of unpaved road surfaced with gravel that has been brought to the site from a quarry or stream bed. In many cases, replacement of gravel on these roads may not always be available or feasible. In 2016, SANRAL estimated between 74-79% of South African roads are gravel (https://www.arrivealive.co.za/The-South-African-National-Roads-Agency-LTD). Most of these roads are found within rural areas but a large percentage of these gravel roads are also found in urban areas. According to the Cornerstone Economic Research (2018), over 80% of Gauteng's road network is considered gravel with more than two thirds of these gravel roads being in poor condition. a larger portion of the unpaved road network in Gauteng is found in outer lying urban areas and within townships (Naidoo, 2023).

The average rainfall in the Highveld varies from about 900 mm in the higher lying areas in the east to about 650 mm in the west. Rainfall is almost exclusively in the form of showers and thundershowers and occurs mainly in the summer from October to March, with the maximum in January. Winters are typically dry, but some rain does occur (DEA, 2011). This combined with

potentially intense traffic in the urban areas, unpaved roads may present a significant local source of PM (Naidoo, 2023).

When a vehicle travels on an unpaved road, the force of the wheels on the road surface causes pulverization of surface material. Particles are lifted and dropped from the rolling wheels, and the road surface is exposed to strong air currents in turbulent shear with the surface. The turbulent wake behind the vehicle continues to act on the road surface after the vehicle has passed. Emissions caused by vehicles can be minimized by paving, windbreaks, frequent water and/or environmentally friendly chemical applications, and using gravel as a means of dust suppression.

LOCATION OF UNPAVED ROADS

Google Earth satellite imagery was used to map out locations of unpaved roads, mainly focusing on densely populated townships within the modelling domain. Based on the satellite imagery, it is noted that there are a few main roads and access roads within townships that are paved. This accounts for a very small fraction of the total length of all roads within a township. From a modelling perspective, a modelling exercise to include all unpaved road segments would be an exceptionally time-consuming exercise and would require exceptionally long model run-times. It was therefore decided to include the unpaved roads as area sources. Area sources corresponding with unpaved roads, which has been used in the modelling is presented in Figure 4-13.

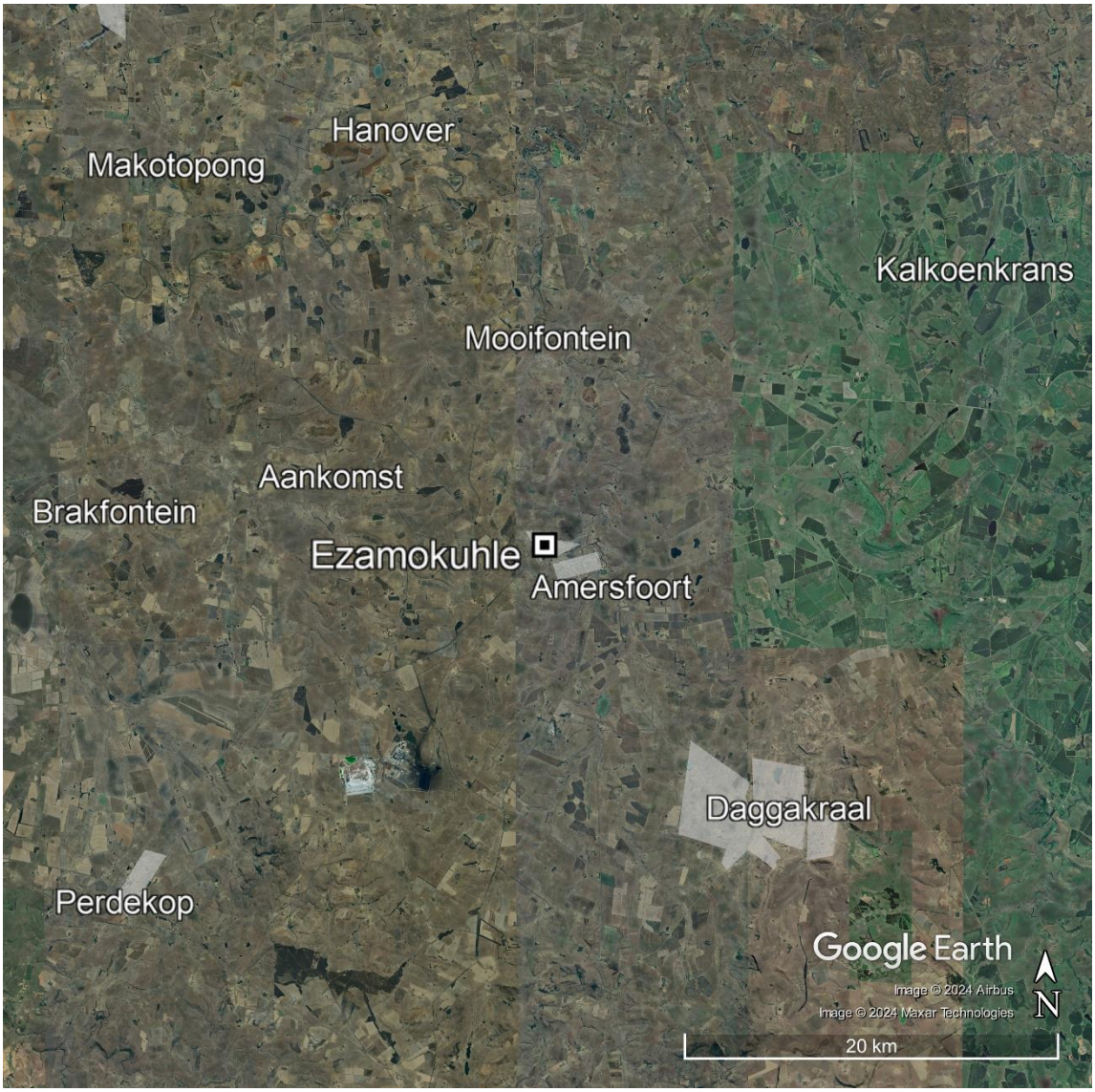

Figure 4-13: Location of areas corresponding with unpaved roads for the Greater Ezamokuhle Airshed

ASSUMPTIONS

For development of the emission inventory, there was no available information for critical input data. A number of assumptions had to be made based on best judgement. To streamline the modelling process, the following profile was created based on a 1 square kilometre of a high-density township:

- Approximately 1000 homes are located within 1 square kilometre of a township, representing 1000 families.
- 50% of these homes have a car, but only half of them are used on a regular basis for travelling to work, dropping off children at school or for shopping. It is therefore assumed that 250 cars travel on the unpaved roads on a daily basis. It is also assumed that each car travels on approximately 1 km of unpaved roads per day.

- Many children and family members depend on public transport for travelling to school or work or to shopping centres. It is assumed that 1 minibus taxi and 1 bus is in operation on a daily basis. It is also assumed that each minbus taxi travels and truck travels on approximately 20 km of unpaved roads per day.
- Goods (for example building material, furniture, food supplies to spaza shops) also need to be transported to and/or from the townships. It is therefore assumed that 1 truck is in operation within the area on a daily basis, travelling 10 km per day.

The total VKT is presented in Table 4-15.

Table 4-15: Total VKT

Trip length (VKT)	Trucks	Buses	Taxis	Cars
Round trip (km)	10	20	20	1
Number of trucks	1	1	1	250
Number of trips	1	1	2	1
Number of days	365	365	365	365
Total distance (km)	3650	7300	14600	91250

In this section, emissions are calculated for exhaust emissions for vehicles travelling on unpaved roads; and particulate emissions from unpaved road surfaces.

4.6.2 Methodology – Vehicle Exhaust Emissions from Unpaved Roads

The EMEP/EEA air pollutant emission inventory guidebook (EMEP/EEA, 2022) provides a methodology, emission factors and relevant activity data to enable exhaust emissions to be calculated for the following categories of road vehicles:

- Passenger cars (NFR code 1.A.3.b.i)
- Light commercial vehicles (1) (< 3.5 t) (NFR code 1.A.3.b.ii)
- Heavy-duty vehicles (2) (> 3.5 t) and buses (NFR code 1.A.3.b.iii)
- Mopeds and motorcycles (3) (NFR code 1.A.3.b.iv)

It does not cover non-exhaust emissions such as fuel evaporation from vehicles (NFR code 1.A.3.b.v), tyre wear and brake wear (NFR code 1.A.3.b.vi), or road wear (NFR code 1.A.3.b.vii).

Emission Factors

The Tier 1 and Tier 2 emission factors have been calculated from detailed emission factors and activity data using the Tier 3 method.

The Tier 1 emission factors have been derived from the Tier 3 methodology using 1995 fleet data for the EU-15. The upper limits of the stated ranges in the emission factors correspond to a typical

uncontrolled (pre-Euro) technology fleet, and the lower limit of the range corresponds to an average EU-15 fleet in 2005. The suitability of these emission factors for a particular country and year depends on the similarity between the national fleet and the assumptions used to derive the Tier 1 emission factors.

The Tier 2 emission factors have been calculated based on average driving and temperature conditions for the EU-15 in 2005. These emission factors assume average urban, rural and highway driving mileage shares and speeds for the EU-15. Again, the suitability of these emission factors depends on the similarity between the national driving conditions and the average of EU-15.

The Tier 3 emission factors have been derived from experimental (measured) data collected in a range of scientific programmes. The emission factors for old-technology passenger cars and light commercial vehicles were taken from earlier COPERT/CORINAIR activities (Eggleston et al., 1989), whilst the emissions from more recent vehicles are calculated on the basis of data from the Artemis project. (Boulter and Barlow, 2005; Boulter and McCrae, 2007).

Tier 2 emission factors are stated in units of grammes per vehicle-kilometre, and for each vehicle technology. These average European emission factors were determined using the Tier 3 methodology which follows in using typical values for driving speeds, ambient temperatures, highway-rural-urban mode mix, trip length, etc. A figure for fuel consumption (g/km), which is derived from carbon balance is also provided, so that fuel-based pollutants such as SO_2 can be calculated.

Vehicle exhaust emissions for unpaved roads was calculated using an estimate of Vehicle Kilometres Travelled (VKT) and Tier 2 exhaust emission factors provided in the EMEP/EEA air pollutant emission inventory guidebook (EMEP/EEA, 2022). Emissions were calculated for passenger cars, light commercial vehicles, heavy-duty vehicles and buses.

Emission factors are based on the “PRE-ECE” and “conventional” technology class. PRE_ECE refers to emission technology of the 1970s and the conventional class refers to a very limited fleet of such vehicles which is still in circulation and no particular emission standards are applicable.

EMISSION RATES ON 1 SQUARE KILOMETRE BASIS

The emission rates for vehicle exhaust emissions from unpaved roads on 1 square kilometre basis is presented in Table 4-16 together with the VKT, fuel consumption and emission factors.

Table 4-16: Emission rates for vehicle exhaust emissions from unpaved roads on a 1 square kilometre basis together with the VKT, fuel consumption and emission factors

	Fuel Consumption Data	Fuel Usage	Emission Factors				Emission Rates			
			Heavy Duty Vehicles - 16-32t				Emission Rates (tonnes/annum)			
VKT (km)	Fuel consumption (g/km) for Diesel (500 ppm Sulphur)	Total Fuel Used By All Trucks (kg)	NO_X (g/km)	SO_2 (kg/kg)	PM_{10} (g/km)	$PM_{2.5}$ (g/km)	NO_X	SO_2	PM_{10}	$PM_{2.5}$
3 650	251.00	916.15	10.70	0.00050	0.42	0.42	0.03906	0.00046	0.00153	0.00153
			Buses				Emission Rates (tonnes/annum)			
VKT (km)	Fuel consumption (g/km) for Diesel (500 ppm Sulphur)	Total Fuel Used By All buses (kg)	NO_X (g/km)	SO_2 (kg/kg)	PM_{10} (g/km)	$PM_{2.5}$ (g/km)	NO_X	SO_2	PM_{10}	$PM_{2.5}$
7 300	2 671.80	2 671.80	16.50	0.00050	0.91	0.91	0.12045	0.00134	0.00664	0.00664
			Taxis				Emission Rates (tonnes/annum)			
VKT (km)	Fuel consumption (g/km) for Petrol (10 ppm Sulphur)	Total Fuel Used By All taxis (kg)	NO_X (g/km)	SO_2 (kg/kg)	PM_{10} (g/km)	$PM_{2.5}$ (g/km)	NO_X	SO_2	PM_{10}	$PM_{2.5}$
14 600	1 241.00	1 241.00	3.09	0.00001	0.0023	0.0023	0.04511	0.00001	0.00003	0.00003
			Passenger Cars				Emission Rates (tonnes/annum)			
VKT (km)	Fuel consumption (g/km) for Petrol (10 ppm Sulphur)	Total Fuel Used By All cars (kg)	NO_X (g/km)	SO_2 (kg/kg)	PM_{10} (g/km)	$PM_{2.5}$ (g/km)	NO_X	SO_2	PM_{10}	$PM_{2.5}$
91 250	7 026.25	7 026.25	2.53	0.00001	0.0022	0.0022	0.30782	0.00009	0.00027	0.00027
							TOTAL Emission Rates (tonnes/annum)			
							NO_X	SO_2	PM_{10}	$PM_{2.5}$
							0.51244	0.00190	0.00846	0.00846

4.6.3 METHODOLOGY – PARTICULATE EMISSIONS FROM UNPAVED ROAD SURFACES

The particulate emissions of concern from unpaved roads are total particulate matter (TPM) including PM_{10} and $PM_{2.5}$. The quantity of dust emissions from a given segment of unpaved road varies with the volume of traffic, the condition of the road, the number of vehicles passes, the vehicle characteristics (e.g. vehicle weight, speed and number of wheels), the properties of the road surface material being disturbed (e.g. silt content, moisture content), and the climatic conditions (e.g., frequency and amounts of precipitation). Dust emissions from unpaved roads have been found to vary directly with the silt content in the road surface material.

In this study, the calculation methodology of unpaved roads emissions from resuspension of loose material on road surfaces due to vehicle travel is based on the USEPA Compilation of Air Pollutant Emission Factors, 5th Edition, Volume 1 (AP-42) Chapter 13 – Miscellaneous Sources, 13.2.2. The following generalised equation is used to determine the annual emissions of each size of PM from unpaved road surfaces (USEPA, 2006):

$$E_x = VKT*EF_x*ADJ*(1-CE/100) \quad (1)$$

Where:

- E_x: Emission of contaminant x (kg)
- VKT: Annual total vehicle kilometres travelled (km)
- EF_x: Emission factor of contaminant x (kg/VKT)
- ADJ: Adjustment factor for precipitation, snow cover and frozen days
- CE: Applied Dust Control Method's efficiency (%)

The following sections describe the process that was followed when using equation 1.

TOTAL VEHICLE KILOMETRES TRAVELLED (VKT)

The VKT represents the kilometres travelled by all vehicles on the unpaved roads. This includes cars, minibus taxis, buses and heavy-duty trucks. The annual VKT should be obtained using the best available data. This can be odometer readings, the length of roads and the number of vehicles and vehicle classes travelling on the unpaved roads on a typical day. If no data is available, surveys should be conducted throughout the year on representative days of operation to estimate the total VKT.

No such data is available for this study. VKT has been calculated using assumptions outlined in the Introduction of this section and is presented in Table 4-15.

EMISSION FACTORS

The USEPA has developed an empirical equation (equation 2) for vehicles travelling on unpaved road surfaces (at industrial sites). The equation takes into account the silt content of the roadway and the mean weight of the vehicles travelling on the road. (For more information, refer to AP 42, Chapter 13: Miscellaneous Sources, Section 2.2, (USEPA, 2006)).

The emission factor in metric units (that is, kilograms/VKT) is calculated using the following equation:

EF = k*(s/12)^a*(W/2.72)^b (2)

Where:

- EF: Size-specific emission factor (kg/VKT)
- s: Surface material silt content (%)
- W: Mean vehicle weight, tonnes (metric)
- k, a, b: Numerical constants for calculation (refer to Table 4-17)

Table 4-17: Numerical constants used in the unpaved industrial road dust emission factor

Constant	$PM_{2.5}$	PM_{10}	TPM
k (kg/VKT)	0.042	0.423	1.381
a	0.9	0.9	0.7
b	0.45	0.45	0.45

The silt content (s) of an unpaved road may be obtained using the USEPA test method (Appendix C.1: Procedures for sampling surface/Bulk dust loading, AP-42, USEPA, 2003). Site-specific values for silt content was not available for unpaved roads in the study area. As recommended by AP42, an appropriate mean value from Table AP-42 13.2.2-1 (USEPA, 2006) (reproduced below in Table 4-18), should used as a default value, in the absence of measured values. It is understood that the use of default values may affect the quality of estimated values. In this study, a silt value of 8.3 (Stone quarrying and processing – Haul road to/from pit) was chosen.

Table 4-18: Typical silt content values of surface material on industrial unpaved roads (USEPA, 2006)

Industry	Road use or surface material	Silt content (%)
Copper smelting	Plant road	17
Iron and steel production	Plant road	6
Sand and gravel processing	Plant road	4.8
Sand and gravel processing	Material storage area	7.1
Stone quarrying and processing	Plant road	10
Stone quarrying and processing	Haul road to/from pit	8.3
Taconite mining and processing	Service road	4.3
Taconite mining and processing	Haul road to/from pit	5.8
Western surface coal mining	Haul road to/from pit	8.4
Western surface coal mining	Plant road	5.1
Western surface coal mining	Scraper route	17
Western surface coal mining	Haul road (freshly graded)	24
Construction sites	Scraper routes	8.5
Lumber sawmills	Log yards	8.4
Municipal solid waste landfills	Disposal routes	6.4

ADJUSTMENT FACTOR (ADJ) FOR PRECIPITATION, SNOW COVER AND FROZEN DAYS (NATURAL MITIGATION)

Road dust emissions are reduced due to the natural mitigation effects of precipitation (rain and snow falls), as well as on frozen or snow-covered roads. Equation 1 assumes that no dust emissions occur on days with precipitation exceeding 0.2 mm or on days when the road surface is covered with snow or is frozen without high traffic volume.

The ADJ value used in equation 1 is determined using the following equation:

ADJ = (Working Days - (p+snow))/Working Days (3)

Where:

- ADJ: Adjustment factor for precipitation, snow cover and frozen days
- Working Days: The number of operating days per year
- p: Estimated Annual Working Days with precipitation exceeding 0.2 mm
- snow: The estimated Annual Working Days when the roads were frozen or snow-covered and wet for winter

With respect to precipitation (and snow-covered days), the number of days with the specified precipitation parameters corresponds to 71 days according to long term climate statistics (SAWB, 1980).

DUST CONTROL METHODS (CE)

Several techniques are used to reduce road dust emissions caused by vehicular travel on unpaved road surfaces, such as the application of water or chemical dust suppressants (Buonicore and Davis, 1992; USEPA, 1987). Watering is the most common control technique used for unpaved road surfaces (AMEC, 2007). The control efficiency of watering depends on the application rate, the elapsed time between applications, traffic volume and meteorological conditions. Chemical stabilization is also used to reduce emissions of road dust from unpaved surfaces. Its control efficiency depends on the material used and the method of application. Table 4-19 lists available dust control methods and their respective efficiencies.

Table 4-19: Dust control methods and efficiencies (USEPA, 2006)

Dust control techniques	Control Efficiency (CE)
Watering twice a day	55%
Watering more than twice a day	70%
Chemical suppressants	80%

In this study, it is assumed that no dust reduction mechanisms are applied on unpaved roads. No control efficiencies have therefore been applied.

EMISSION RATES ON 1 SQUARE KILOMETRE BASIS

The emission rates for particulates from unpaved road surfaces on a 1 square kilometre basis is presented in Table 4-20 together with the VKT, emission factors, adjustment factor for natural mitigations, and the emission rate before and after mitigation.

Table 4-20: Emission rates for particulates from unpaved roads on a 1 square kilometre basis together with the VKT, emission factors, adjustment factor for natural mitigations, and the emission rate before and after mitigation

Vehicle Type	Pollutant	VKT (km)	EF Uncontrolled kg/VKT)	Total Release (tonnes)	Adjustment factor ADJ for natural mitigations	Annual adjusted emissions for natural mitigation (tonnes)
Trucks	TPM	3650	3.05	11.12	0.81	8.96
	PM_{10}		0.87	3.17	0.81	2.55
	$PM_{2.5}$		0.09	0.32	0.81	0.26
Buses	TPM	7300	2.39	17.44	0.81	14.05
	PM_{10}		0.68	4.97	0.81	4.00
	$PM_{2.5}$		0.07	0.50	0.81	0.40
Taxis	TPM	14600	1.12	16.42	0.81	13.23
	PM_{10}		0.32	4.68	0.81	3.77
	$PM_{2.5}$		0.03	0.47	0.81	0.38
Cars	TPM	91250	0.80	72.83	0.81	58.66
	PM_{10}		0.23	20.76	0.81	16.72
	$PM_{2.5}$		0.02	2.08	0.81	1.67

4.6.4 Emission Inventory

The Emission Inventory for the Vehicles – Unpaved Roads category is presented in Table 4-21 for all pollutants in the Ezamokuhle modelling domain. It must be noted that the emissions presented is the total emissions made up of vehicle exhaust emissions and emissions from unpaved road surfaces.

Table 4-21: Emission Inventory for the Vehicles – Unpaved Roads Category

Pollutant	SO_2	NO_X	PM_{10}	$PM_{2.5}$	TPM
Emission Rate (tonnes/annum)	0.1	23.6	1 247.2	125.1	4 374.1

4.7 ALL SOURCES

In order to assess potential cumulative impacts and possible synergistic effects, emissions from all source categories are modelled at once. In this section, the total emissions for SO_2, NO_X, PM_{10}, $PM_{2.5}$ and dustfall are presented for the primary and secondary modelling domains.

PRIMARY MODELLING GRID: GREATER EZAMOKUHLE AIRSHED

A summary of emissions of SO_2, NO_X, PM_{10}, $PM_{2.5}$ and dustfall for each source category for the Greater Ezamokuhle Airshed is presented in Table 4-22.

Table 4-22 is used to calculate the percent contribution of SO_2, NO_X, PM_{10}, $PM_{2.5}$ and dustfall for the Greater Ezamokuhle Airshed as a function of the six emission source categories and is presented in Table 4-23.

Pie charts are used to illustrate the percent contribution for each pollutant. These are compared with the percent contribution for each pollutant for the Ezamokuhle Airshed in Figure 4-14 for SO_2, Figure 4-15 for NO_X, Figure 4-16 for PM_{10}, Figure 4-17 for $PM_{2.5}$ and Figure 4-18 for dustfall.

A basemap showing all emission source categories within the Greater Ezamokuhle Airshed (primary, coarse resolution modelling domain) is presented in Figure 4-19.

SECONDARY MODELLING GRID: EZAMOKUHLE AIRSHED

A summary of emissions of SO_2, NO_X, PM_{10}, $PM_{2.5}$ and dustfall for each source category for the Ezamokuhle Airshed is presented in Table 4-24.

Table 4-24 is used to calculate the percent contribution of SO_2, NO_X, PM_{10}, $PM_{2.5}$ and dustfall for the Ezamokuhle Airshed as a function of the six emission source categories and is presented in Table 4-25.

Pie charts are used to illustrate the percent contribution for each pollutant. These are compared with the percent contribution for each pollutant for the Greater Ezamokuhle Airshed in Figure 4-14 for SO_2, Figure 4-15 for NO_X, Figure 4-16 for PM_{10}, Figure 4-17 for $PM_{2.5}$ and Figure 4-18 for dustfall.

A basemap showing all emission source categories within the Ezamokuhle Airshed (secondary, fine resolution modelling domain), together with discrete receptors is presented in Figure 4-20.

Table 4-22: Emission Inventory for SO_2, NO_X, PM_{10}, $PM_{2.5}$ and dustfall for the six emission source categories in the Greater Ezamokuhle Airshed

	Emission rate (tonnes/annum)				
Emission Source Category	**SO_2**	**NO_X**	**PM_{10}**	**$PM_{2.5}$**	**TPM**
Power Generation	182 926.00	109 677.00	14 693.28	5 962.01	
Residential Fuel Burning	48.10	20.15	109.18	109.18	
Waste Burning	1.08	2.73	8.23	7.77	
Biomass Burning	59.50	11.95	487.11	483.38	
Vehicles – Paved Roads	1.27	178.64	3.33	3.33	
Vehicles – Unpaved Roads	0.09	23.62	1 247.22	125.07	4 374.15
All Sources	183 036.03	109 914.08	16 548.37	6 690.76	4 374.15

Table 4-23: Emission source contribution (%) of SO_2, NO_X, PM_{10}, $PM_{2.5}$ and dustfall as a function of the six emission source categories for the Greater Ezamokuhle Airshed

	Emission Source Contribution (%)				
Emission Source Category	**SO_2**	**NO_X**	**PM_{10}**	**$PM_{2.5}$**	**TPM**
Power Generation	99.94	99.78	88.79	89.11	0.00
Residential Fuel Burning	0.03	0.02	0.66	1.63	0.00
Waste Burning	0.00	0.00	0.05	0.12	0.00
Biomass Burning	0.03	0.01	2.94	7.22	0.00
Vehicles – Paved Roads	0.00	0.16	0.02	0.05	0.00
Vehicles – Unpaved Roads	0.00	0.02	7.54	1.87	100.00
All Sources	100.00	100.00	100.00	100.00	100.00

Table 4-24: Emission Inventory for SO_2, NO_X, PM_{10}, $PM_{2.5}$ and dustfall for the six emission source categories in the Ezamokuhle Airshed

	Emission rate (tonnes/annum)				
Emission Source Category	**SO_2**	**NO_X**	**PM_{10}**	**$PM_{2.5}$**	**TPM**
Power Generation	0.00	0.00	0.00	0.00	
Residential Fuel Burning	7.84	2.90	13.26	13.26	
Waste Burning	0.21	0.54	1.62	1.53	
Biomass Burning	0.15	0.03	1.21	1.20	
Vehicles – Paved Roads	0.18	25.02	0.47	0.47	
Vehicles – Unpaved Roads	0.01	2.28	120.23	12.06	421.66
All Sources	8.39	30.77	136.78	28.51	421.66

Table 4-25: Emission source contribution (%) of SO_2, NO_X, PM_{10}, $PM_{2.5}$ and dustfall as a function of the six emission source categories for the Ezamokuhle Airshed

	Emission Source Contribution (%)				
Emission Source Category	**SO_2**	**NO_X**	**PM_{10}**	**$PM_{2.5}$**	**TPM**
Power Generation	0.00	0.00	0.00	0.00	0.00
Residential Fuel Burning	93.48	9.44	9.69	46.50	0.00
Waste Burning	2.53	1.75	1.18	5.37	0.00
Biomass Burning	1.76	0.10	0.88	4.20	0.00
Vehicles – Paved Roads	2.13	81.32	0.34	1.64	0.00
Vehicles – Unpaved Roads	0.10	7.40	87.90	42.29	100.00
All Sources	100.00	100.00	100.00	100.00	100.00

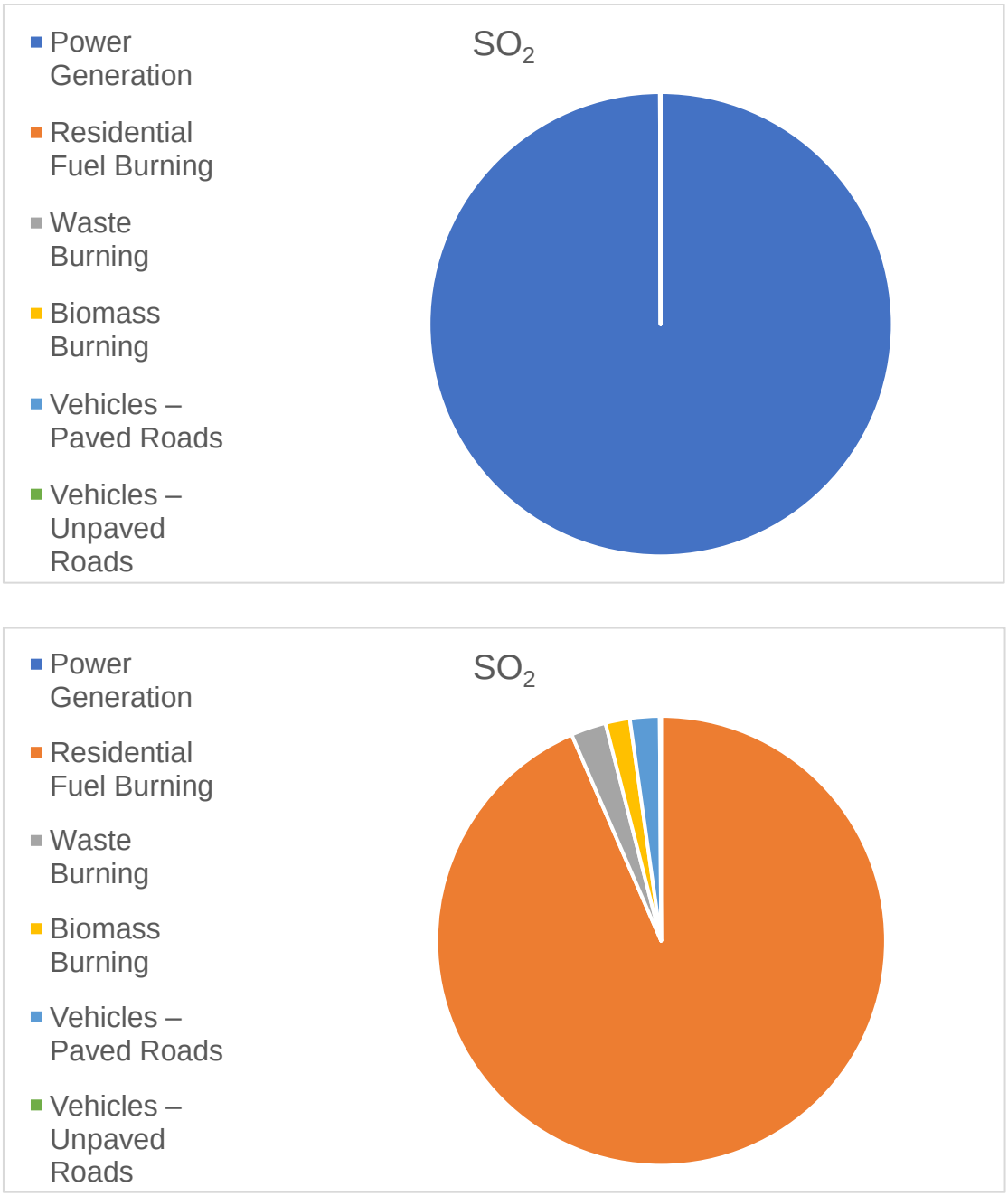

Figure 4-14: Emission source contribution (%) of SO_2 as a function of the six emission source categories for the Greater Ezamokuhle Airshed (top) and for the Ezamokuhle Airshed (bottom)

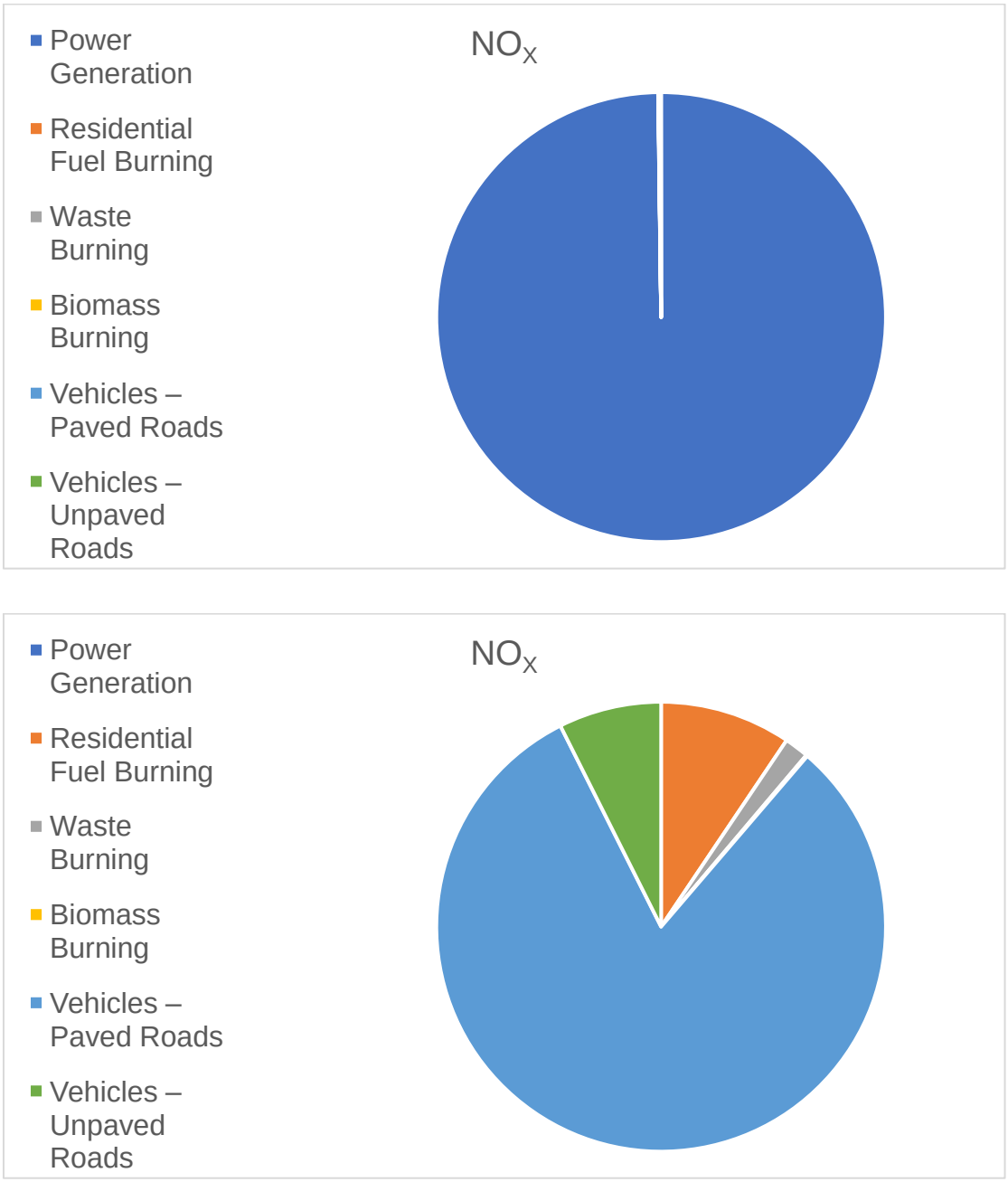

Figure 4-15: Emission source contribution (%) of NO_X as a function of the six emission source categories for the Greater Ezamokuhle Airshed (top) and for the Ezamokuhle Airshed (bottom)

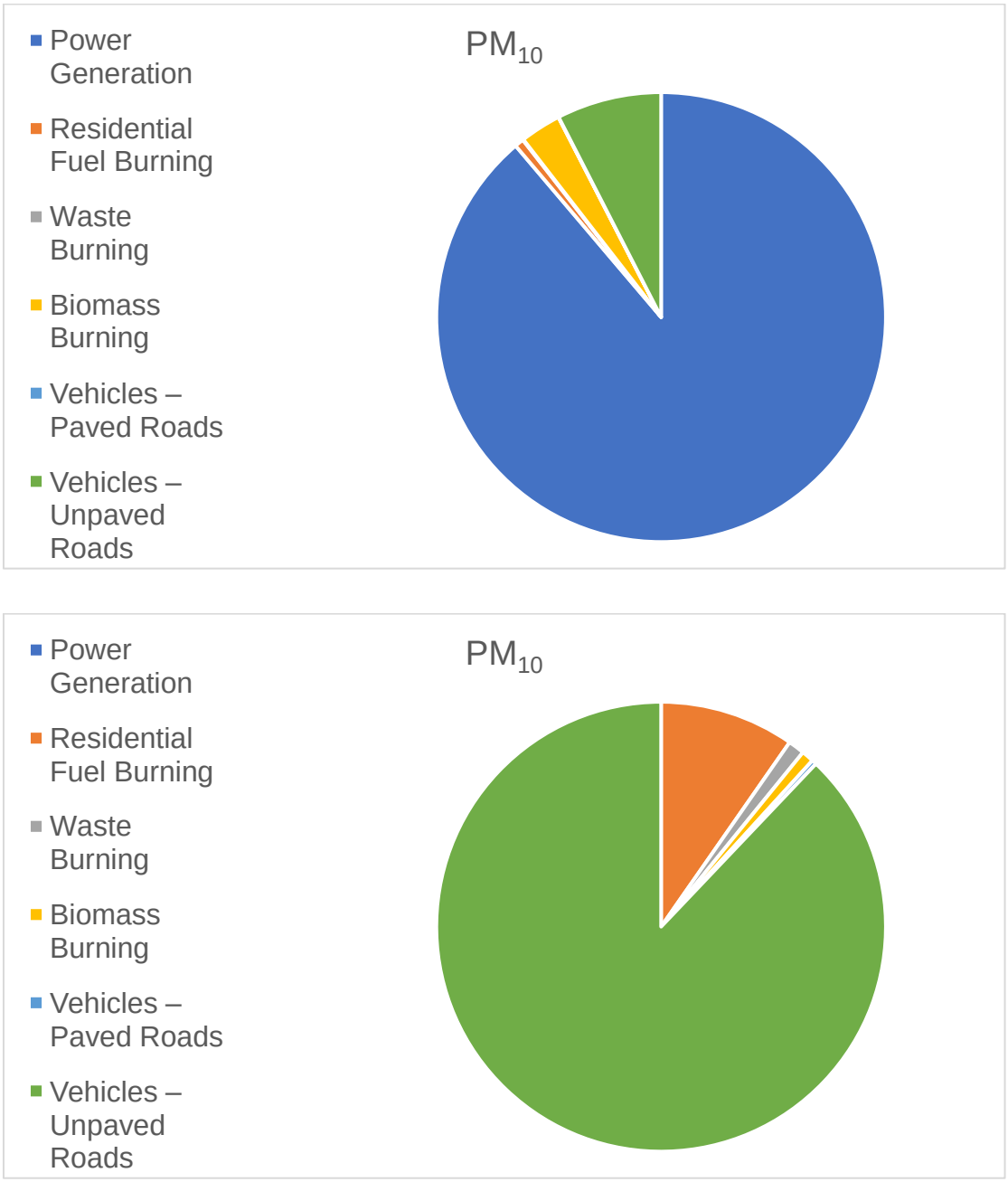

Figure 4-16: Emission source contribution (%) of PM_{10} as a function of the six emission source categories for the Greater Ezamokuhle Airshed (top) and for the Ezamokuhle Airshed (bottom)

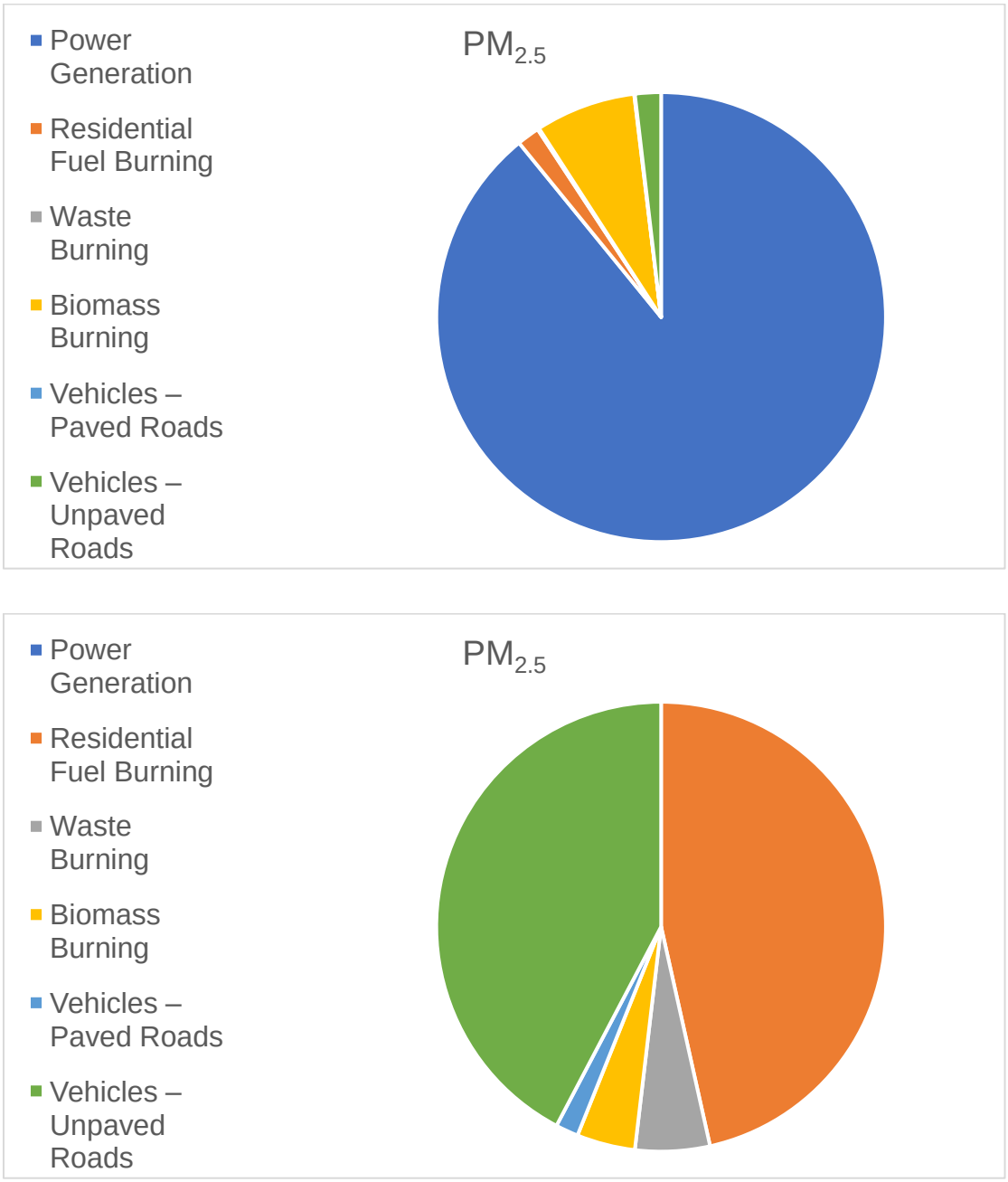

Figure 4-17: Emission source contribution (%) of $PM_{2.5}$ as a function of the six emission source categories for the Greater Ezamokuhle Airshed (top) and for the Ezamokuhle Airshed (bottom)

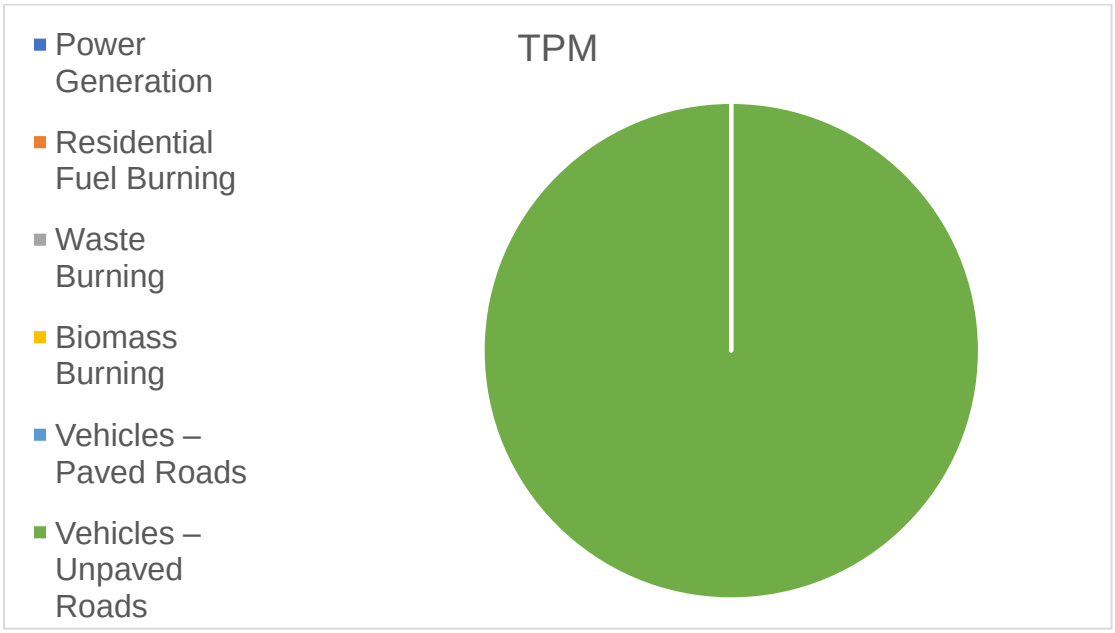

Figure 4-18: Emission source contribution (%) of dustfall as a function of the six emission source categories for the Greater Ezamokuhle Airshed and for the Ezamokuhle Airshed

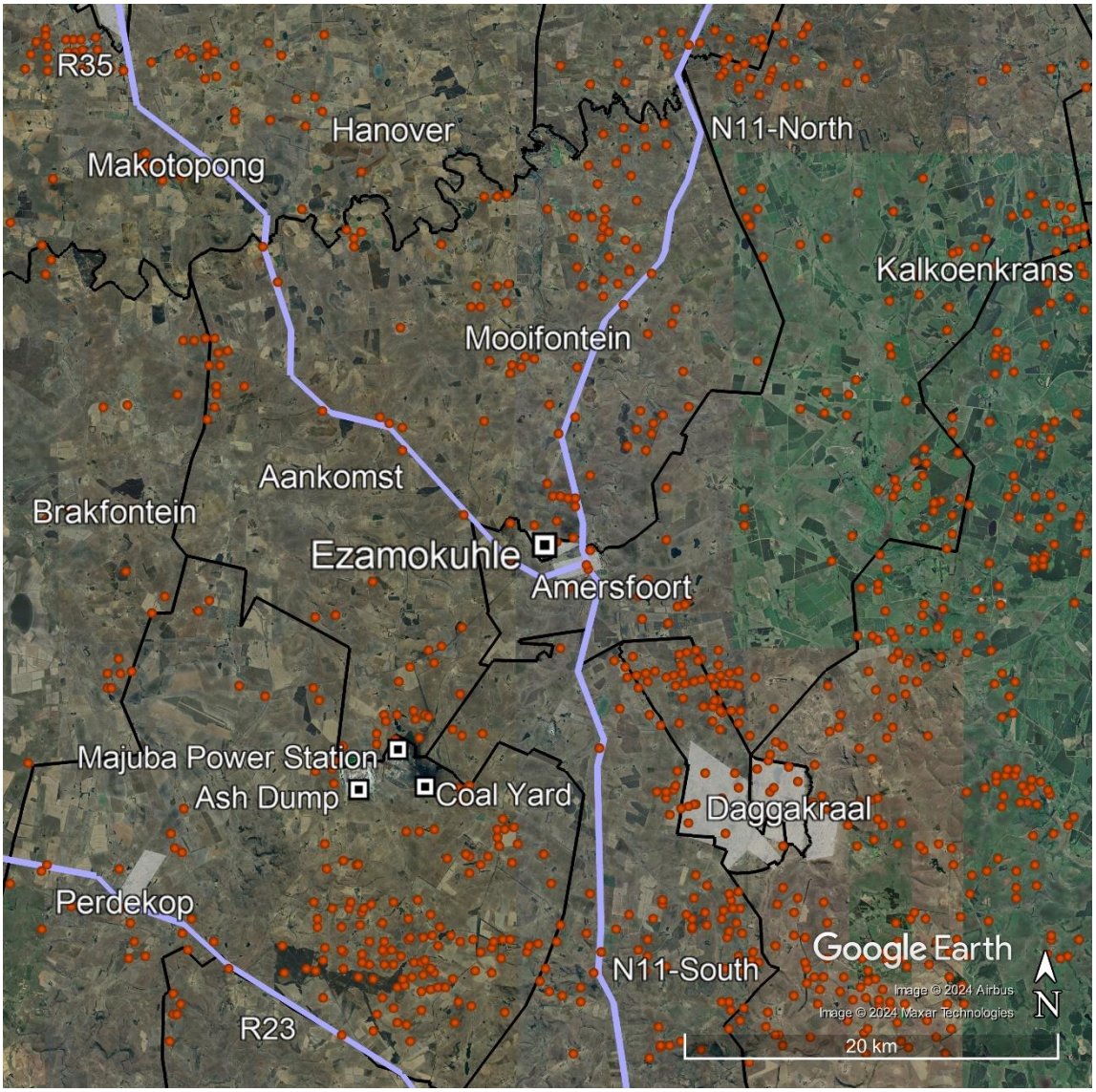

Figure 4-19: Overview of all emission source categories within the Greater Ezamokuhle Airshed

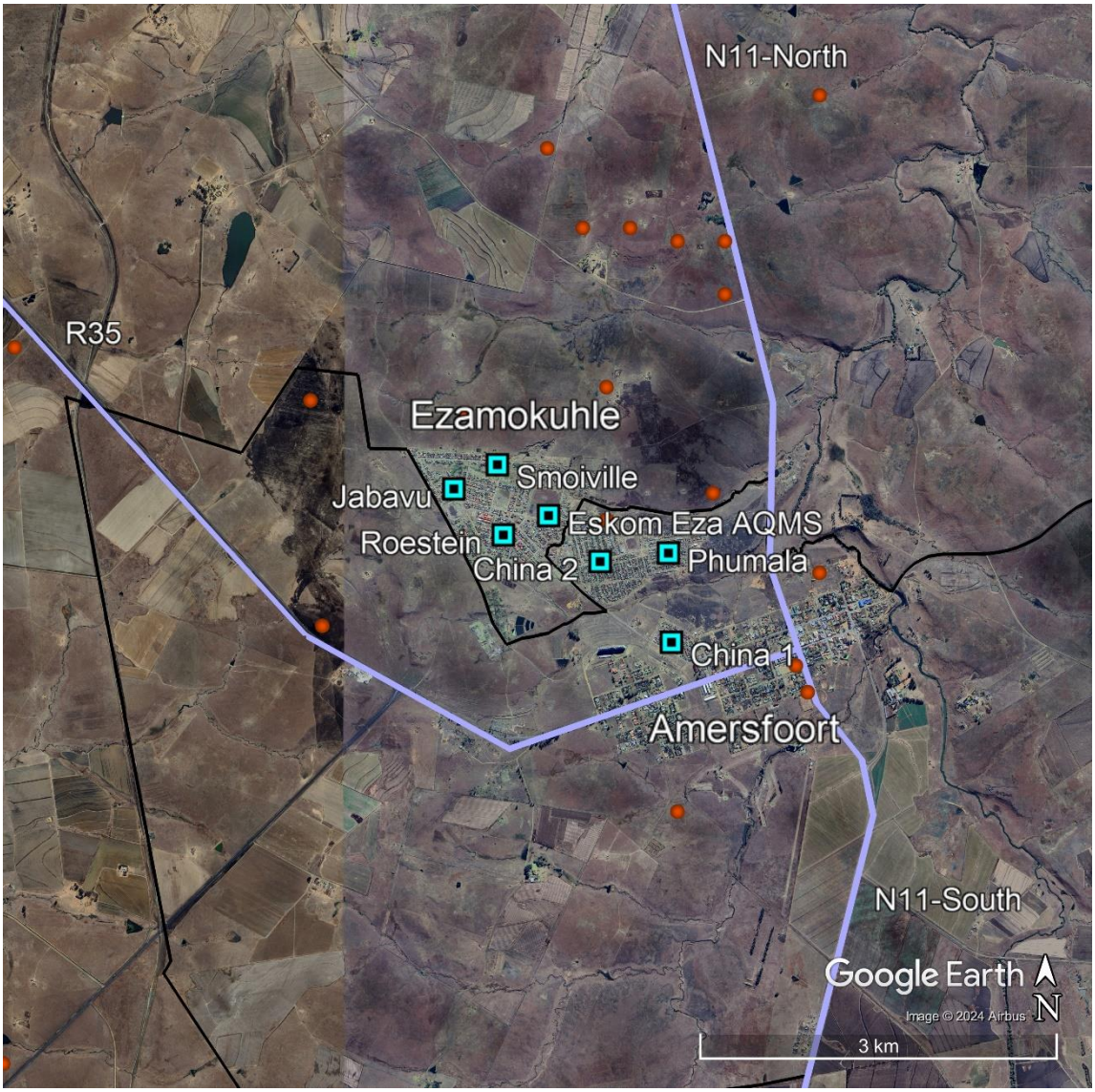

Figure 4-20: Overview of all emission source categories within the Ezamokuhle airshed, together with discrete receptors

5. RESULTS & DISCUSSION

The CALPUFF dispersion model uses mathematical formulations to characterize the atmospheric processes that disperse a pollutant emitted by a source. In this study, the CALPUFF dispersion model was used to predict ambient concentrations and dustfall rates within the modelling domain, based on emissions from seven emission source categories and meteorological data for a three-year period spanning from 2020 to 2022. In this section, model predicted results are presented for SO_2, NO_2, PM_{10} and $PM_{2.5}$ and assessed against the respective NAAQS. Model predicted dustfall rates are presented and assessed against the National Dustfall Standard.

This section is made up of several sub-sections as follows:

- Predicted SO_2 ambient concentrations
    - 1-hour SO_2
    - 24-hour SO_2
    - Annual SO_2
- Predicted NO_2 ambient concentrations
    - 1-hour NO_2
    - Annual NO_2
- Predicted PM_{10} ambient concentrations
    - 24-hour PM_{10}
    - Annual PM_{10}
- Predicted $PM_{2.5}$ ambient concentrations
    - 24-hour $PM_{2.5}$
    - Annual $PM_{2.5}$
- Predicted dustfall rates
- Source Contribution
    - SO_2 ambient concentrations
    - NO_2 ambient concentrations
    - PM_{10} ambient concentrations
    - $PM_{2.5}$ ambient concentrations

In each subsection for SO_2, NO_2, PM_{10} and $PM_{2.5}$, model predicted ambient concentrations at each discrete receptor and at the point of maximum within the modelling domain, resulting from the seven emission source categories are presented in the form of a table. The 1-hour and 24-hour concentrations are based on the 99^{th} percentile. In the table where dustfall rates are presented, the model predicted dustfall rates are presented at each discrete receptor and at the point of maximum

within the modelling domain, resulting from the Vehicles – Unpaved Roads emission source category as TPM was only considered for this emission source category.

This is then followed by bar graphs which graphically illustrate the respective predicted ambient concentrations or dustfall rates at each of the discrete receptors for each source category. Below each graph is a corresponding contour plot representing the respective model predicted ambient concentrations or dustfall rates throughout the Greater Ezamokuhle Airshed. Contour plots representing model predicted ambient concentrations for the Ezamokuhle airshed is only presented for the All Sources category.

5.1 PREDICTED SO_2 AMBIENT CONCENTRATIONS

5.1.1 1-HOUR SO_2

Model predicted 1-hour SO_2 ambient concentrations at discrete receptors and at the point of maximum for the seven emission source categories are presented in Table 5-1. If applicable, exceedances of the NAAQS are highlighted in red.

Bar graphs for model predicted 1-hour SO_2 ambient concentrations at discrete receptors are presented in the following order:

- Figure 5-1 for the Power Generation emission source category
- Figure 5-3 for the Residential Fuel Burning emission source category
- Figure 5-5 for the Waste Burning emission source category
- Figure 5-7 for the Biomass Burning emission source category
- Figure 5-9 for the Vehicles – Paved Roads emission source category
- Figure 5-11 for the Vehicles – Unpaved Roads emission source category
- Figure 5-13 for the All Sources emission source category

Contour plots for model predicted 1-hour SO_2 ambient concentrations for the Greater Ezamokuhle Airshed are presented in the following order:

- Figure 5-2 for the Power Generation emission source category
- Figure 5-4 for the Residential Fuel Burning emission source category
- Figure 5-6 for the Waste Burning emission source category
- Figure 5-8 for the Biomass Burning emission source category
- Figure 5-10 for the Vehicles – Paved Roads emission source category
- Figure 5-12 for the Vehicles – Unpaved Roads emission source category
- Figure 5-14 for the All Sources emission source category

Contour plots for model predicted 1-hour SO_2 ambient concentrations for the Ezamokuhle airshed is presented in Figure 5-15 for the All Sources emission source category.

With respect to contour plots for the primary and Ezamokuhle airshed, areas of exceedance of the NAAQS is coloured in red.

Table 5-1: Model predicted 1-hour SO_2 ambient concentrations (99th percentile) in µg/m^3 at discrete receptors and at the point of maximum for the seven emission source categories

Discrete Receptors	Power Generation	Residential Fuel Burning	Waste Burning	Biomass Burning	Vehicles – Paved Roads	Vehicles – Unpaved Roads	All Sources
China 1	94.36	16.59	0.55	0.16	0.14	0.02	98.65
China 2	101.12	14.65	0.46	0.15	0.08	0.02	104.01
Phumala	94.38	10.19	0.33	0.15	0.05	0.01	95.19
Jabavu	95.15	31.34	0.66	0.19	0.02	0.01	103.16
Roestein	101.31	24.32	0.53	0.15	0.03	0.01	106.80
Smoiville	94.96	33.92	0.71	0.16	0.02	0.01	100.02
Eskom Eza AQMS	100.72	9.66	0.29	0.15	0.03	0.01	102.75
Eskom Majuba AQMS	141.10	0.38	0.01	0.95	0.01	0.00	141.10
Maximum	201.97	113.09	1.70	3.55	1.65	0.05	201.98
	NAAQS – 1-hour SO_2 (350 µg/m^3)						

According to Table 5-1, model predicted 1-hour SO_2 ambient concentrations are below the 1-hour SO_2 NAAQS of 350 µg/m^3 at all discrete receptors and at the point of maximum for all seven emission source categories, both in the Greater Ezamokuhle Airshed and in the Ezamokuhle Airshed. There are no exceedances of the NAAQS both in the Greater Ezamokuhle Airshed and in the Ezamokuhle Airshed (Figure 3-3).

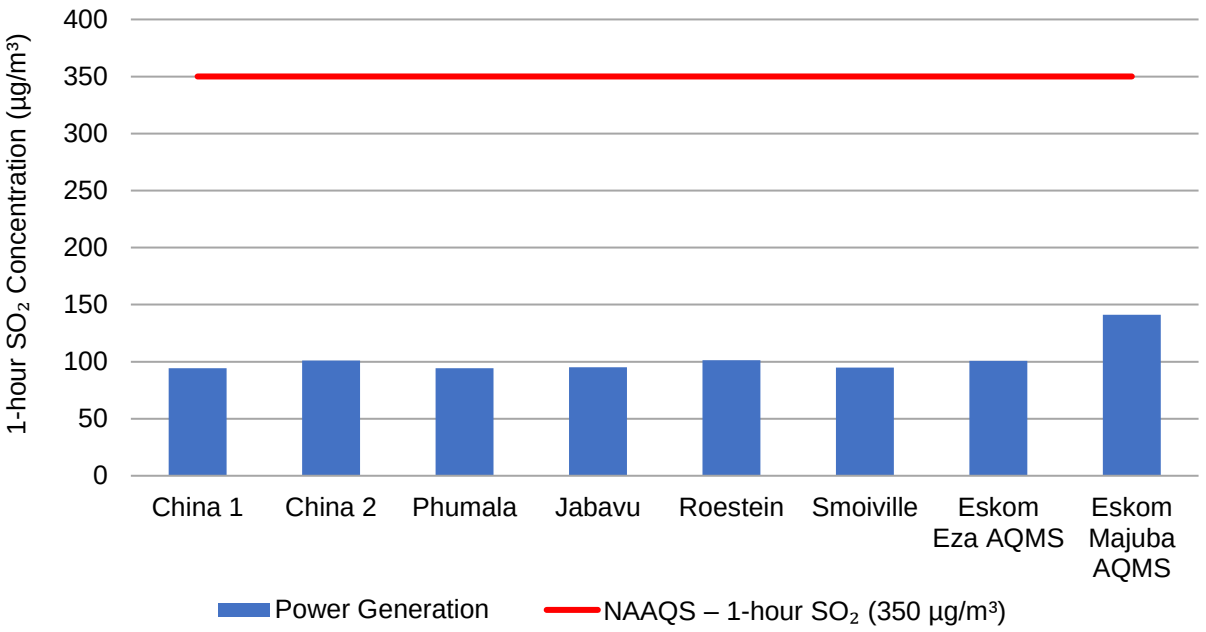

Figure 5-1: Model predicted 1-hour SO_2 ambient concentrations (99th percentile) in µg/m³ at discrete receptors for the Power Generation emission source category

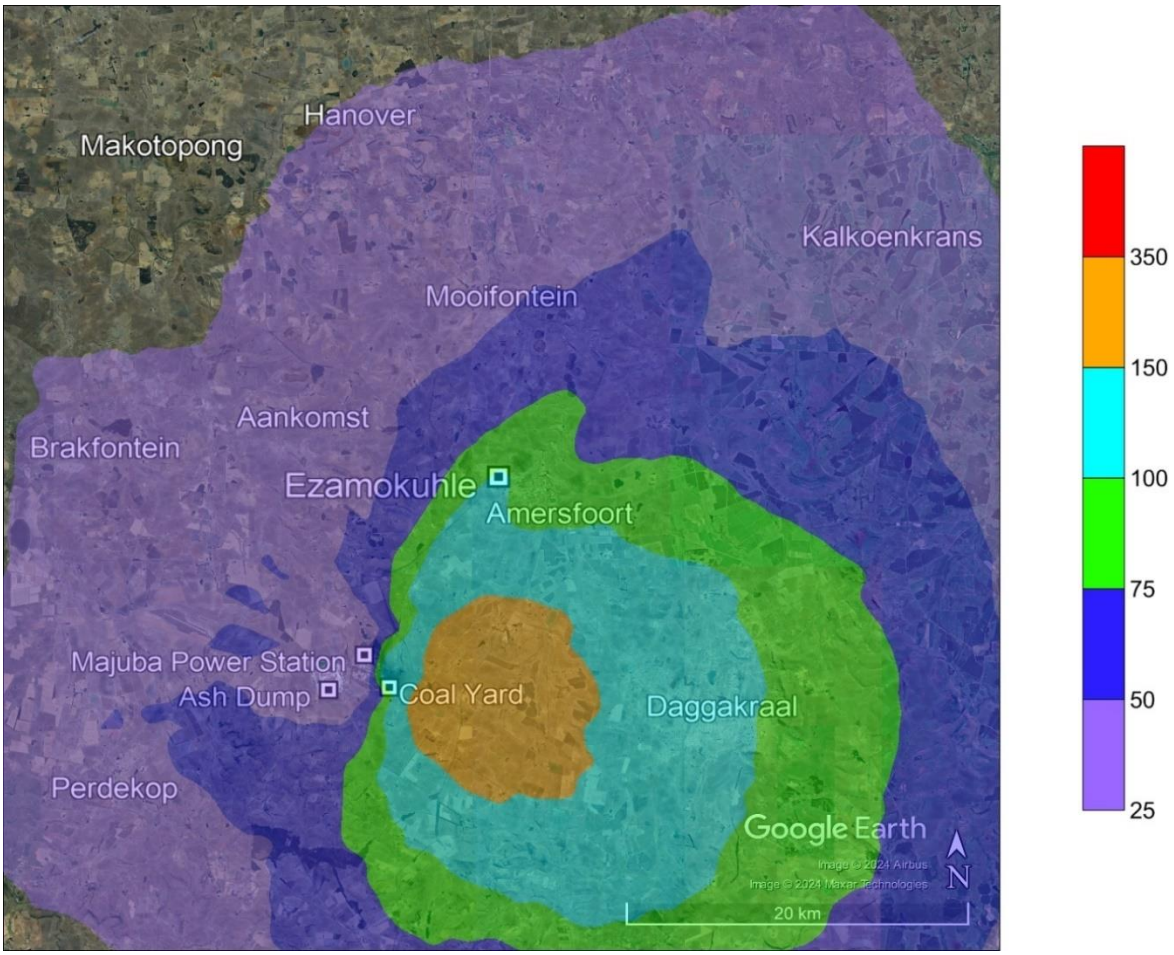

Figure 5-2: Model predicted 1-hour SO_2 ambient concentrations (99th percentile) in µg/m³ for the Power Generation emission source category within the Greater Ezamokuhle Airshed

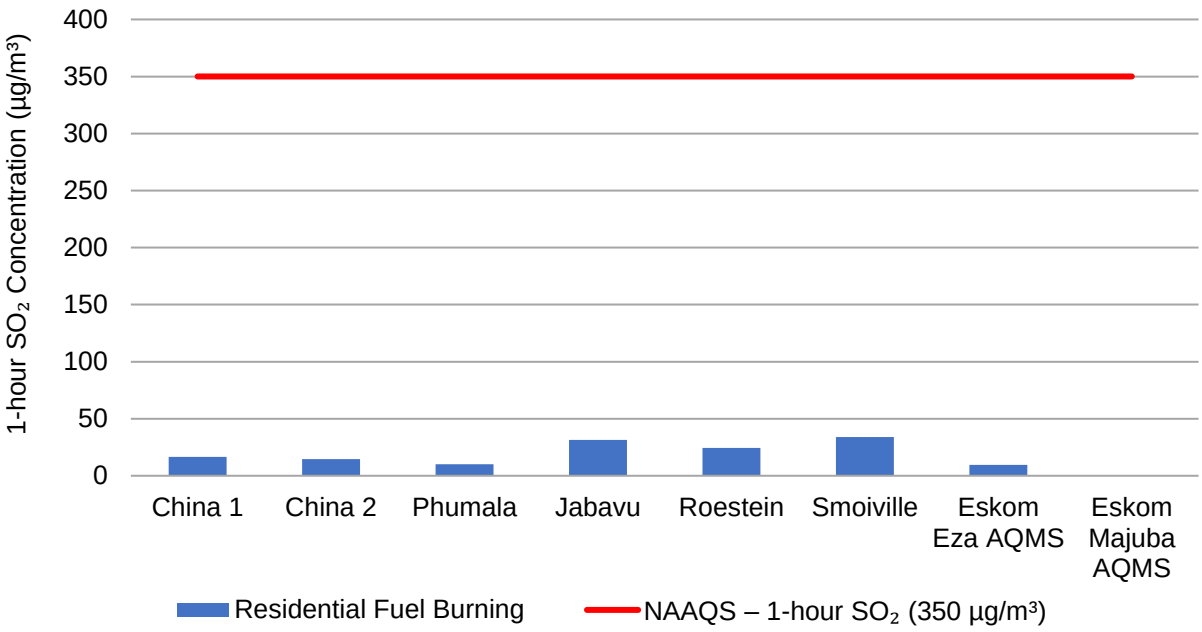

Figure 5-3: Model predicted 1-hour SO_2 ambient concentrations (99th percentile) in µg/m³ at discrete receptors for the Residential Fuel Burning emission source category

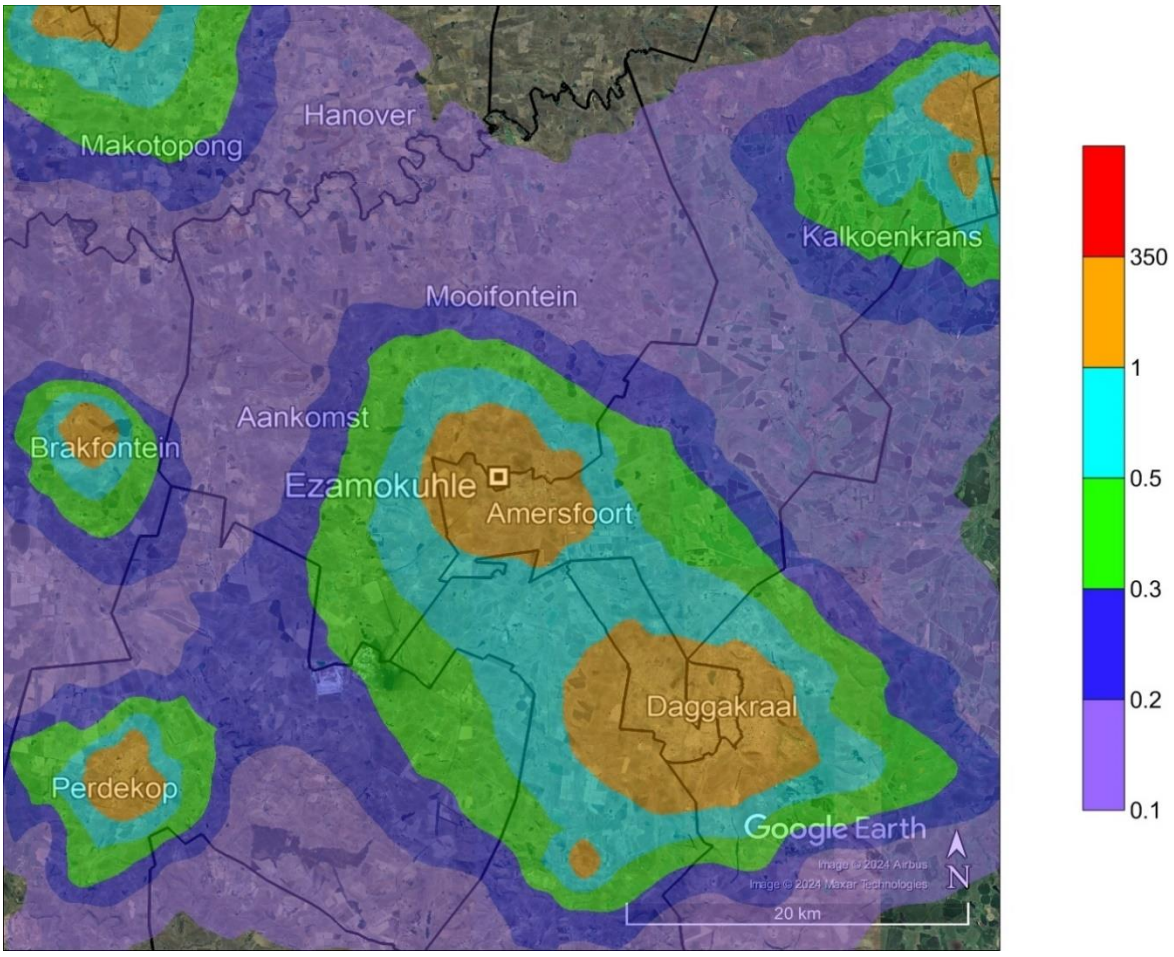

Figure 5-4: Model predicted 1-hour SO_2 ambient concentrations (99th percentile) in µg/m³ for the Residential Fuel Burning emission source category within the Greater Ezamokuhle Airshed

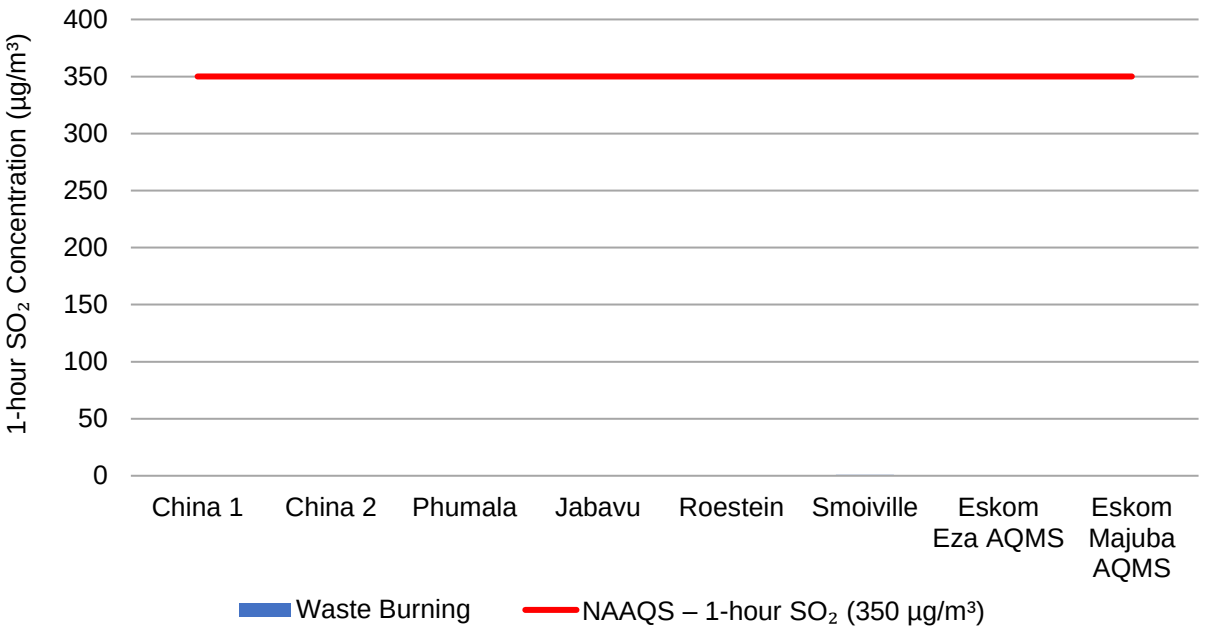

Figure 5-5: Model predicted 1-hour SO_2 ambient concentrations (99th percentile) in µg/m³ at discrete receptors for the Waste Burning emission source category

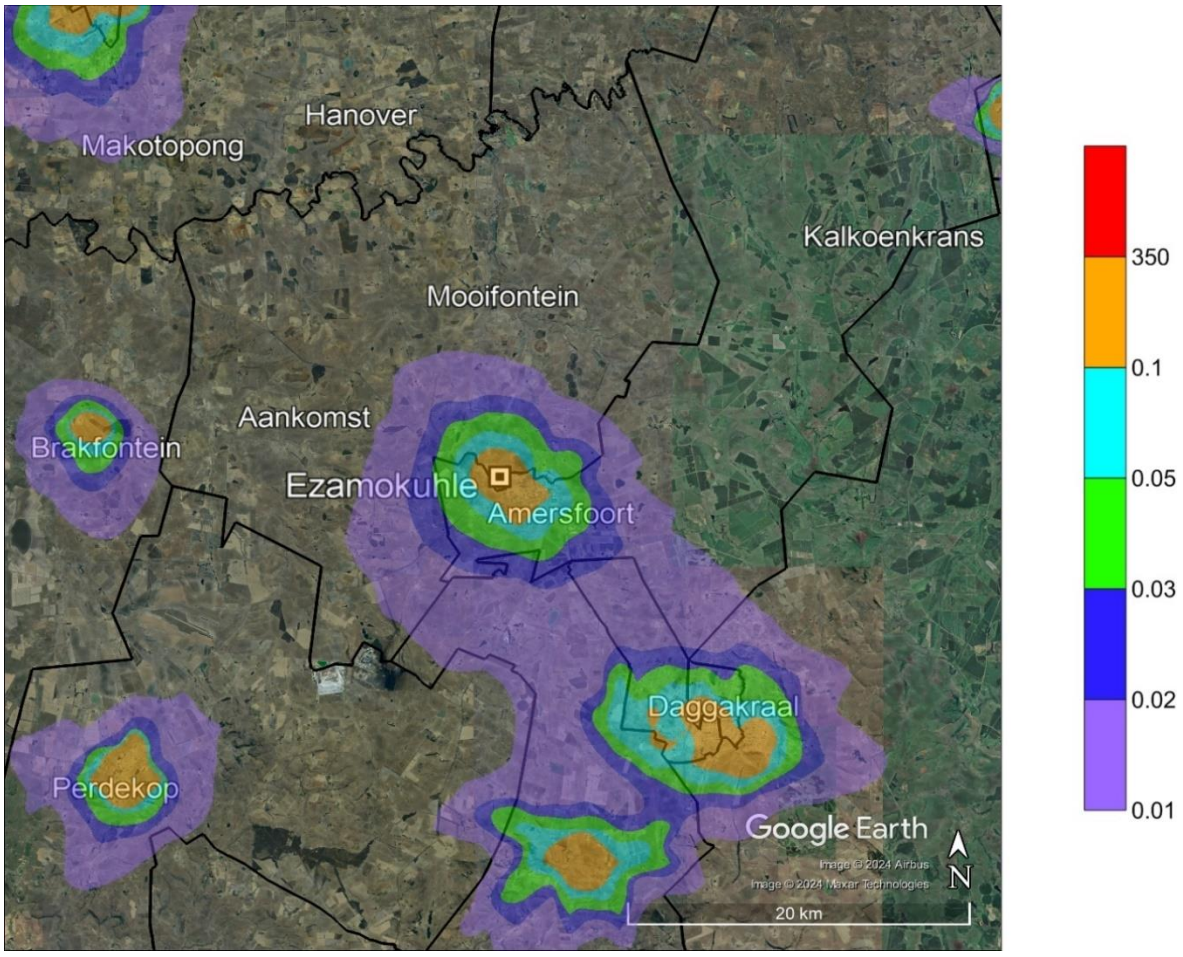

Figure 5-6: Model predicted 1-hour SO_2 ambient concentrations (99th percentile) in µg/m³ for the Waste Burning emission source category within the Greater Ezamokuhle Airshed

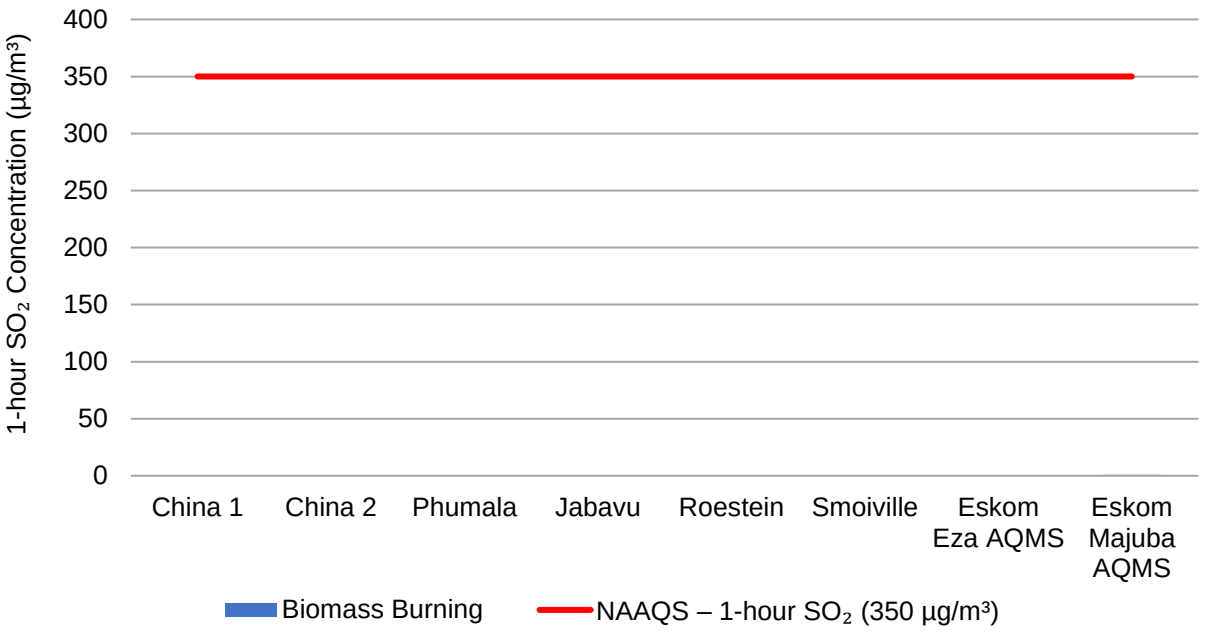

Figure 5-7: Model predicted 1-hour SO_2 ambient concentrations (99th percentile) in µg/m³ at discrete receptors for the Biomass Burning emission source category

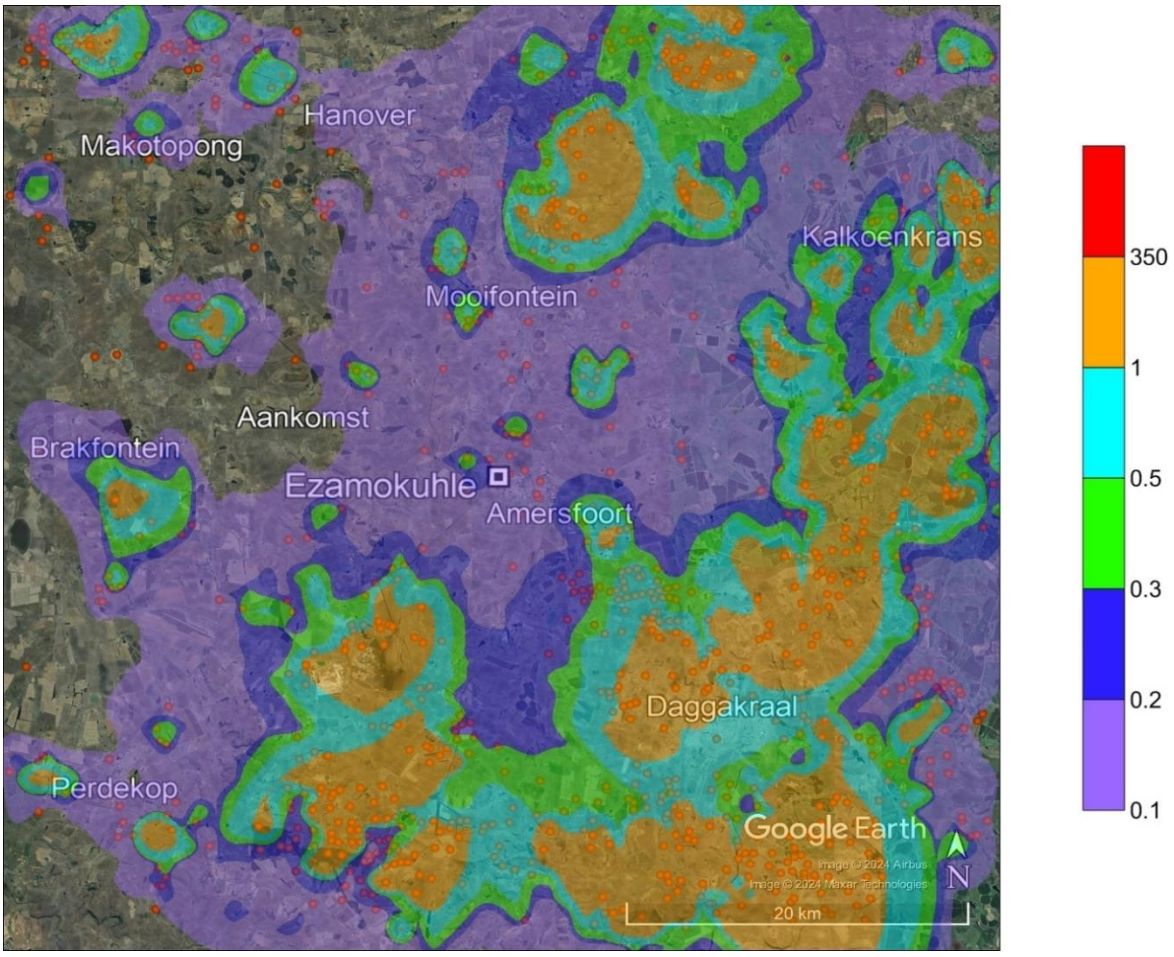

Figure 5-8: Model predicted 1-hour SO_2 ambient concentrations (99th percentile) in µg/m³ for the Biomass Burning emission source category within the Greater Ezamokuhle Airshed

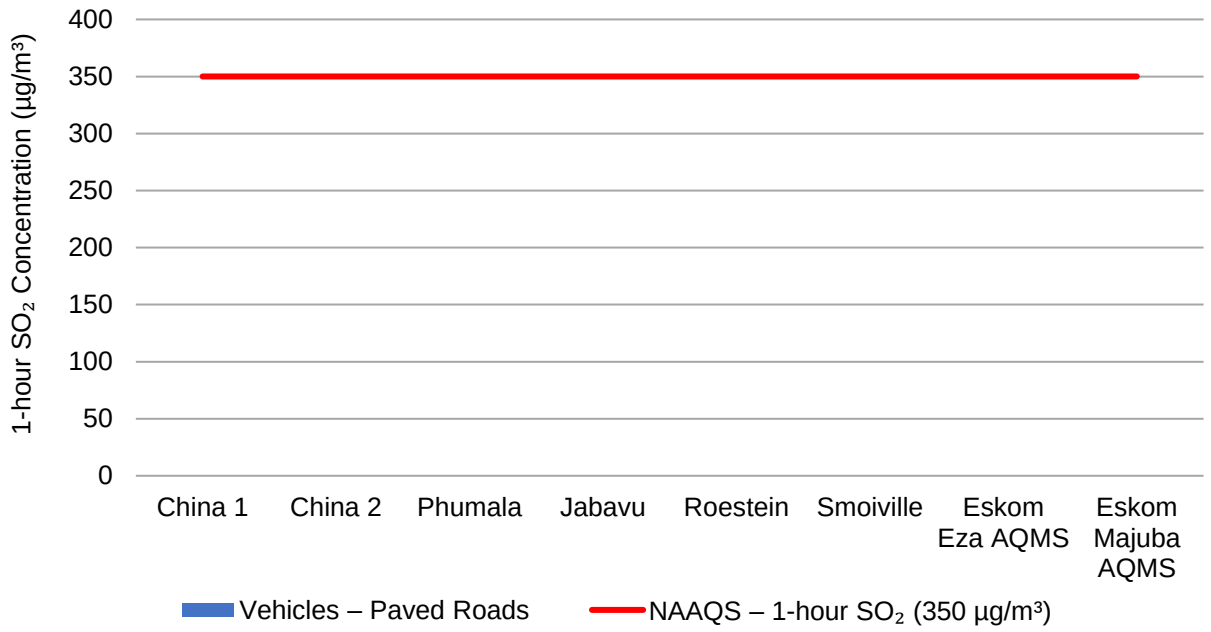

Figure 5-9: Model predicted 1-hour SO_2 ambient concentrations (99th percentile) in µg/m³ at discrete receptors for the Vehicles – Paved Roads emission source category

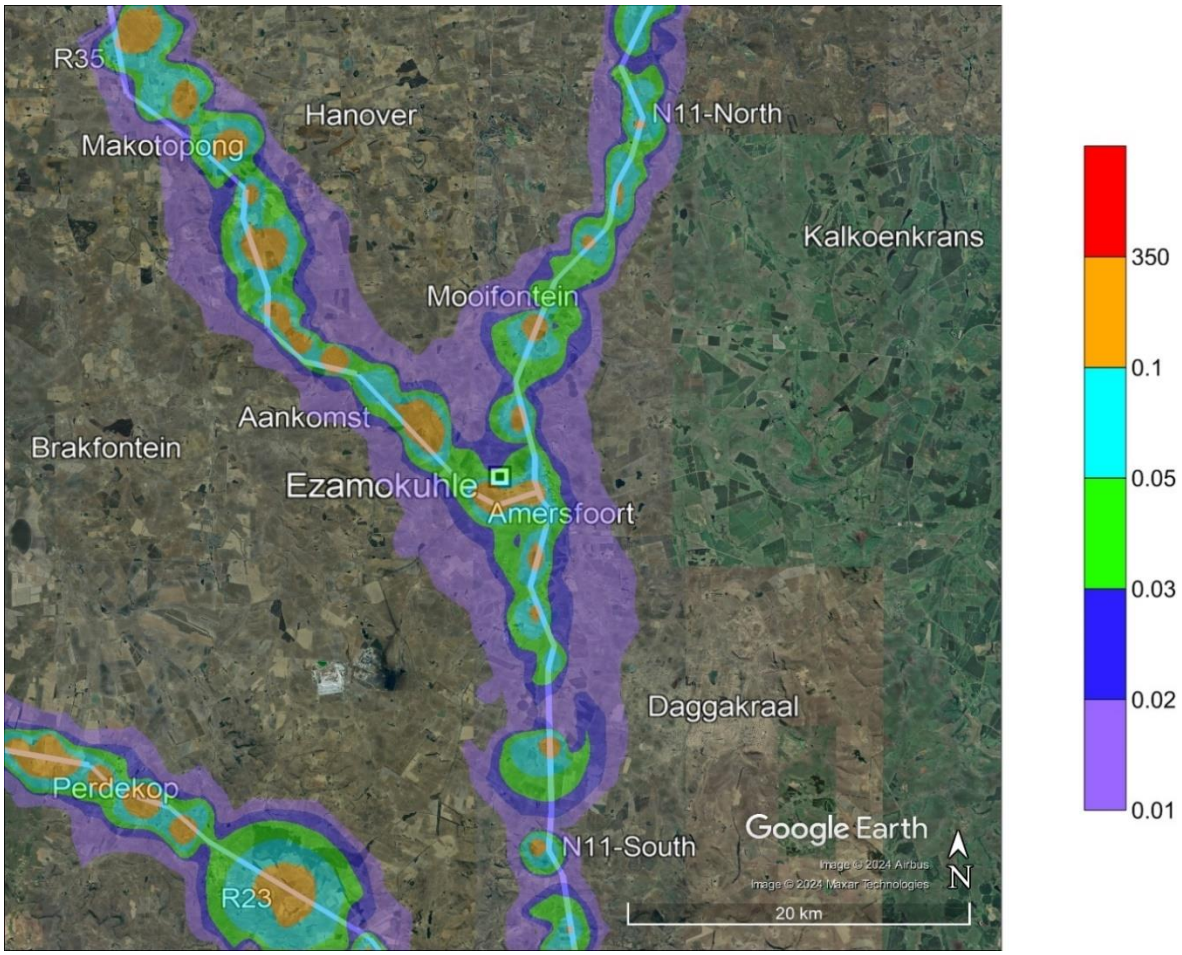

Figure 5-10: Model predicted 1-hour SO_2 ambient concentrations (99th percentile) in µg/m³ for the Vehicles – Paved Roads emission source category within the Greater Ezamokuhle Airshed

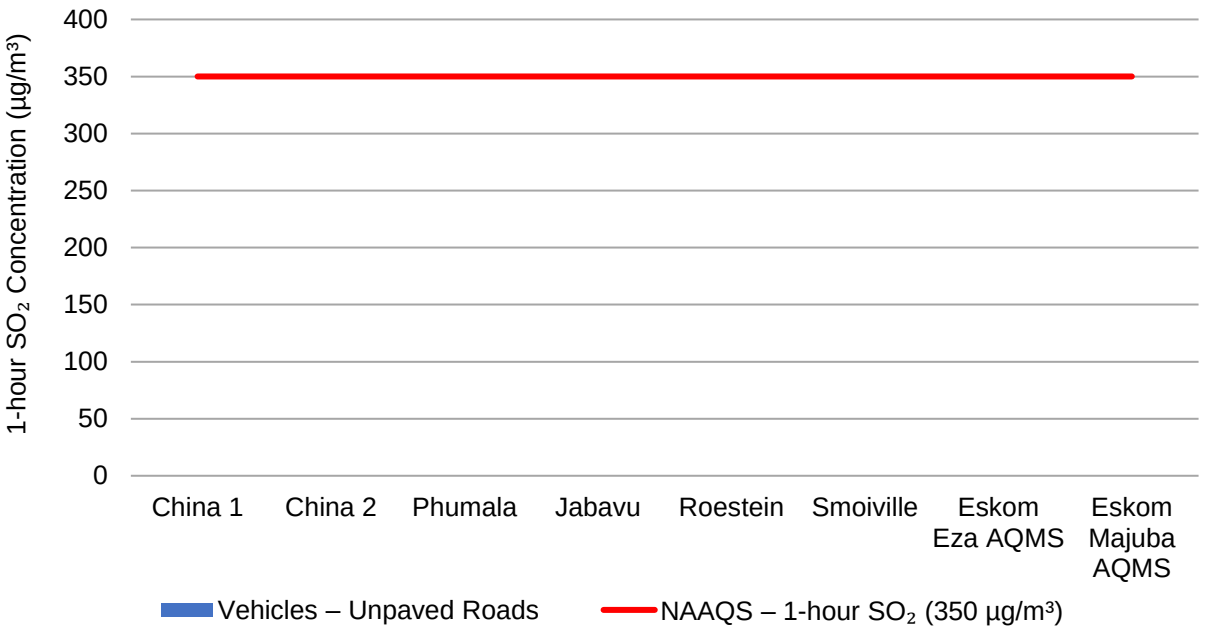

Figure 5-11: Model predicted 1-hour SO_2 ambient concentrations (99th percentile) in µg/m³ at discrete receptors for the Vehicles – Unpaved Roads emission source category

Figure 5-12: Model predicted 1-hour SO_2 ambient concentrations (99th percentile) in µg/m³ for the Vehicles – Unpaved Roads emission source category within the Greater Ezamokuhle Airshed

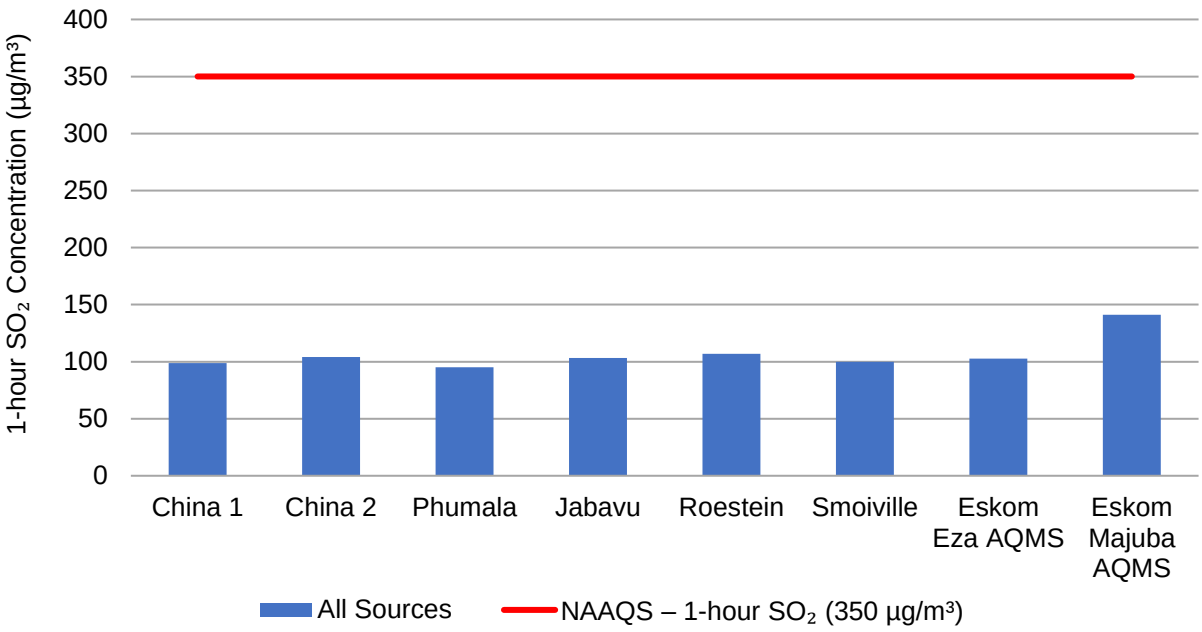

Figure 5-13: Model predicted 1-hour SO_2 ambient concentrations (99th percentile) in µg/m³ at discrete receptors for the All Sources emission source category

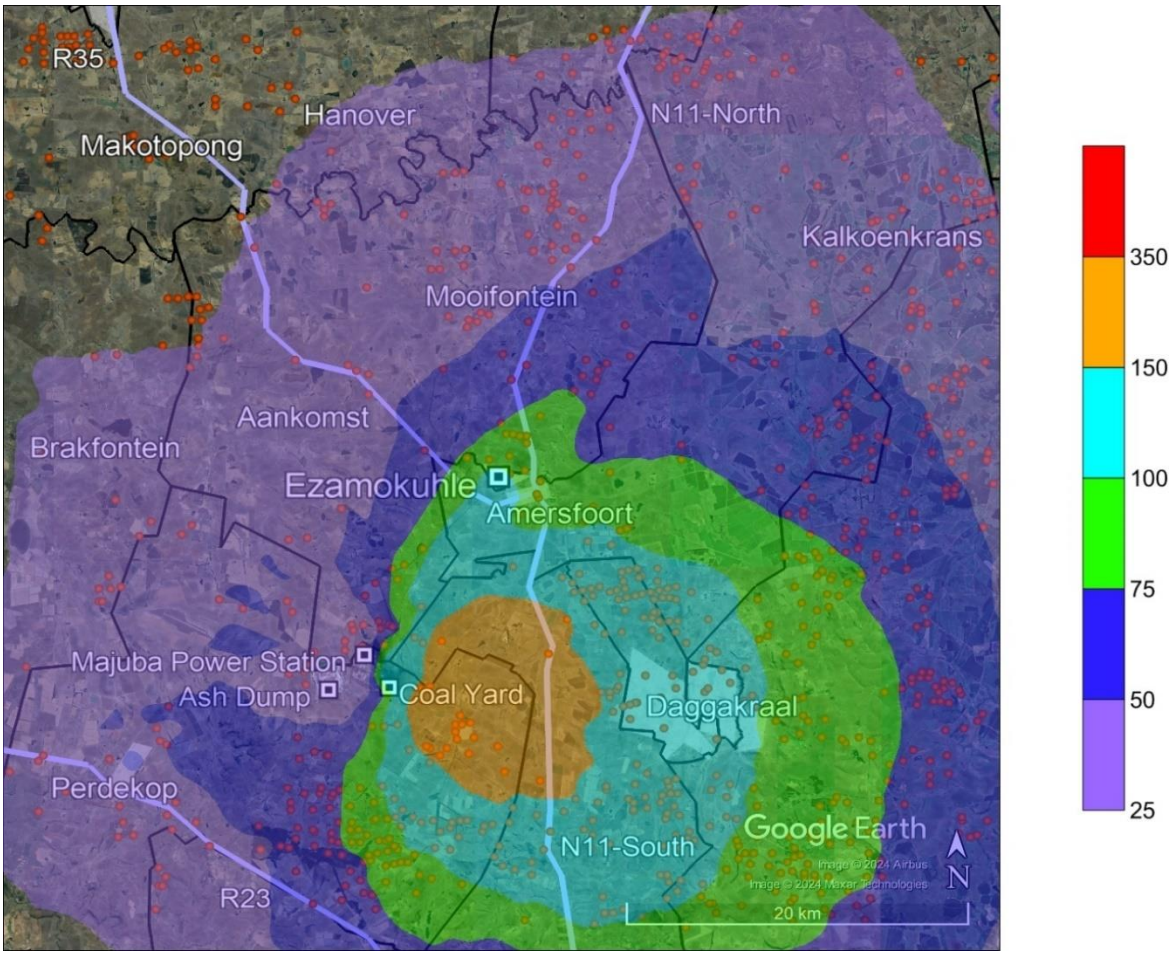

Figure 5-14: Model predicted 1-hour SO_2 ambient concentrations (99th percentile) in µg/m³ for the All Sources emission source category within the Greater Ezamokuhle Airshed

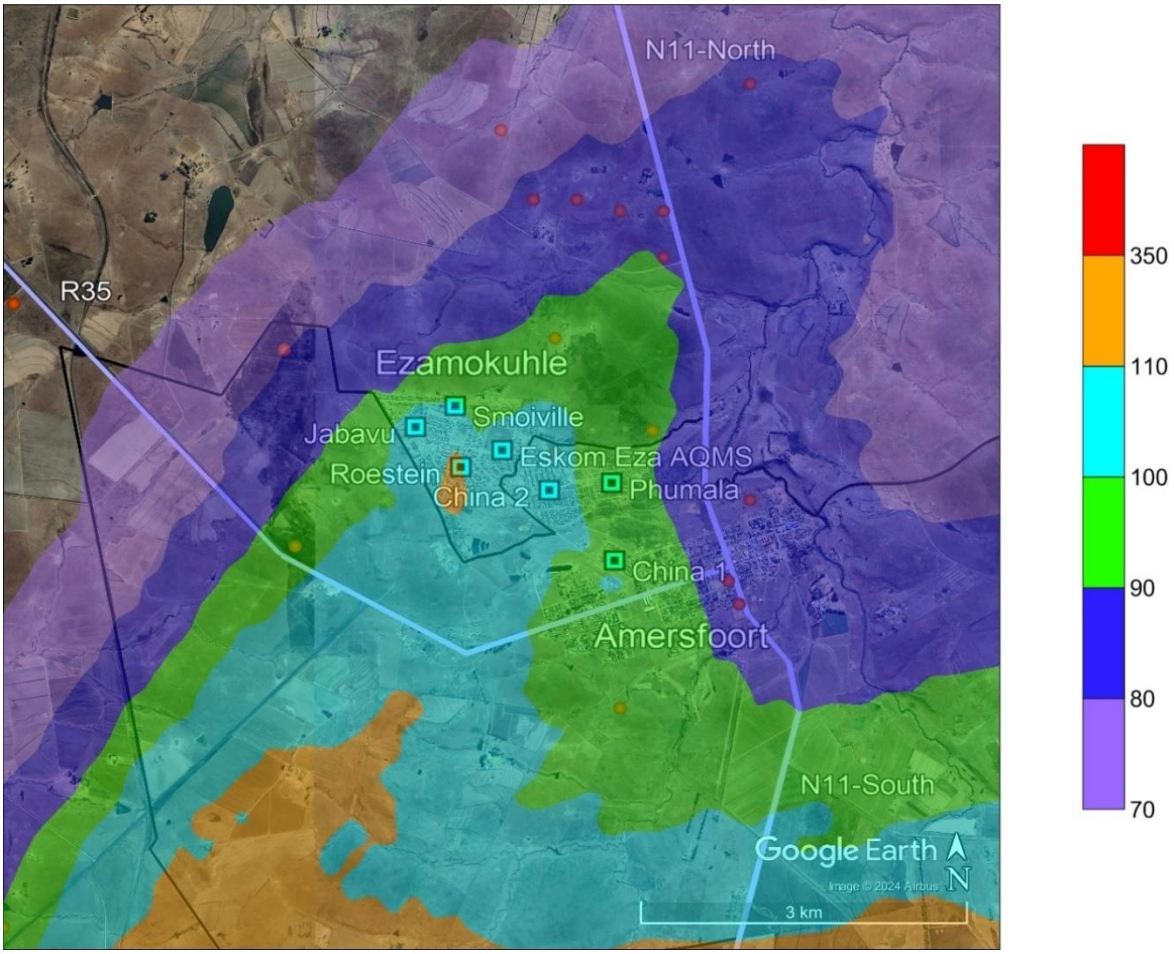

Figure 5-15: Model predicted 1-hour SO_2 ambient concentrations (99th percentile) in µg/m^3 for the All Sources emission source category within Ezamokuhle airshed

5.1.2 24-HOUR SO_2

Model predicted 24-hour SO_2 ambient concentrations at discrete receptors and at the point of maximum for the seven emission source categories are presented in Table 5-2. If applicable, exceedances of the NAAQS are highlighted in red.

Bar graphs for model predicted 24-hour SO_2 ambient concentrations at discrete receptors are presented in the following order:

- Figure 5-16 for the Power Generation emission source category
- Figure 5-18 for the Residential Fuel Burning emission source category
- Figure 5-20 for the Waste Burning emission source category
- Figure 5-22 for the Biomass Burning emission source category
- Figure 5-24 for the Vehicles – Paved Roads emission source category
- Figure 5-26 for the Vehicles – Unpaved Roads emission source category
- Figure 5-28 for the All Sources emission source category

Contour plots for model predicted 24-hour SO_2 ambient concentrations for the Greater Ezamokuhle Airshed are presented in the following order:

- Figure 5-17 for the Power Generation emission source category
- Figure 5-19 for the Residential Fuel Burning emission source category
- Figure 5-21 for the Waste Burning emission source category
- Figure 5-23 for the Biomass Burning emission source category
- Figure 5-25 for the Vehicles – Paved Roads emission source category
- Figure 5-27 for the Vehicles – Unpaved Roads emission source category
- Figure 5-29 for the All Sources emission source category

Contour plots for model predicted 24-hour SO_2 ambient concentrations for the Ezamokuhle airshed is presented in Figure 5-30 for the All Sources emission source category.

With respect to contour plots for the primary and Ezamokuhle airshed, areas of exceedance of the NAAQS is coloured in red.

Table 5-2: Model predicted 24-hour SO_2 ambient concentrations (99th percentile) in µg/m^3 at discrete receptors and at the point of maximum for the seven emission source categories

Discrete Receptors	Power Generation	Residential Fuel Burning	Waste Burning	Biomass Burning	Vehicles – Paved Roads	Vehicles – Unpaved Roads	All Sources
China 1	40.58	8.74	0.29	0.08	0.06	0.01	45.86
China 2	42.27	7.92	0.25	0.07	0.03	0.01	46.60
Phumala	41.52	4.90	0.16	0.07	0.02	0.01	43.38
Jabavu	45.65	17.50	0.36	0.09	0.01	0.01	53.62
Roestein	44.36	12.98	0.28	0.07	0.01	0.01	49.44
Smoiville	40.29	18.44	0.39	0.07	0.01	0.01	49.73
Eskom Eza AQMS	42.44	4.46	0.13	0.07	0.02	0.00	43.92
Eskom Majuba AQMS	73.82	0.11	0.00	0.51	0.00	0.00	74.00
Maximum	110.85	47.62	0.84	2.14	0.54	0.02	111.68
	NAAQS – 24-hour SO_2 (125 µg/m^3)						

According to Table 5-2, model predicted 24-hour SO_2 ambient concentrations are below the 24-hour SO_2 NAAQS of 125 µg/m^3 at all discrete receptors and at the point of maximum for all seven emission source categories, both in the Greater Ezamokuhle Airshed and in the Ezamokuhle Airshed. There are no exceedances of the NAAQS both in the Greater Ezamokuhle Airshed and in the Ezamokuhle Airshed.

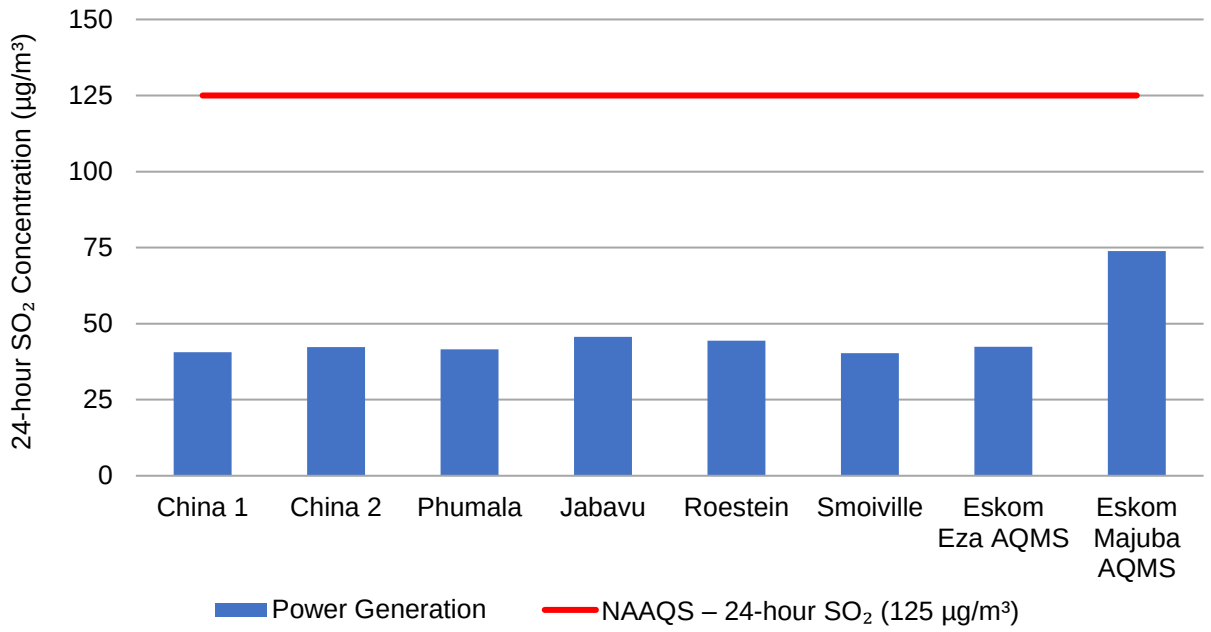

Figure 5-16: Model predicted 24-hour SO_2 ambient concentrations (99th percentile) in µg/m^3 at discrete receptors for the Power Generation emission source category

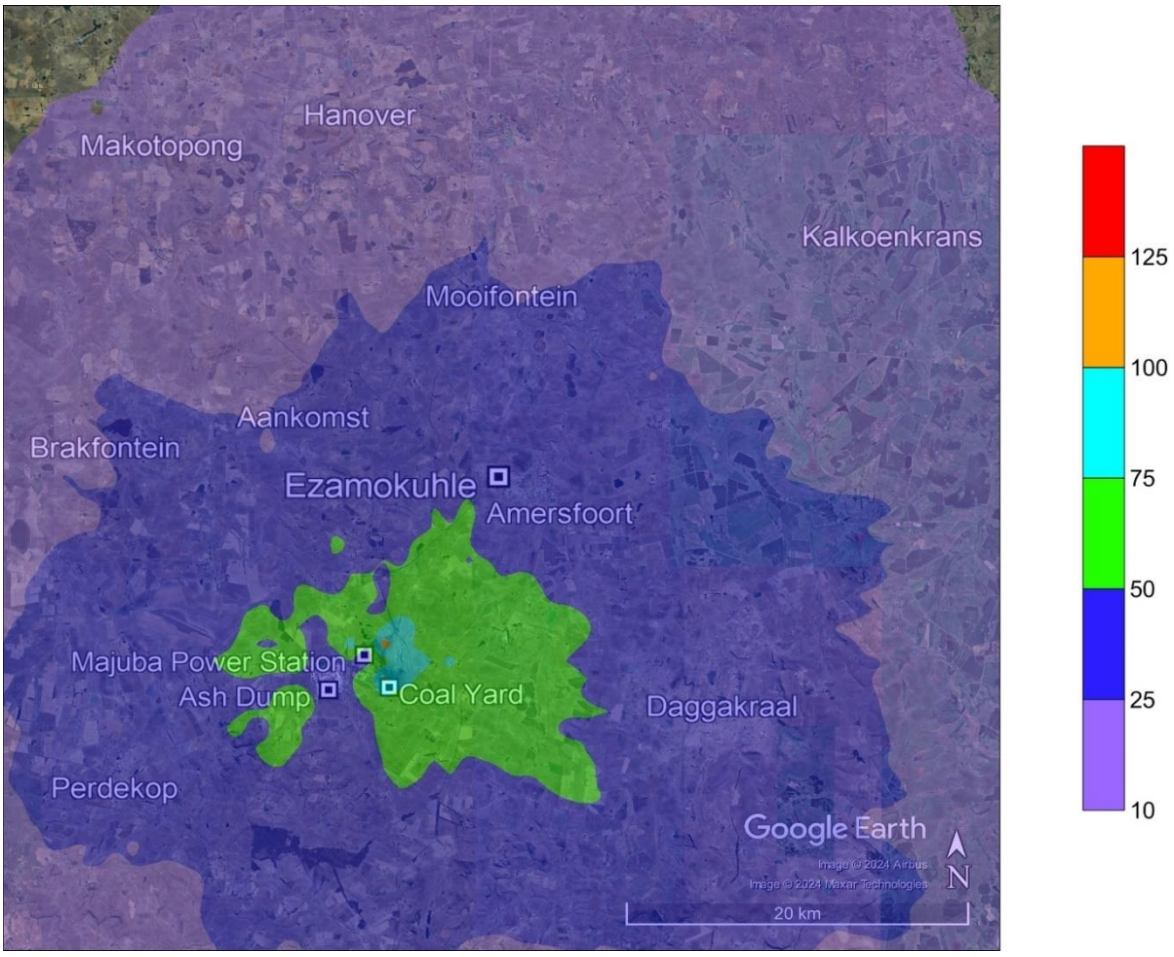

Figure 5-17: Model predicted 24-hour SO_2 ambient concentrations (99th percentile) in µg/m^3 for the Power Generation emission source category within the Greater Ezamokuhle Airshed

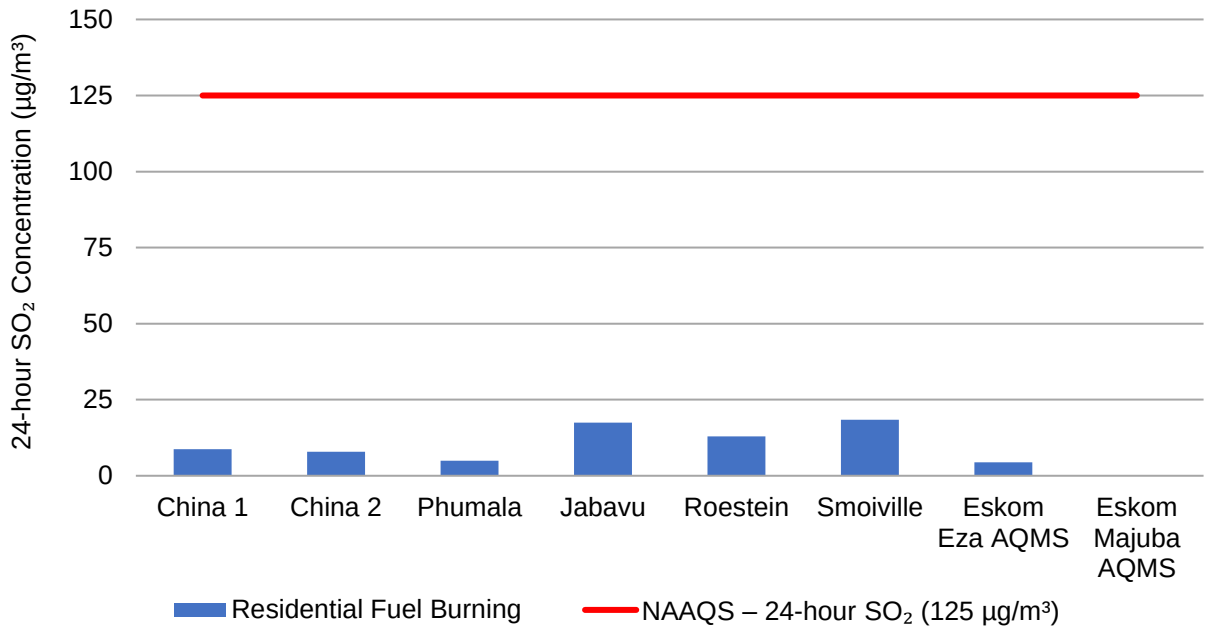

Figure 5-18: Model predicted 24-hour SO_2 ambient concentrations (99th percentile) in µg/m³ at discrete receptors for the Residential Fuel Burning emission source category

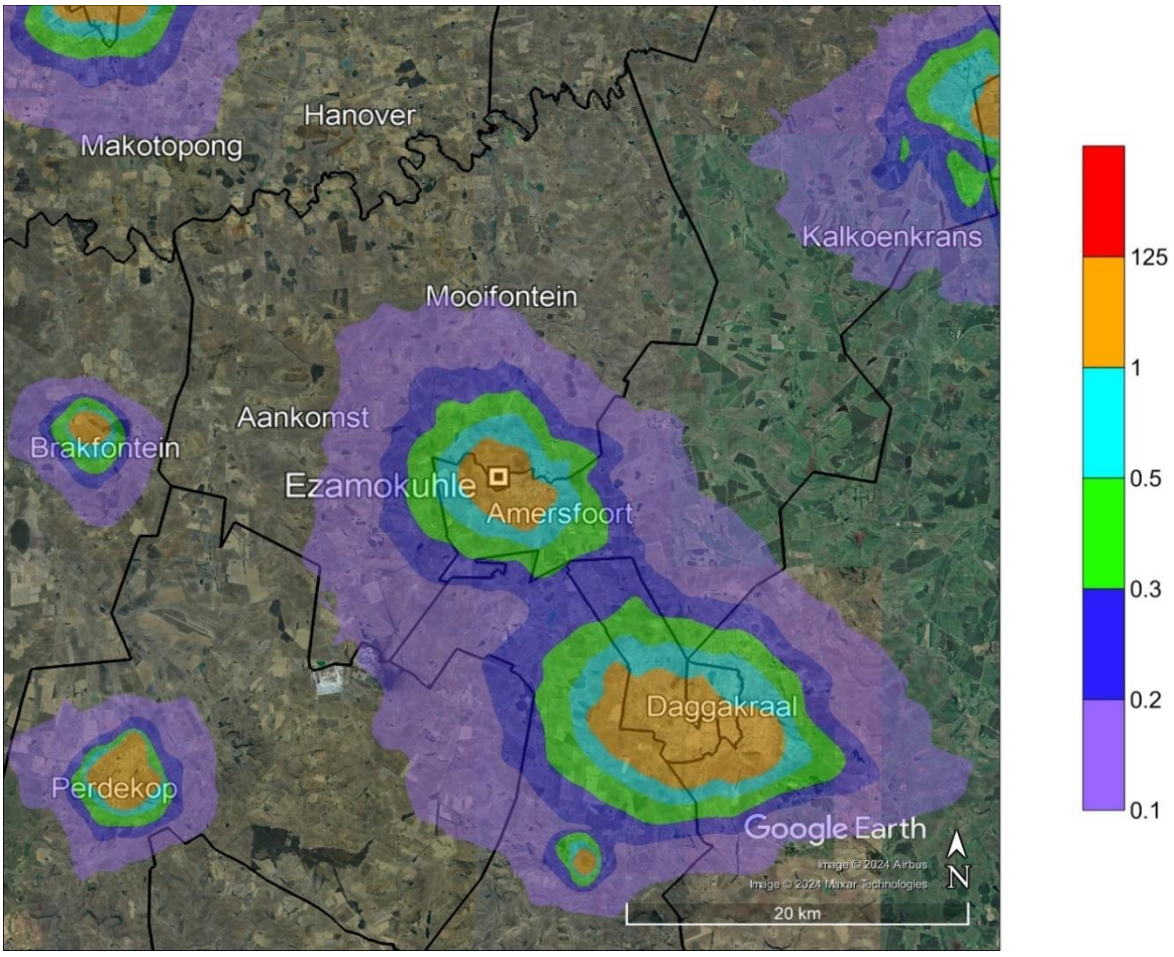

Figure 5-19: Model predicted 24-hour SO_2 ambient concentrations (99th percentile) in µg/m³ for the Residential Fuel Burning emission source category within the Greater Ezamokuhle Airshed

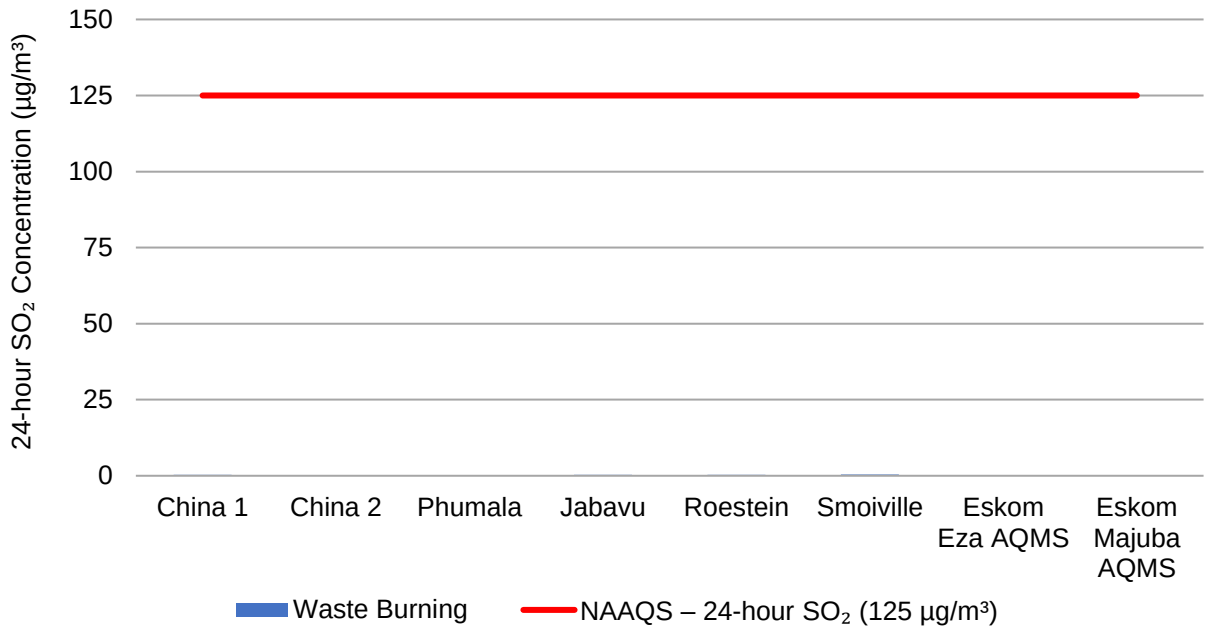

Figure 5-20: Model predicted 24-hour SO_2 ambient concentrations (99th percentile) in µg/m³ at discrete receptors for the Waste Burning emission source category

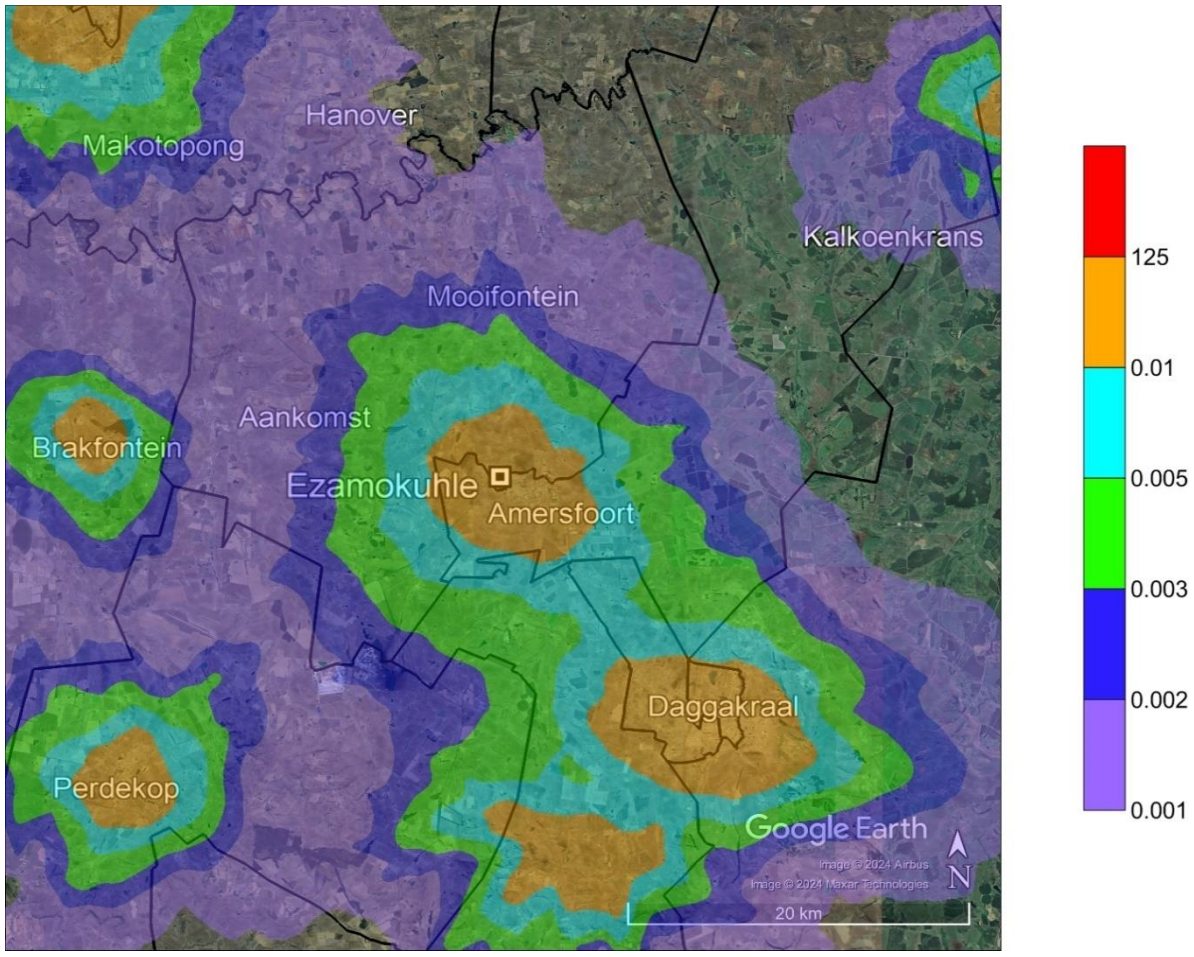

Figure 5-21: Model predicted 24-hour SO_2 ambient concentrations (99th percentile) in µg/m³ for the Waste Burning emission source category within the Greater Ezamokuhle Airshed

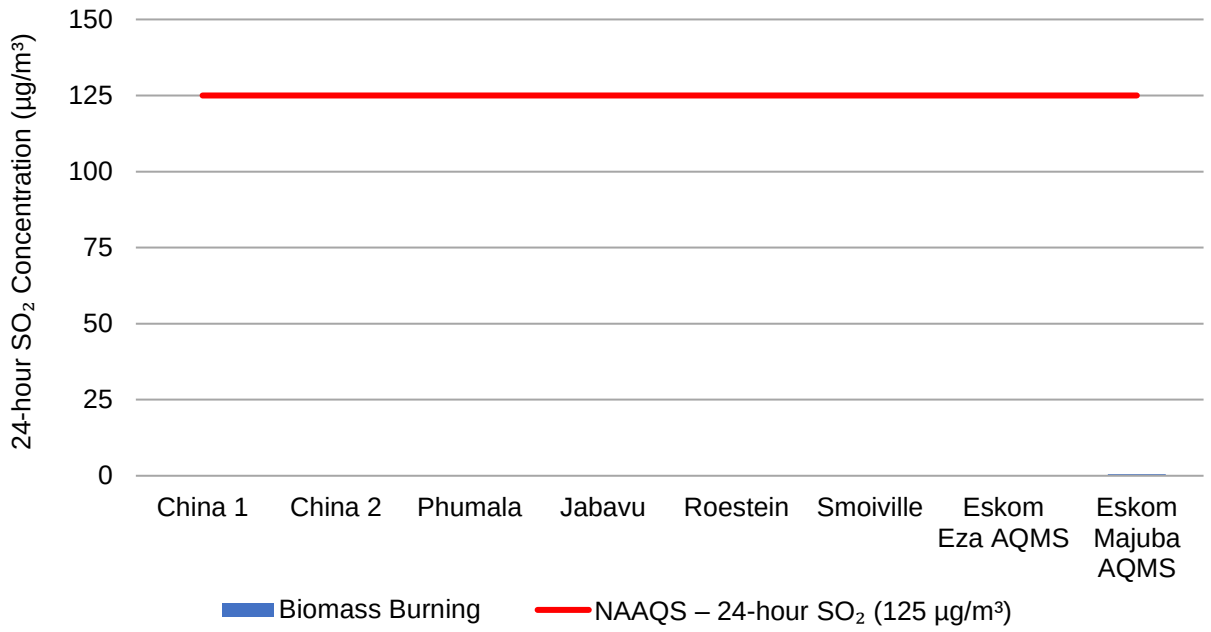

Figure 5-22: Model predicted 24-hour SO_2 ambient concentrations (99th percentile) in µg/m³ at discrete receptors for the Biomass Burning emission source category

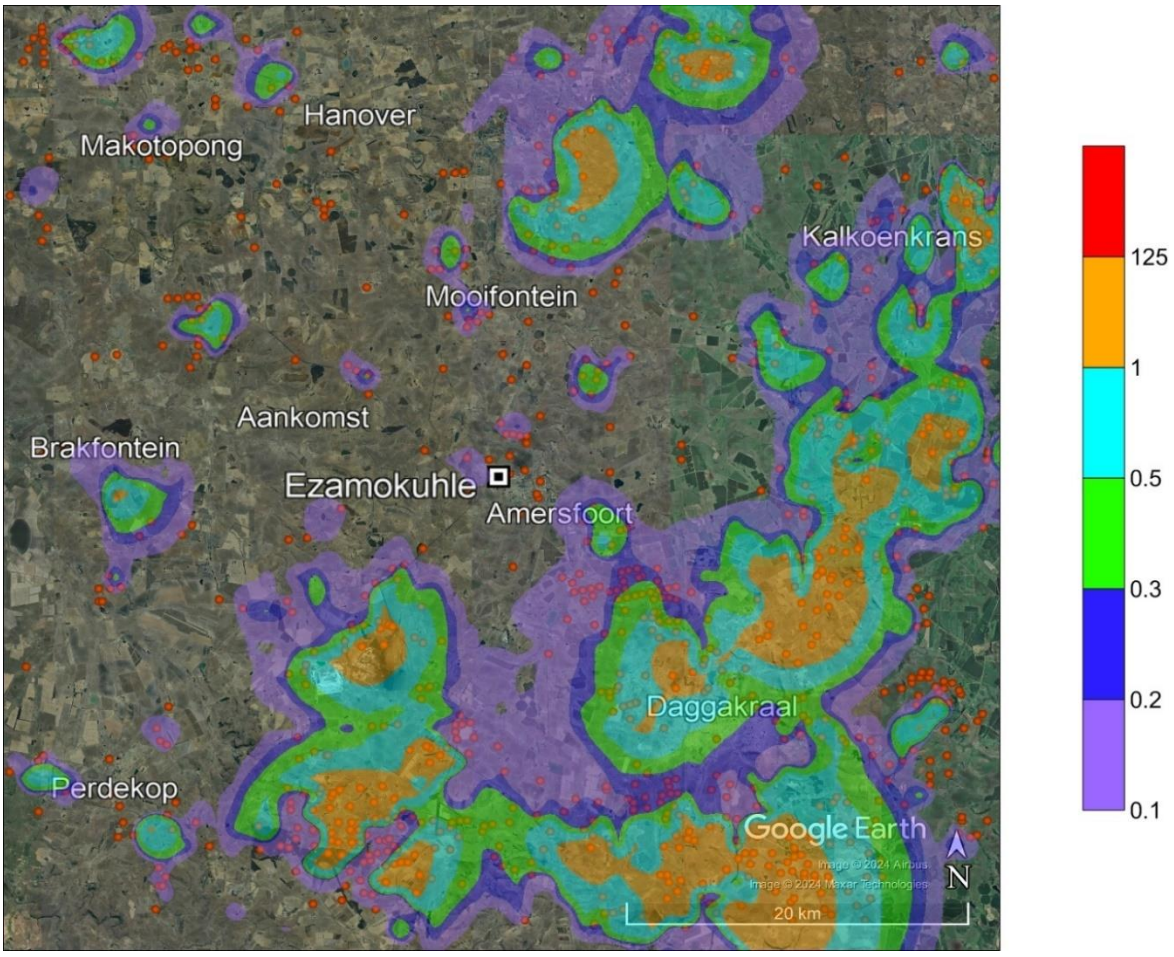

Figure 5-23: Model predicted 24-hour SO_2 ambient concentrations (99th percentile) in µg/m³ for the Biomass Burning emission source category within the Greater Ezamokuhle Airshed

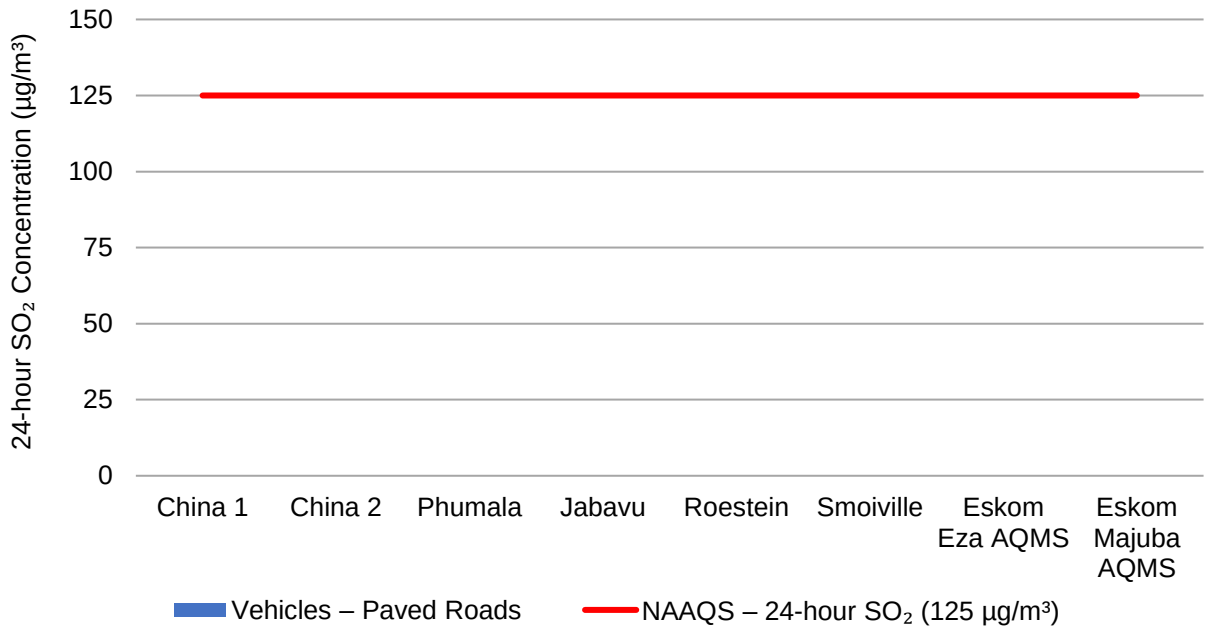

Figure 5-24: Model predicted 24-hour SO_2 ambient concentrations (99th percentile) in µg/m³ at discrete receptors for the Vehicles – Paved Roads emission source category

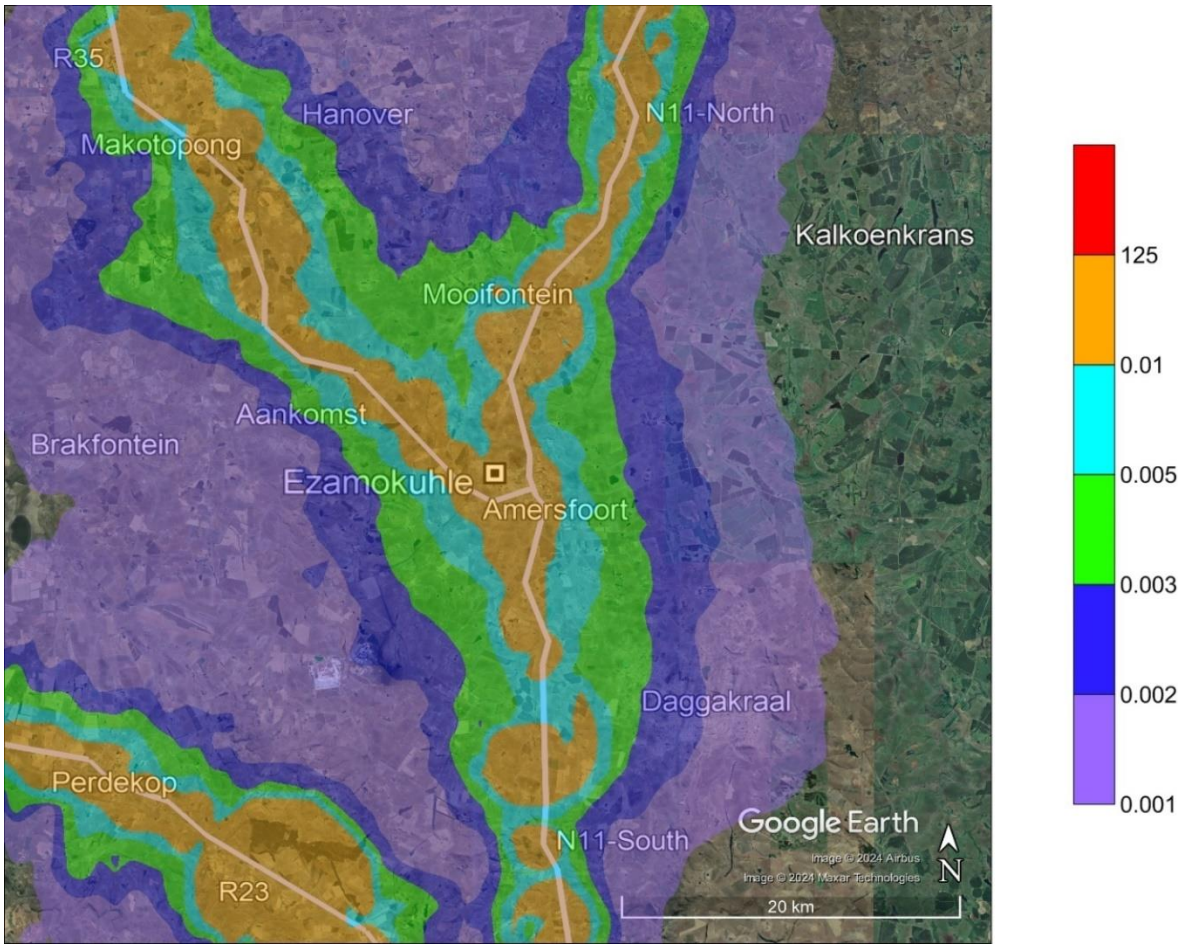

Figure 5-25: Model predicted 24-hour SO_2 ambient concentrations (99th percentile) in µg/m³ for the Vehicles – Paved Roads emission source category within the Greater Ezamokuhle Airshed

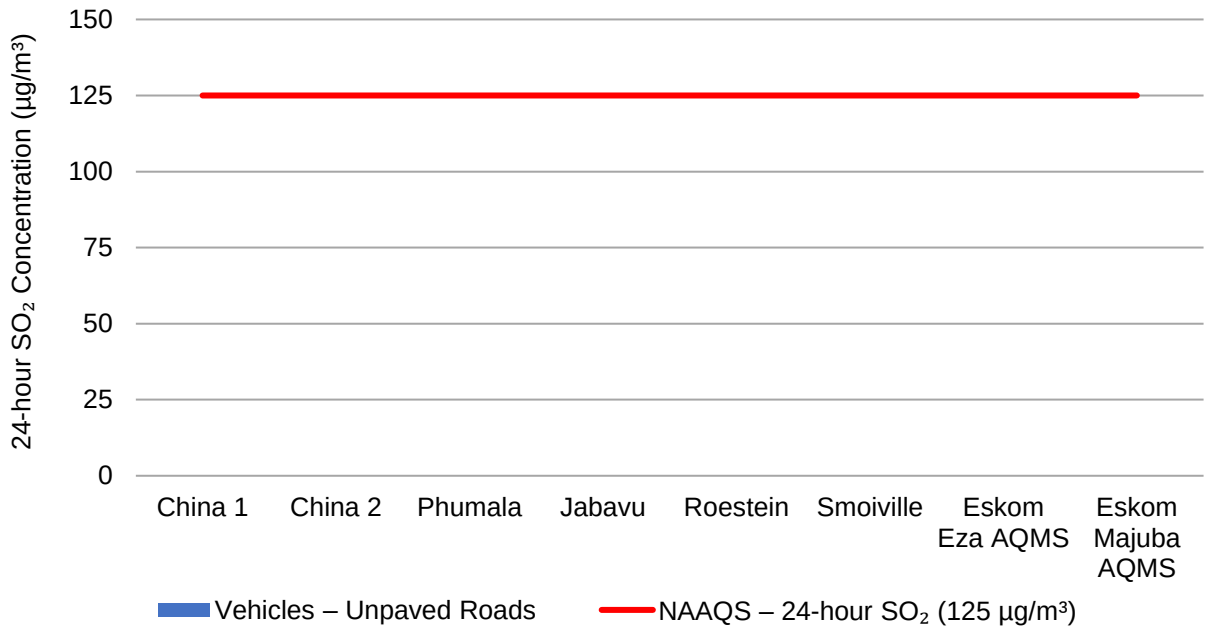

Figure 5-26: Model predicted 24-hour SO_2 ambient concentrations (99th percentile) in µg/m³ at discrete receptors for the Vehicles – Unpaved Roads emission source category

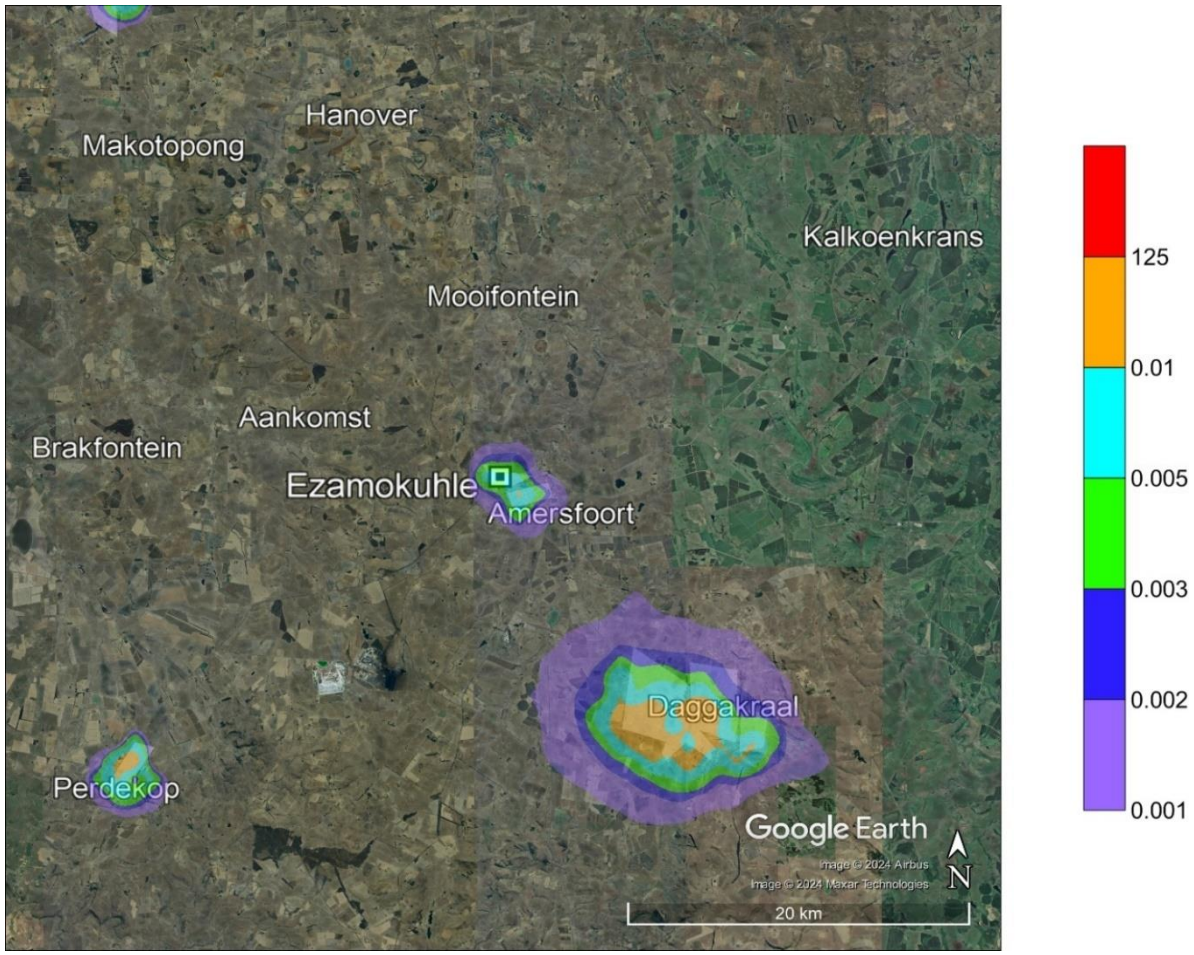

Figure 5-27: Model predicted 24-hour SO_2 ambient concentrations (99th percentile) in µg/m³ for the Vehicles – Unpaved Roads emission source category within the Greater Ezamokuhle Airshed

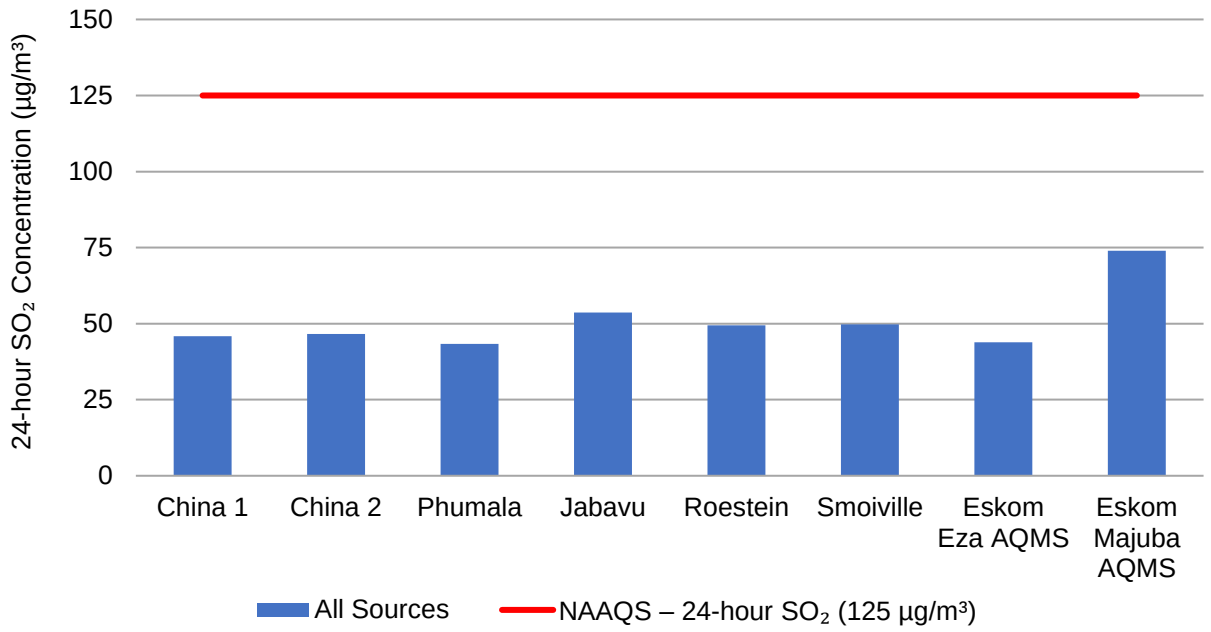

Figure 5-28: Model predicted 24-hour SO_2 ambient concentrations (99th percentile) in µg/m³ at discrete receptors for the All Sources emission source category

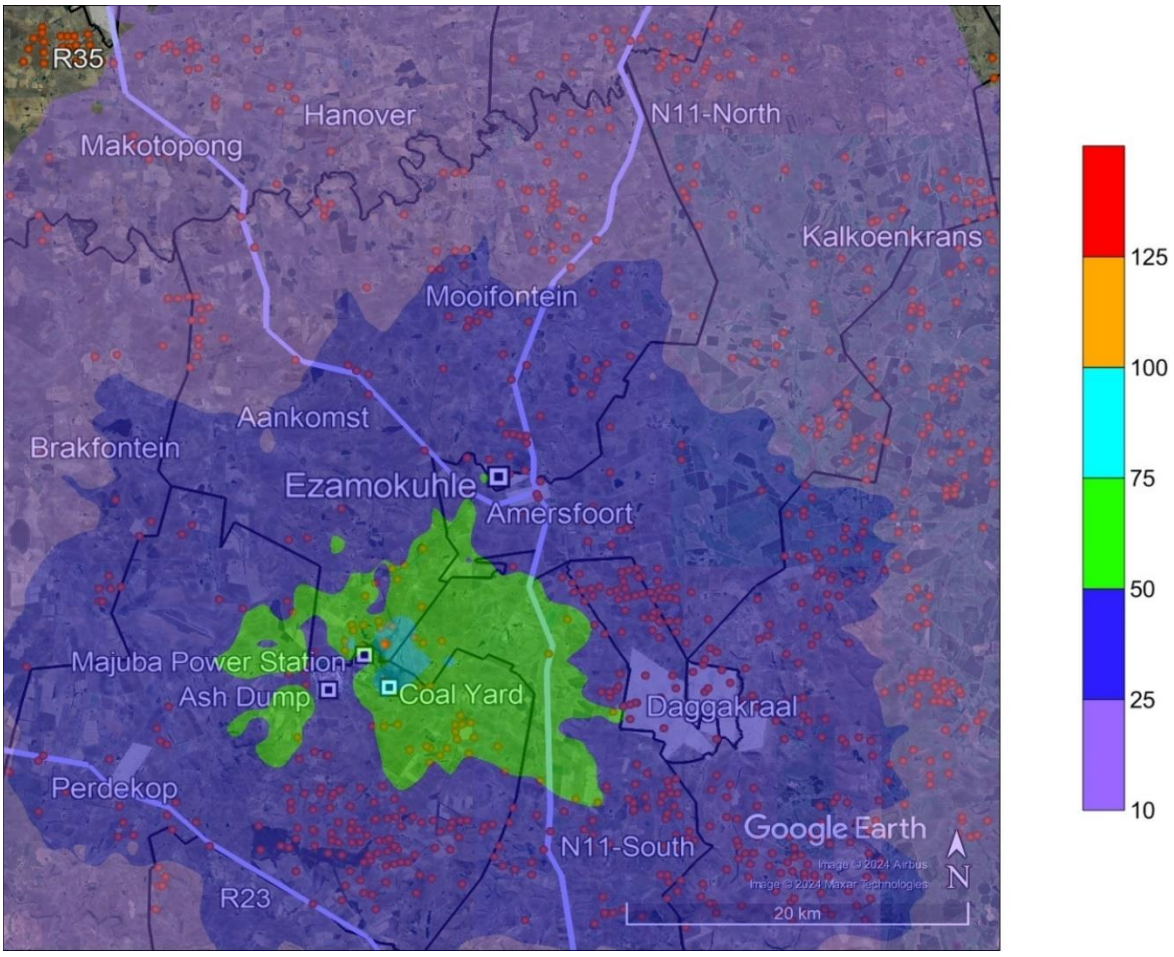

Figure 5-29: Model predicted 24-hour SO_2 ambient concentrations (99th percentile) in µg/m³ for the All Sources emission source category within the Greater Ezamokuhle Airshed

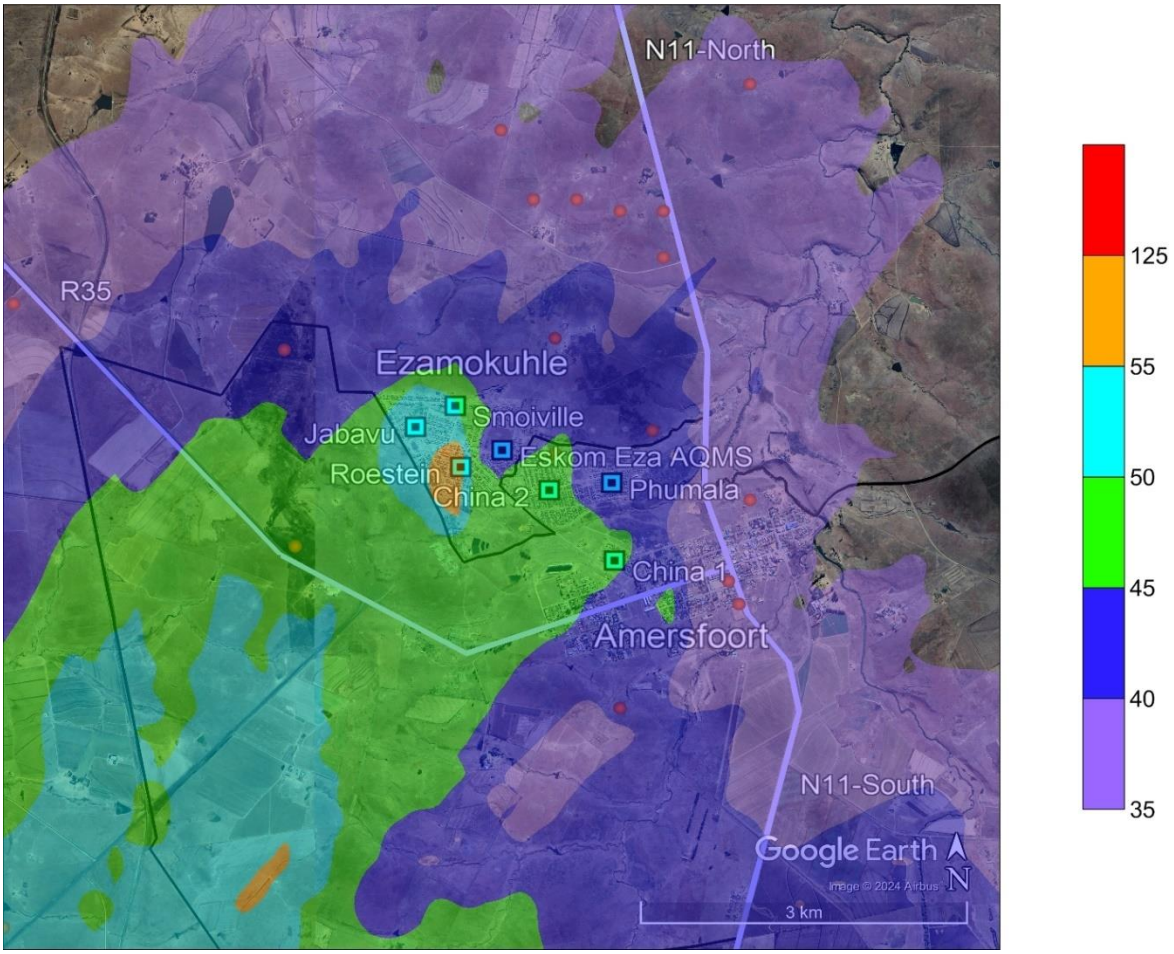

Figure 5-30: Model predicted 24-hour SO_2 ambient concentrations (99th percentile) in µg/m^3 for the All Sources emission source category within Ezamokuhle airshed

5.1.3 ANNUAL SO_2

Model predicted annual SO_2 ambient concentrations at discrete receptors and at the point of maximum for the seven emission source categories are presented in Table 5-3. If applicable, exceedances of the NAAQS are highlighted in red.

Bar graphs for model predicted annual SO_2 ambient concentrations at discrete receptors are presented in the following order:

- Figure 5-31 for the Power Generation emission source category
- Figure 5-33 for the Residential Fuel Burning emission source category
- Figure 5-35 for the Waste Burning emission source category
- Figure 5-37 for the Biomass Burning emission source category
- Figure 5-39 for the Vehicles – Paved Roads emission source category
- Figure 5-41 for the Vehicles – Unpaved Roads emission source category
- Figure 5-43 for the All Sources emission source category

Contour plots for model predicted annual SO_2 ambient concentrations for the Greater Ezamokuhle Airshed are presented in the following order:

- Figure 5-32 for the Power Generation emission source category
- Figure 5-34 for the Residential Fuel Burning emission source category
- Figure 5-36 for the Waste Burning emission source category
- Figure 5-38 for the Biomass Burning emission source category
- Figure 5-40 for the Vehicles – Paved Roads emission source category
- Figure 5-42 for the Vehicles – Unpaved Roads emission source category
- Figure 5-44 for the All Sources emission source category

Contour plots for model predicted annual SO_2 ambient concentrations for the Ezamokuhle airshed is presented in Figure 5-45 for the All Sources emission source category.

With respect to contour plots for the primary and Ezamokuhle airshed, areas of exceedance of the NAAQS is coloured in red.

Table 5-3: Model predicted annual SO_2 ambient concentrations in µg/m^3 at discrete receptors and at the point of maximum for the seven emission source categories

Discrete Receptors	Power Generation	Residential Fuel Burning	Waste Burning	Biomass Burning	Vehicles – Paved Roads	Vehicles – Unpaved Roads	All Sources
China 1	2.90	3.73	0.12	0.02	0.02	0.00	6.80
China 2	2.97	3.27	0.10	0.02	0.01	0.00	6.38
Phumala	2.87	1.96	0.06	0.02	0.00	0.00	4.91
Jabavu	2.90	7.51	0.16	0.03	0.00	0.00	10.60
Roestein	3.00	5.19	0.11	0.02	0.00	0.00	8.33
Smoiville	2.88	9.31	0.19	0.02	0.00	0.00	12.42
Eskom Eza AQMS	2.96	1.78	0.05	0.02	0.00	0.00	4.81
Eskom Majuba AQMS	6.02	0.02	0.00	0.16	0.00	0.00	6.21
Maximum	7.72	11.51	0.32	0.78	0.13	0.01	14.73
	NAAQS – annual SO_2 (50 µg/m^3)						

According to Table 5-3, model predicted annual SO_2 ambient concentrations are below the annual SO_2 NAAQS of 50 µg/m^3 at all discrete receptors and at the point of maximum for all seven emission source categories, both in the Greater Ezamokuhle Airshed and in the Ezamokuhle Airshed. There are no exceedances of the NAAQS both in the Greater Ezamokuhle Airshed and in the Ezamokuhle Airshed.

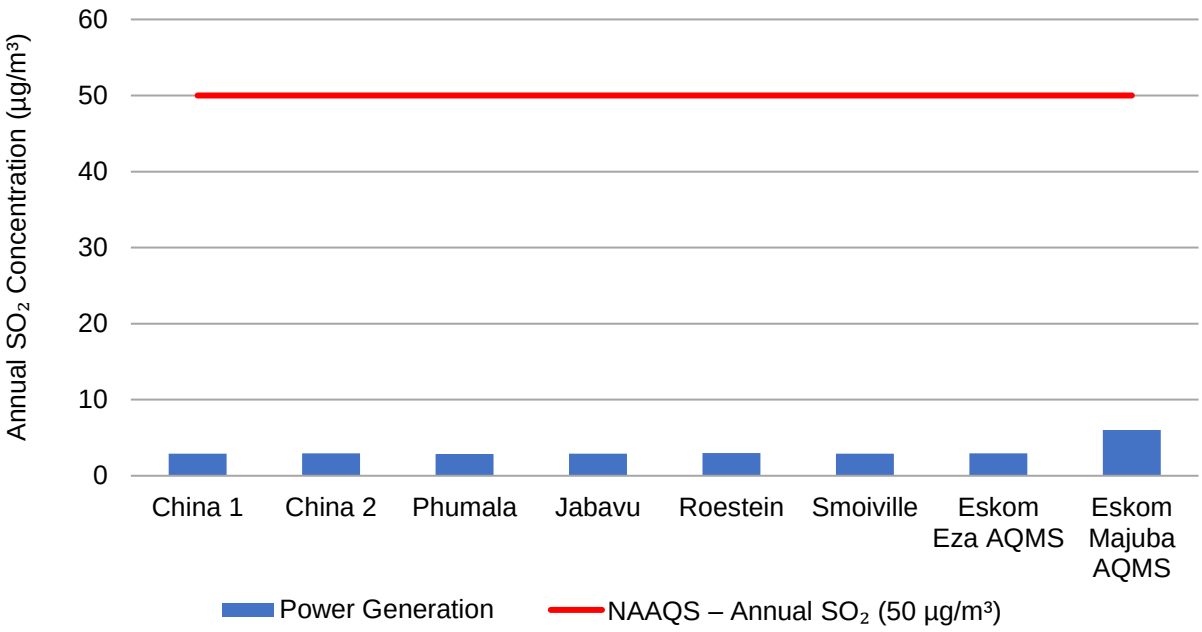

Figure 5-31: Model predicted annual SO_2 ambient concentrations in µg/m³ at discrete receptors for the Power Generation emission source category

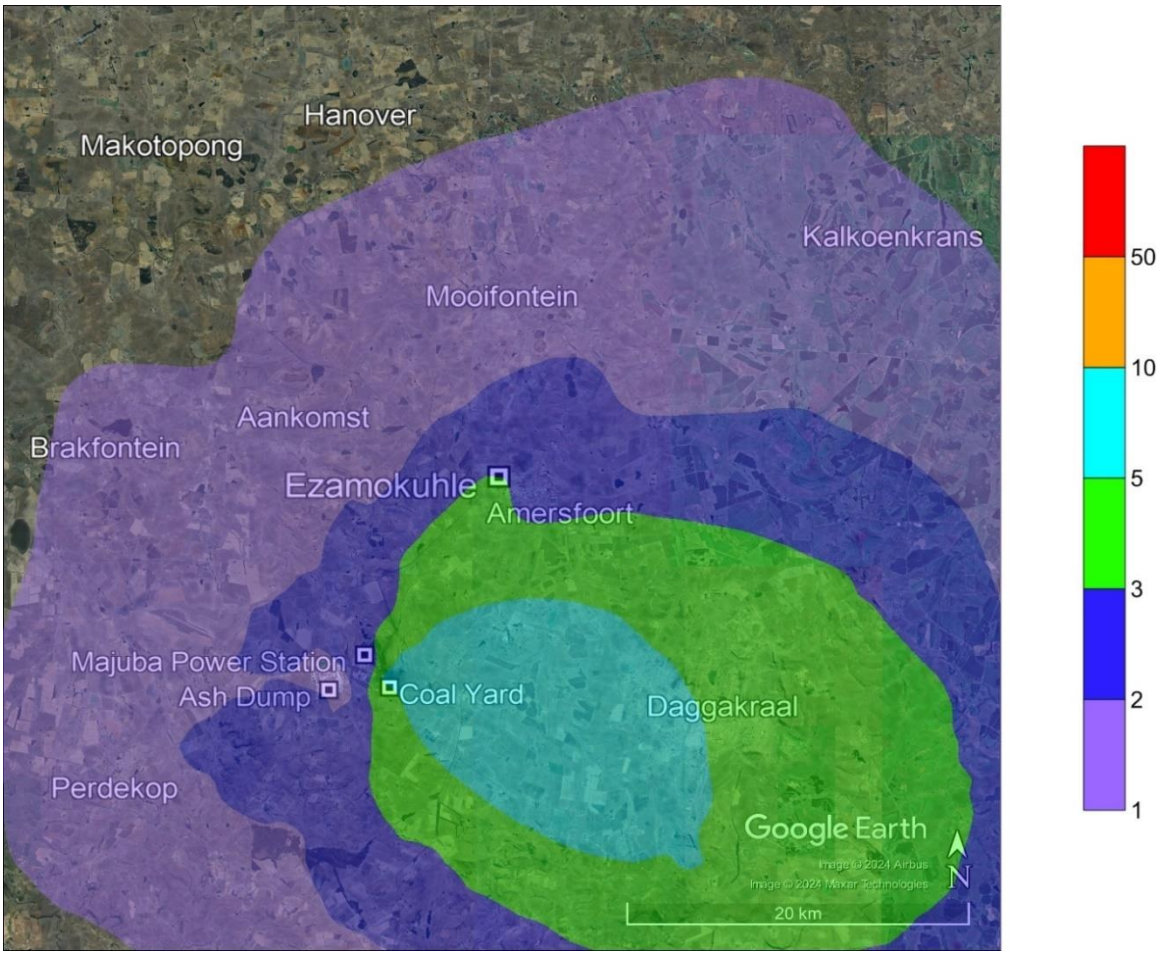

Figure 5-32: Model predicted annual SO_2 ambient concentrations in µg/m³ for the Power Generation emission source category within the Greater Ezamokuhle Airshed

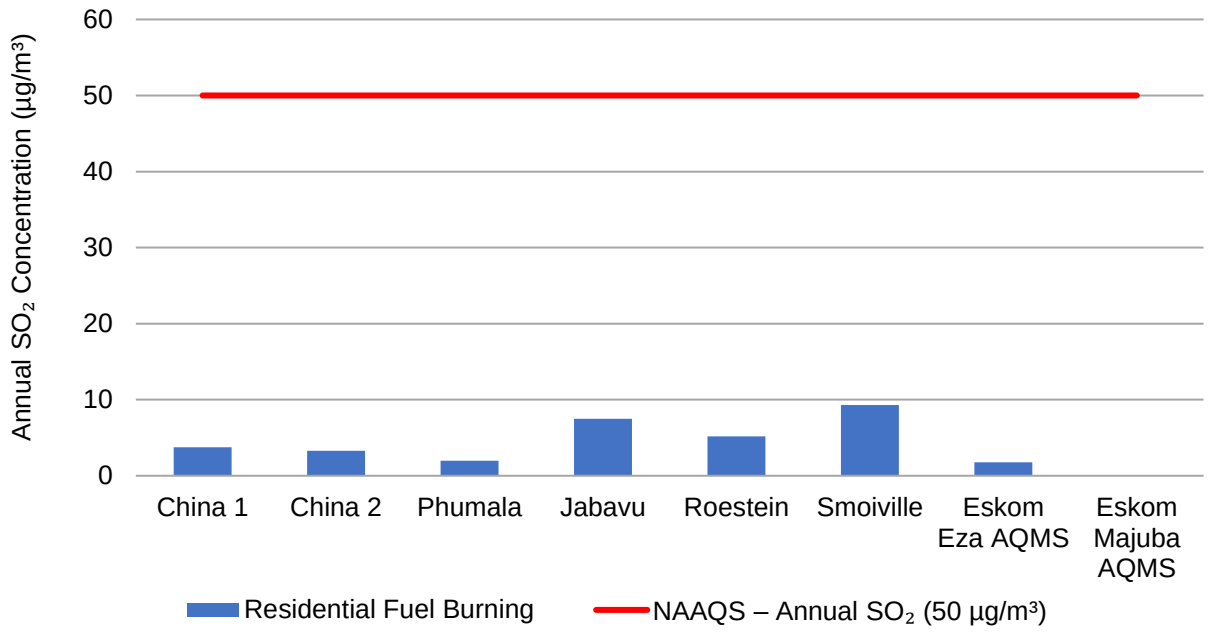

Figure 5-33: Model predicted annual SO_2 ambient concentrations in µg/m³ at discrete receptors for the Residential Fuel Burning emission source category

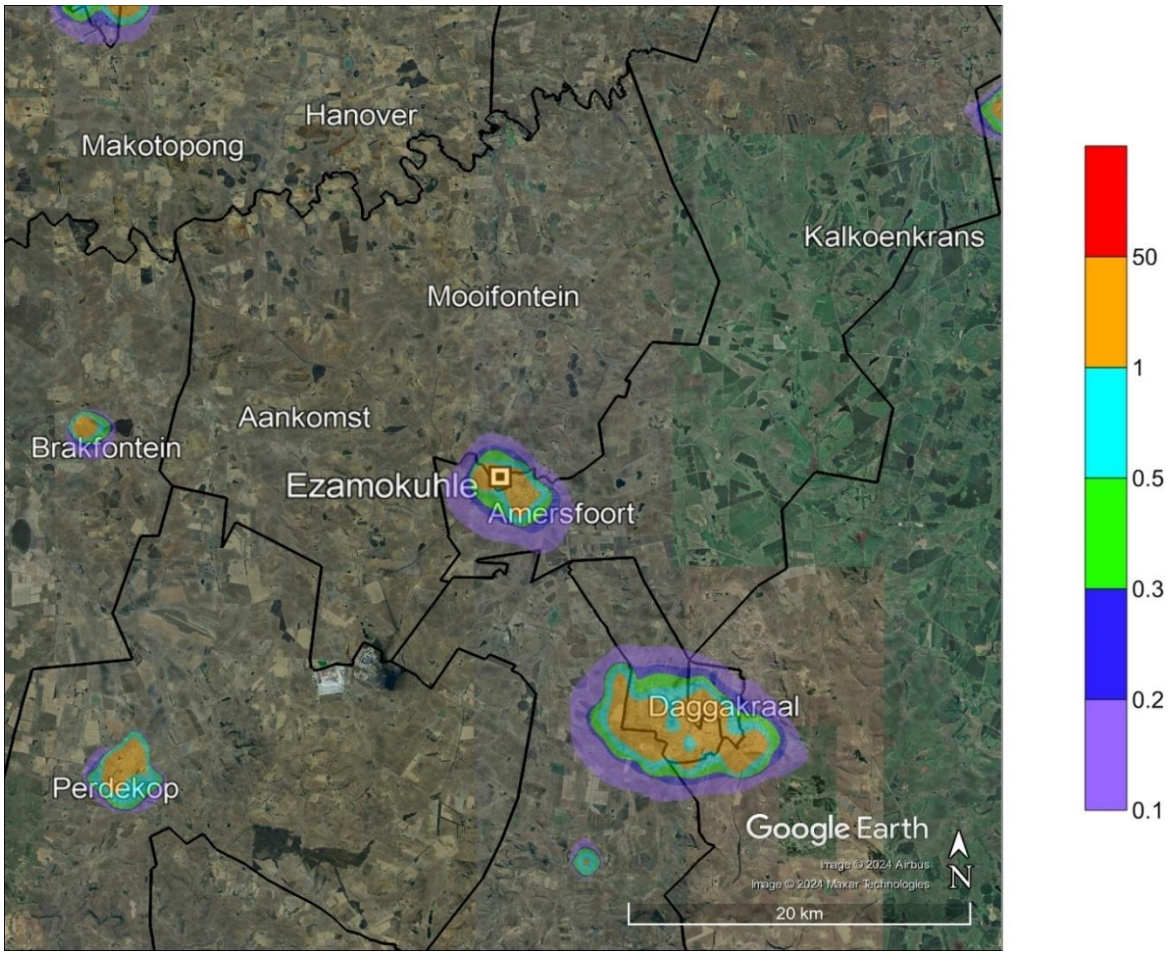

Figure 5-34: Model predicted annual SO_2 ambient concentrations in µg/m³ for the Residential Fuel Burning emission source category within the Greater Ezamokuhle Airshed

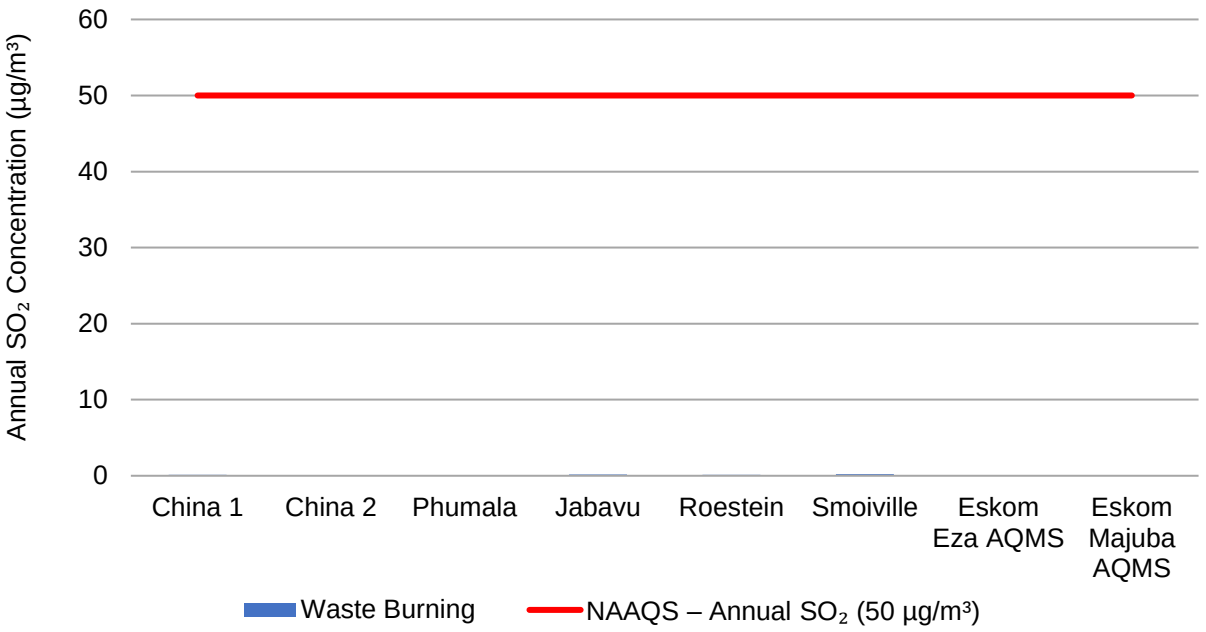

Figure 5-35: Model predicted annual SO_2 ambient concentrations in µg/m³ at discrete receptors for the Waste Burning emission source category

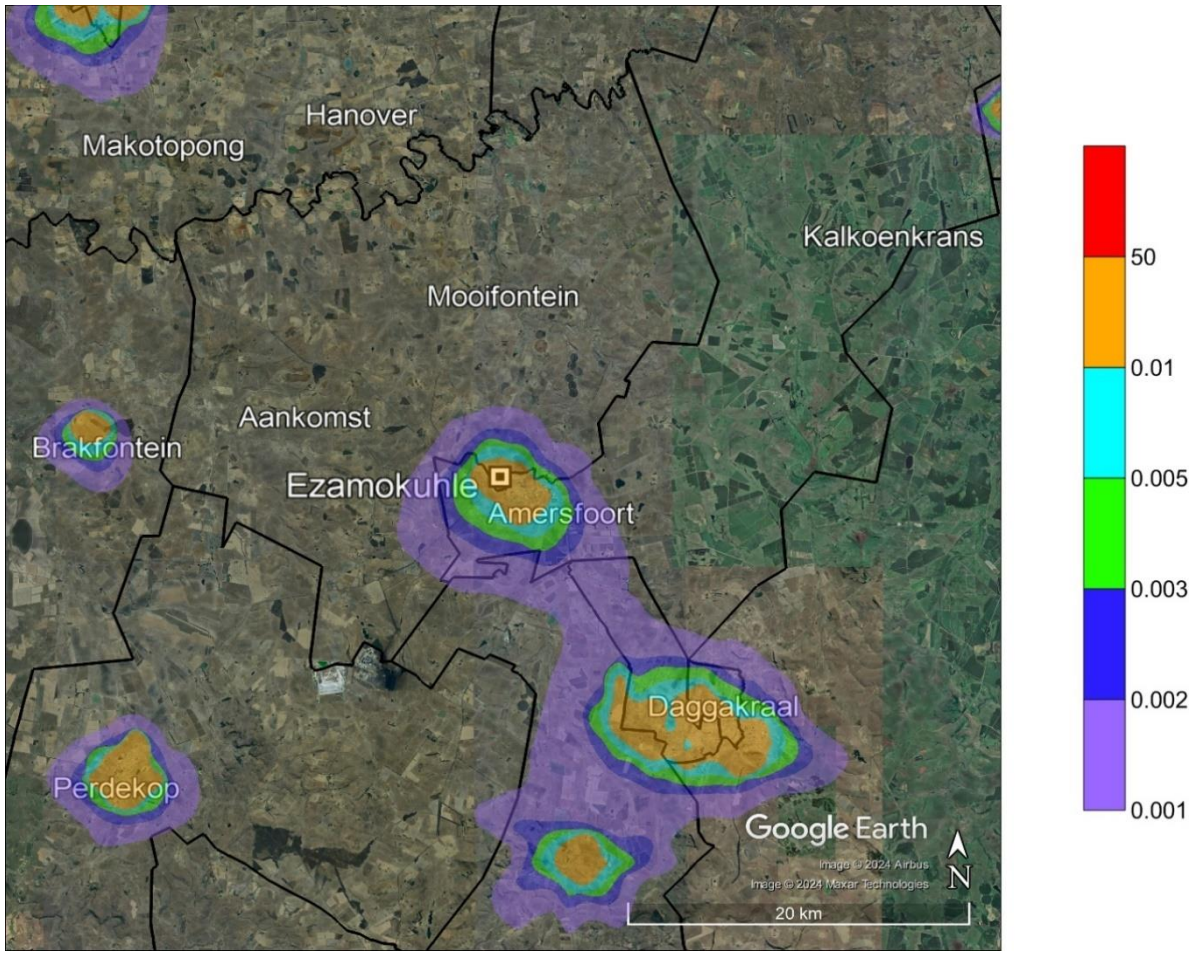

Figure 5-36: Model predicted annual SO_2 ambient concentrations in µg/m³ for the Waste Burning emission source category within the Greater Ezamokuhle Airshed

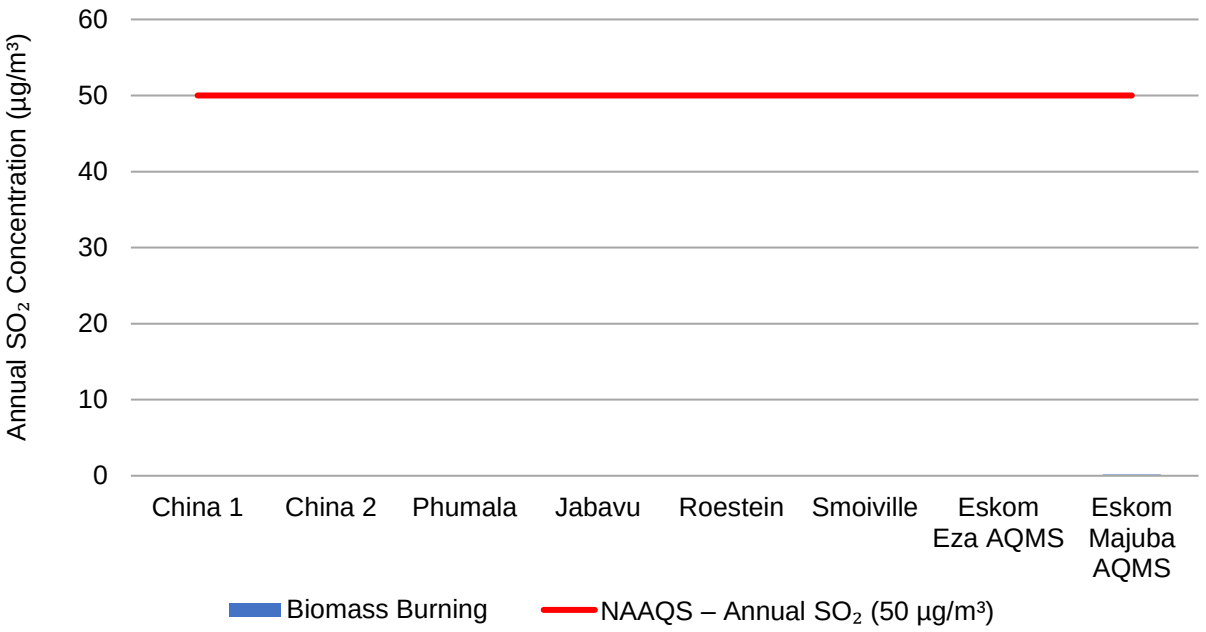

Figure 5-37: Model predicted annual SO_2 ambient concentrations in µg/m³ at discrete receptors for the Biomass Burning emission source category

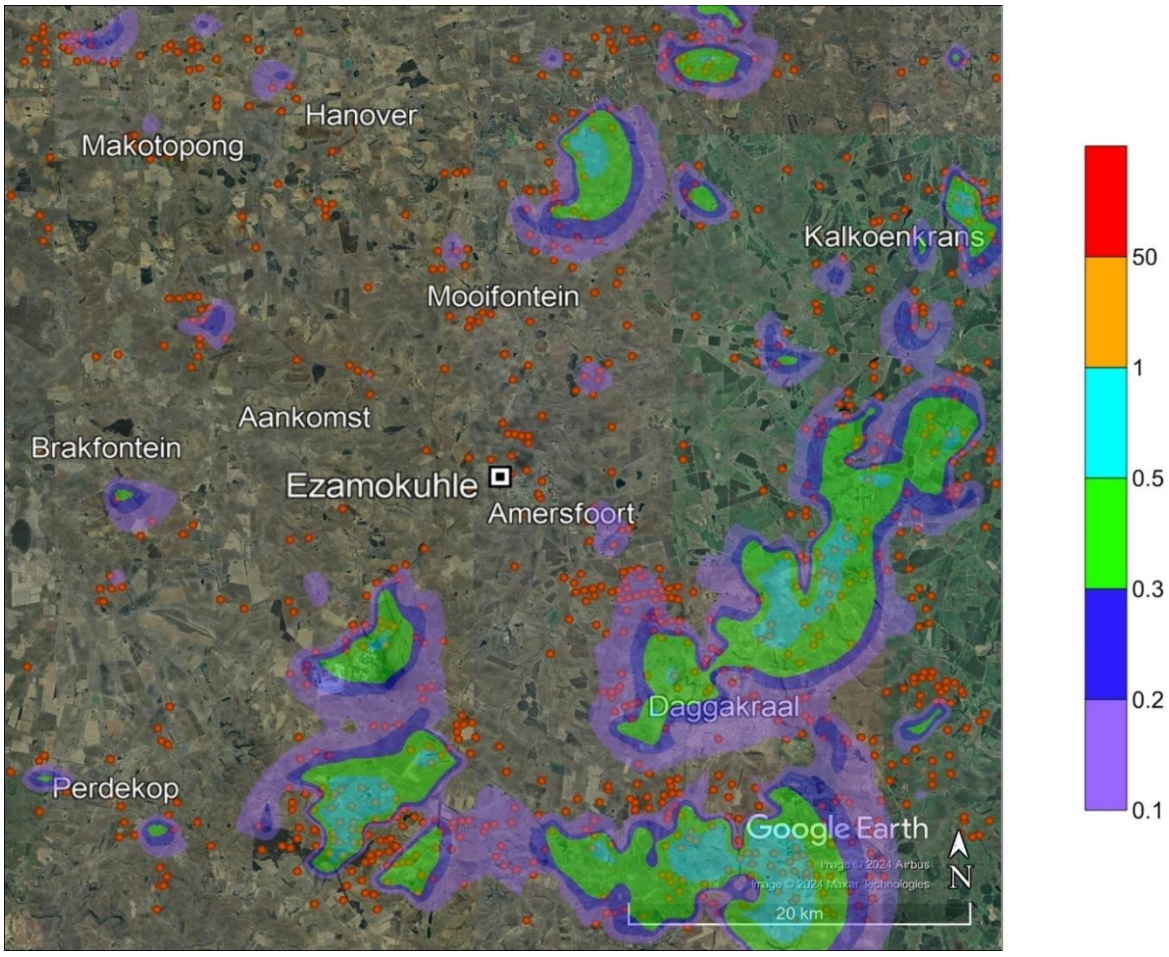

Figure 5-38: Model predicted annual SO_2 ambient concentrations in µg/m³ for the Biomass Burning emission source category within the Greater Ezamokuhle Airshed

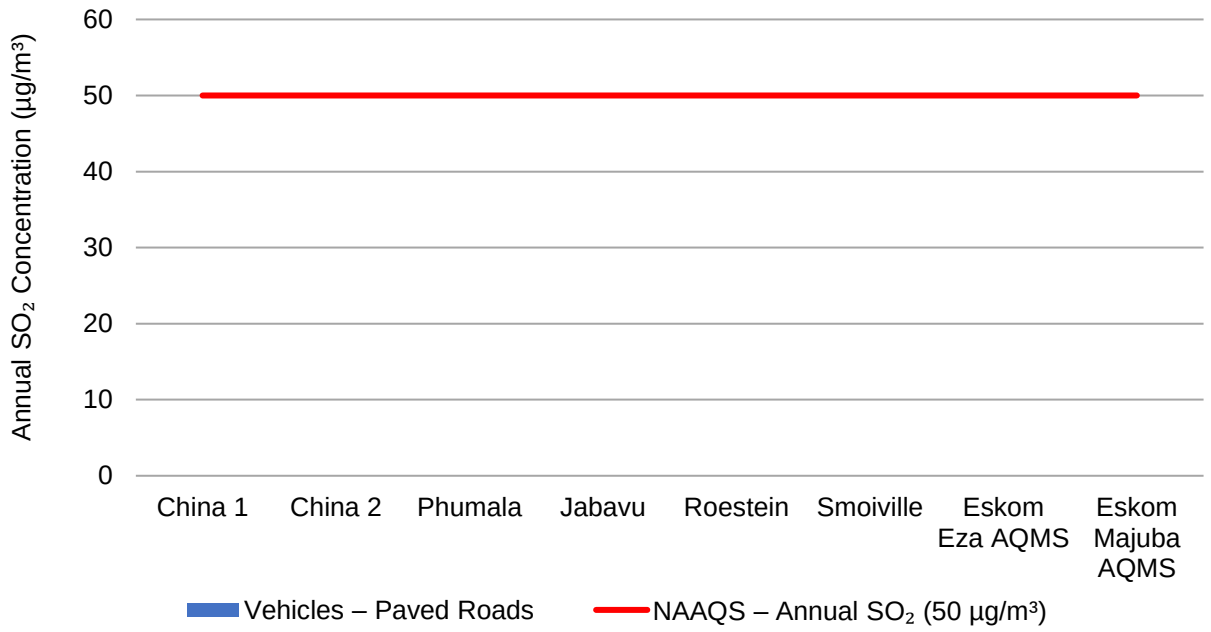

Figure 5-39: Model predicted annual SO_2 ambient concentrations in µg/m³ at discrete receptors for the Vehicles – Paved Roads emission source category

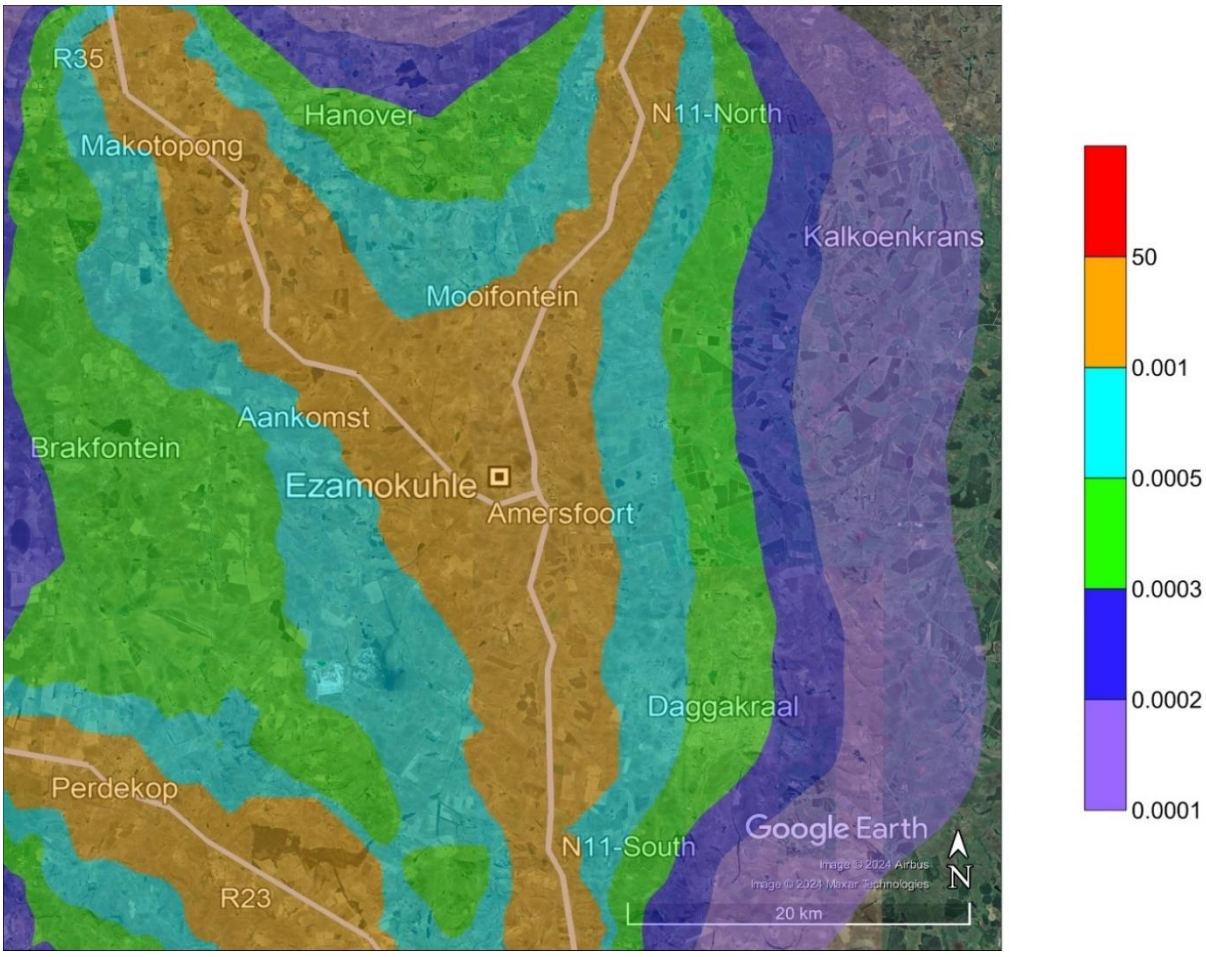

Figure 5-40: Model predicted annual SO_2 ambient concentrations in µg/m³ for the Vehicles – Paved Roads emission source category within the Greater Ezamokuhle Airshed

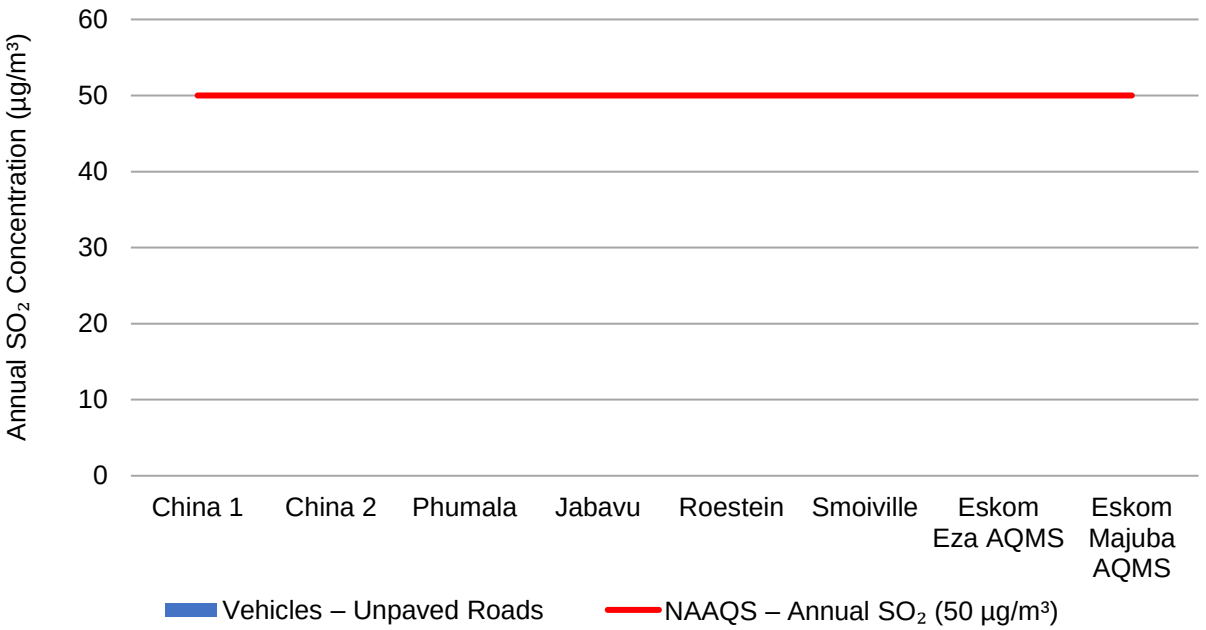

Figure 5-41: Model predicted annual SO_2 ambient concentrations in µg/m³ at discrete receptors for the Vehicles – Unpaved Roads emission source category

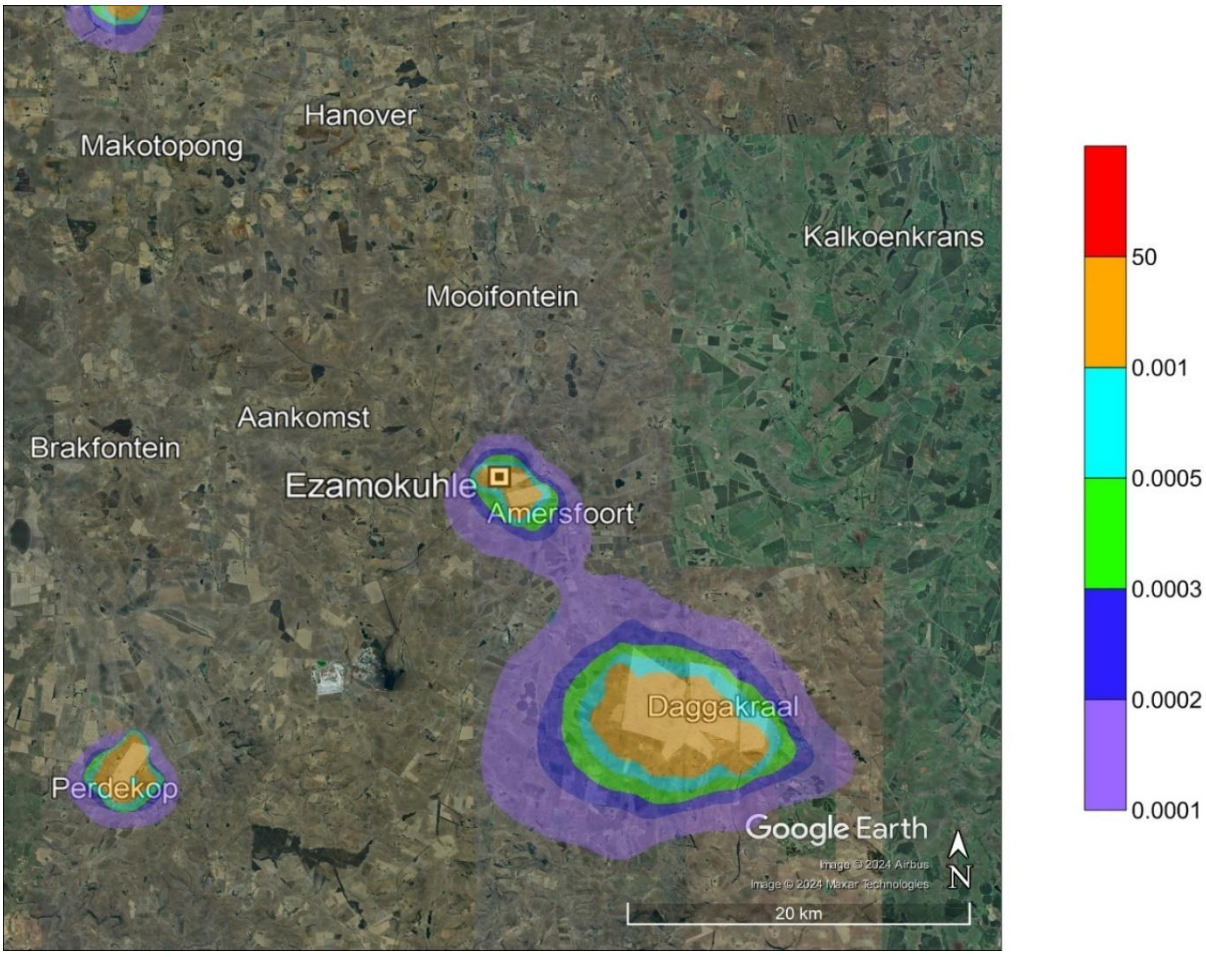

Figure 5-42: Model predicted annual SO_2 ambient concentrations in µg/m³ for the Vehicles – Unpaved Roads emission source category within the Greater Ezamokuhle Airshed

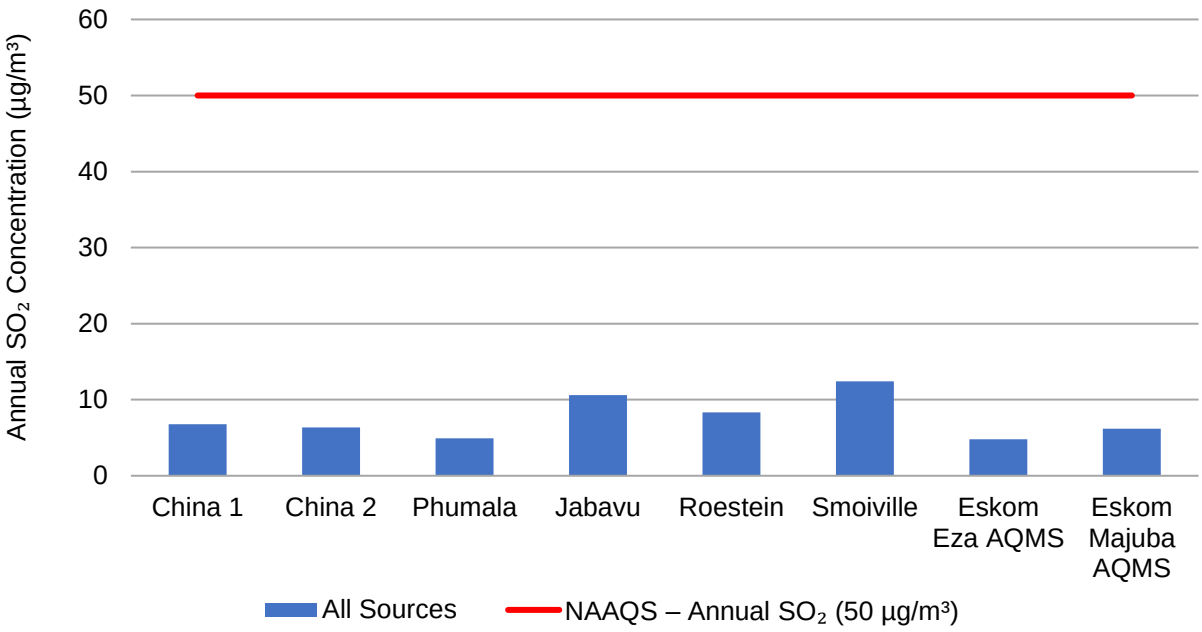

Figure 5-43: Model predicted annual SO_2 ambient concentrations in µg/m³ at discrete receptors for the All Sources emission source category

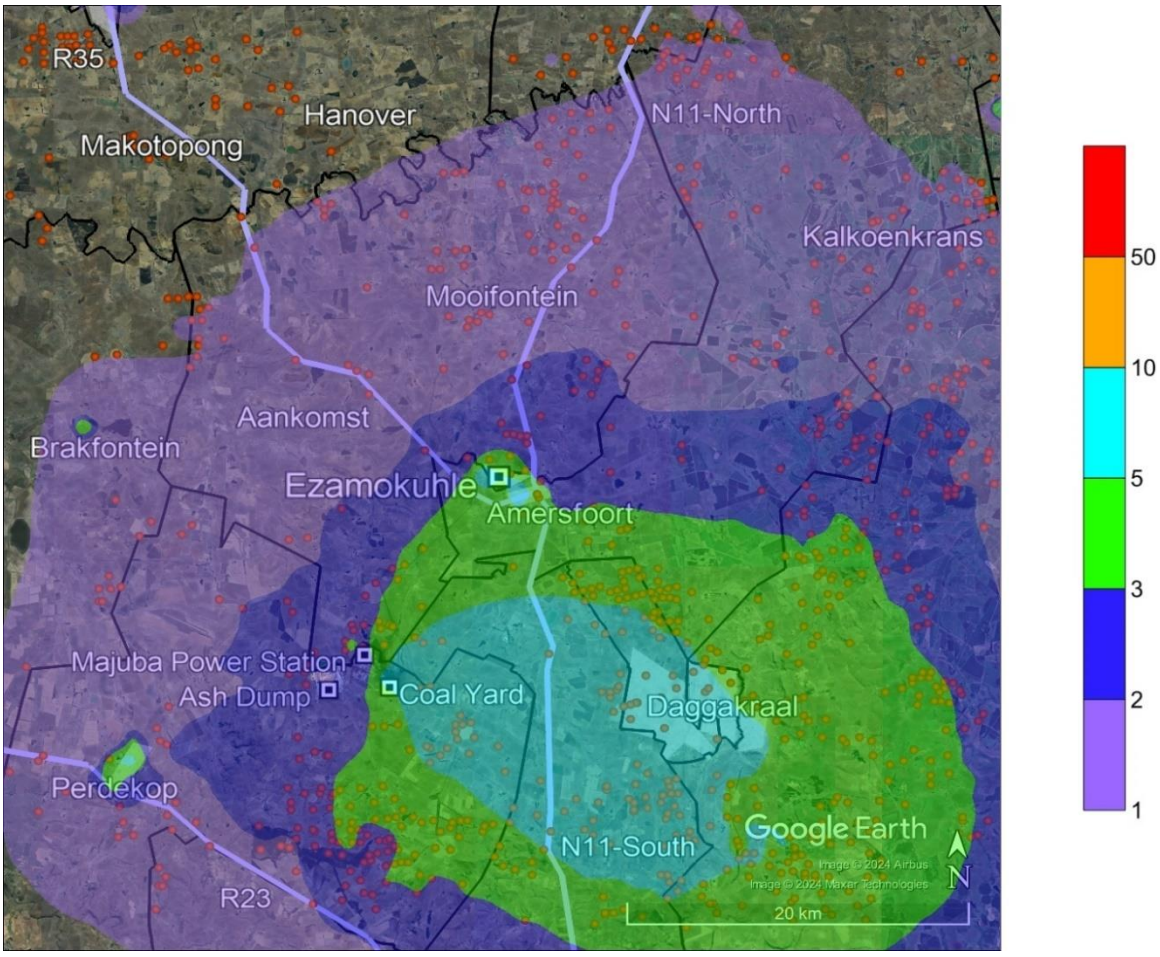

Figure 5-44: Model predicted annual SO_2 ambient concentrations in µg/m³ for the All Sources emission source category within the Greater Ezamokuhle Airshed

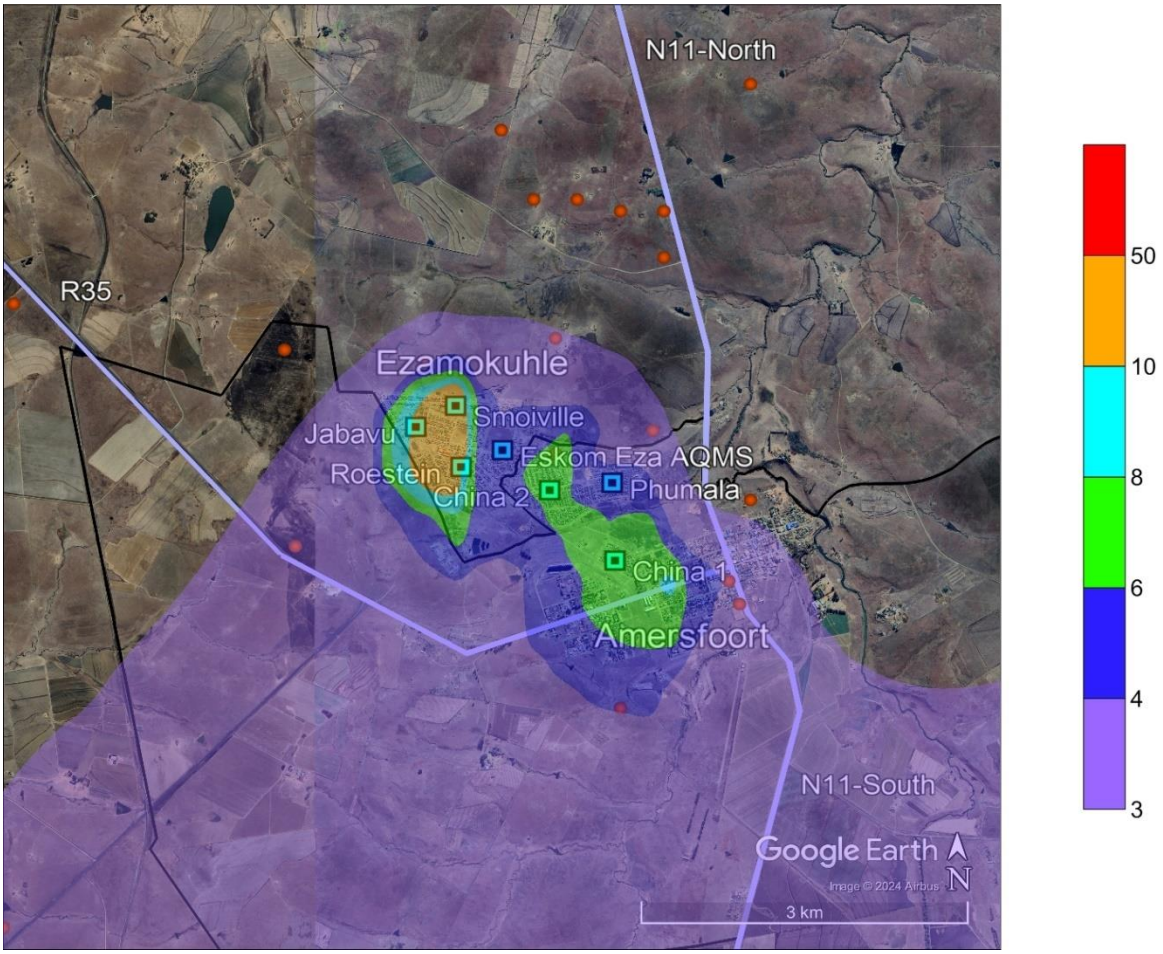

Figure 5-45: Model predicted annual SO_2 ambient concentrations in µg/m³ for the All Sources emission source category within Ezamokuhle airshed

5.1.4 SO_2 SOURCE CONTRIBUTION ANALYSIS

In this study, the SO_2 source contribution analysis is based on model predicted annual SO_2 ambient concentrations at the discrete receptors for the six emission source categories which include power generation, residential fuel burning, waste burning, biomass burning, vehicles – paved roads and vehicles – unpaved roads (Table 5-3). Table 5-3 is used to calculate the percent contribution of SO_2 at each discrete receptor as a function of the six source categories, and is presented in Table 5-4.

Table 5-4: SO_2 source contribution (%) at discrete receptors for the six emission source categories based on model predicted annual SO_2 ambient concentrations

Discrete Receptors	Power Generation	Residential Fuel Burning	Waste Burning	Biomass Burning	Vehicles – Paved Roads	Vehicles – Unpaved Roads	All Sources
China 1	42.64	54.90	1.80	0.28	0.32	0.07	100.00
China 2	46.52	51.36	1.62	0.31	0.13	0.06	100.00
Phumala	58.33	39.86	1.28	0.38	0.10	0.05	100.00
Jabavu	27.37	70.85	1.48	0.25	0.03	0.03	100.00
Roestein	36.06	62.30	1.32	0.25	0.04	0.03	100.00
Smoiville	23.23	74.96	1.57	0.19	0.02	0.03	100.00
Eskom Eza AQMS	61.52	36.90	1.04	0.42	0.07	0.04	100.00
Eskom Majuba AQMS	97.00	0.38	0.01	2.60	0.01	0.00	100.00

SO_2 ambient concentrations (in terms of $\mu g/m^3$) for each emission source category at each discrete receptor is presented in the form of a stacked bar graph in Figure 5-46. The total SO_2 ambient concentrations at each discrete receptor (which is made up of individual contributions representing each of the six emission source categories) represents the All Sources emission source category. The SO_2 source contribution in terms of percentages is presented in the form of a stacked bar graph in Figure 5-47. The sum of individual contributions resulting from each emission source category makes up 100%.

The source contribution analysis indicates that power generation and residential fuel burning are the main contributors to ambient SO_2 levels in the region. Ambient contributions from waste burning, biomass burning and vehicles are much smaller in comparison.

Power generation sources account for approximately 97% of the total SO_2 ambient concentrations at the Eskom Majuba AQMS but are much lower at the Eskom Ezamokuhle AQMS and ward centroid discrete receptors (23-62%). This is expected as the Eskom Majuba Power Station is located close to the Eskom Majuba AQMS in comparison with the Eskom Ezamokuhle AQMS and ward centroid discrete receptors.

Residential fuel burning sources account for approximately 0.4% of the total SO_2 ambient concentrations at the Eskom Majuba AQMS but are much higher at the Eskom Ezamokuhle AQMS and ward centroid discrete receptors (36-75%). This is expected as residential areas are located further away from the Eskom Majuba AQMS in comparison with the Eskom Ezamokuhle AQMS and ward centroid discrete receptors.

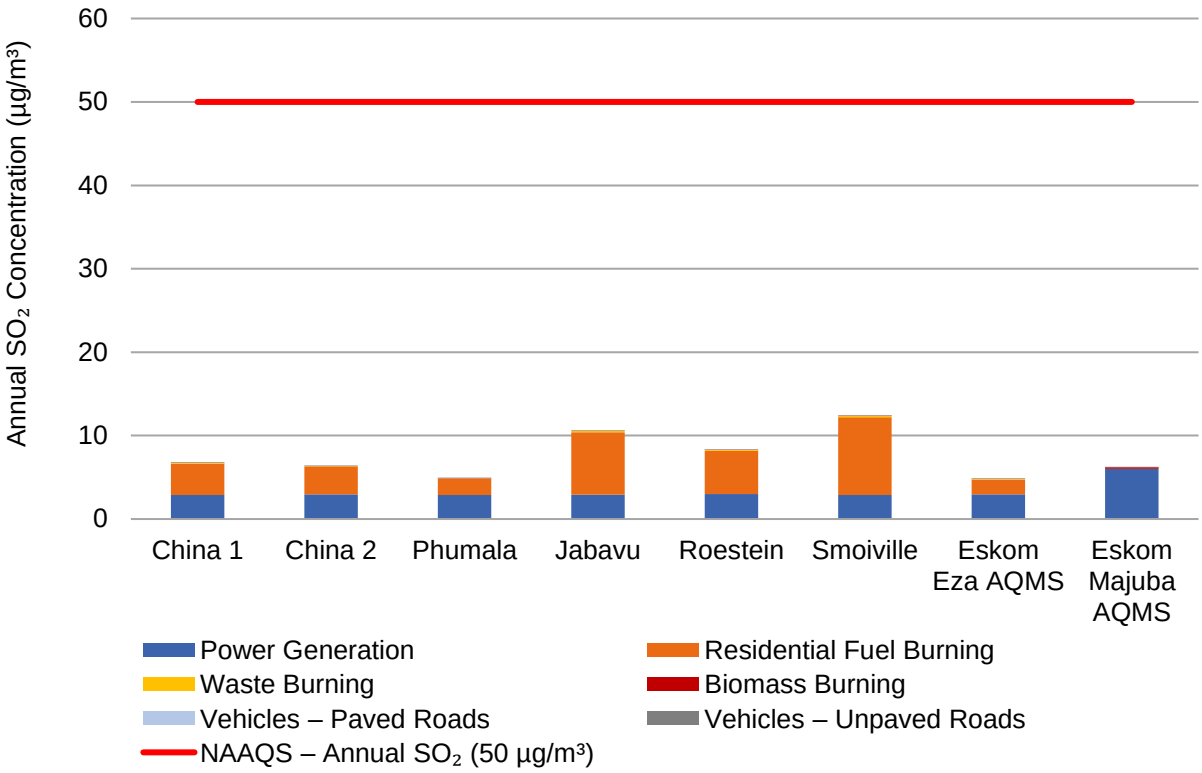

Figure 5-46: Stacked bar graph representing model predicted annual SO_2 ambient concentrations in µg/m³ at discrete receptors for the six emission source categories

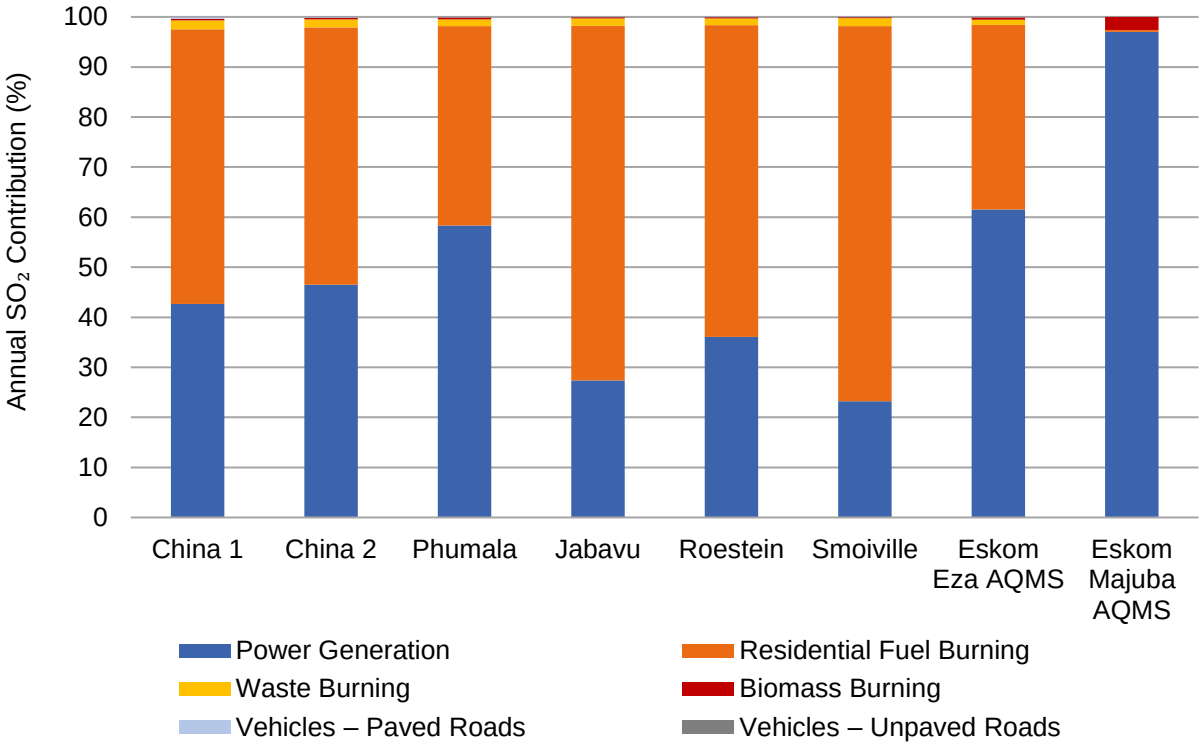

Figure 5-47: Stacked bar graph representing the percent contribution of SO_2 ambient concentrations at discrete receptors as a function of source category

5.2 PREDICTED NO_2 AMBIENT CONCENTRATIONS

5.2.1 1-HOUR NO_2

Model predicted 1-hour NO_2 ambient concentrations at discrete receptors and at the point of maximum for the seven emission source categories are presented in Table 5-5. If applicable, exceedances of the NAAQS are highlighted in red.

Bar graphs for model predicted 1-hour NO_2 ambient concentrations at discrete receptors are presented in the following order:

- Figure 5-48 for the Power Generation emission source category
- Figure 5-50 for the Residential Fuel Burning emission source category
- Figure 5-52 for the Waste Burning emission source category
- Figure 5-54 for the Biomass Burning emission source category
- Figure 5-56 for the Vehicles – Paved Roads emission source category
- Figure 5-58 for the Vehicles – Unpaved Roads emission source category
- Figure 5-60 for the All Sources emission source category

Contour plots for model predicted 1-hour NO_2 ambient concentrations for the Greater Ezamokuhle Airshed are presented in the following order:

- Figure 5-49 for the Power Generation emission source category
- Figure 5-51 for the Residential Fuel Burning emission source category
- Figure 5-53 for the Waste Burning emission source category
- Figure 5-55 for the Biomass Burning emission source category
- Figure 5-57 for the Vehicles – Paved Roads emission source category
- Figure 5-59 for the Vehicles – Unpaved Roads emission source category
- Figure 5-61 for the All Sources emission source category

Contour plots for model predicted 1-hour NO_2 ambient concentrations for the Ezamokuhle airshed is presented in Figure 5-62 for the All Sources emission source category.

With respect to contour plots for the primary and Ezamokuhle airshed, areas of exceedance of the NAAQS is coloured in red.

Table 5-5: Model predicted 1-hour NO_2 ambient concentrations (99th percentile) in µg/m^3 at discrete receptors and at the point of maximum for the seven emission source categories

Discrete Receptors	Power Generation	Residential Fuel Burning	Waste Burning	Biomass Burning	Vehicles – Paved Roads	Vehicles – Unpaved Roads	All Sources
China 1	38.86	4.63	1.09	0.02	15.09	4.85	48.29
China 2	41.75	4.16	0.93	0.02	9.12	3.77	43.37
Phumala	39.33	2.90	0.66	0.02	5.01	2.68	39.86
Jabavu	38.31	9.40	1.30	0.03	2.56	2.96	42.54
Roestein	40.56	7.30	1.06	0.02	3.04	2.50	43.70
Smoiville	39.20	10.19	1.41	0.02	2.59	3.08	40.61
Eskom Eza AQMS	41.54	2.75	0.57	0.02	3.38	2.14	42.13
Eskom Majuba AQMS	65.33	0.11	0.02	0.15	0.63	0.21	65.34
Maximum	93.67	31.78	3.41	0.55	184.39	10.86	191.16
	NAAQS – 1-hour NO_2 (200 µg/m^3)						

According to Table 5-5, model predicted 1-hour NO_2 ambient concentrations are below the 1-hour NO_2 NAAQS of 200 µg/m^3 at all discrete receptors and at the point of maximum for all seven emission source categories, both in the Greater Ezamokuhle Airshed and in the Ezamokuhle Airshed. There are no exceedances of the NAAQS both in the Greater Ezamokuhle Airshed and in the Ezamokuhle Airshed (Figure 3-3).

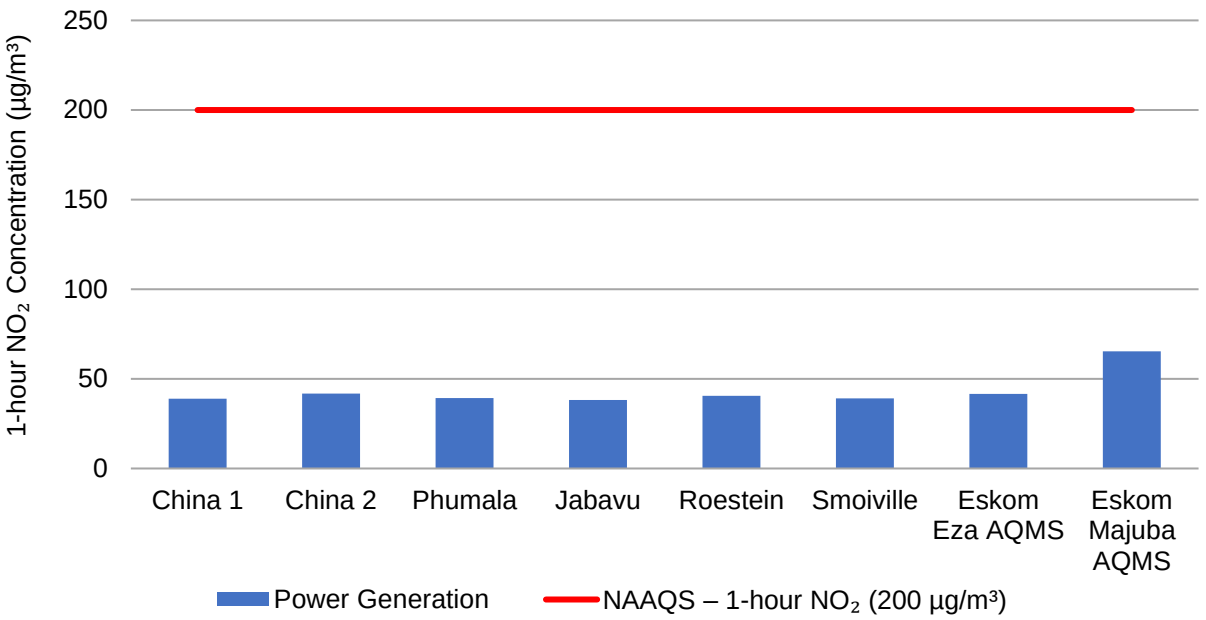

Figure 5-48: Model predicted 1-hour NO_2 ambient concentrations (99th percentile) in µg/m³ at discrete receptors for the Power Generation emission source category

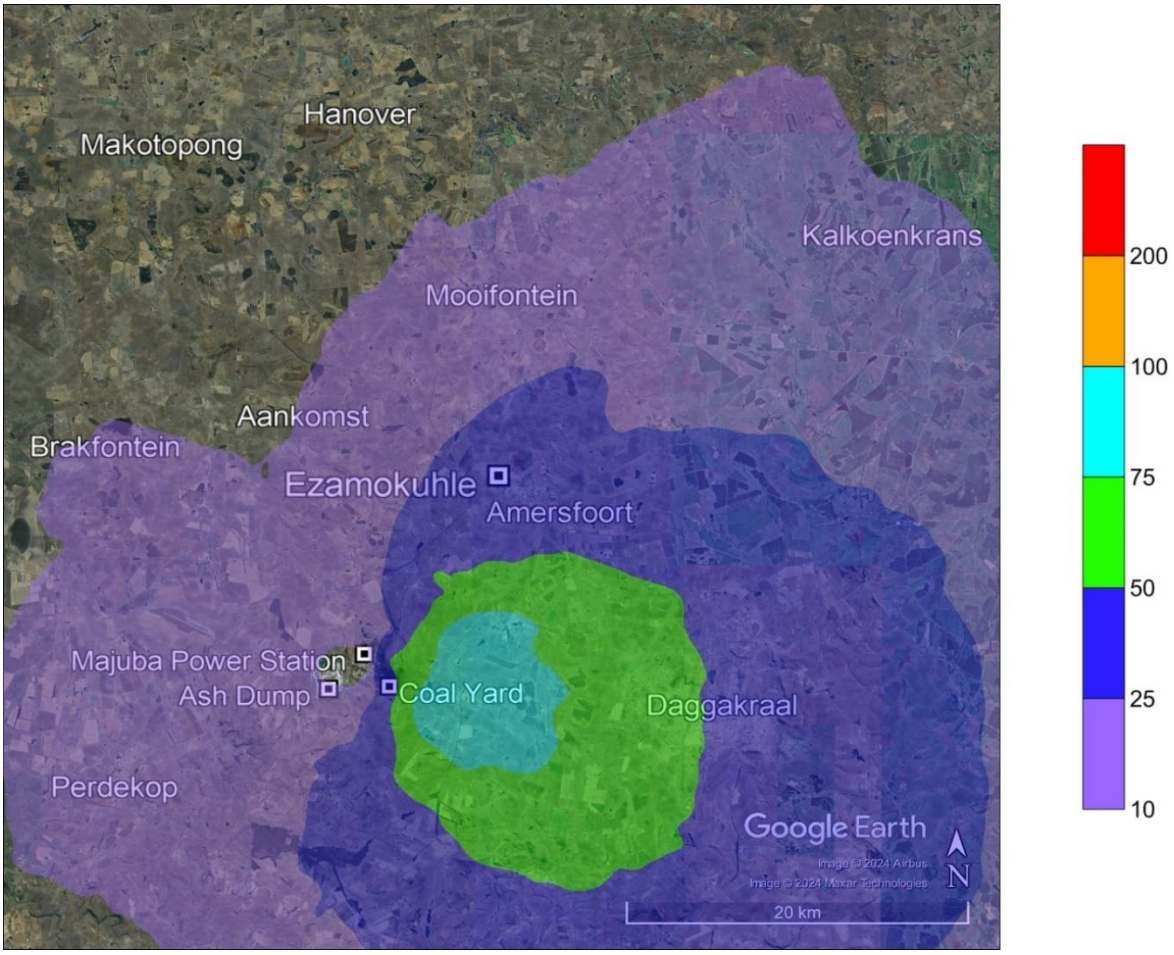

Figure 5-49: Model predicted 1-hour NO_2 ambient concentrations (99th percentile) in µg/m³ for the Power Generation emission source category within the Greater Ezamokuhle Airshed

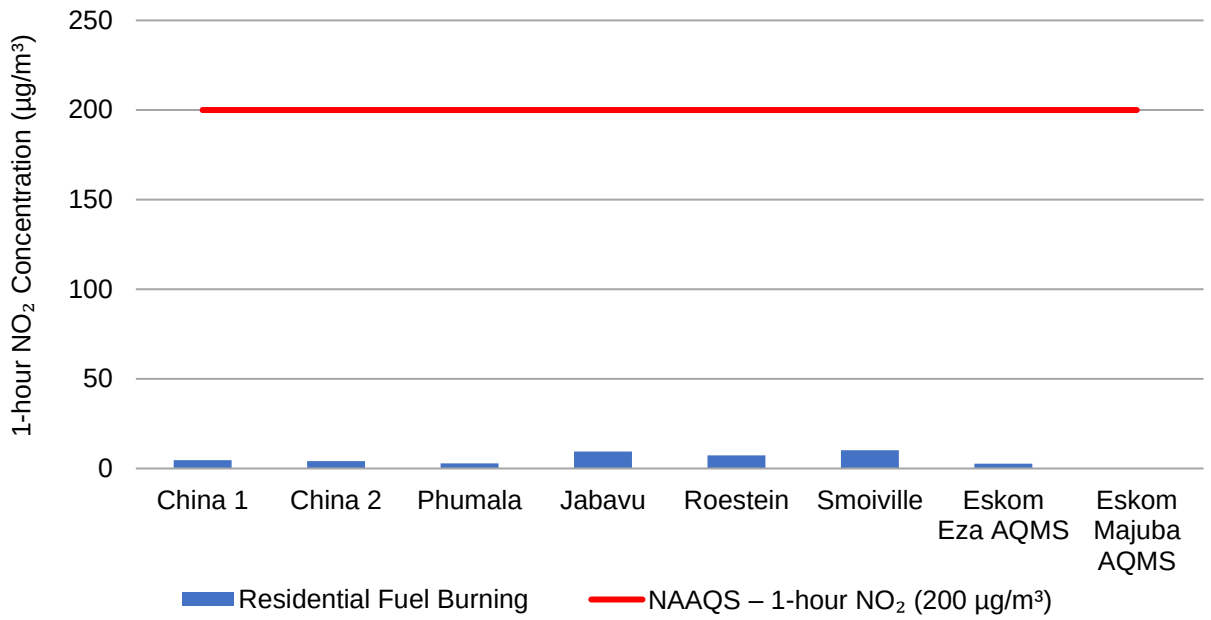

Figure 5-50: Model predicted 1-hour NO_2 ambient concentrations (99th percentile) in µg/m³ at discrete receptors for the Residential Fuel Burning emission source category

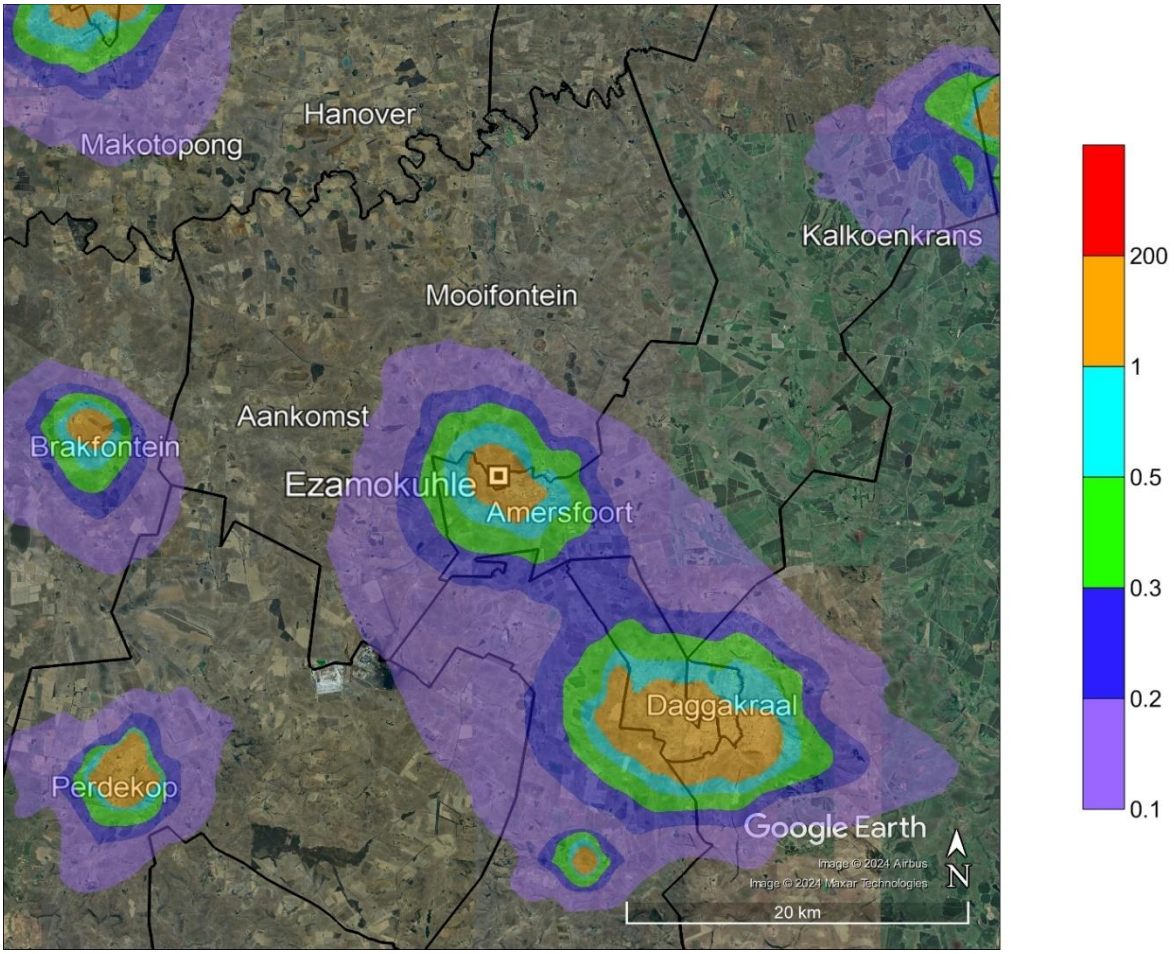

Figure 5-51: Model predicted 1-hour NO_2 ambient concentrations (99th percentile) in µg/m³ for the Residential Fuel Burning emission source category within the Greater Ezamokuhle Airshed

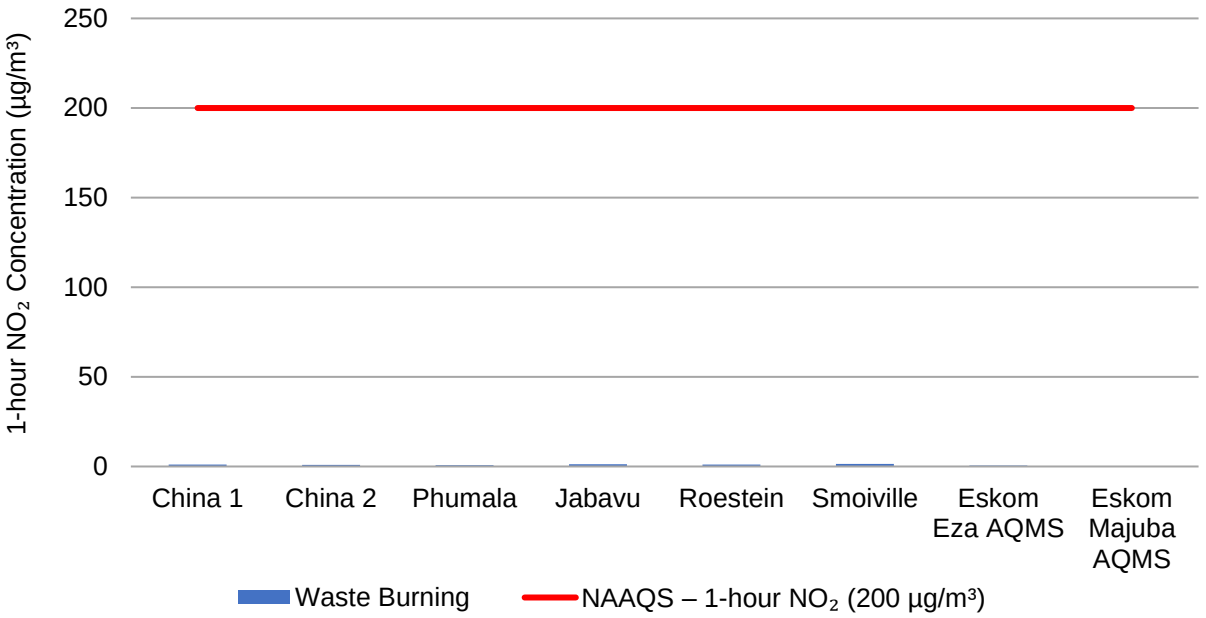

Figure 5-52: Model predicted 1-hour NO_2 ambient concentrations (99th percentile) in µg/m³ at discrete receptors for the Waste Burning emission source category

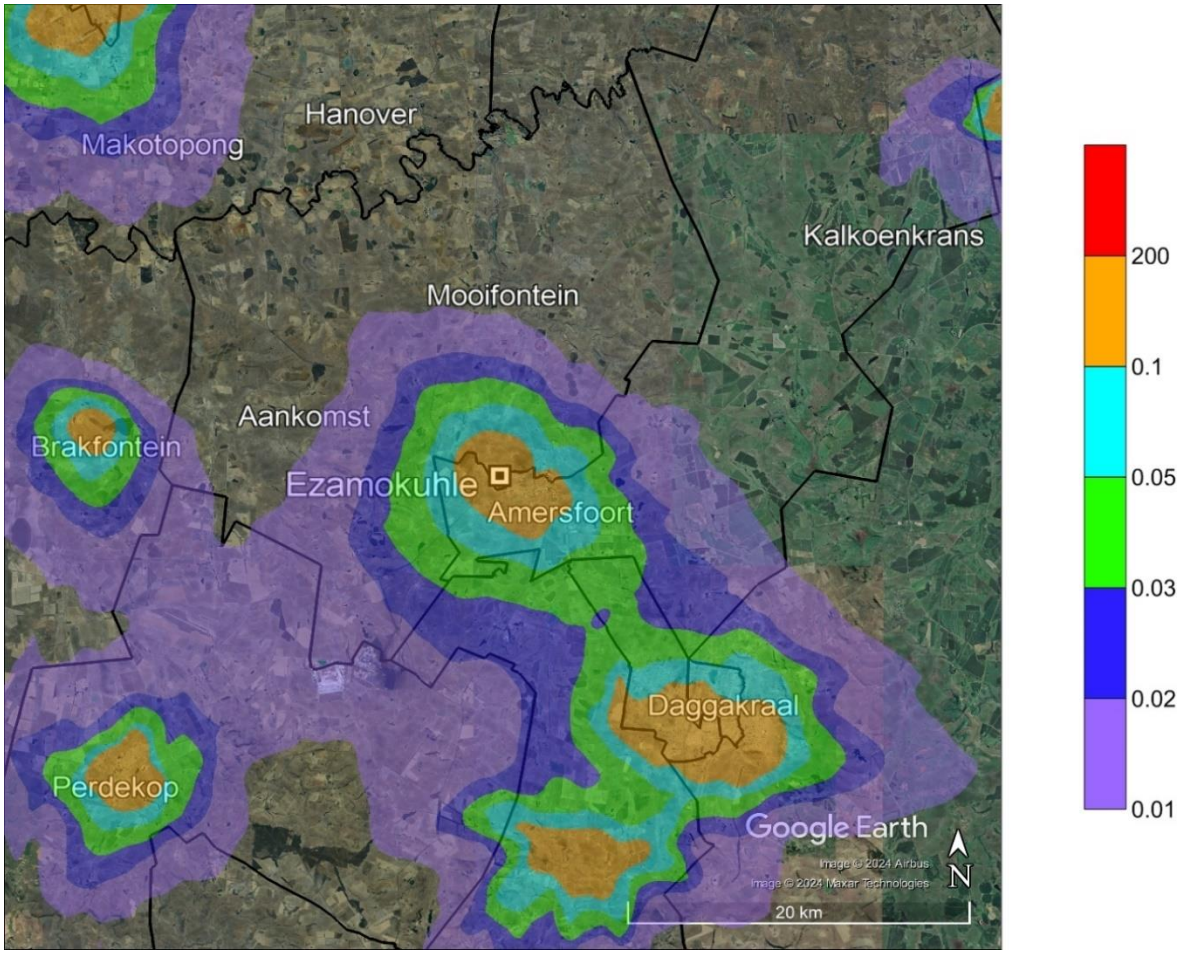

Figure 5-53: Model predicted 1-hour NO_2 ambient concentrations (99th percentile) in µg/m³ for the Waste Burning emission source category within the Greater Ezamokuhle Airshed

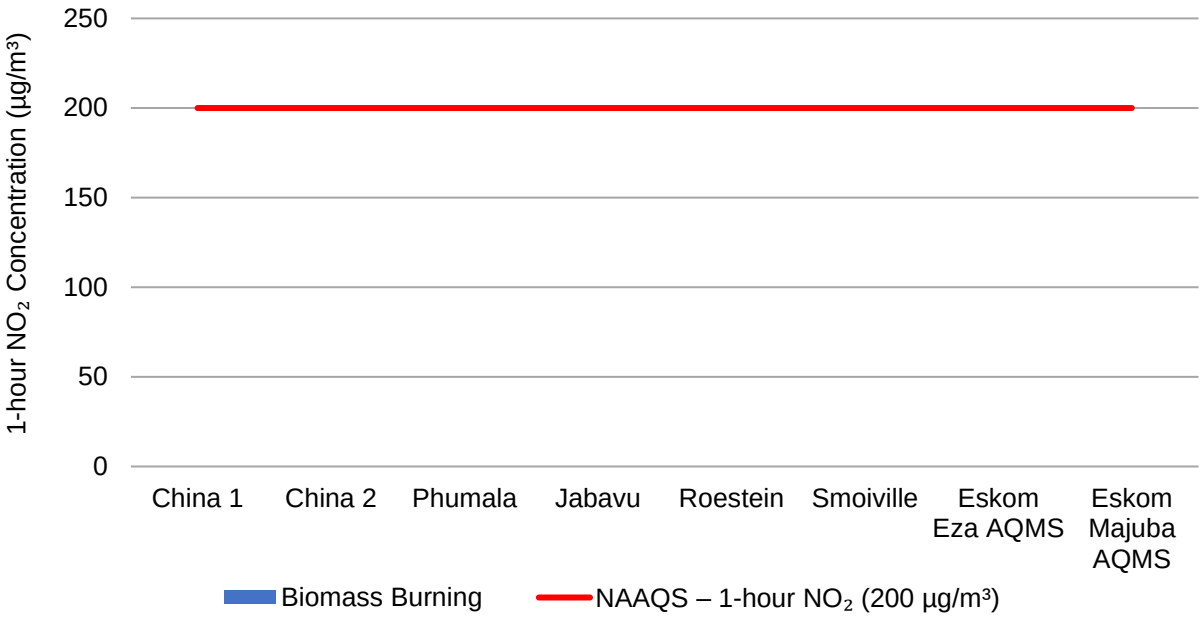

Figure 5-54: Model predicted 1-hour NO_2 ambient concentrations (99th percentile) in µg/m³ at discrete receptors for the Biomass Burning emission source category

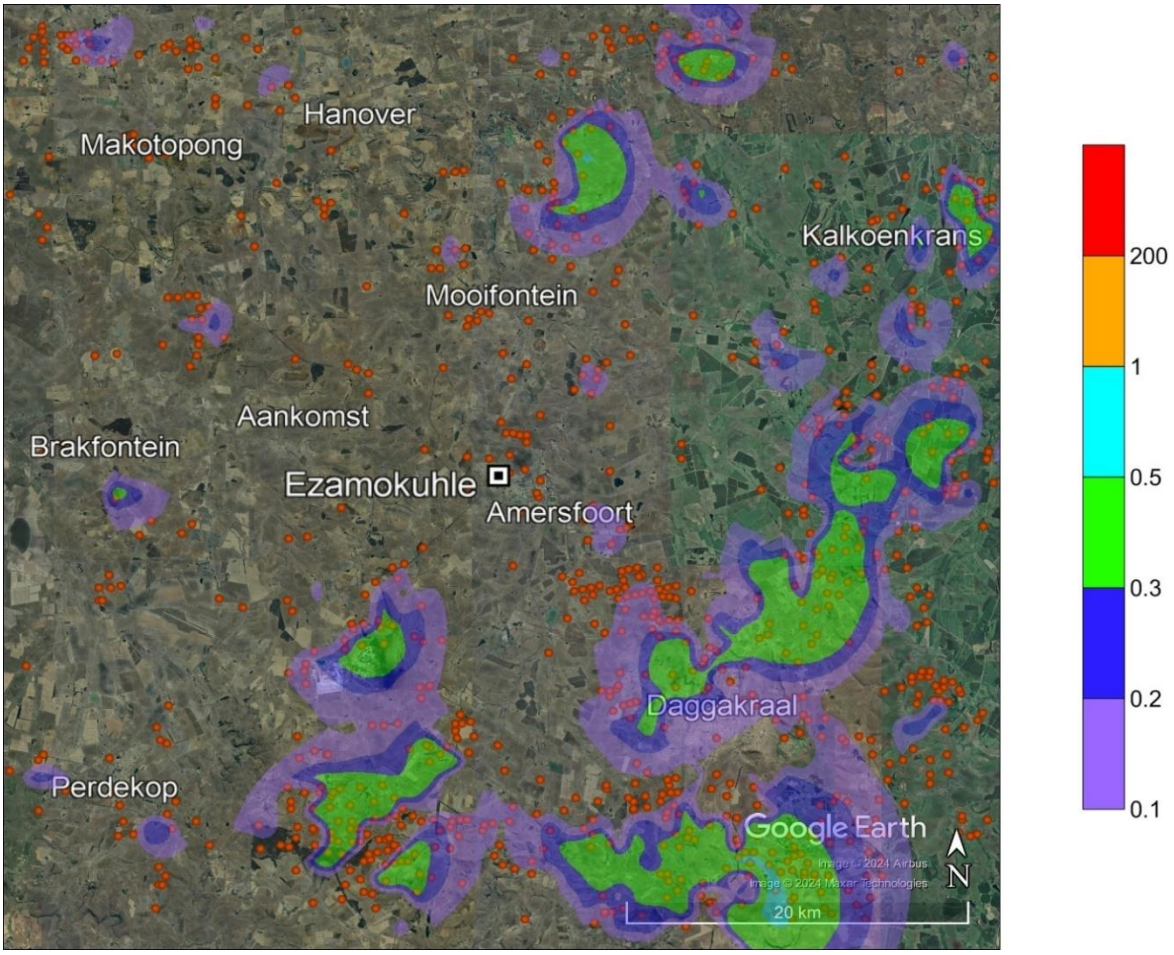

Figure 5-55: Model predicted 1-hour NO_2 ambient concentrations (99th percentile) in µg/m³ for the Biomass Burning emission source category within the Greater Ezamokuhle Airshed

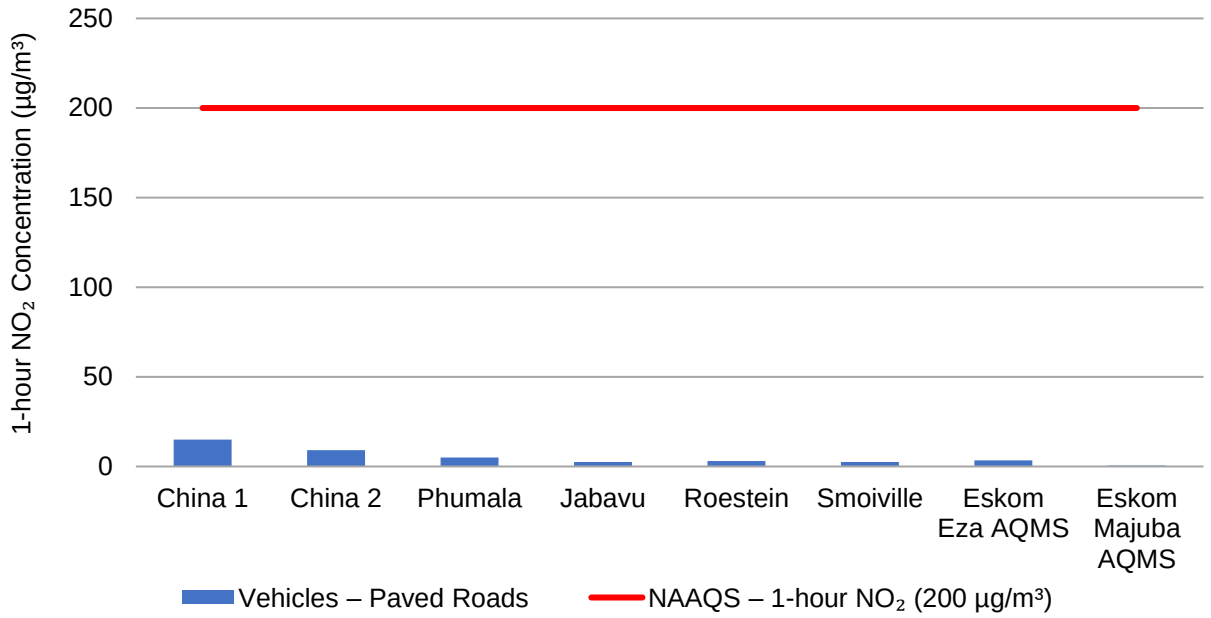

Figure 5-56: Model predicted 1-hour NO_2 ambient concentrations (99th percentile) in µg/m³ at discrete receptors for the Vehicles – Paved Roads emission source category

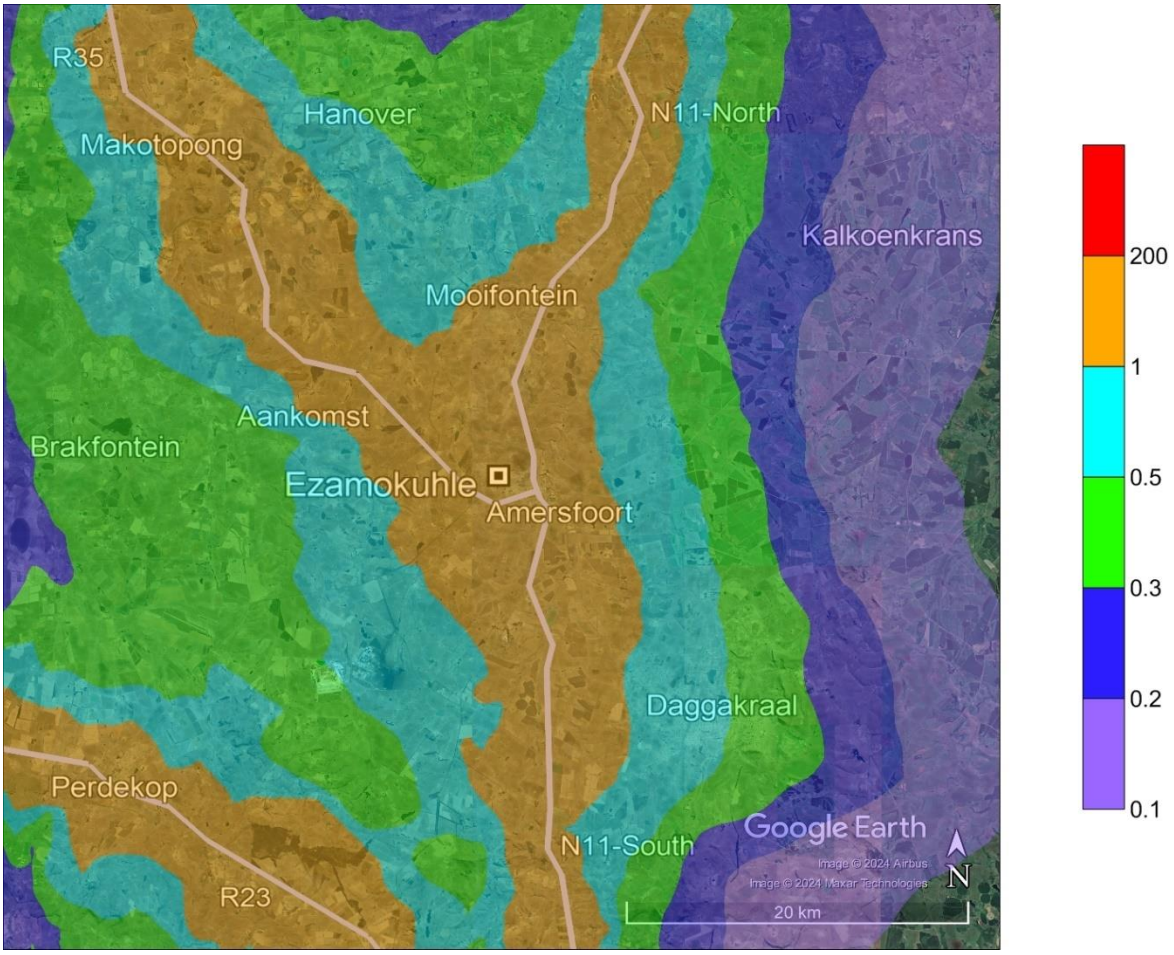

Figure 5-57: Model predicted 1-hour NO_2 ambient concentrations (99th percentile) in µg/m³ for the Vehicles – Paved Roads emission source category within the Greater Ezamokuhle Airshed

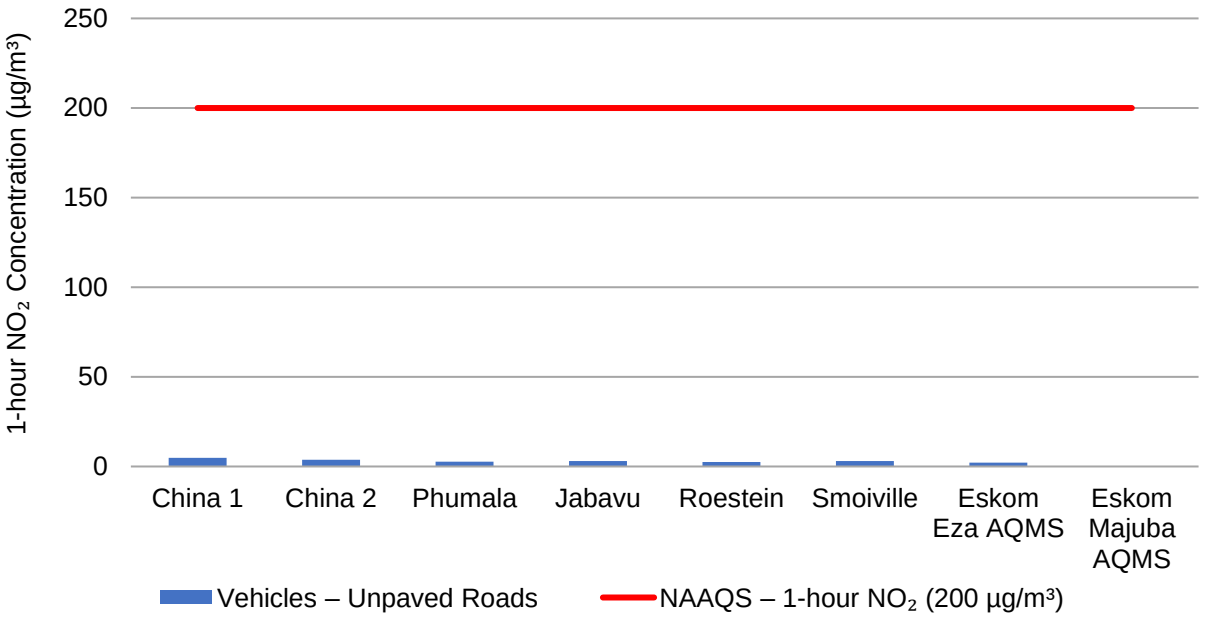

Figure 5-58: Model predicted 1-hour NO_2 ambient concentrations (99th percentile) in µg/m³ at discrete receptors for the Vehicles – Unpaved Roads emission source category

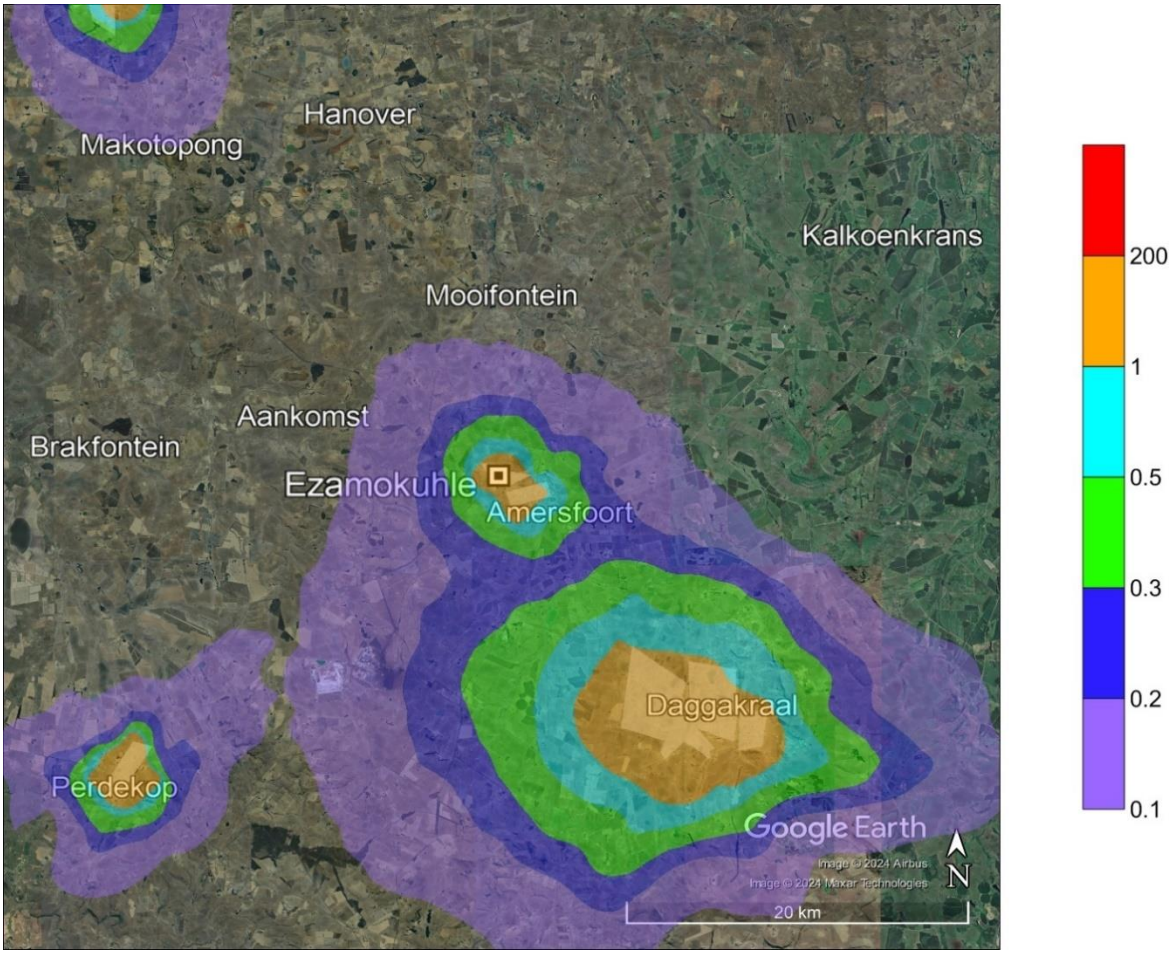

Figure 5-59: Model predicted 1-hour NO_2 ambient concentrations (99th percentile) in µg/m³ for the Vehicles – Unpaved Roads emission source category within the Greater Ezamokuhle Airshed

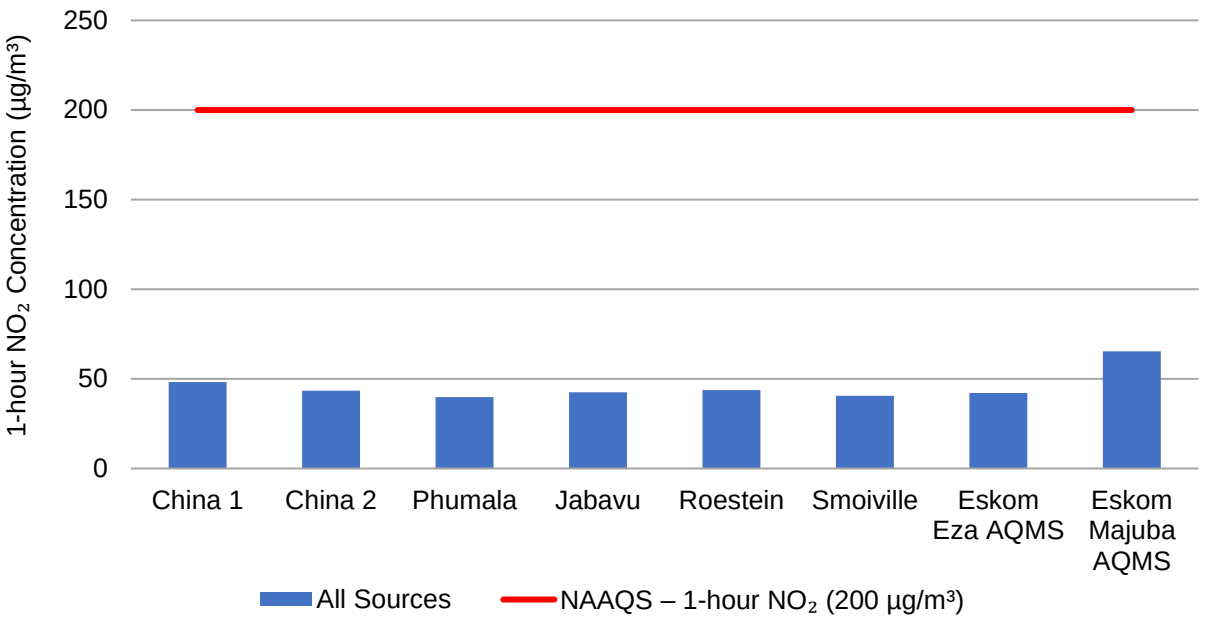

Figure 5-60: Model predicted 1-hour NO_2 ambient concentrations (99th percentile) in µg/m³ at discrete receptors for the All Sources emission source category

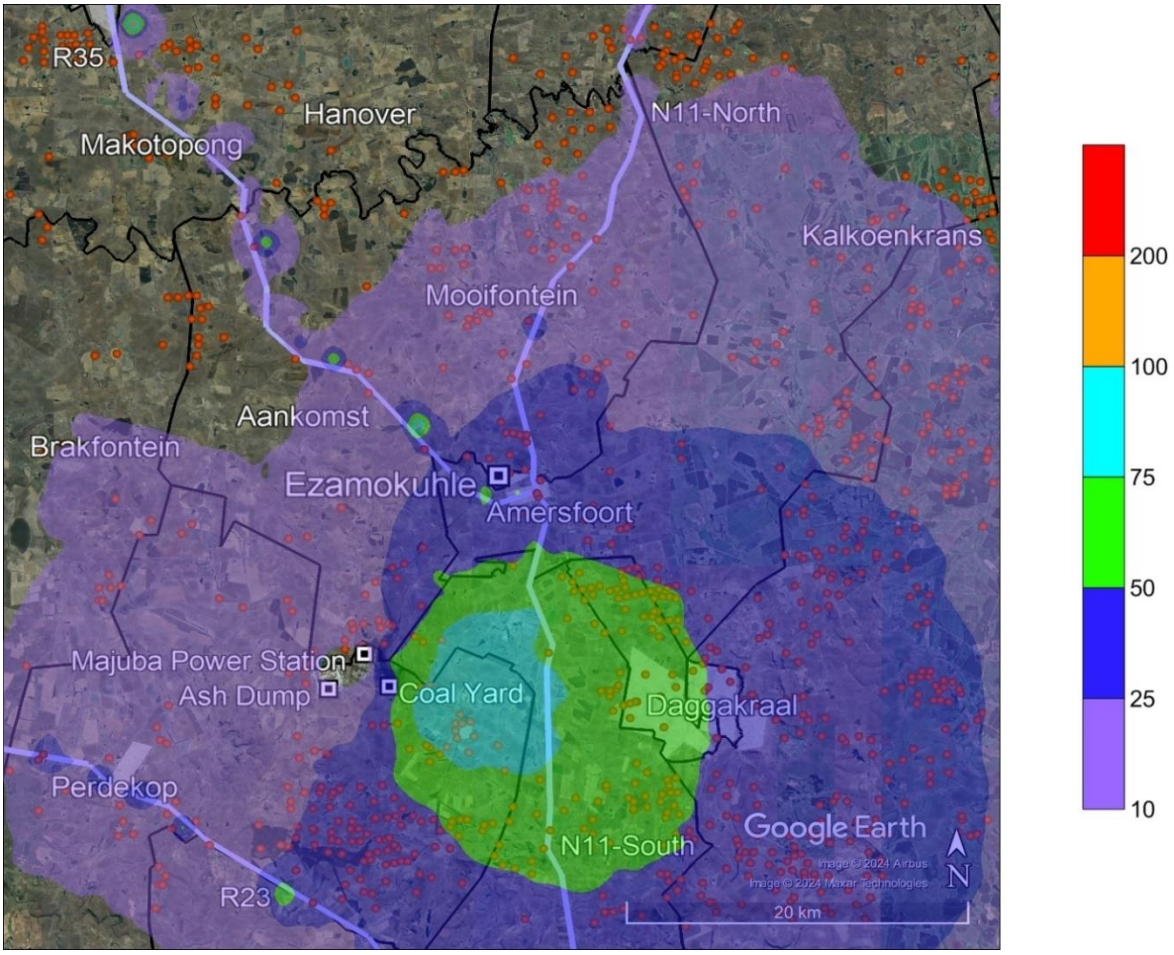

Figure 5-61: Model predicted 1-hour NO_2 ambient concentrations (99th percentile) in µg/m³ for the All Sources emission source category within the Greater Ezamokuhle Airshed

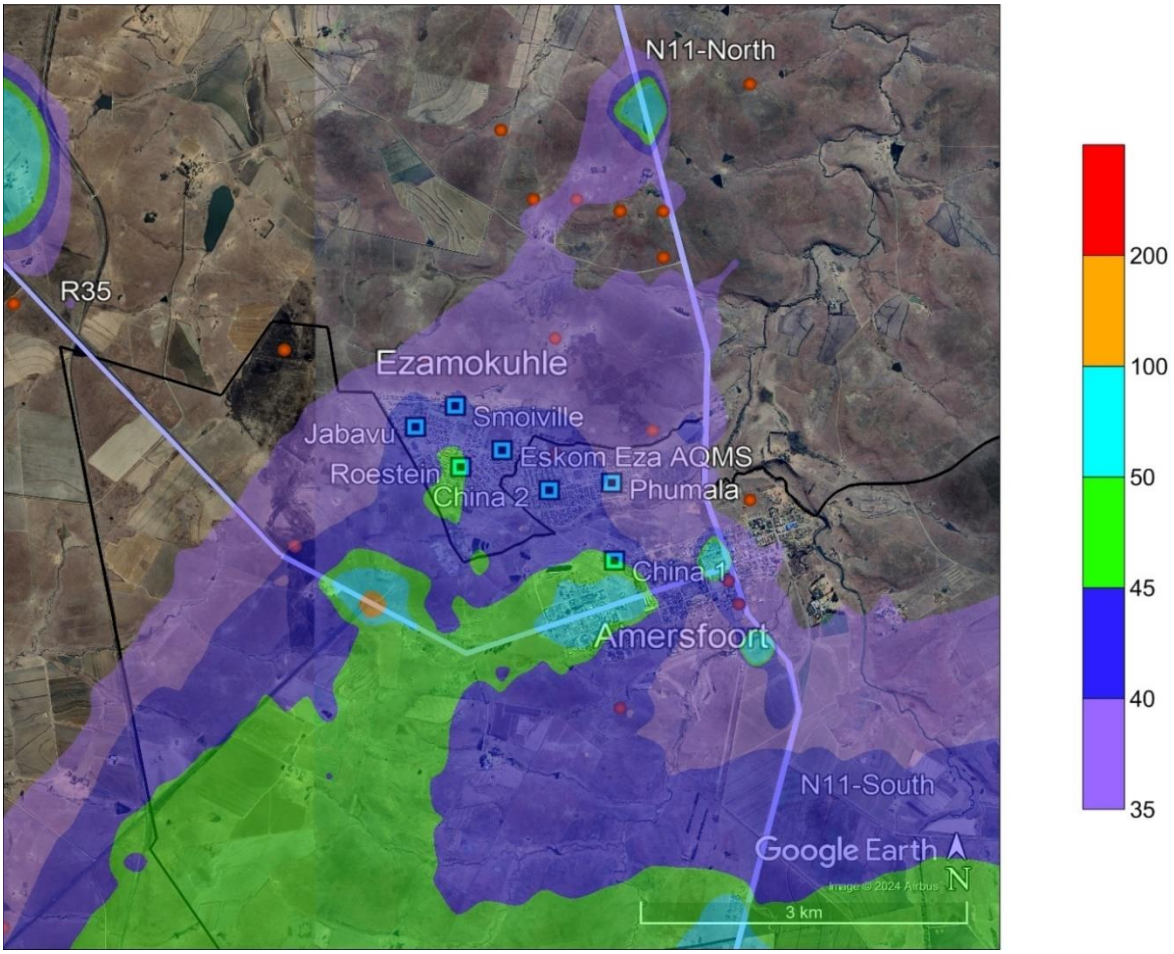

Figure 5-62: Model predicted 1-hour NO_2 ambient concentrations (99th percentile) in µg/m^3 for the All Sources emission source category within Ezamokuhle airshed

5.2.2 ANNUAL NO_2

Model predicted annual NO_2 ambient concentrations at discrete receptors and at the point of maximum for the seven emission source categories are presented in Table 5-6. If applicable, exceedances of the NAAQS are highlighted in red.

Bar graphs for model predicted annual NO_2 ambient concentrations at discrete receptors are presented in the following order:

- Figure 5-63 for the Power Generation emission source category
- Figure 5-65 for the Residential Fuel Burning emission source category
- Figure 5-67 for the Waste Burning emission source category
- Figure 5-69 for the Biomass Burning emission source category
- Figure 5-71 for the Vehicles – Paved Roads emission source category
- Figure 5-73 for the Vehicles – Unpaved Roads emission source category
- Figure 5-75 for the All Sources emission source category

Contour plots for model predicted annual NO_2 ambient concentrations for the Greater Ezamokuhle Airshed are presented in the following order:

- Figure 5-64 for the Power Generation emission source category
- Figure 5-66 for the Residential Fuel Burning emission source category
- Figure 5-68 for the Waste Burning emission source category
- Figure 5-70 for the Biomass Burning emission source category
- Figure 5-72 for the Vehicles – Paved Roads emission source category
- Figure 5-74 for the Vehicles – Unpaved Roads emission source category
- Figure 5-76 for the All Sources emission source category

Contour plots for model predicted annual NO_2 ambient concentrations for the Ezamokuhle airshed is presented in Figure 5-77 for the All Sources emission source category.

With respect to contour plots for the primary and Ezamokuhle airshed, areas of exceedance of the NAAQS is coloured in red.

Table 5-6: Model predicted annual NO_2 ambient concentrations in µg/m^3 at discrete receptors and at the point of maximum for the seven emission source categories

Discrete Receptors	Power Generation	Residential Fuel Burning	Waste Burning	Biomass Burning	Vehicles – Paved Roads	Vehicles – Unpaved Roads	All Sources
China 1	1.13	1.05	0.24	0.00	2.38	0.96	5.77
China 2	1.16	0.93	0.21	0.00	0.93	0.80	4.04
Phumala	1.11	0.56	0.13	0.00	0.51	0.50	2.81
Jabavu	1.14	2.28	0.31	0.00	0.33	0.71	4.77
Roestein	1.18	1.57	0.22	0.00	0.37	0.46	3.81
Smoiville	1.13	2.83	0.39	0.00	0.33	0.78	5.46
Eskom Eza AQMS	1.16	0.52	0.10	0.00	0.39	0.36	2.53
Eskom Majuba AQMS	2.68	0.01	0.00	0.03	0.07	0.01	2.79
Maximum	3.46	3.49	0.64	0.12	14.45	2.02	15.93
	NAAQS – annual NO_2 (40 µg/m^3)						

According to Table 5-6, model predicted annual NO_2 ambient concentrations are below the annual NO_2 NAAQS of 40 µg/m^3 at all discrete receptors and at the point of maximum for all seven emission source categories, both in the Greater Ezamokuhle Airshed and in the Ezamokuhle Airshed. There are no exceedances of the NAAQS both in the Greater Ezamokuhle Airshed and in the Ezamokuhle Airshed.

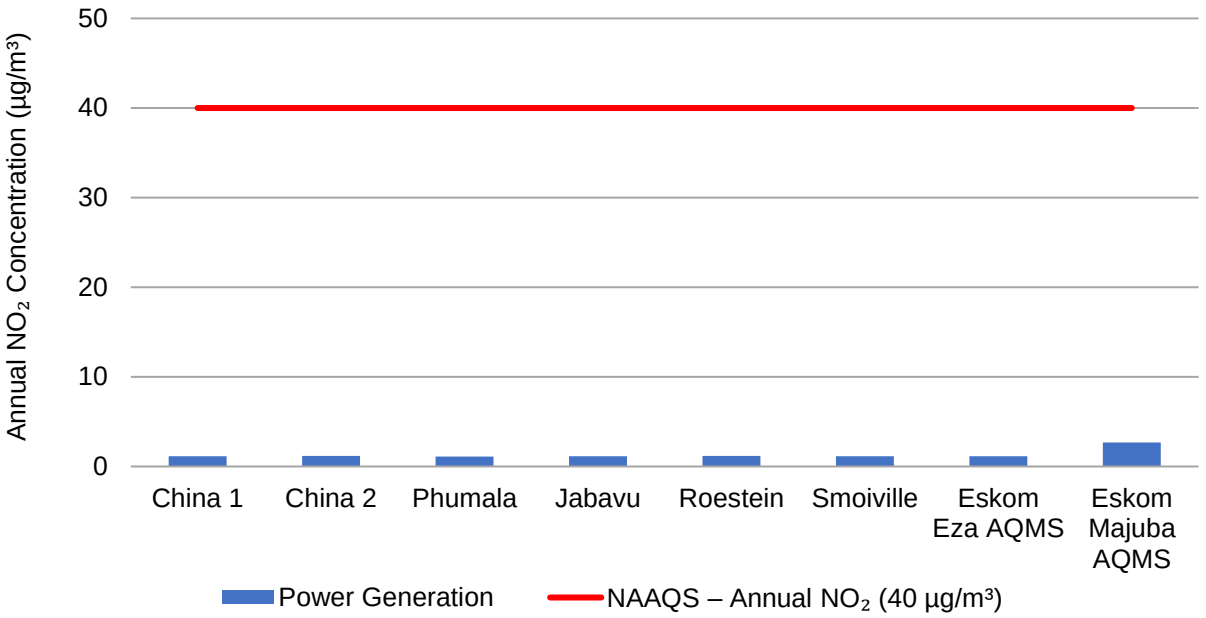

Figure 5-63: Model predicted annual NO_2 ambient concentrations in µg/m³ at discrete receptors for the Power Generation emission source category

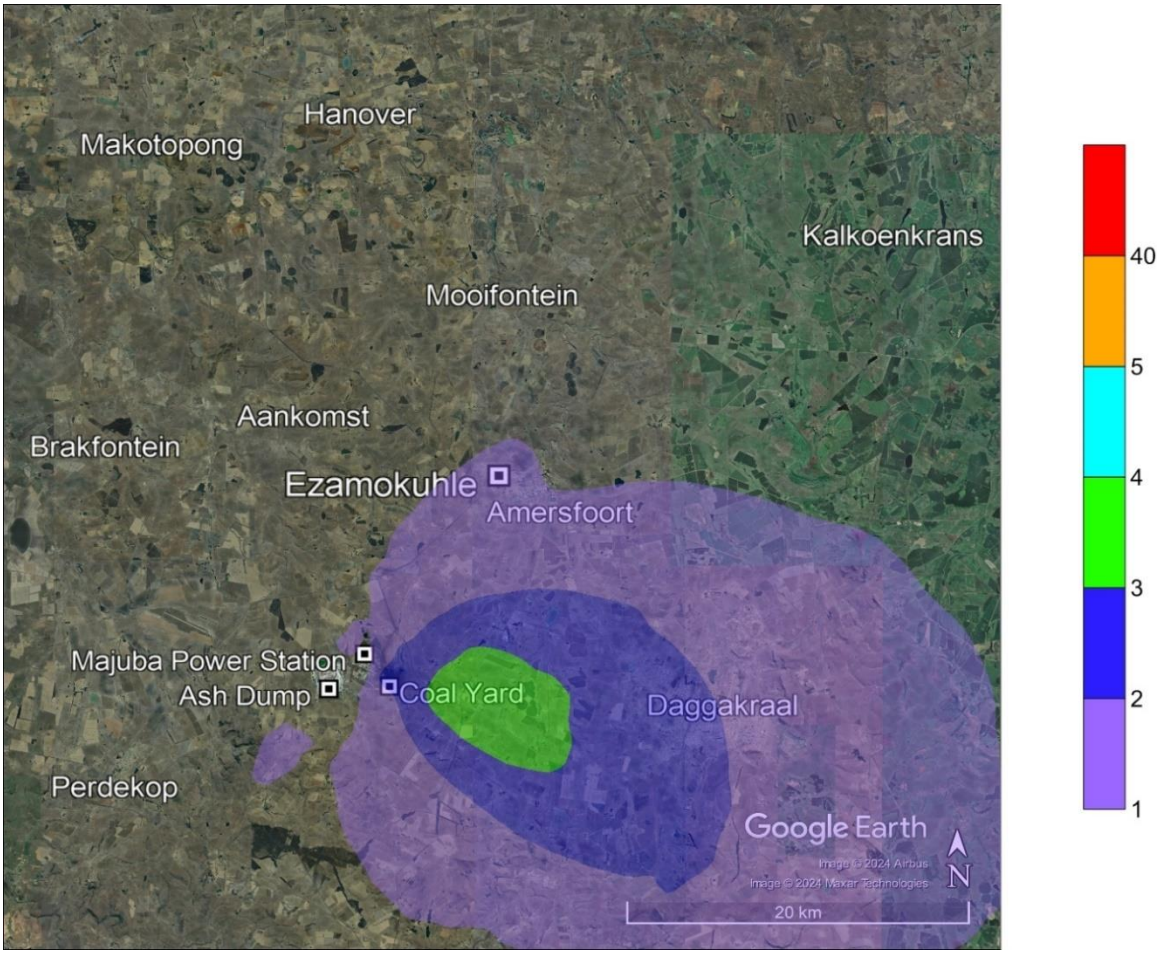

Figure 5-64: Model predicted annual NO_2 ambient concentrations in µg/m³ for the Power Generation emission source category within the Greater Ezamokuhle Airshed

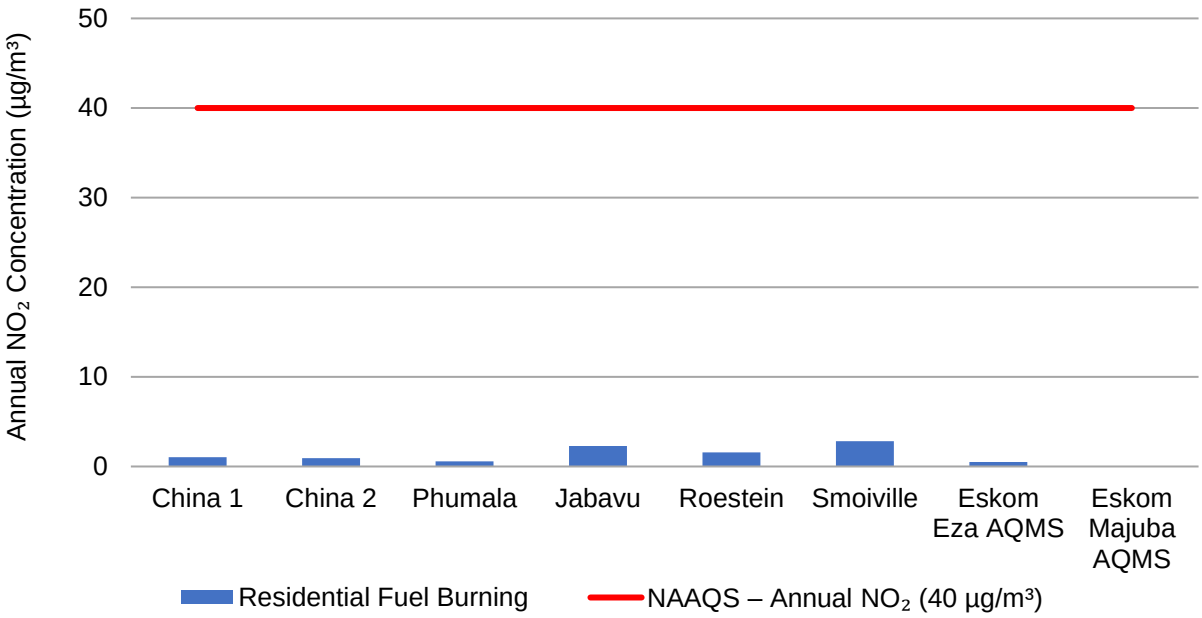

Figure 5-65: Model predicted annual NO_2 ambient concentrations in µg/m³ at discrete receptors for the Residential Fuel Burning emission source category

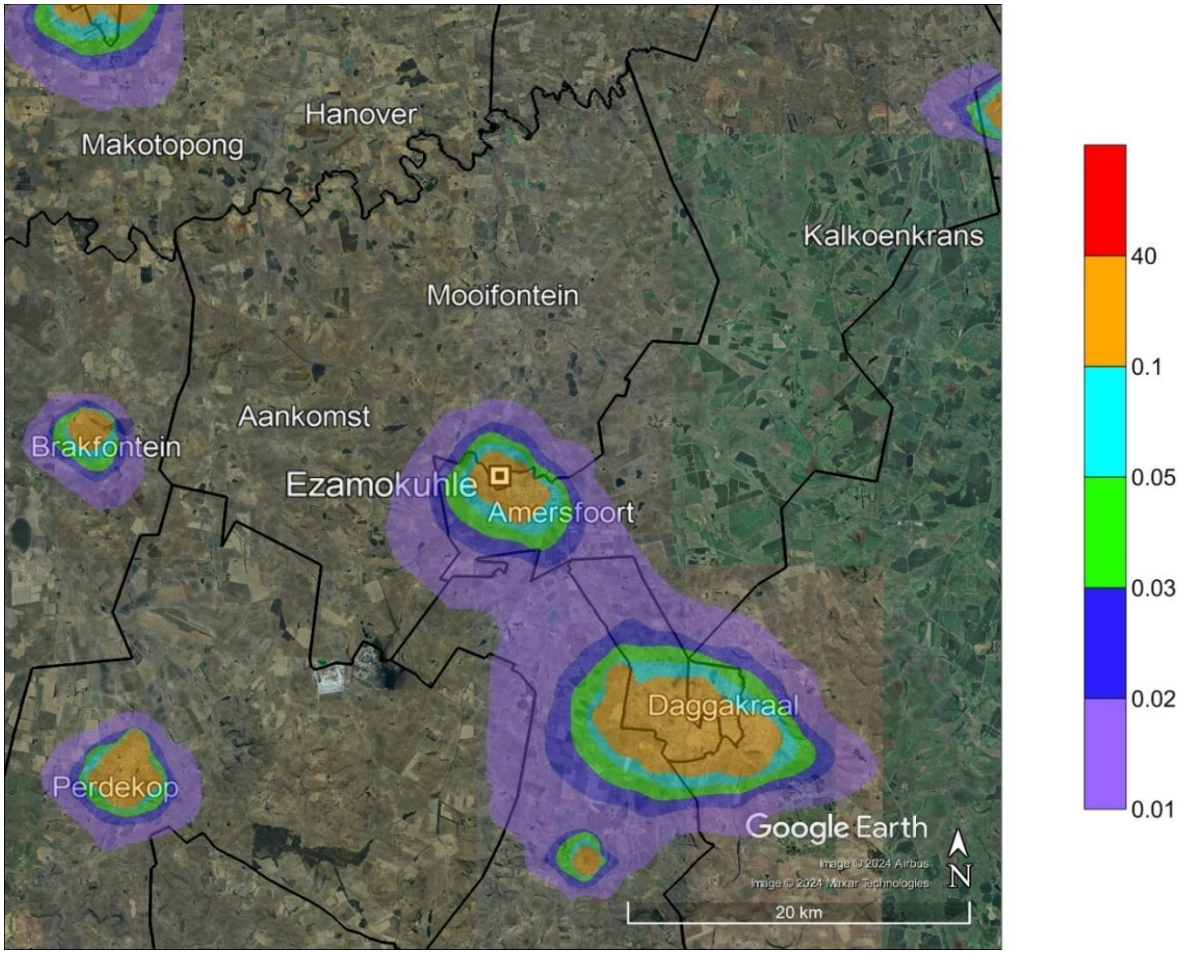

Figure 5-66: Model predicted annual NO_2 ambient concentrations in µg/m³ for the Residential Fuel Burning emission source category within the Greater Ezamokuhle Airshed

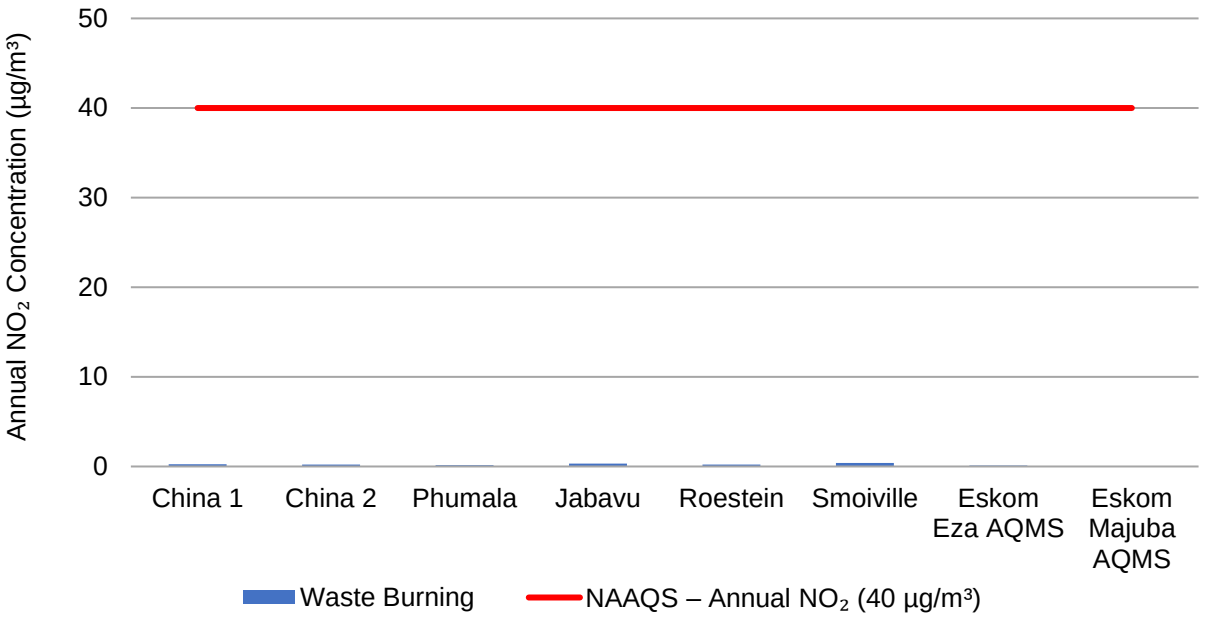

Figure 5-67: Model predicted annual NO_2 ambient concentrations in µg/m³ at discrete receptors for the Waste Burning emission source category

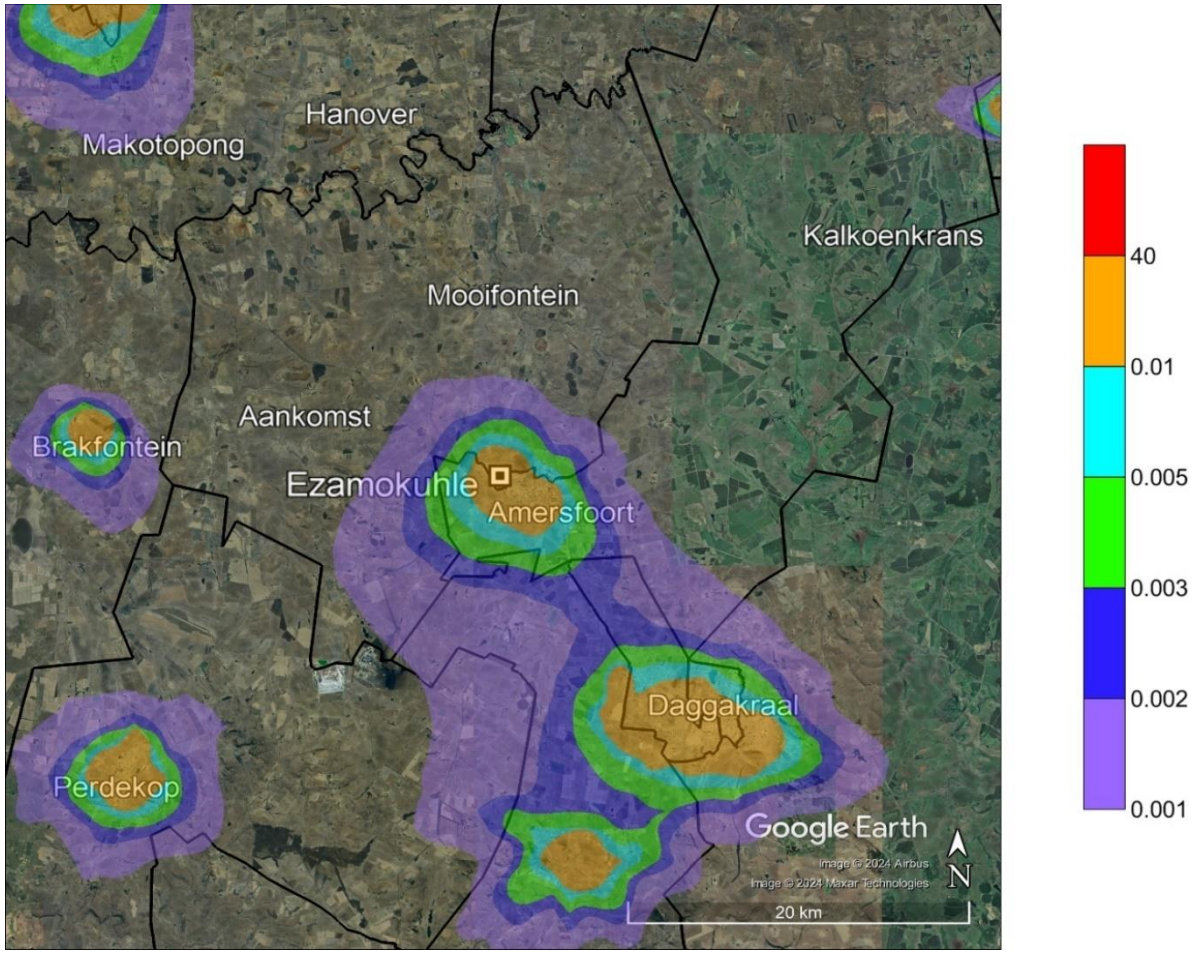

Figure 5-68: Model predicted annual NO_2 ambient concentrations in µg/m³ for the Waste Burning emission source category within the Greater Ezamokuhle Airshed

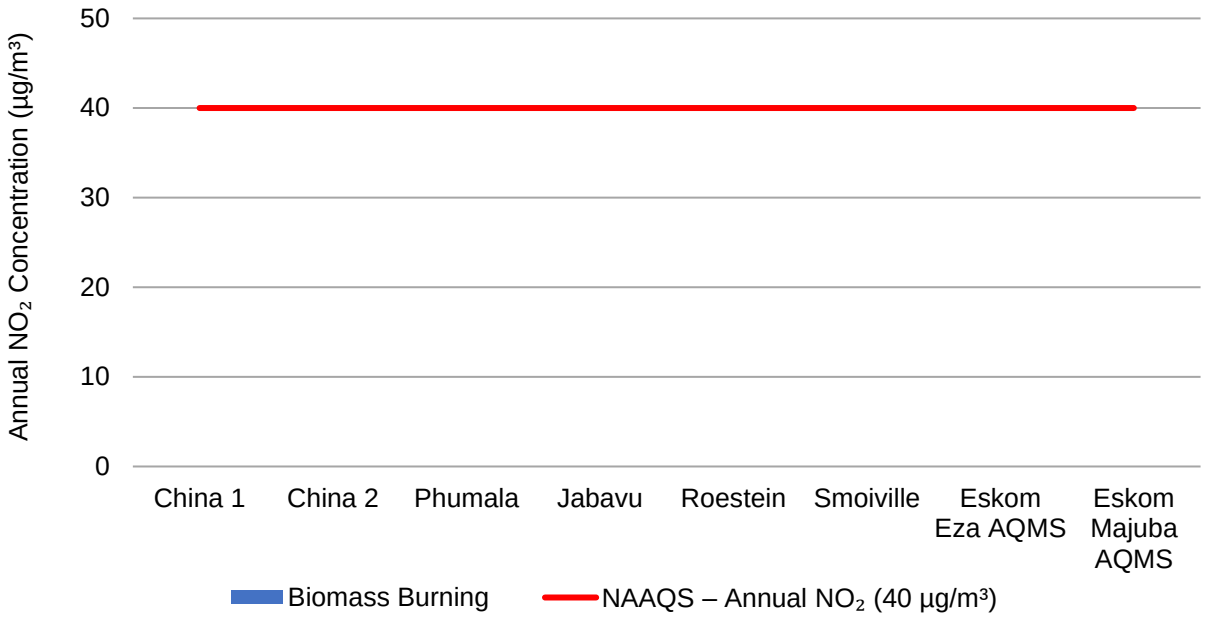

Figure 5-69: Model predicted annual NO_2 ambient concentrations in µg/m³ at discrete receptors for the Biomass Burning emission source category

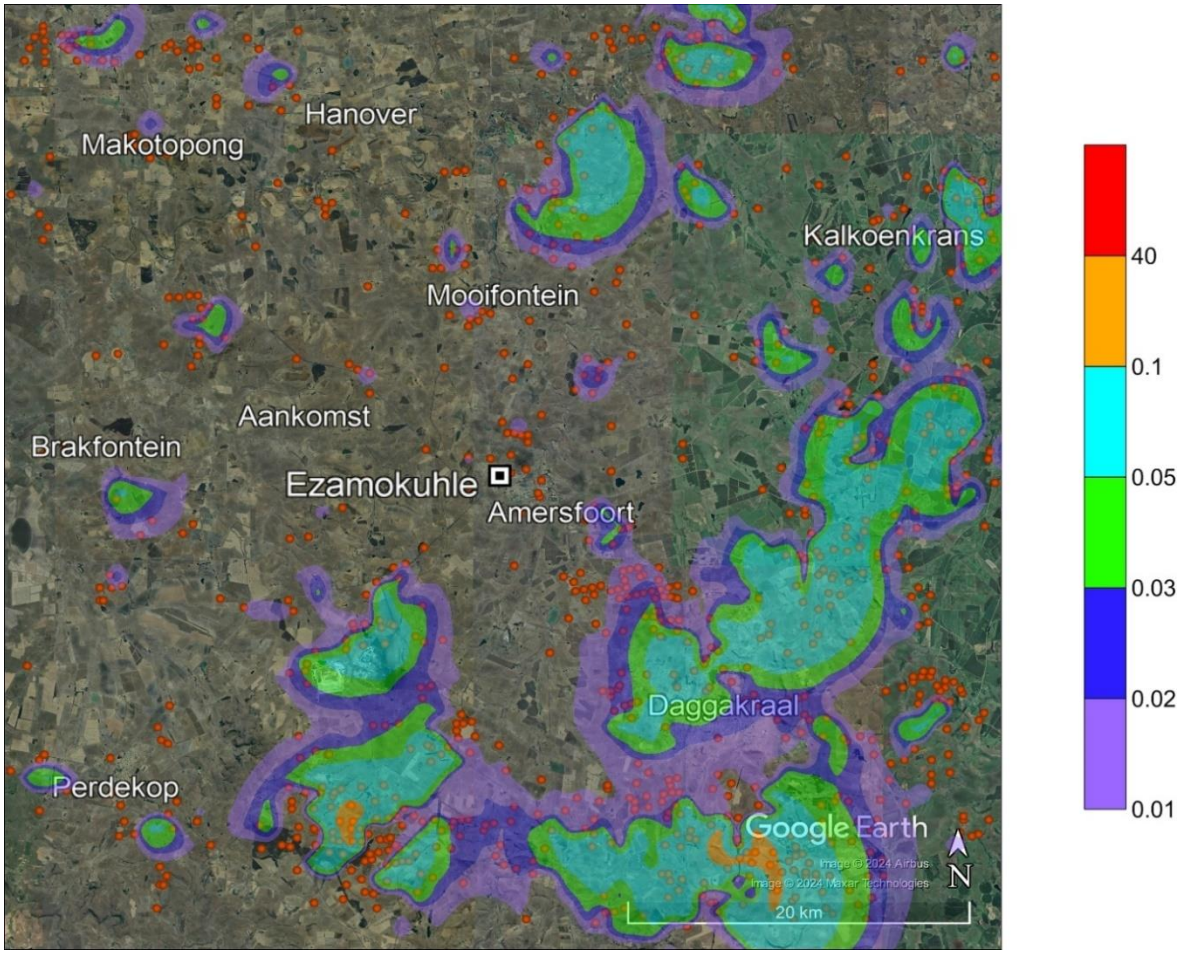

Figure 5-70: Model predicted annual NO_2 ambient concentrations in µg/m³ for the Biomass Burning emission source category within the Greater Ezamokuhle Airshed

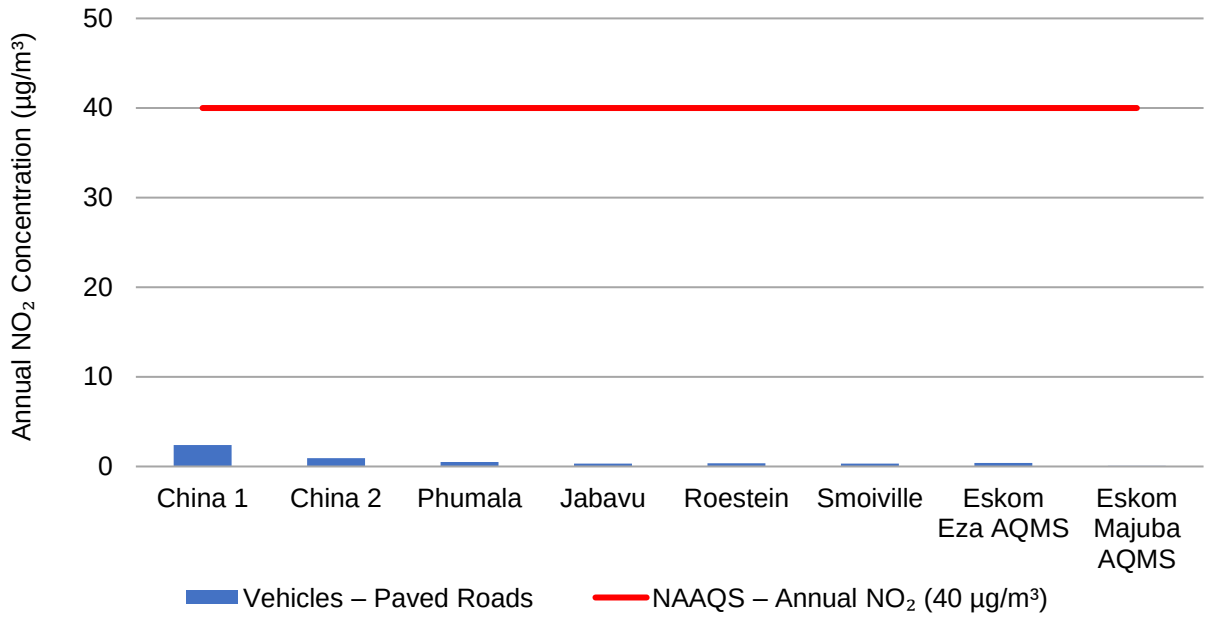

Figure 5-71: Model predicted annual NO_2 ambient concentrations in µg/m^3 at discrete receptors for the Vehicles – Paved Roads emission source category

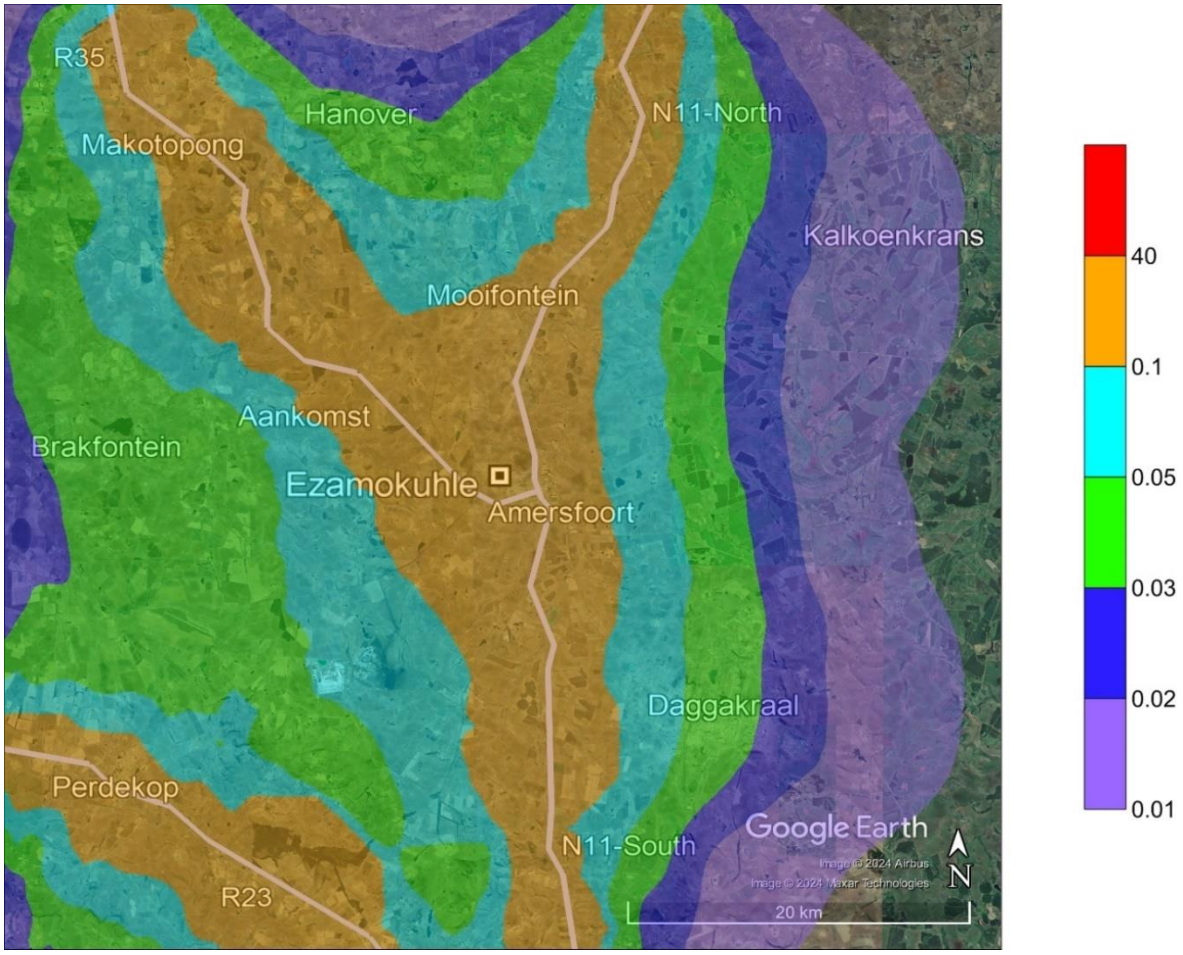

Figure 5-72: Model predicted annual NO_2 ambient concentrations in µg/m^3 for the Vehicles – Paved Roads emission source category within the Greater Ezamokuhle Airshed

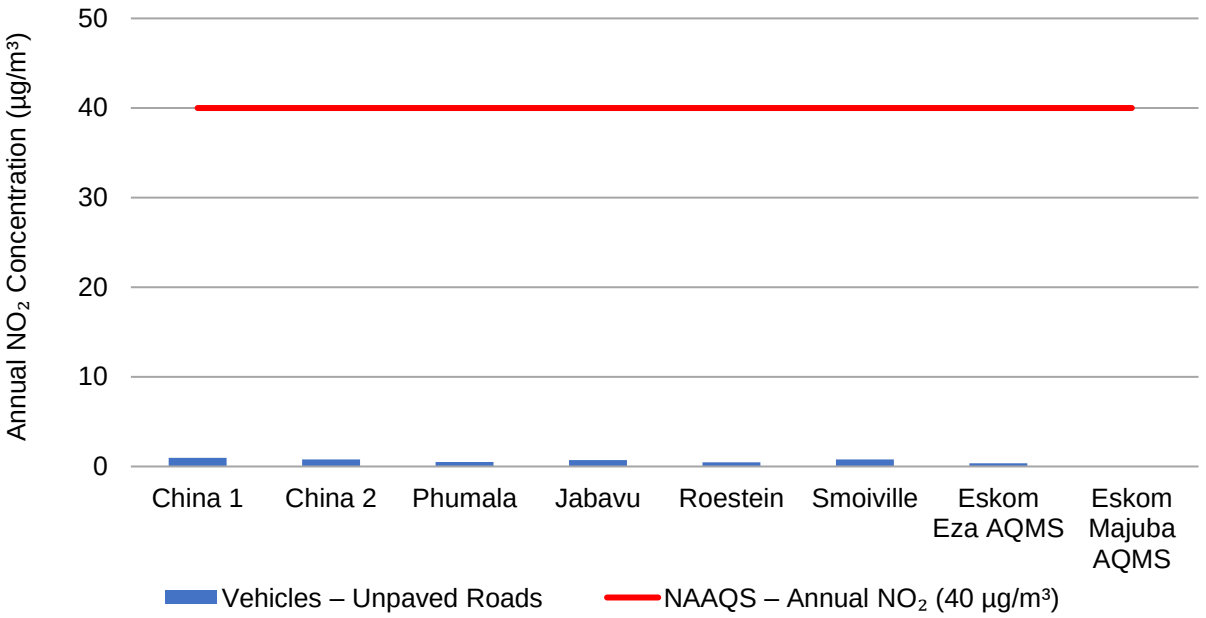

Figure 5-73: Model predicted annual NO_2 ambient concentrations in µg/m³ at discrete receptors for the Vehicles – Unpaved Roads emission source category

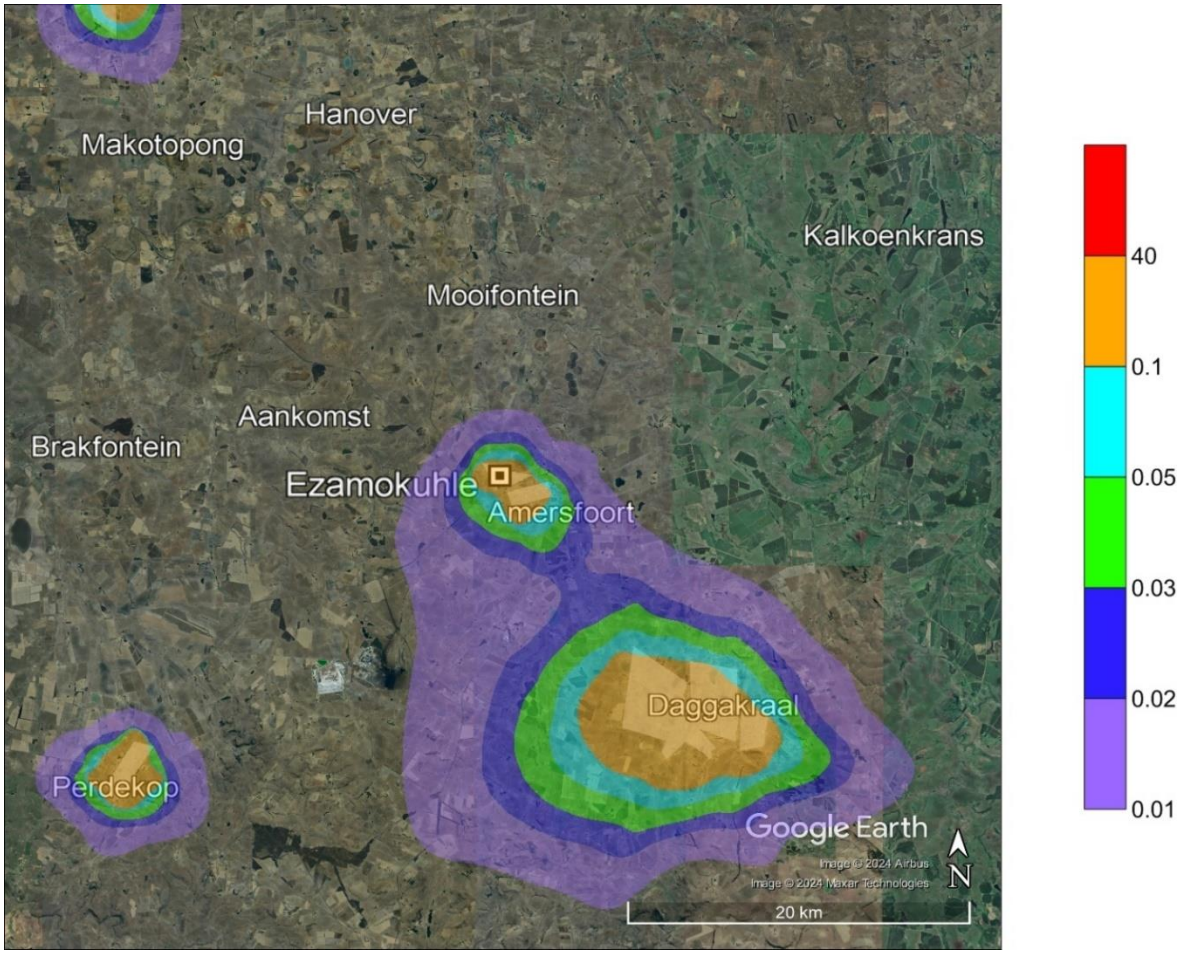

Figure 5-74: Model predicted annual NO_2 ambient concentrations in µg/m³ for the Vehicles – Unpaved Roads emission source category within the Greater Ezamokuhle Airshed

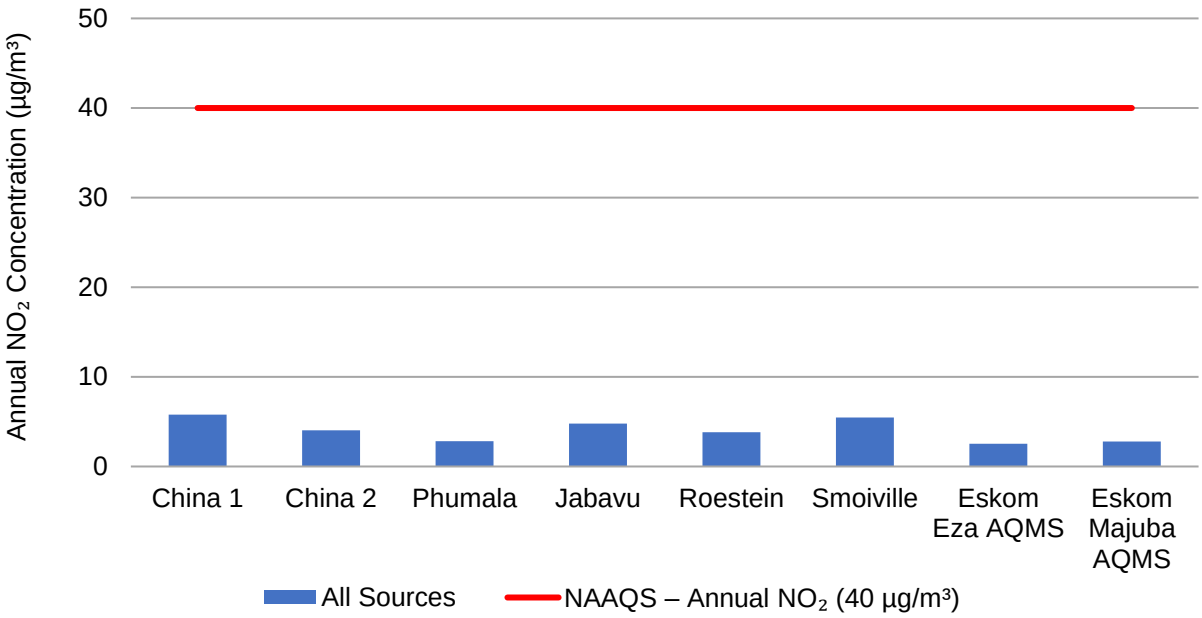

Figure 5-75: Model predicted annual NO_2 ambient concentrations in µg/m³ at discrete receptors for the All Sources emission source category

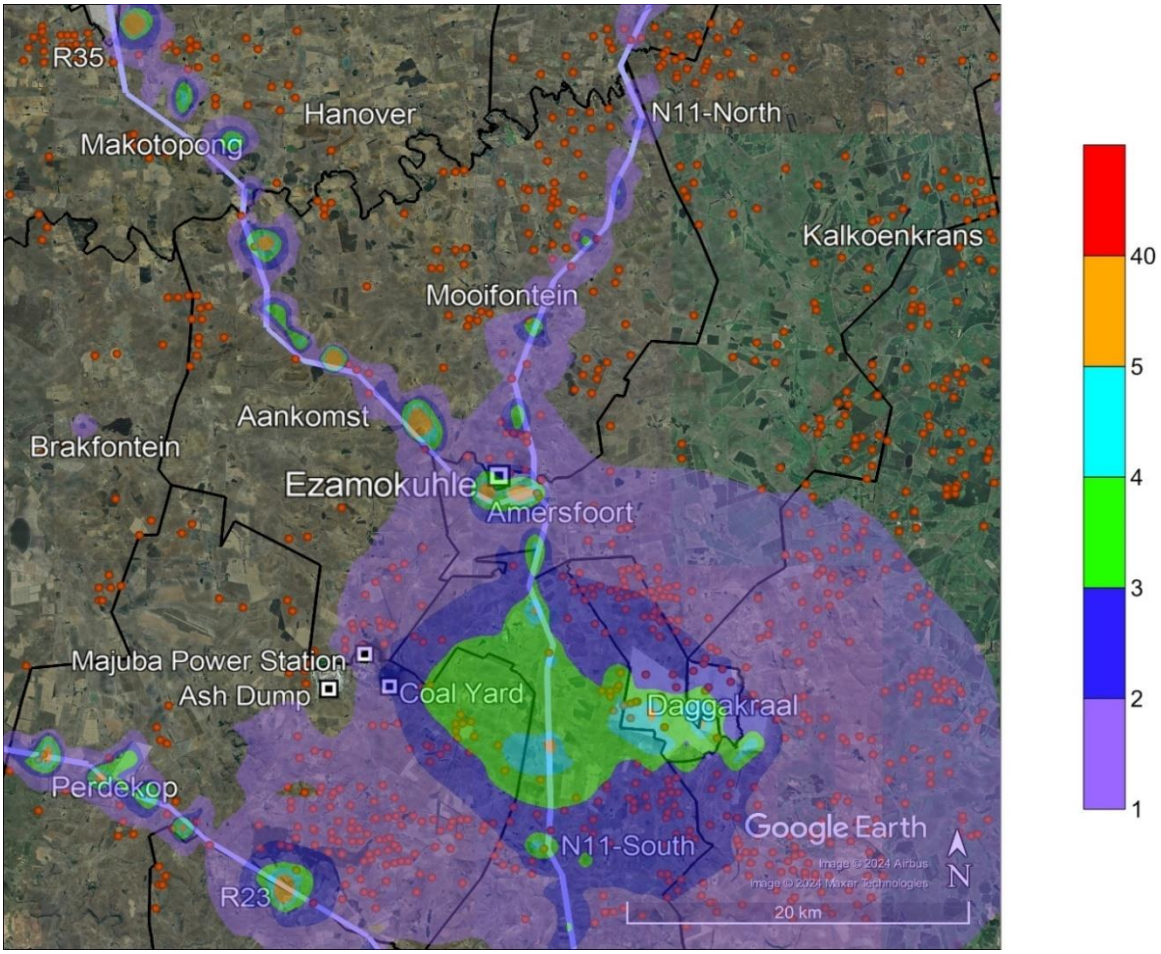

Figure 5-76: Model predicted annual NO_2 ambient concentrations in µg/m³ for the All Sources emission source category within the Greater Ezamokuhle Airshed

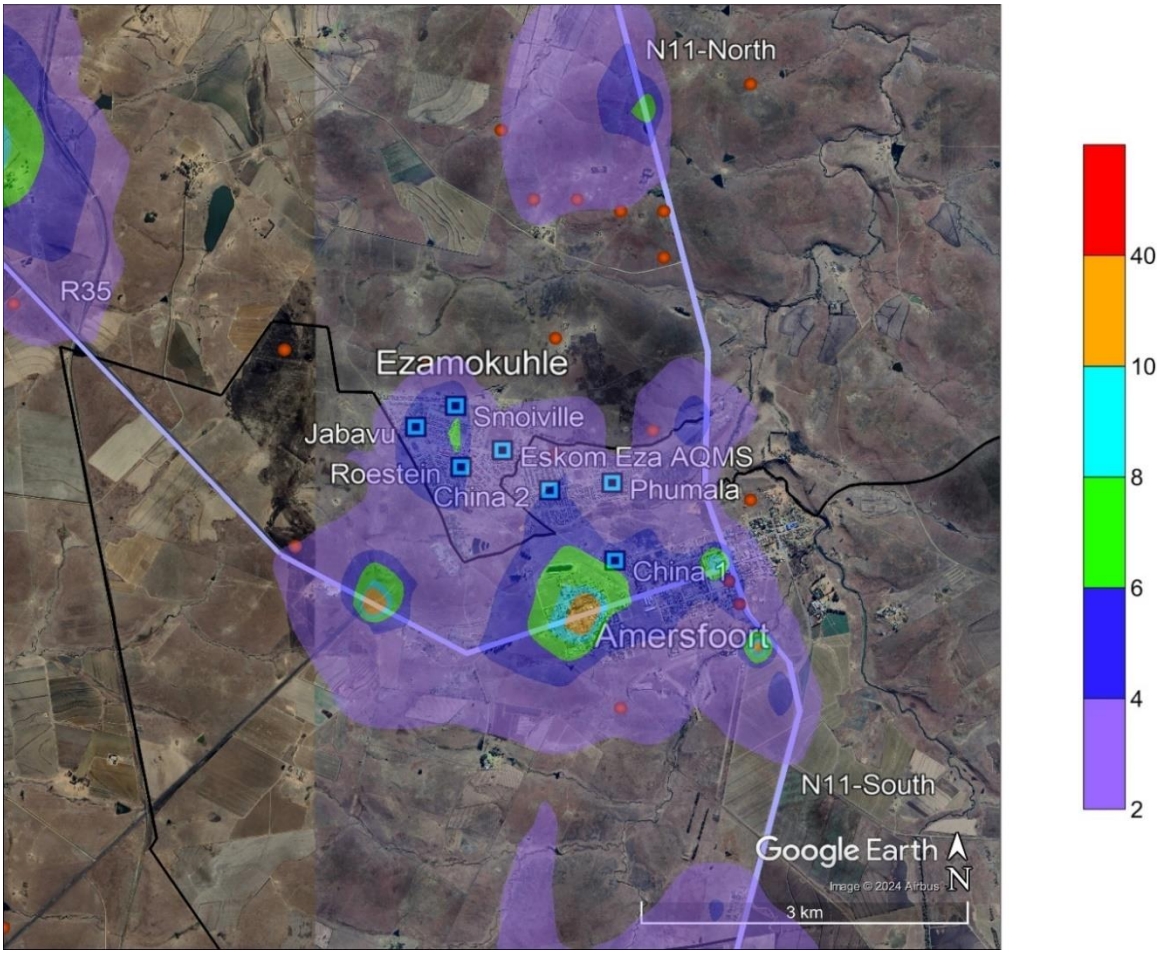

Figure 5-77: Model predicted annual NO_2 ambient concentrations in µg/m³ for the All Sources emission source category within Ezamokuhle airshed

5.2.3 NO_2 SOURCE CONTRIBUTION ANALYSIS

In this study, the NO_2 source contribution analysis is based on model predicted annual NO_2 ambient concentrations at the discrete receptors for the six emission source categories which include power generation, residential fuel burning, waste burning, biomass burning, vehicles – paved roads and vehicles – unpaved roads (Table 5-6). Table 5-6 is used to calculate the percent contribution of NO_2 at each discrete receptor as a function of the six source categories and is presented in Table 5-7.

Table 5-7: NO_2 source contribution (%) at discrete receptors for the six emission source categories based on model predicted annual NO_2 ambient concentrations

Discrete Receptors	Power Generation	Residential Fuel Burning	Waste Burning	Biomass Burning	Vehicles – Paved Roads	Vehicles – Unpaved Roads	All Sources
China 1	19.59	18.25	4.23	0.05	41.19	16.71	100.00
China 2	28.76	23.12	5.12	0.07	23.08	19.85	100.00
Phumala	39.68	19.77	4.50	0.10	18.26	17.69	100.00
Jabavu	23.80	47.73	6.59	0.08	7.01	14.79	100.00
Roestein	31.00	41.18	5.79	0.08	9.77	12.19	100.00
Smoiville	20.65	51.81	7.17	0.06	6.04	14.27	100.00
Eskom Eza AQMS	45.92	20.40	3.95	0.12	15.25	14.37	100.00
Eskom Majuba AQMS	96.08	0.24	0.03	0.90	2.38	0.37	100.00

NO_2 ambient concentrations (in terms of $\mu g/m^3$) for each emission source category at each discrete receptor is presented in the form of a stacked bar graph in Figure 5-78. The total NO_2 ambient concentrations at each discrete receptor (which is made up of individual contributions representing each of the six emission source categories) represents the All Sources emission source category. The NO_2 source contribution in terms of percentages is presented in the form of a stacked bar graph in Figure 5-79. The sum of individual contributions resulting from each emission source category makes up 100%. The source contribution analysis indicates that power generation, residential fuel burning and vehicles are the main contributors to ambient NO_2 levels in the region. Ambient contributions from waste burning and biomass burning are much smaller in comparison.

Power generation sources account for approximately 96% of the total NO_2 ambient concentrations at the Eskom Majuba AQMS but are much lower at the Eskom Ezamokuhle AQMS and ward centroid discrete receptors (19-46%). This is expected as the Eskom Majuba Power Station is located close to the Eskom Majuba AQMS in comparison with the Eskom Ezamokuhle AQMS and ward centroid discrete receptors.

Residential fuel burning sources account for approximately 0.2% of the total NO_2 ambient concentrations at the Eskom Majuba AQMS but are much higher at the Eskom Ezamokuhle AQMS and ward centroid discrete receptors (18-52%). This is expected as residential areas are located further away from the Eskom Majuba AQMS in comparison with the Eskom Ezamokuhle AQMS and ward centroid discrete receptors.

Vehicle emission sources from paved and unpaved roads account for approximately 2.4% and 0.4% respectively, of the total NO_2 ambient concentrations at the Eskom Majuba AQMS but are much higher at the Eskom Ezamokuhle AQMS and ward centroid discrete receptors (6-42%). This is expected as residential areas and the dense network of paved roads is located further away from the Eskom Majuba AQMS in comparison with the Eskom Ezamokuhle AQMS and ward centroid discrete receptors.

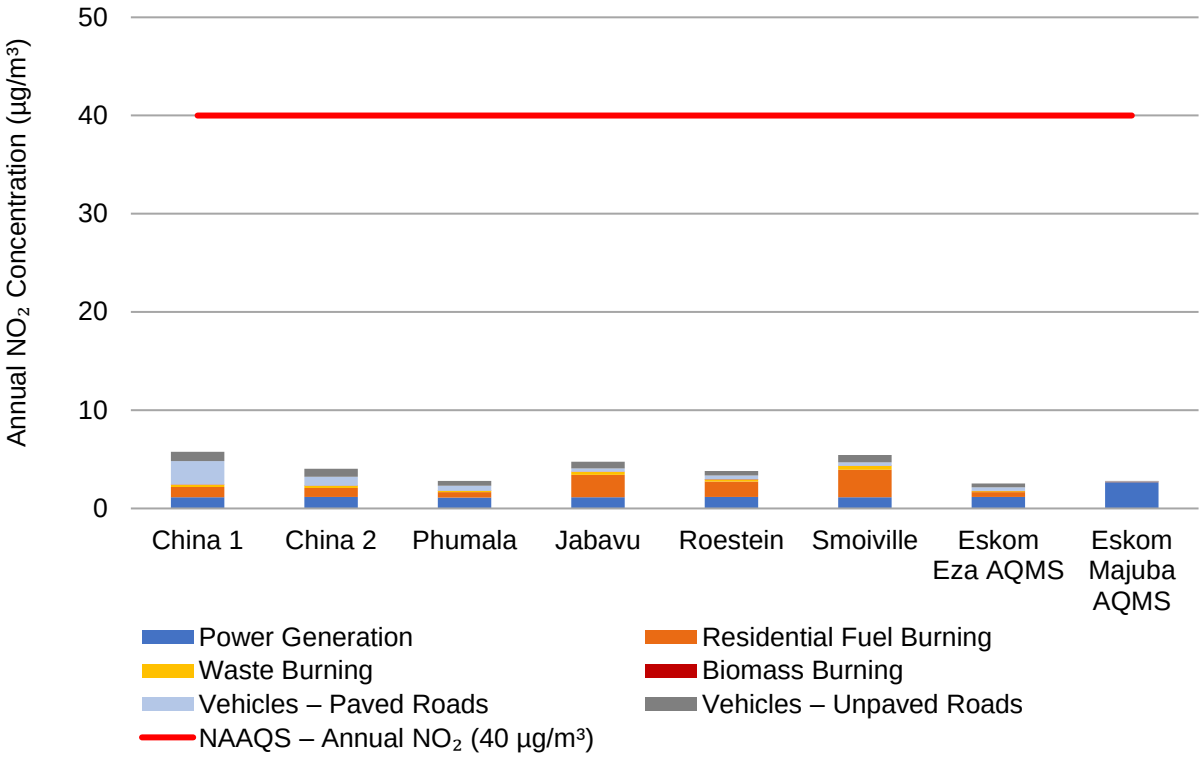

Figure 5-78: Stacked bar graph representing model predicted annual NO_2 ambient concentrations in µg/m³ at discrete receptors for the six emission source categories

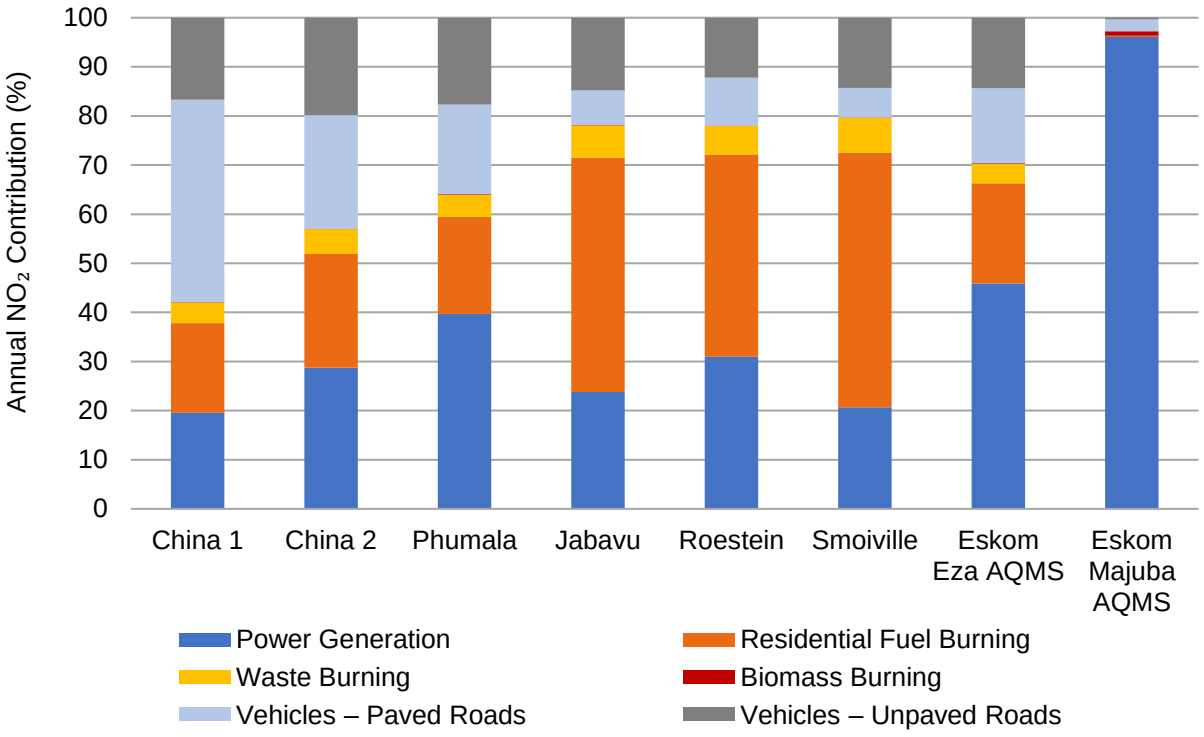

Figure 5-79: Stacked bar graph representing the percent contribution of NO_2 ambient concentrations at discrete receptors as a function of source category

5.3 PREDICTED PM_{10} AMBIENT CONCENTRATIONS

5.3.1 24-HOUR PM_{10}

Model predicted 24-hour PM_{10} ambient concentrations at discrete receptors and at the point of maximum for the seven emission source categories are presented in Table 5-8. If applicable, exceedances of the NAAQS are highlighted in red.

Bar graphs for model predicted 24-hour PM_{10} ambient concentrations at discrete receptors are presented in the following order:

- Figure 5-80 for the Power Generation emission source category
- Figure 5-82 for the Residential Fuel Burning emission source category
- Figure 5-84 for the Waste Burning emission source category
- Figure 5-86 for the Biomass Burning emission source category
- Figure 5-88 for the Vehicles – Paved Roads emission source category
- Figure 5-90 for the Vehicles – Unpaved Roads emission source category
- Figure 5-92 for the All Sources emission source category

Contour plots for model predicted 24-hour PM_{10} ambient concentrations for the Greater Ezamokuhle Airshed are presented in the following order:

- Figure 5-81 for the Power Generation emission source category
- Figure 5-83 for the Residential Fuel Burning emission source category
- Figure 5-85 for the Waste Burning emission source category
- Figure 5-87 for the Biomass Burning emission source category
- Figure 5-89 for the Vehicles – Paved Roads emission source category
- Figure 5-91 for the Vehicles – Unpaved Roads emission source category
- Figure 5-93 for the All Sources emission source category

Contour plots for model predicted 24-hour PM_{10} ambient concentrations for the Ezamokuhle airshed is presented in Figure 5-94 for the All Sources emission source category.

With respect to contour plots for the primary and Ezamokuhle airshed, areas of exceedance of the NAAQS is coloured in red.

Table 5-8: Model predicted 24-hour PM_{10} ambient concentrations (99th percentile) in µg/m^3 at discrete receptors and at the point of maximum for the seven emission source categories

Discrete Receptors	Power Generation	Residential Fuel Burning	Waste Burning	Biomass Burning	Vehicles – Paved Roads	Vehicles – Unpaved Roads	All Sources
China 1	30.33	13.36	2.22	0.63	0.24	161.22	192.35
China 2	27.34	12.56	1.92	0.57	0.15	136.95	168.69
Phumala	27.23	7.55	1.23	0.58	0.11	85.71	106.51
Jabavu	32.18	32.76	2.80	0.71	0.09	116.81	165.78
Roestein	27.78	23.80	2.18	0.57	0.10	84.41	125.62
Smoiville	29.05	34.55	3.02	0.61	0.09	117.25	161.29
Eskom Eza AQMS	28.11	7.40	0.99	0.58	0.11	67.07	92.55
Eskom Majuba AQMS	215.58	0.24	0.02	4.20	0.03	5.50	218.02
Maximum	709.21	72.45	6.46	17.55	1.50	331.07	714.79
	NAAQS – 24-hour PM_{10} (75 µg/m^3)						

According to Table 5-8, model predicted 24-hour PM_{10} ambient concentrations exceed the 24-hour PM_{10} NAAQS of 75 µg/m^3 at the Eskom Majuba AQMS and at the point of maximum for the Power Generation emission source category; and at all ward centroid discrete receptors and point of maximum for the Vehicles – Unpaved Roads emission source category in the Ezamokuhle Airshed.

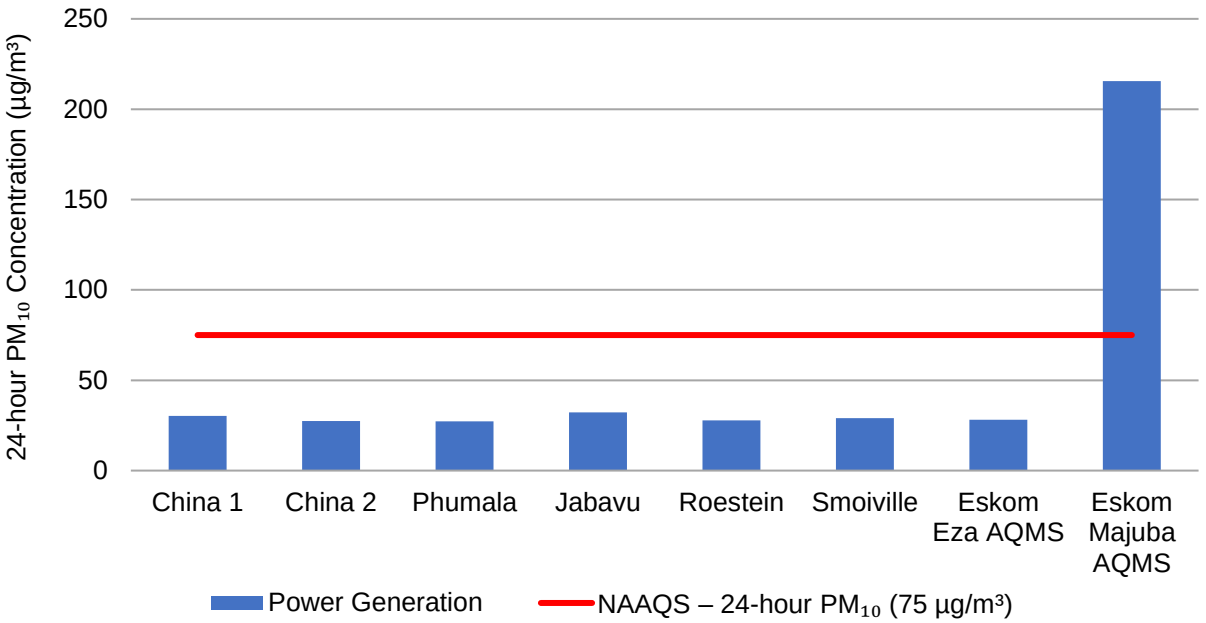

Figure 5-80: Model predicted 24-hour PM_{10} ambient concentrations (99th percentile) in µg/m³ at discrete receptors for the Power Generation emission source category

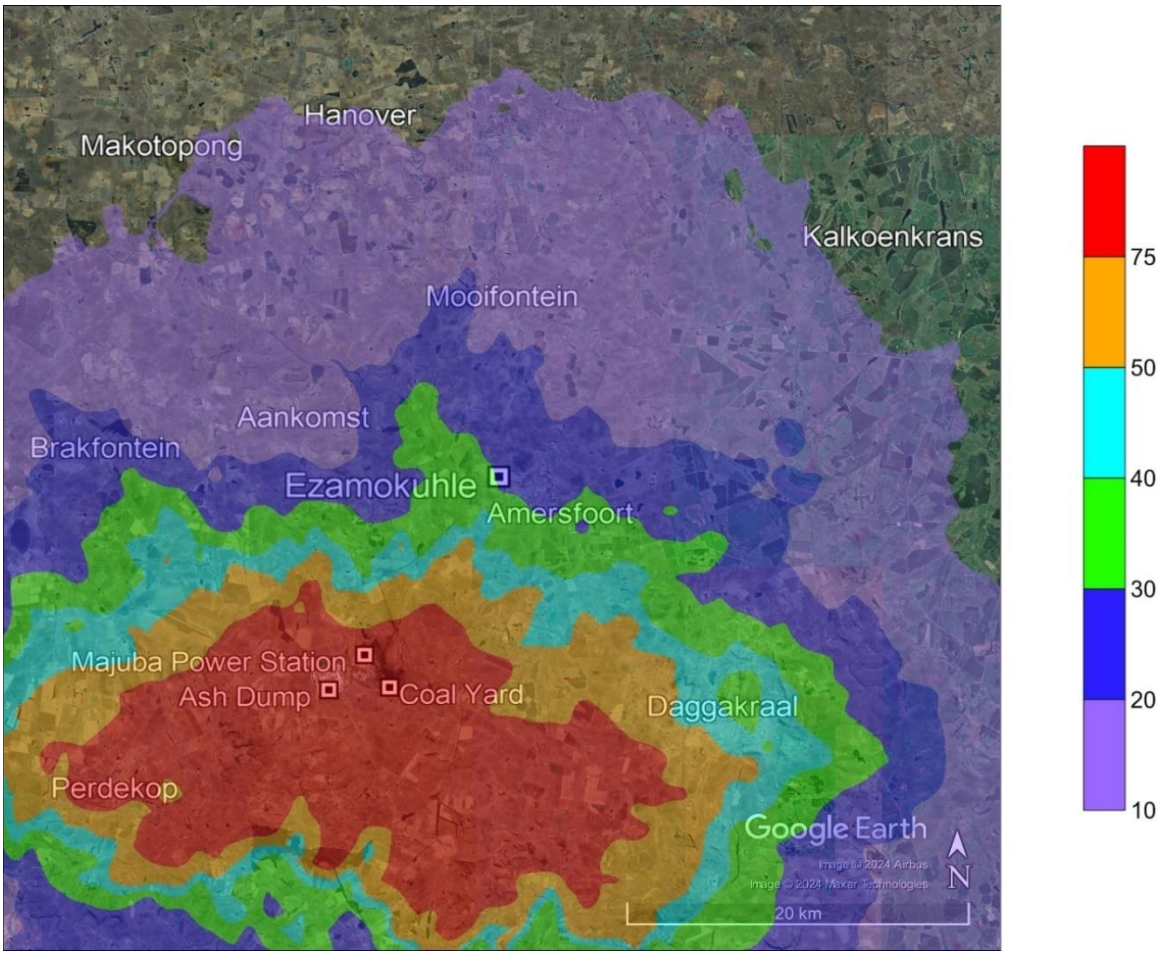

Figure 5-81: Model predicted 24-hour PM_{10} ambient concentrations (99th percentile) in µg/m³ for the Power Generation emission source category within the Greater Ezamokuhle Airshed

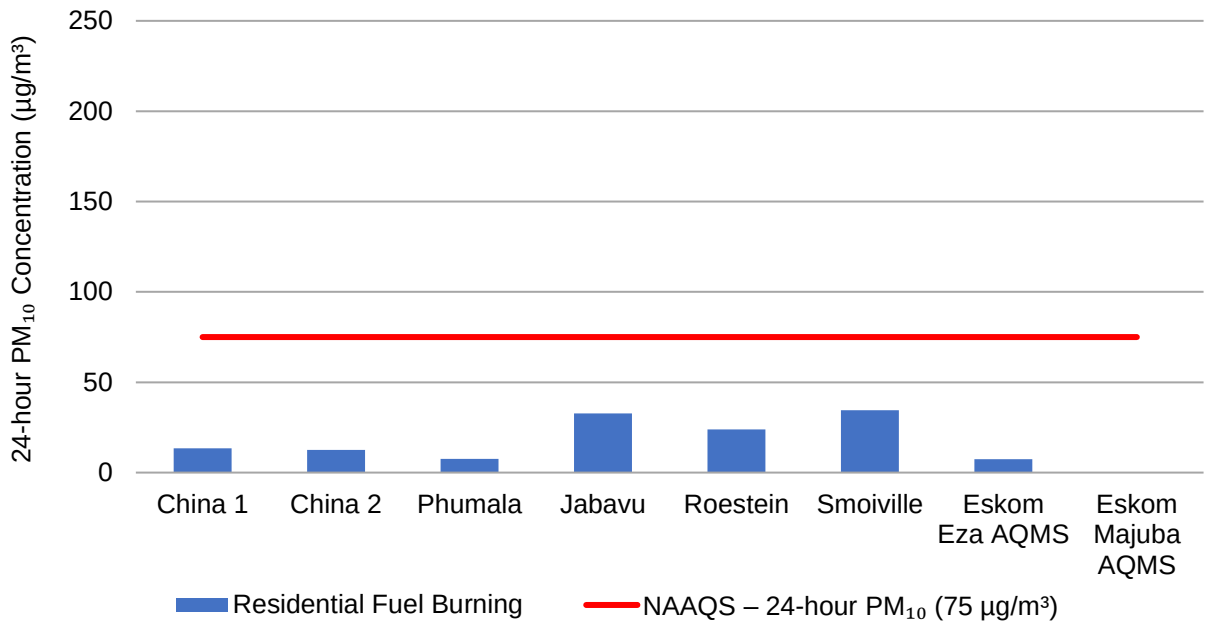

Figure 5-82: Model predicted 24-hour PM_{10} ambient concentrations (99th percentile) in µg/m³ at discrete receptors for the Residential Fuel Burning emission source category

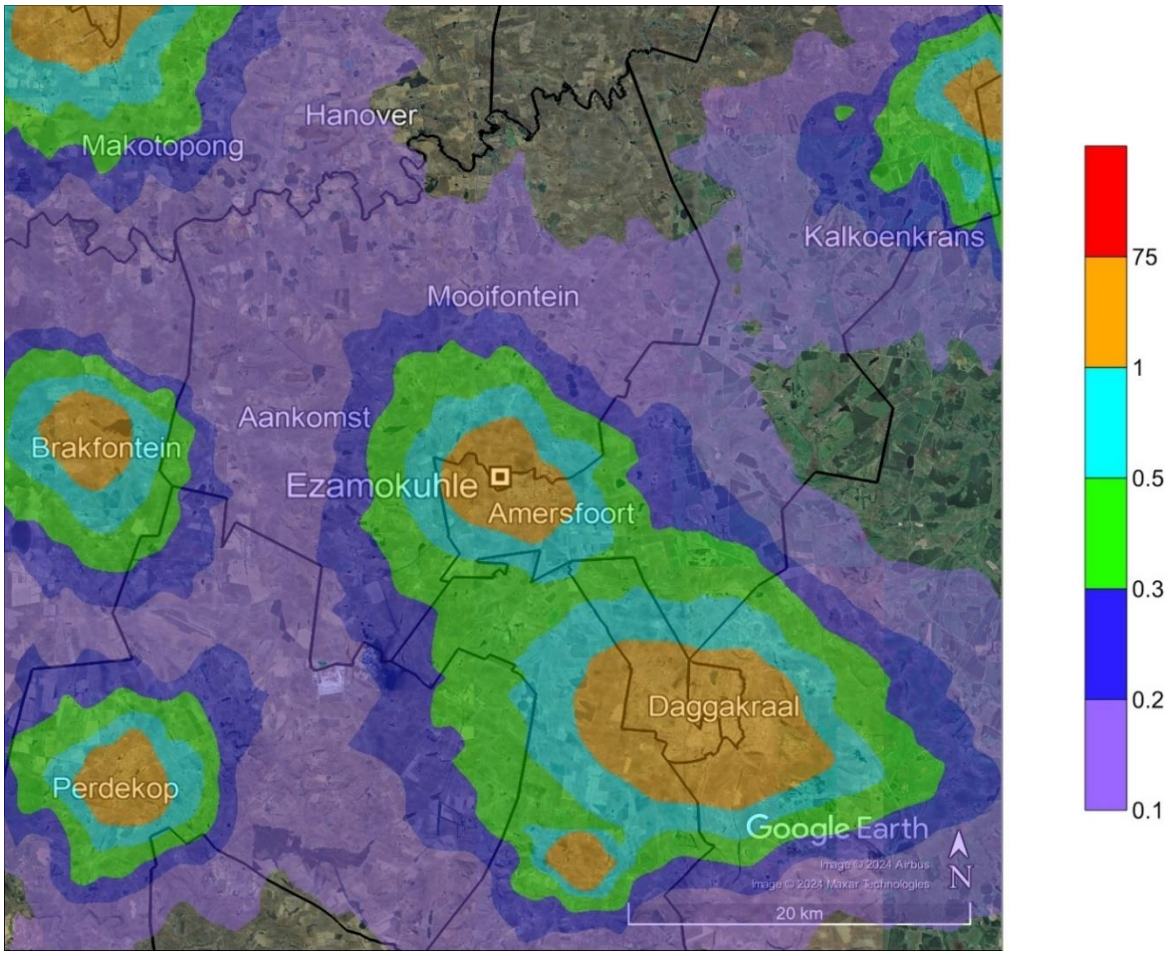

Figure 5-83: Model predicted 24-hour PM_{10} ambient concentrations (99th percentile) in µg/m³ for the Residential Fuel Burning emission source category within the Greater Ezamokuhle Airshed

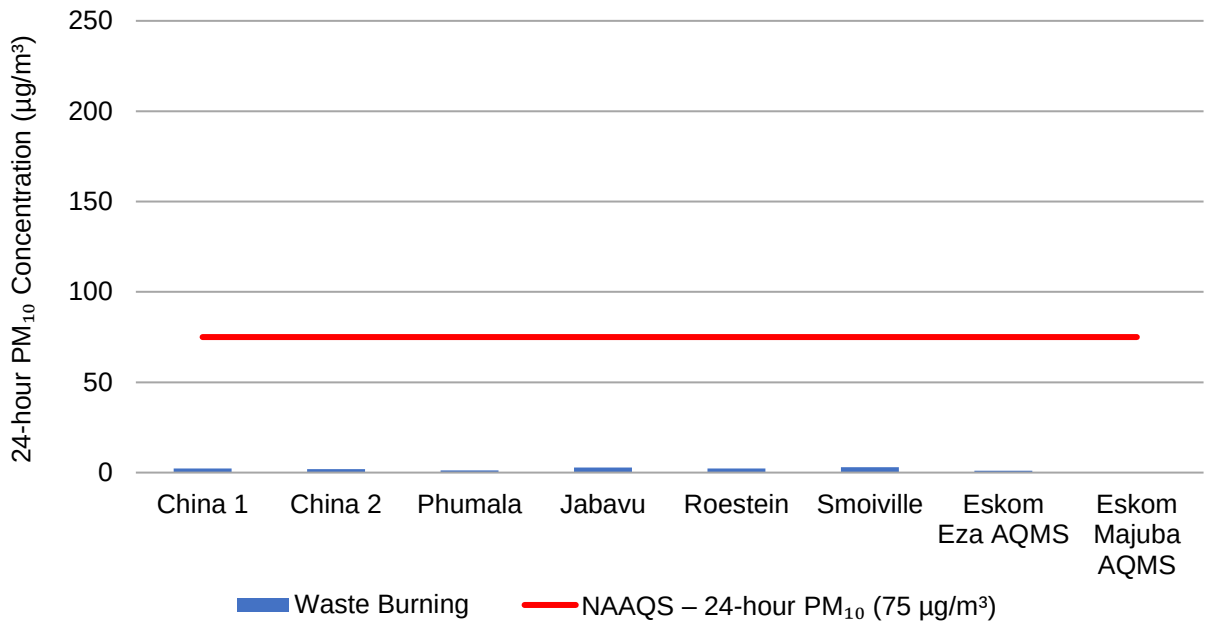

Figure 5-84: Model predicted 24-hour PM_{10} ambient concentrations (99th percentile) in µg/m³ at discrete receptors for the Waste Burning emission source category

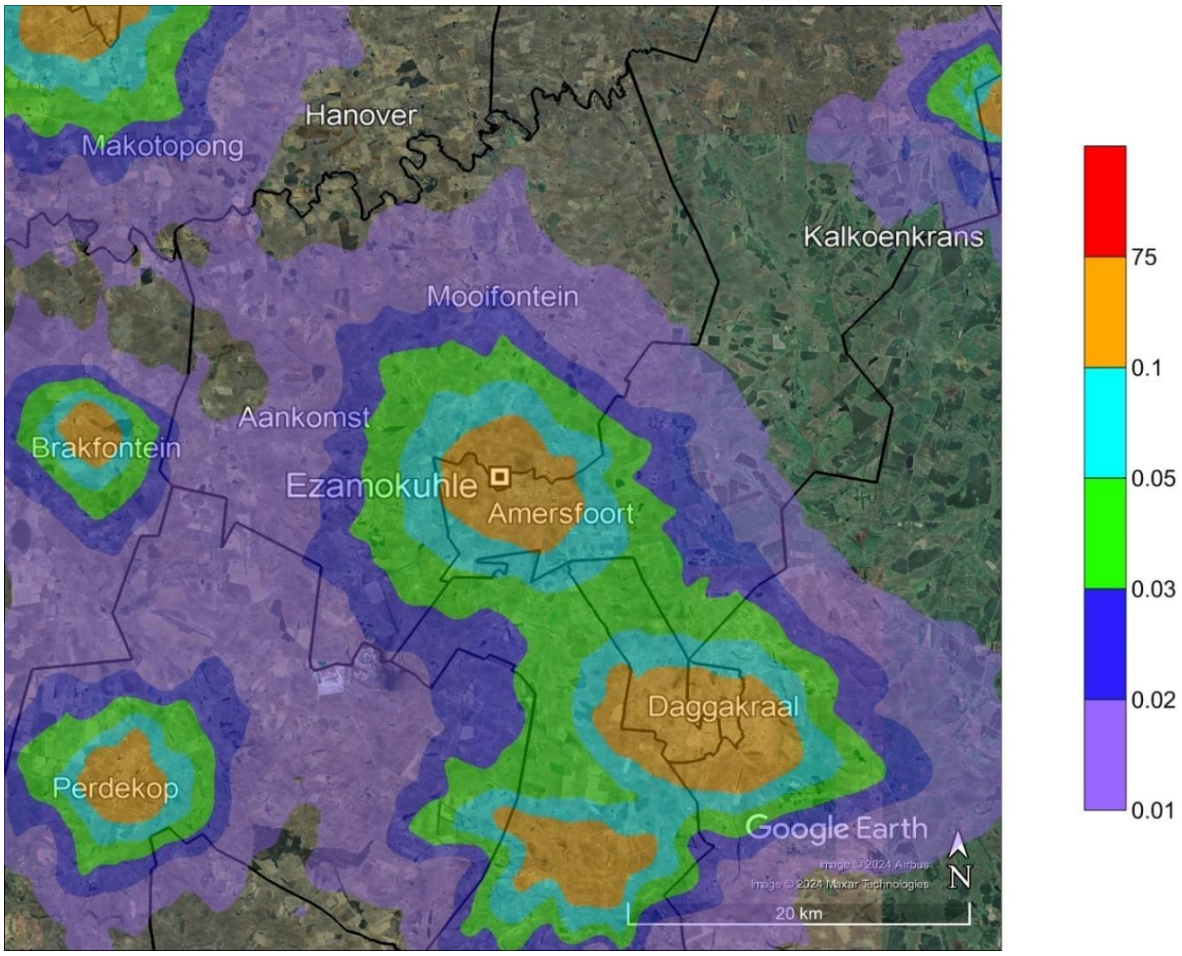

Figure 5-85: Model predicted 24-hour PM_{10} ambient concentrations (99th percentile) in µg/m³ for the Waste Burning emission source category within the Greater Ezamokuhle Airshed

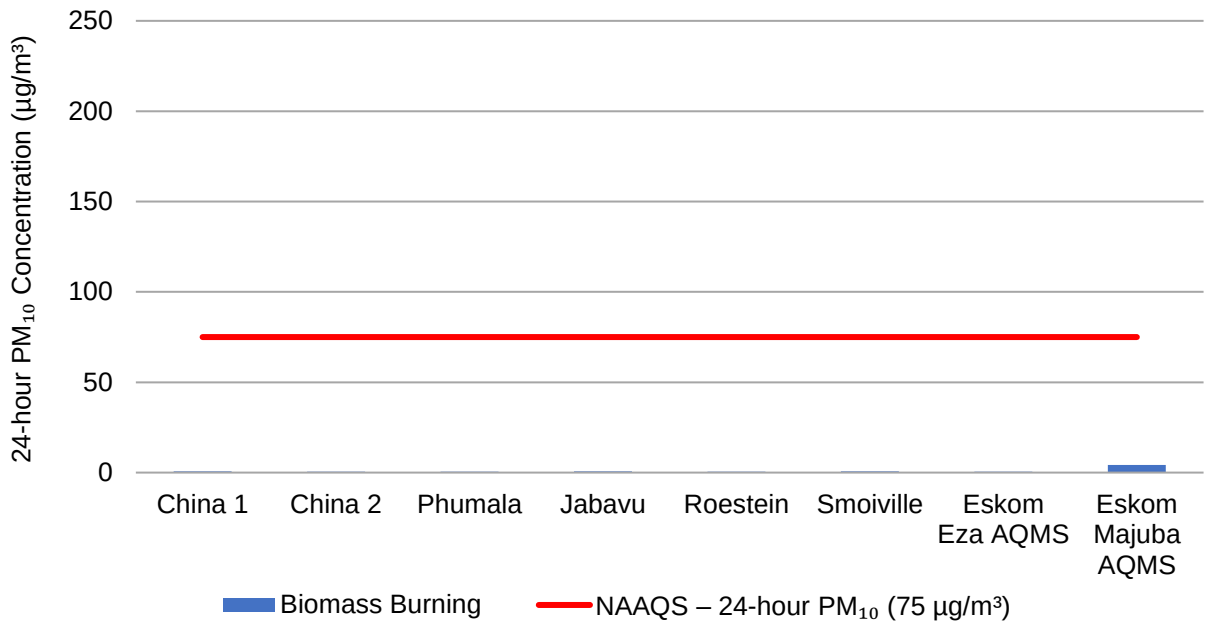

Figure 5-86: Model predicted 24-hour PM_{10} ambient concentrations (99th percentile) in µg/m³ at discrete receptors for the Biomass Burning emission source category

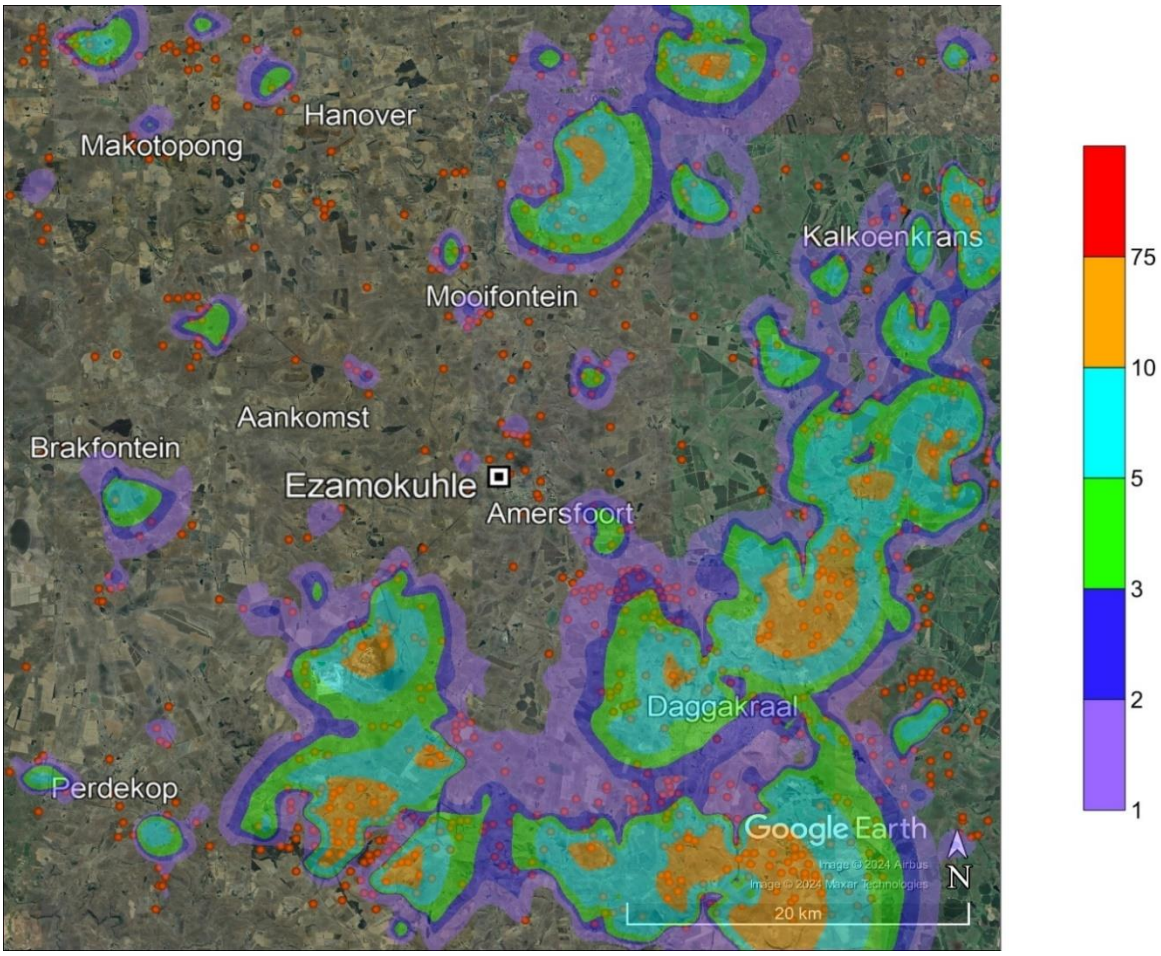

Figure 5-87: Model predicted 24-hour PM_{10} ambient concentrations (99th percentile) in µg/m³ for the Biomass Burning emission source category within the Greater Ezamokuhle Airshed

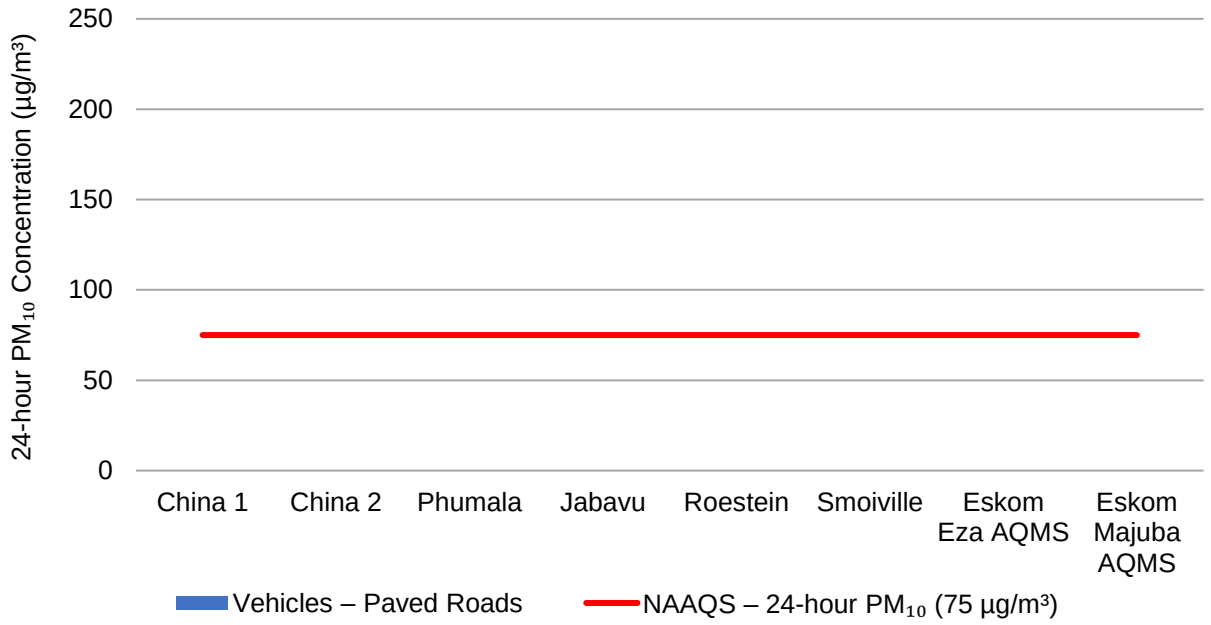

Figure 5-88: Model predicted 24-hour PM_{10} ambient concentrations (99th percentile) in µg/m³ at discrete receptors for the Vehicles – Paved Roads emission source category

Figure 5-89: Model predicted 24-hour PM_{10} ambient concentrations (99th percentile) in µg/m³ for the Vehicles – Paved Roads emission source category within the Greater Ezamokuhle Airshed

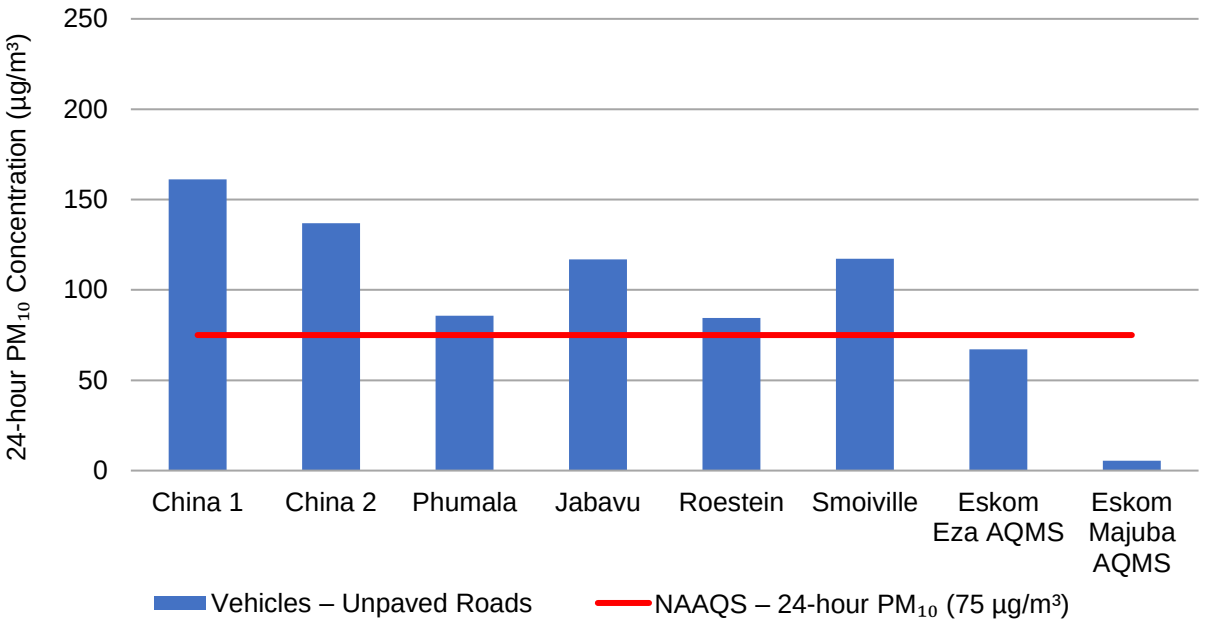

Figure 5-90: Model predicted 24-hour PM_{10} ambient concentrations (99th percentile) in µg/m³ at discrete receptors for the Vehicles – Unpaved Roads emission source category

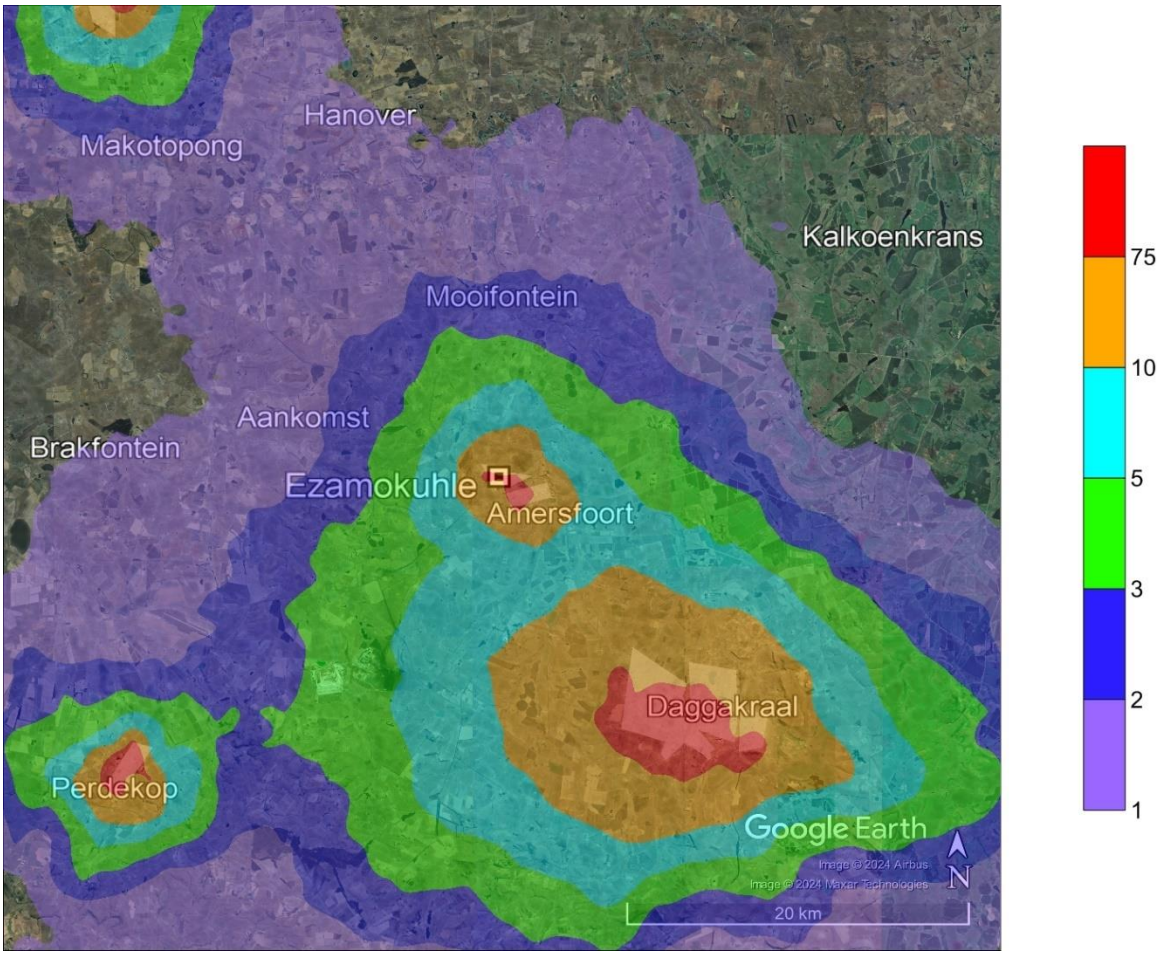

Figure 5-91: Model predicted 24-hour PM_{10} ambient concentrations (99th percentile) in µg/m³ for the Vehicles – Unpaved Roads emission source category within the Greater Ezamokuhle Airshed

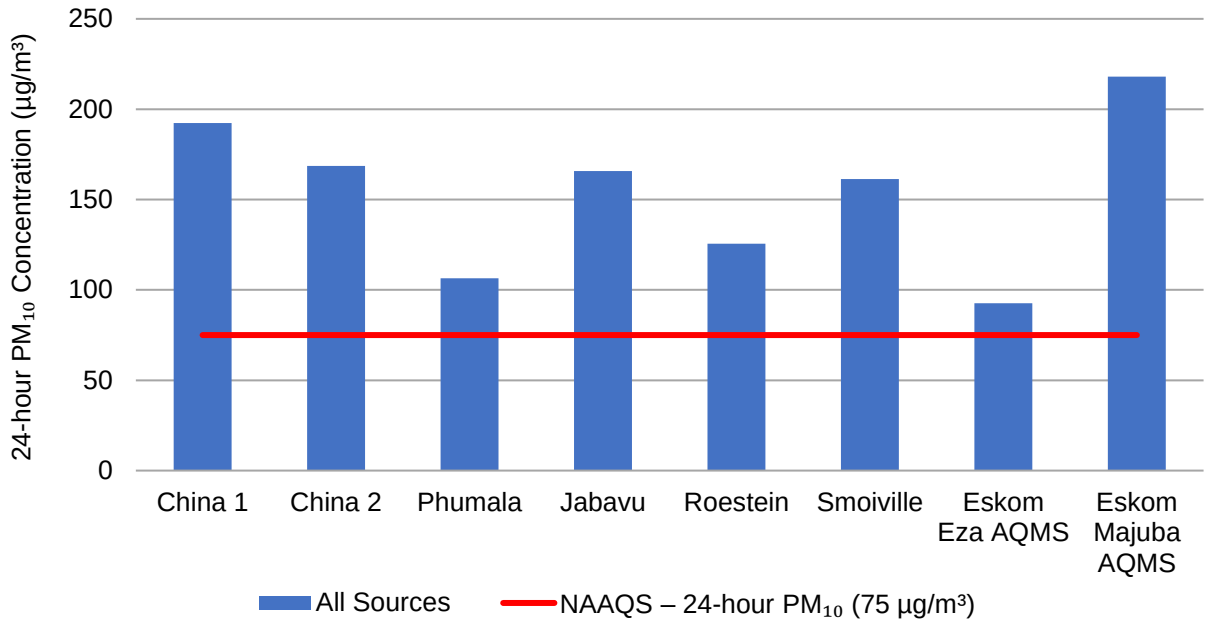

Figure 5-92: Model predicted 24-hour PM_{10} ambient concentrations (99th percentile) in µg/m³ at discrete receptors for the All Sources emission source category

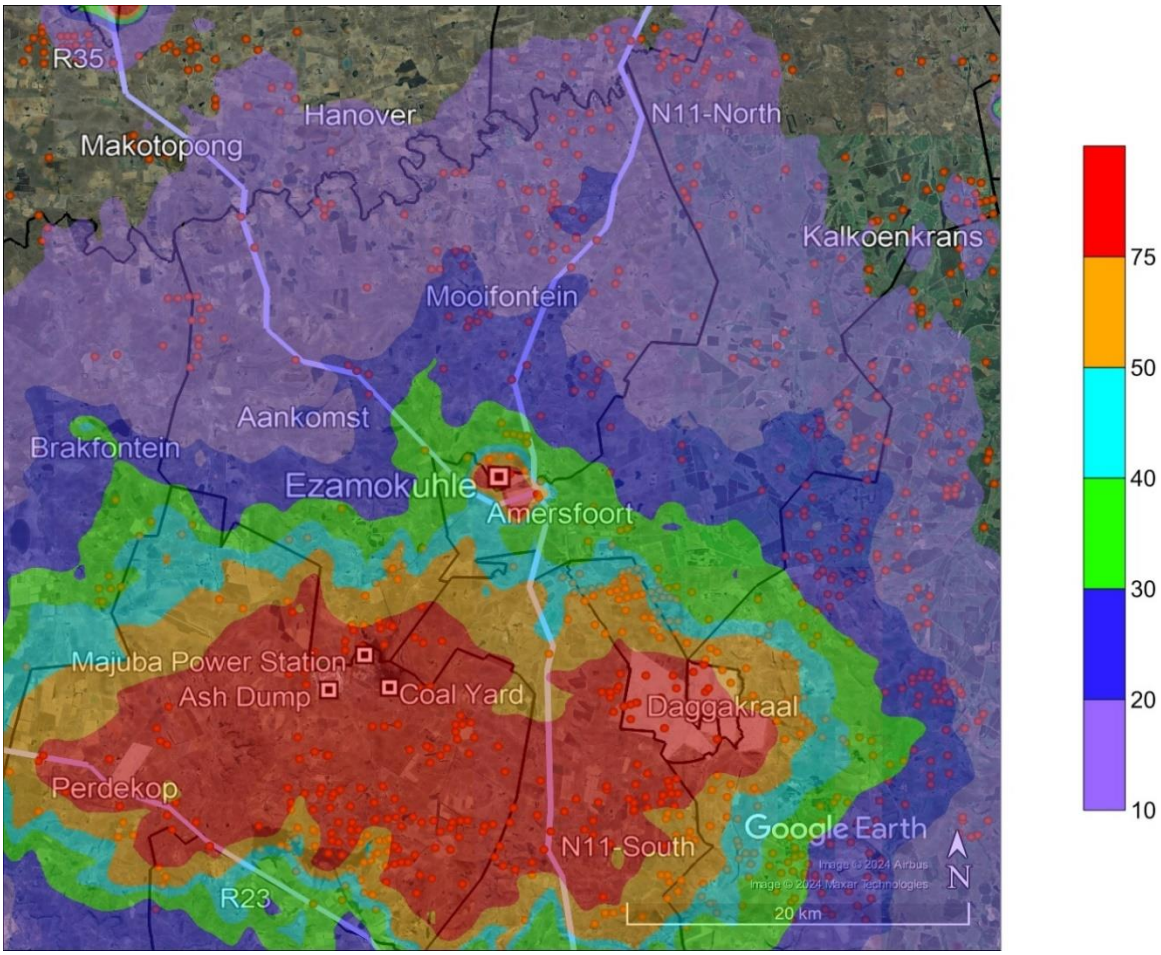

Figure 5-93: Model predicted 24-hour PM_{10} ambient concentrations (99th percentile) in µg/m³ for the All Sources emission source category within the Greater Ezamokuhle Airshed

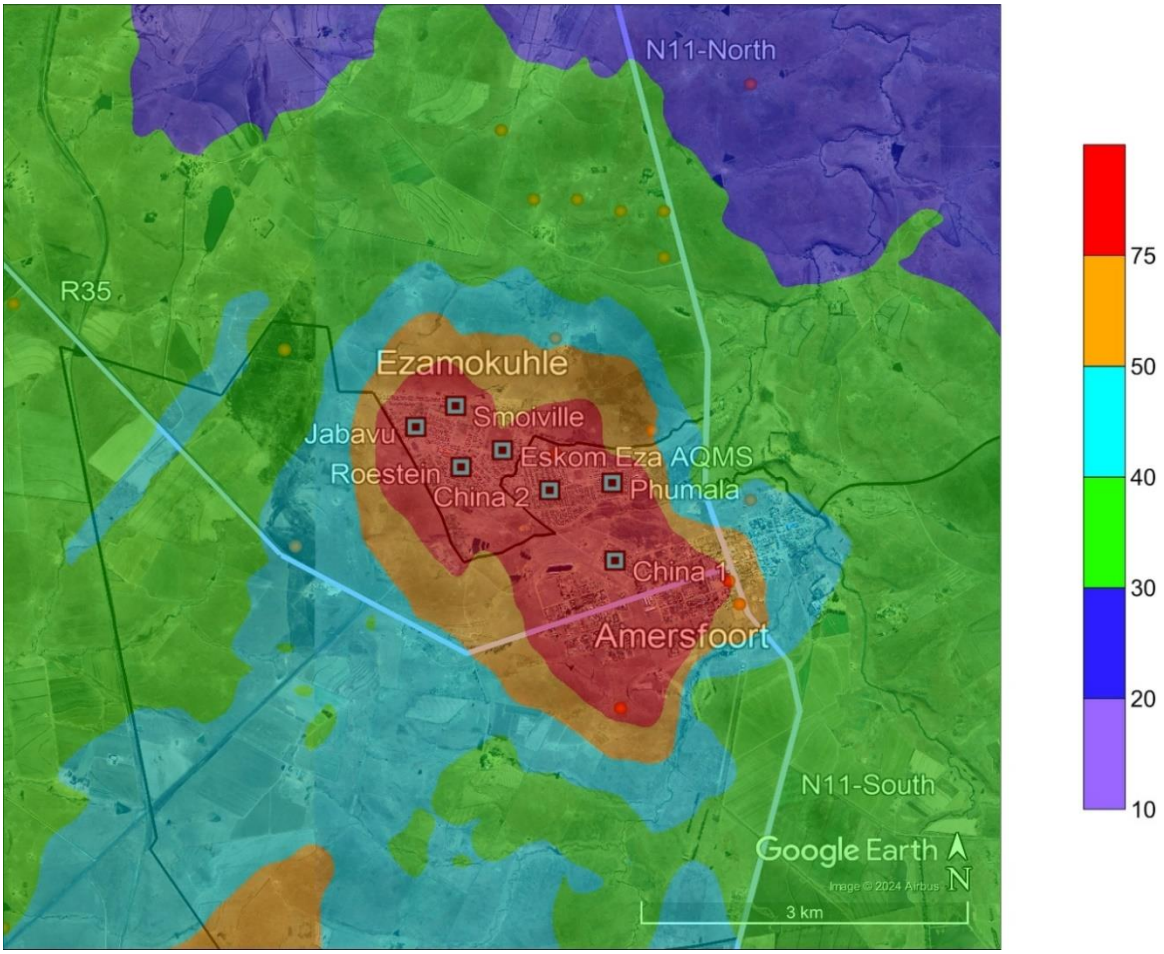

Figure 5-94: Model predicted 24-hour PM_{10} ambient concentrations (99th percentile) in µg/m^3 for the All Sources emission source category within Ezamokuhle airshed

5.3.2 ANNUAL PM_{10}

Model predicted annual PM_{10} ambient concentrations at discrete receptors and at the point of maximum for the seven emission source categories are presented in Table 5-9. If applicable, exceedances of the NAAQS are highlighted in red.

Bar graphs for model predicted annual PM_{10} ambient concentrations at discrete receptors are presented in the following order:

- Figure 5-95 for the Power Generation emission source category
- Figure 5-97 for the Residential Fuel Burning emission source category
- Figure 5-99 for the Waste Burning emission source category
- Figure 5-101 for the Biomass Burning emission source category
- Figure 5-103 for the Vehicles – Paved Roads emission source category
- Figure 5-105 for the Vehicles – Unpaved Roads emission source category
- Figure 5-107 for the All Sources emission source category

Contour plots for model predicted annual PM_{10} ambient concentrations for the Greater Ezamokuhle Airshed are presented in the following order:

- Figure 5-96 for the Power Generation emission source category
- Figure 5-98 for the Residential Fuel Burning emission source category
- Figure 5-100 for the Waste Burning emission source category
- Figure 5-102 for the Biomass Burning emission source category
- Figure 5-104 for the Vehicles – Paved Roads emission source category
- Figure 5-106 for the Vehicles – Unpaved Roads emission source category
- Figure 5-108 for the All Sources emission source category

Contour plots for model predicted annual PM_{10} ambient concentrations for the Ezamokuhle airshed is presented in Figure 5-109 for the All Sources emission source category.

With respect to contour plots for the primary and Ezamokuhle airshed, areas of exceedance of the NAAQS is coloured in red.

Table 5-9: Model predicted annual PM_{10} ambient concentrations in µg/m³ at discrete receptors and at the point of maximum for the seven emission source categories

Discrete Receptors	Power Generation	Residential Fuel Burning	Waste Burning	Biomass Burning	Vehicles – Paved Roads	Vehicles – Unpaved Roads	All Sources
China 1	2.13	5.71	0.93	0.16	0.07	64.67	73.68
China 2	2.15	5.13	0.79	0.16	0.03	53.61	61.87
Phumala	1.99	3.03	0.48	0.16	0.02	33.28	38.96
Jabavu	2.35	14.05	1.20	0.22	0.02	47.17	65.01
Roestein	2.27	9.66	0.84	0.17	0.02	31.09	44.05
Smoiville	2.21	17.41	1.49	0.19	0.02	51.97	73.29
Eskom Eza AQMS	2.17	2.96	0.38	0.17	0.02	24.35	30.05
Eskom Majuba AQMS	26.90	0.05	0.00	1.33	0.01	0.76	29.05
Maximum	102.63	21.53	2.42	6.39	0.35	135.09	146.28
	NAAQS – annual PM_{10} (40 µg/m³)						

According to Table 5-9, model predicted annual PM_{10} ambient concentrations exceed the annual PM_{10} NAAQS of 40 µg/m³ at the point of maximum for the Power Generation and Vehicles – Unpaved Roads emission source category; and at China 1, China 2, Jabavu and Smoiville discrete receptors for the Vehicles – Unpaved Roads emission source category in the Ezamokuhle Airshed.

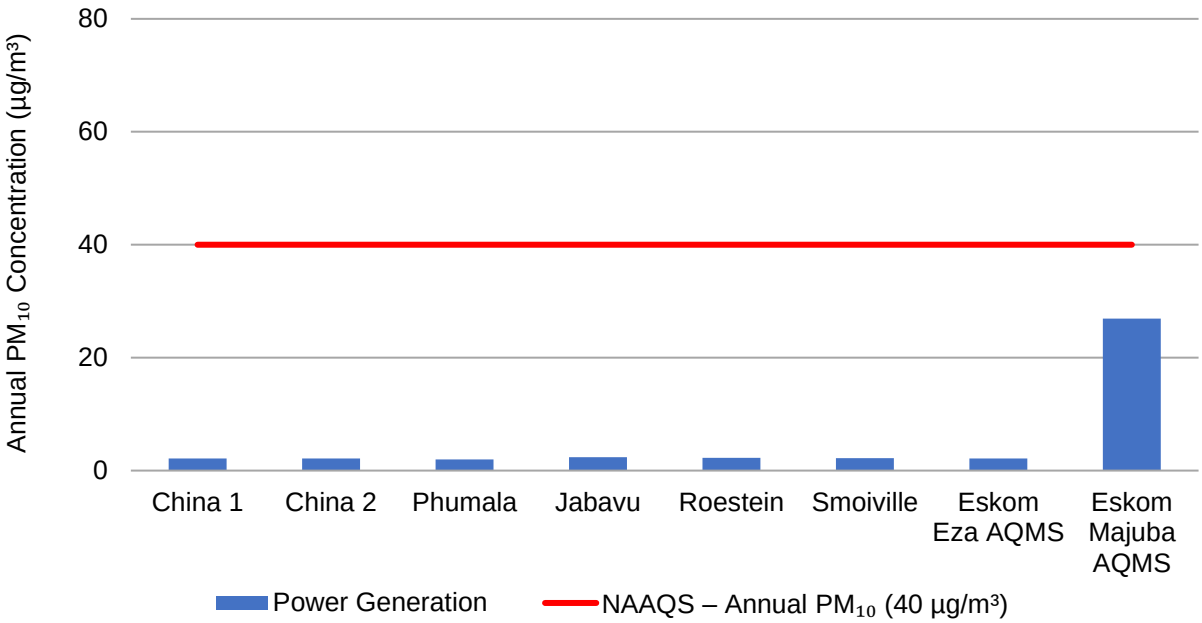

Figure 5-95: Model predicted annual PM_{10} ambient concentrations in µg/m³ at discrete receptors for the Power Generation emission source category

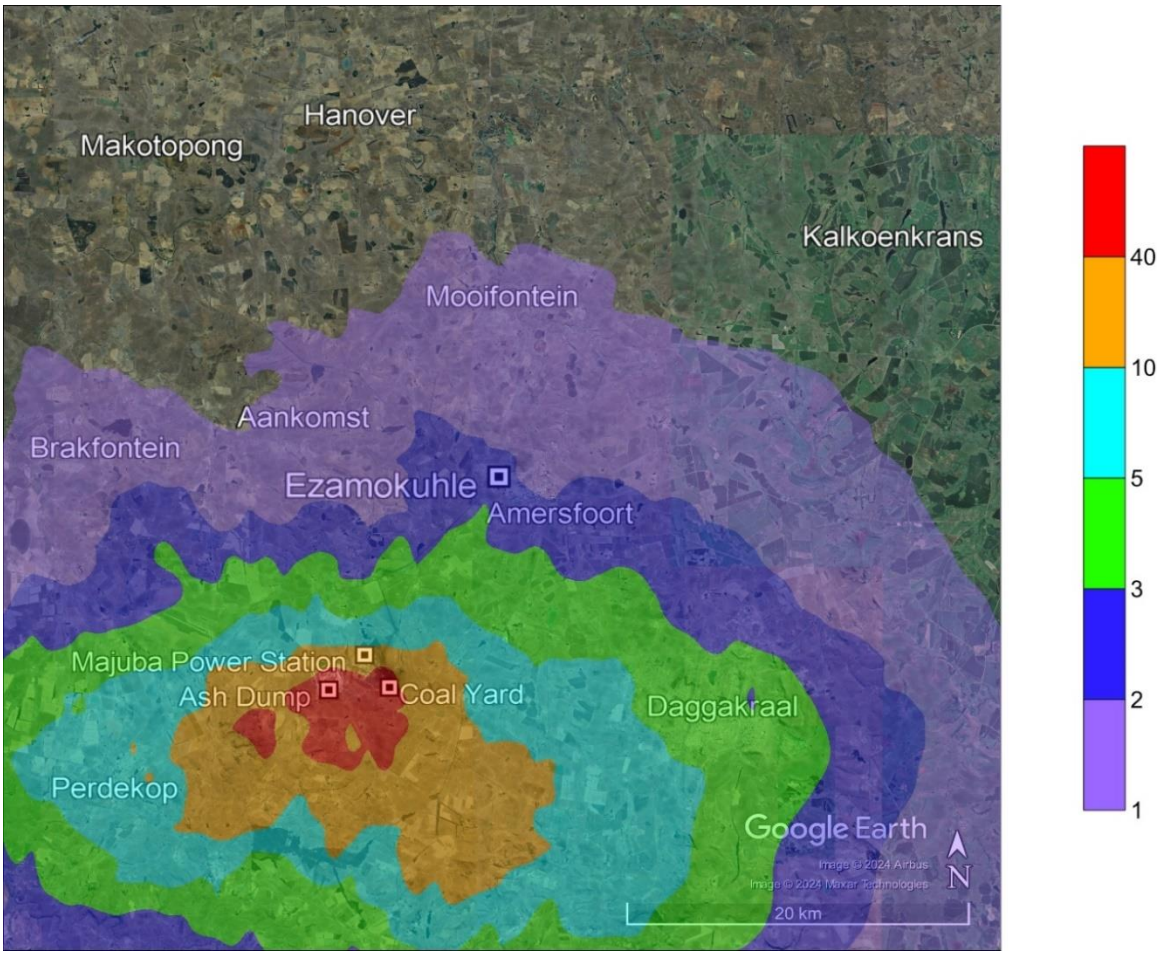

Figure 5-96: Model predicted annual PM_{10} ambient concentrations in µg/m³ for the Power Generation emission source category within the Greater Ezamokuhle Airshed

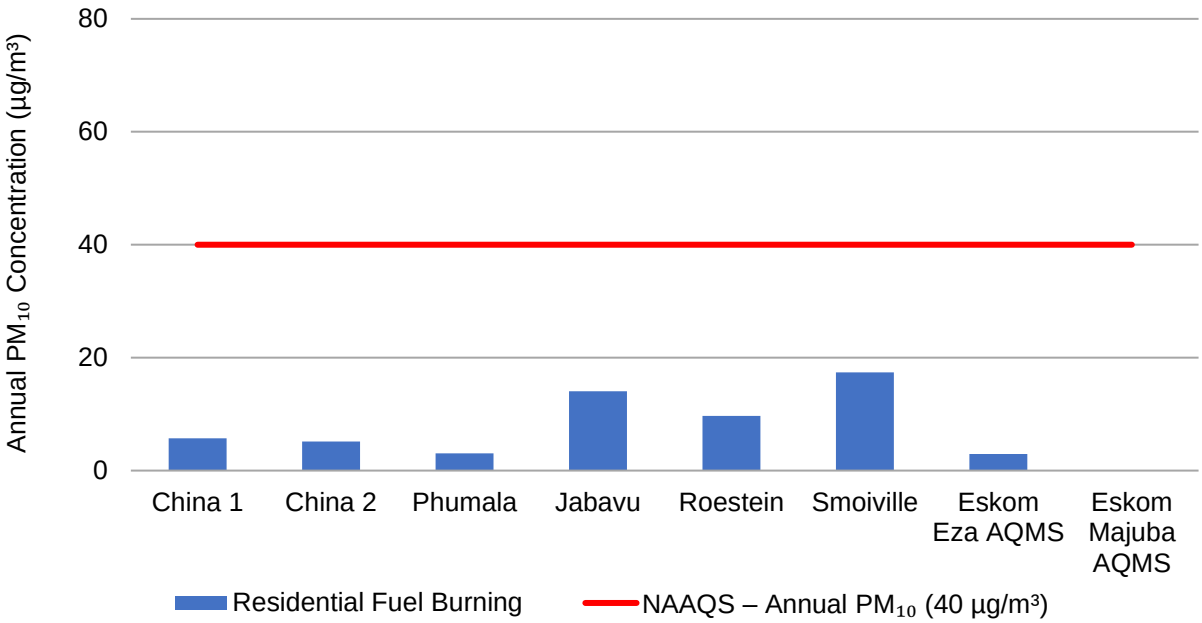

Figure 5-97: Model predicted annual PM_{10} ambient concentrations in µg/m³ at discrete receptors for the Residential Fuel Burning emission source category

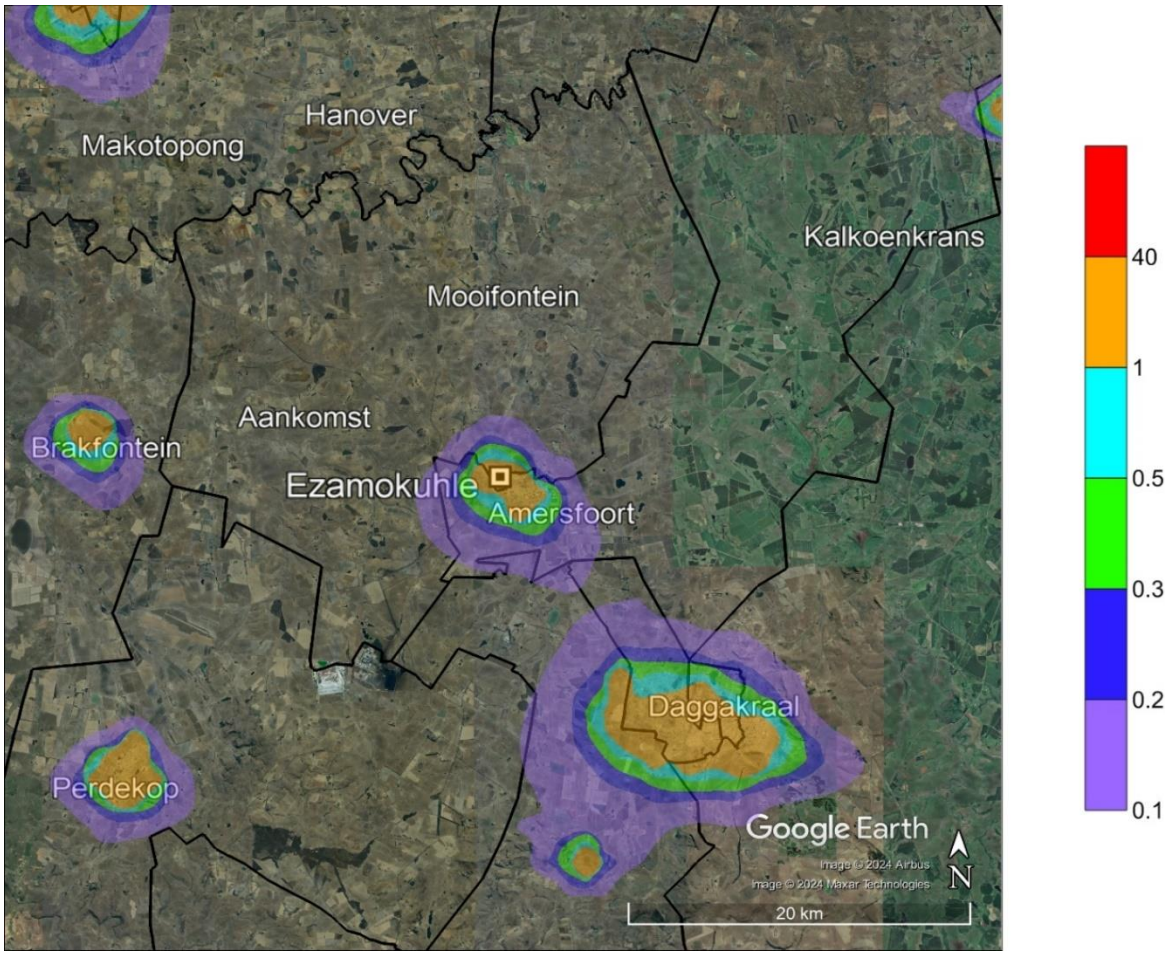

Figure 5-98: Model predicted annual PM_{10} ambient concentrations in µg/m³ for the Residential Fuel Burning emission source category within the Greater Ezamokuhle Airshed

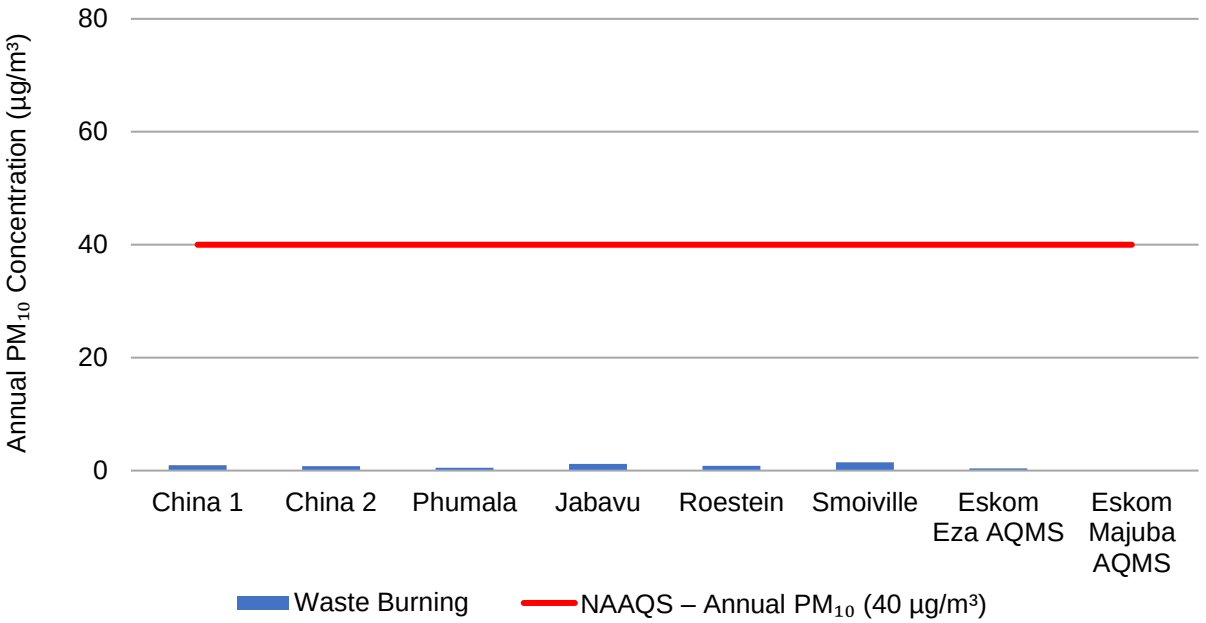

Figure 5-99: Model predicted annual PM_{10} ambient concentrations in µg/m³ at discrete receptors for the Waste Burning emission source category

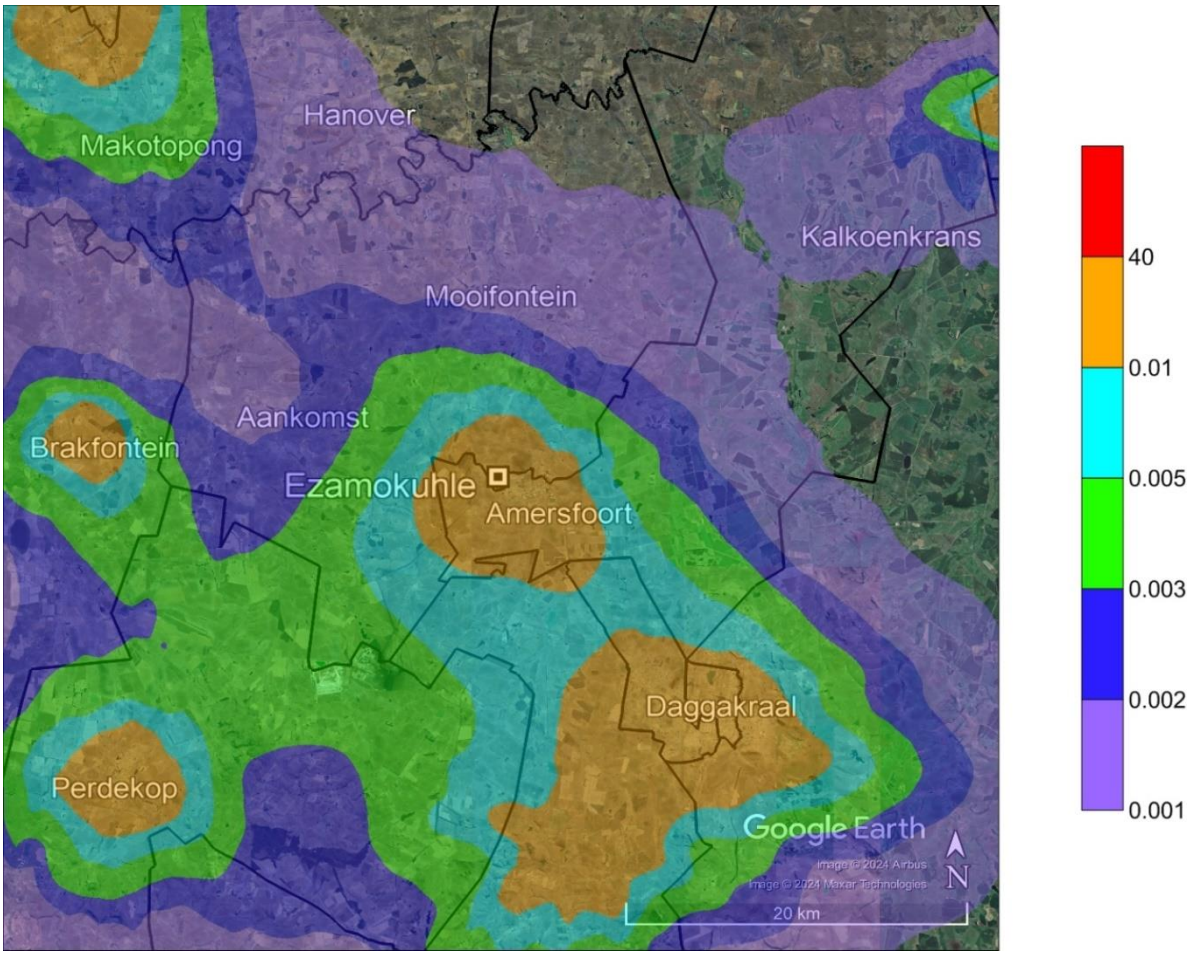

Figure 5-100: Model predicted annual PM_{10} ambient concentrations in µg/m³ for the Waste Burning emission source category within the Greater Ezamokuhle Airshed

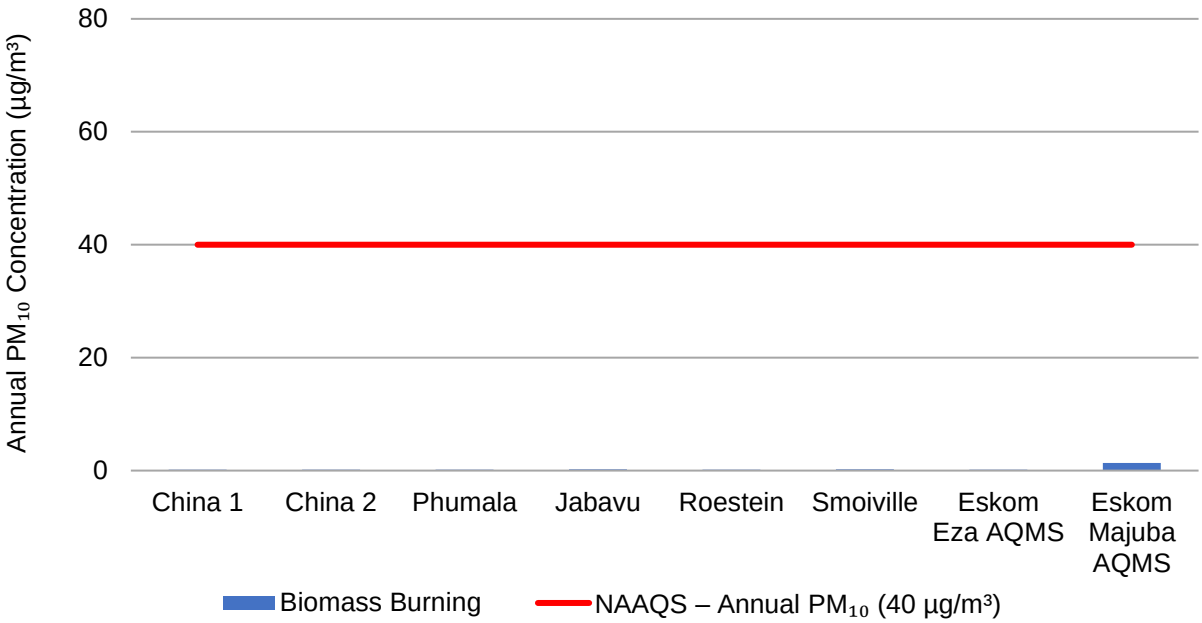

Figure 5-101: Model predicted annual PM_{10} ambient concentrations in µg/m³ at discrete receptors for the Biomass Burning emission source category

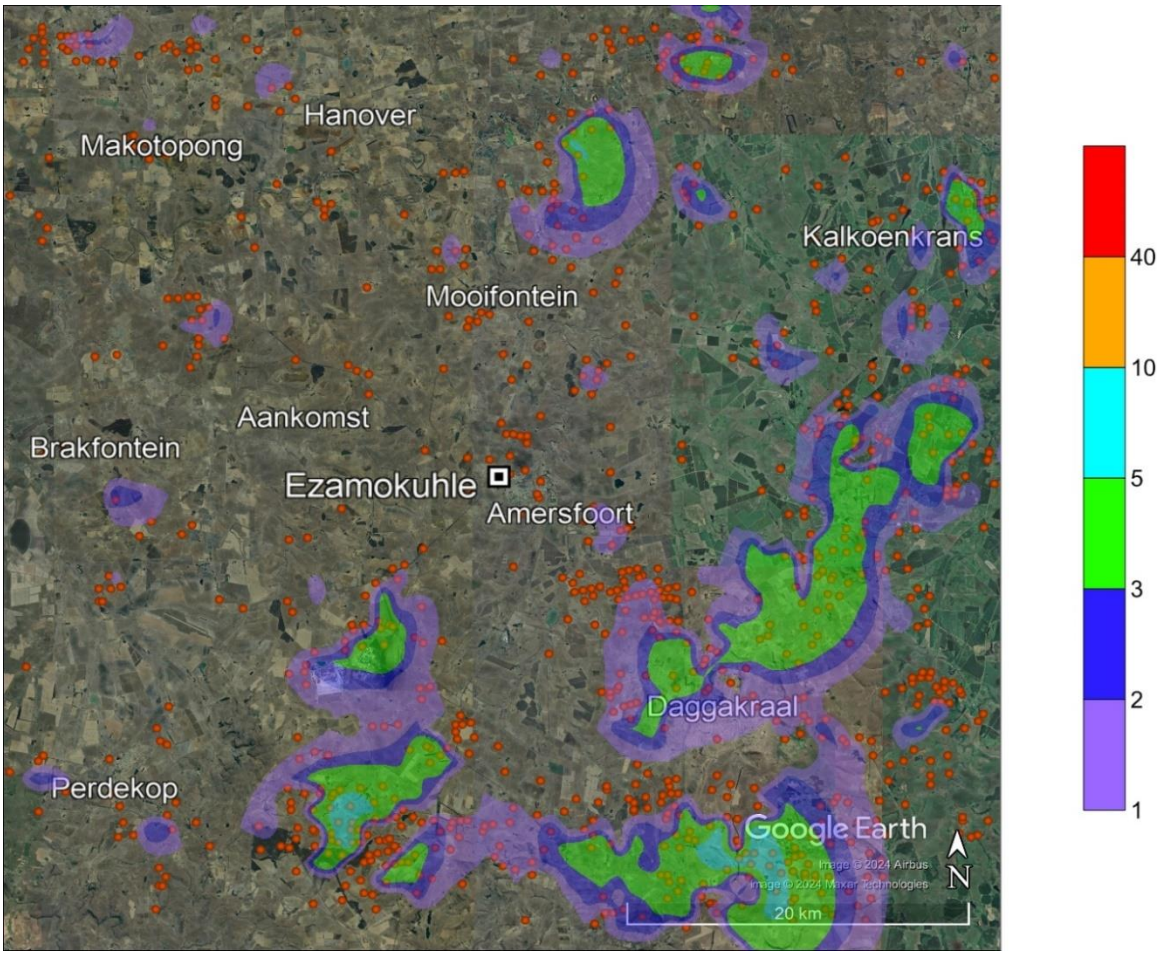

Figure 5-102: Model predicted annual PM_{10} ambient concentrations in µg/m³ for the Biomass Burning emission source category within the Greater Ezamokuhle Airshed

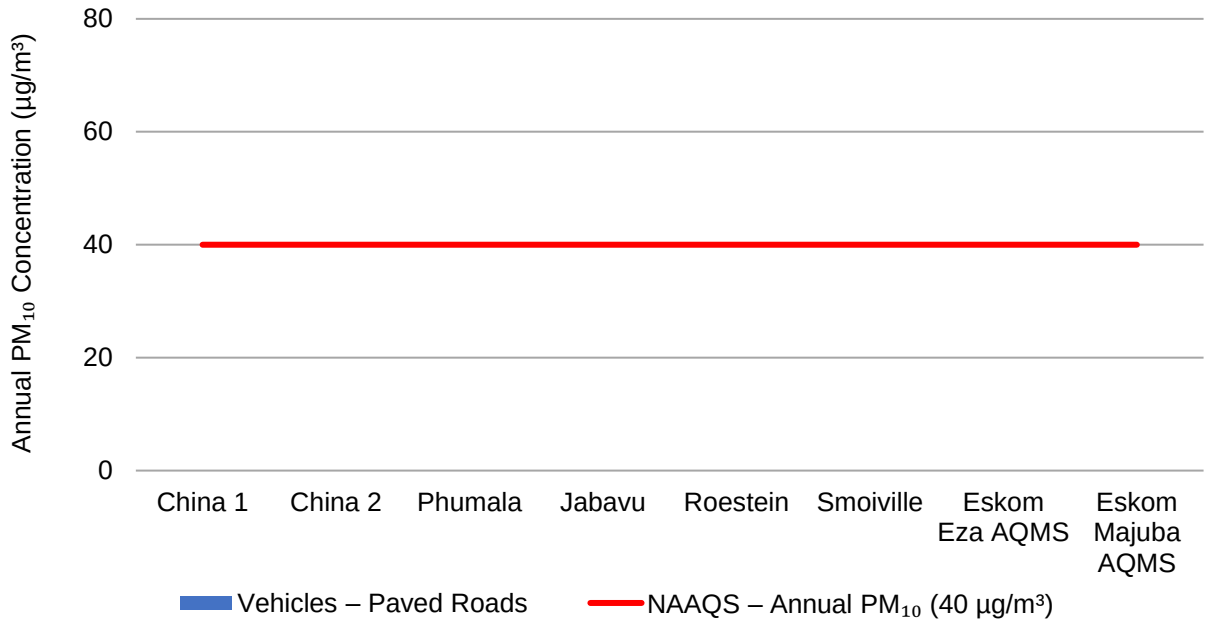

Figure 5-103: Model predicted annual PM_{10} ambient concentrations in µg/m³ at discrete receptors for the Vehicles – Paved Roads emission source category

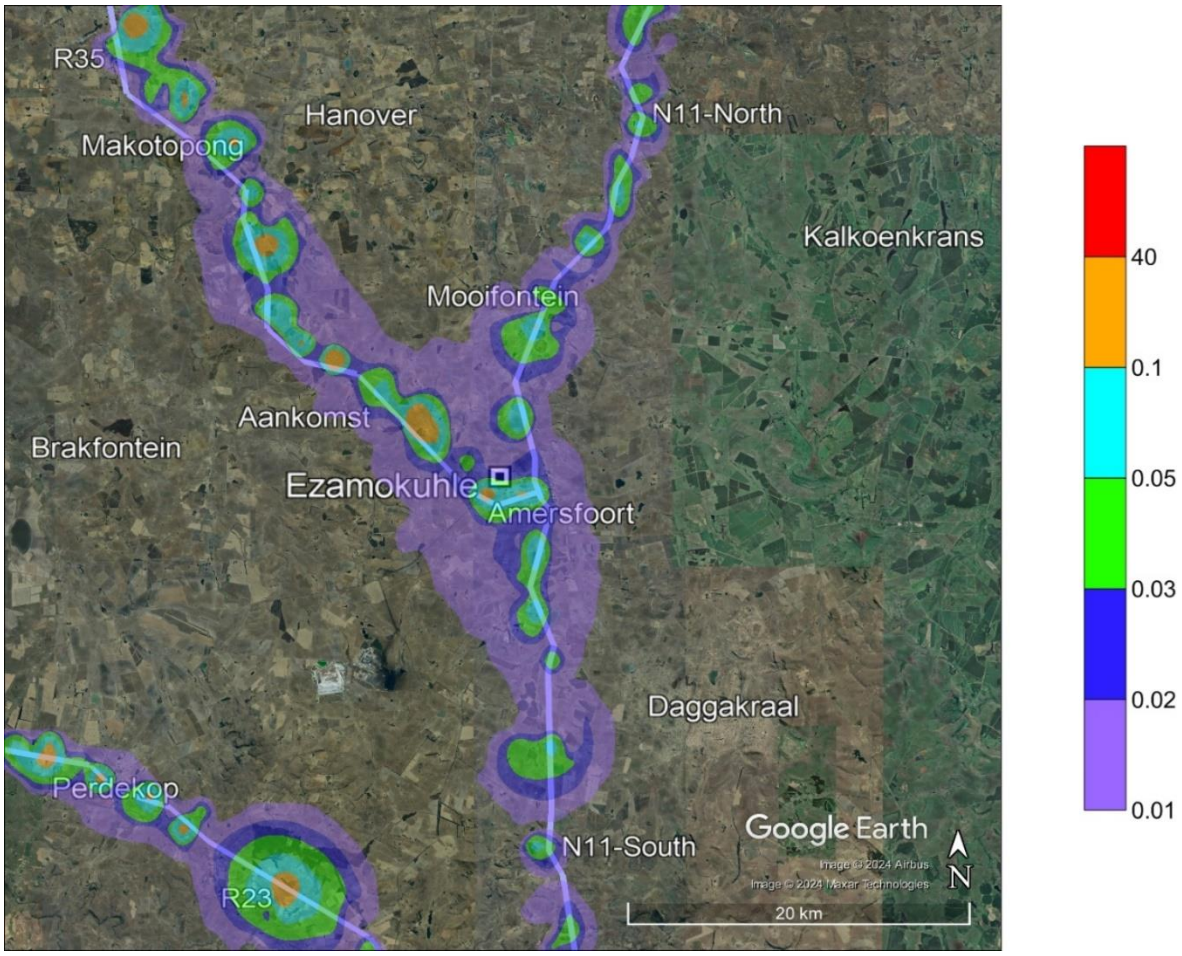

Figure 5-104: Model predicted annual PM_{10} ambient concentrations in µg/m³ for the Vehicles – Paved Roads emission source category within the Greater Ezamokuhle Airshed

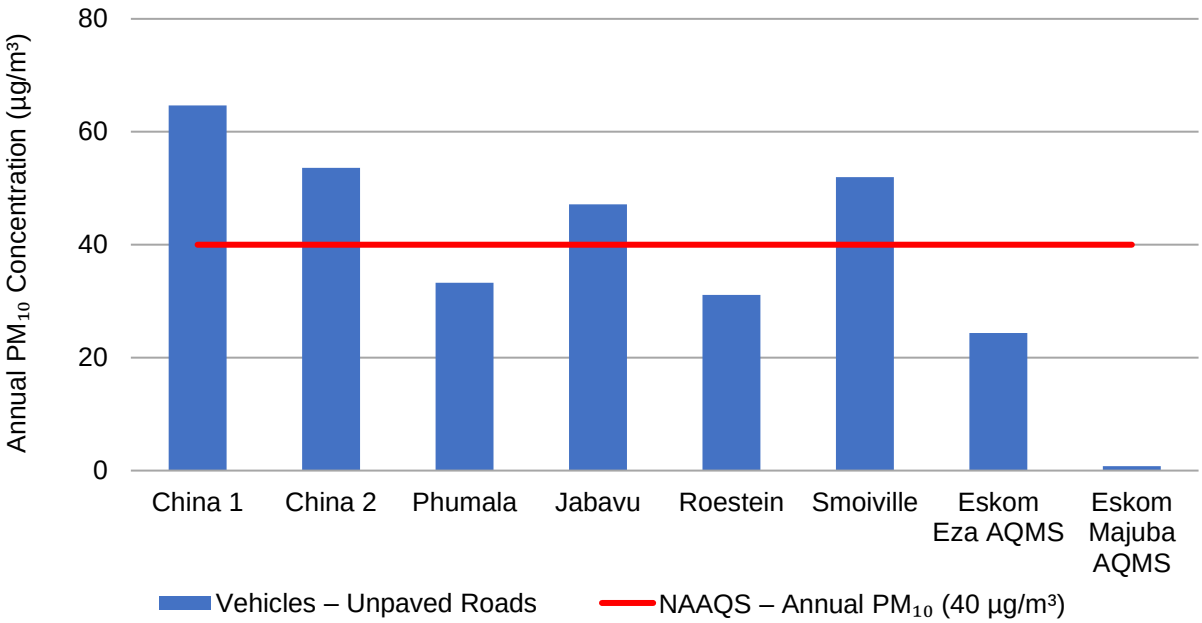

Figure 5-105: Model predicted annual PM_{10} ambient concentrations in µg/m³ at discrete receptors for the Vehicles – Unpaved Roads emission source category

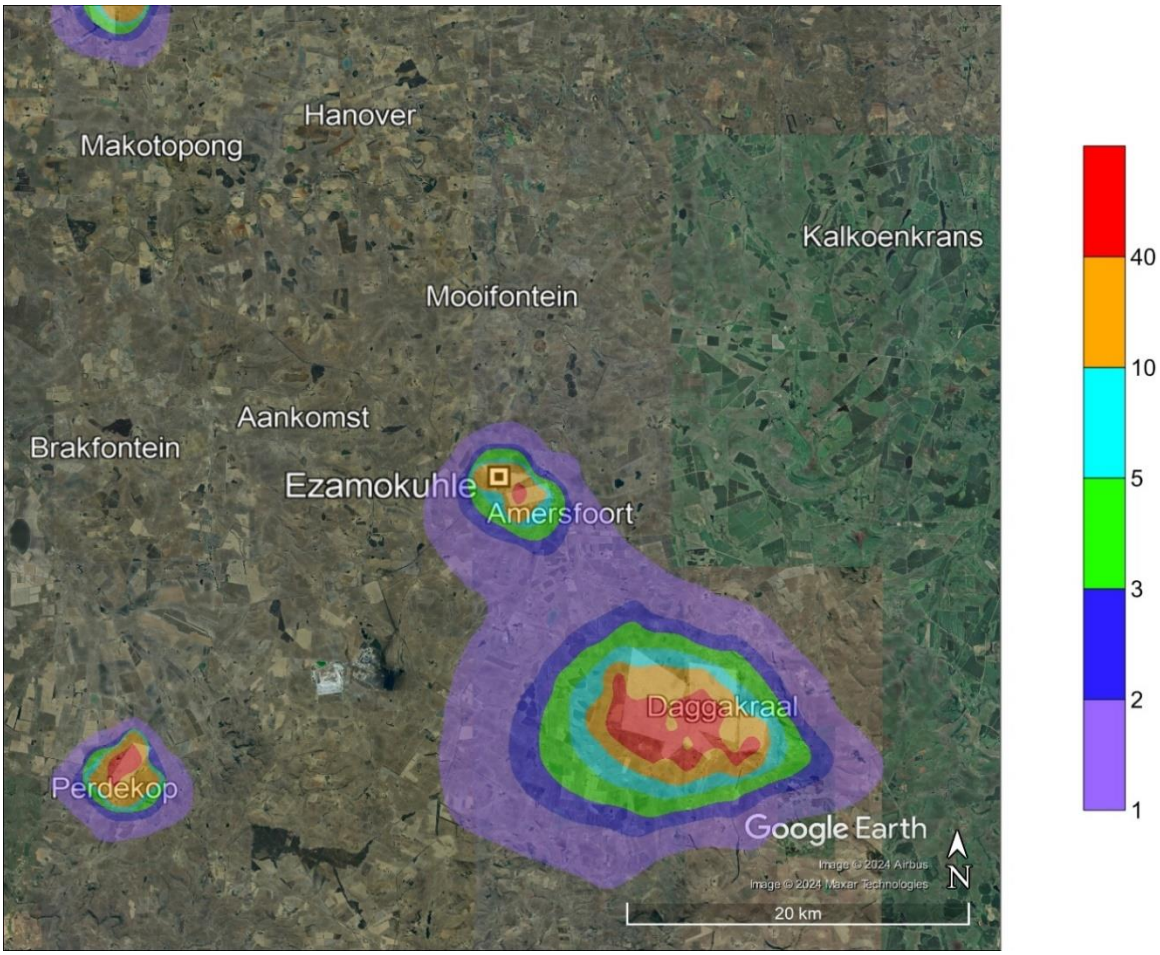

Figure 5-106: Model predicted annual PM_{10} ambient concentrations in µg/m³ for the Vehicles – Unpaved Roads emission source category within the Greater Ezamokuhle Airshed

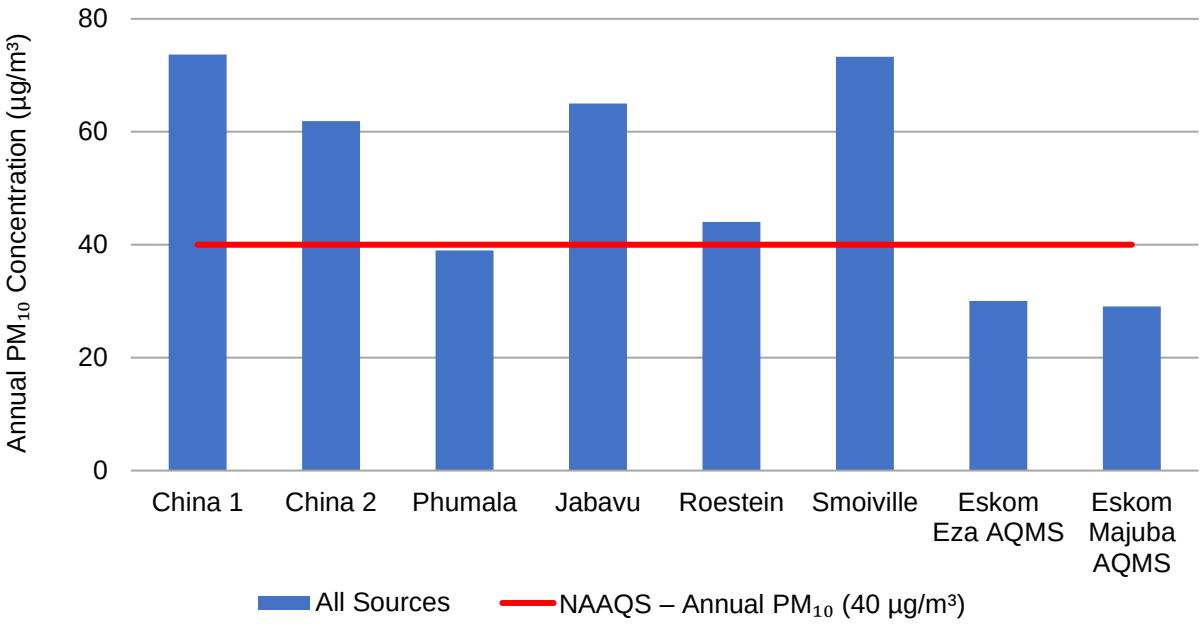

Figure 5-107: Model predicted annual PM_{10} ambient concentrations in µg/m³ at discrete receptors for the All Sources emission source category

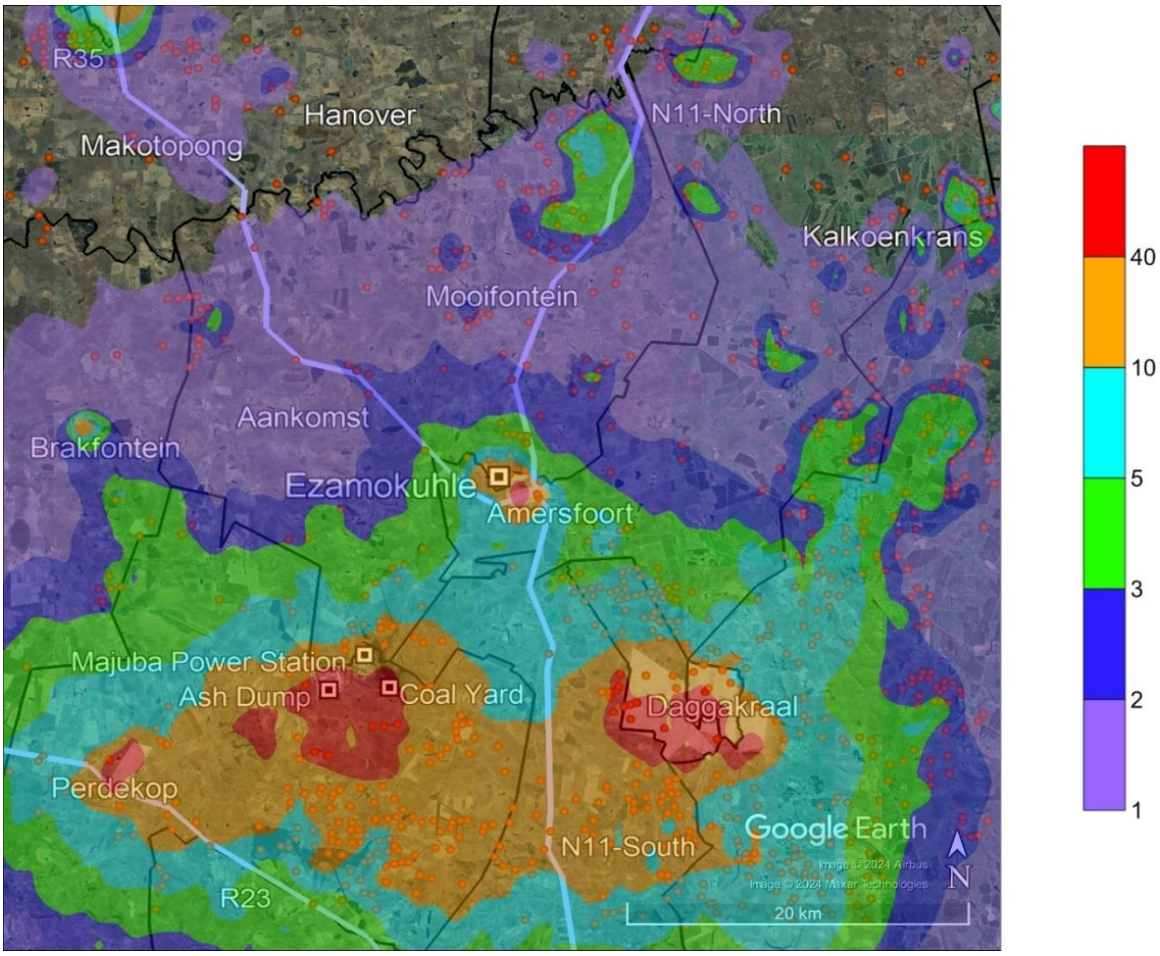

Figure 5-108: Model predicted annual PM_{10} ambient concentrations in µg/m³ for the All Sources emission source category within the Greater Ezamokuhle Airshed

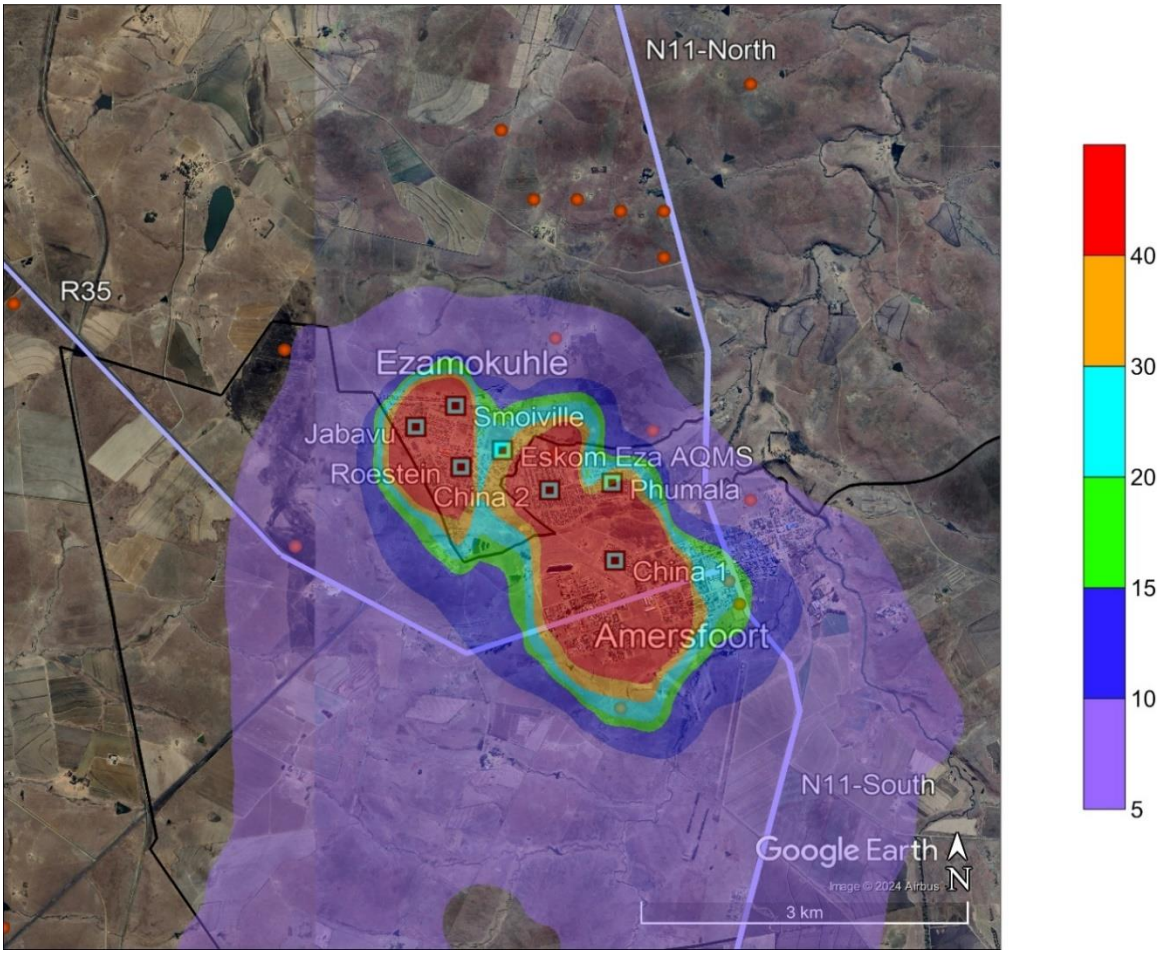

Figure 5-109: Model predicted annual PM_{10} ambient concentrations in µg/m³ for the All Sources emission source category within Ezamokuhle airshed

5.3.3 PM_{10} SOURCE CONTRIBUTION ANALYSIS

In this study, the PM_{10} source contribution analysis is based on model predicted annual PM_{10} ambient concentrations at the discrete receptors for the six emission source categories which include power generation, residential fuel burning, waste burning, biomass burning, vehicles – paved roads and vehicles – unpaved roads (Table 5-9). Table 5-9 is used to calculate the percent contribution of PM_{10} at each discrete receptor as a function of the six source categories, and is presented in Table 5-10.

Table 5-10: PM_{10} source contribution (%) at discrete receptors for the six emission source categories based on model predicted annual PM_{10} ambient concentrations

Discrete Receptors	Power Generation	Residential Fuel Burning	Waste Burning	Biomass Burning	Vehicles – Paved Roads	Vehicles – Unpaved Roads	All Sources
China 1	2.89	7.76	1.27	0.22	0.09	87.77	100.00
China 2	3.47	8.29	1.28	0.26	0.05	86.65	100.00
Phumala	5.11	7.77	1.24	0.40	0.06	85.42	100.00
Jabavu	3.62	21.61	1.85	0.34	0.03	72.56	100.00
Roestein	5.16	21.92	1.91	0.39	0.04	70.58	100.00
Smoiville	3.02	23.75	2.03	0.26	0.03	70.91	100.00
Eskom Eza AQMS	7.22	9.85	1.27	0.56	0.07	81.03	100.00
Eskom Majuba AQMS	92.61	0.18	0.01	4.56	0.02	2.61	100.00

PM_{10} ambient concentrations (in terms of $\mu g/m^3$) for each emission source category at each discrete receptor is presented in the form of a stacked bar graph in Figure 5-110. The total PM_{10} ambient concentrations at each discrete receptor (which is made up of individual contributions representing each of the six emission source categories) represents the All Sources emission source category. The PM_{10} source contribution in terms of percentages is presented in the form of a stacked bar graph in Figure 5-111. The sum of individual contributions resulting from each emission source category makes up 100%.

The source contribution analysis indicates that power generation, residential fuel burning and vehicles travelling on unpaved road surfaces are the main contributors to ambient PM_{10} levels in the region. Ambient contributions from waste burning, biomass burning and vehicles travelling on paved roads are much smaller in comparison.

Power generation sources account for approximately 93% of the total PM_{10} ambient concentrations at the Eskom Majuba AQMS but are much lower at the Eskom Ezamokuhle AQMS and ward centroid discrete receptors (2-8%). This is expected as the Eskom Majuba Power Station ash dump and coal stockpile are located close to the Eskom Majuba AQMS in comparison with the Eskom Ezamokuhle AQMS and ward centroid discrete receptors.

Residential fuel burning sources account for approximately 0.2% of the total PM_{10} ambient concentrations at the Eskom Majuba AQMS but are much higher at the Eskom Ezamokuhle AQMS and ward centroid discrete receptors (7-24%). This is expected as residential areas are located further away from the Eskom Majuba AQMS in comparison with the Eskom Ezamokuhle AQMS and ward centroid discrete receptors.

Vehicle emission sources from unpaved roads account for approximately 2.6% of the total PM_{10} ambient concentrations at the Eskom Majuba AQMS but are much higher at the Eskom Ezamokuhle AQMS and ward centroid discrete receptors (70-88%). This is expected as residential areas and the dense network of unpaved roads is located further away from the Eskom Majuba AQMS in comparison with the Eskom Ezamokuhle AQMS and ward centroid discrete receptors.

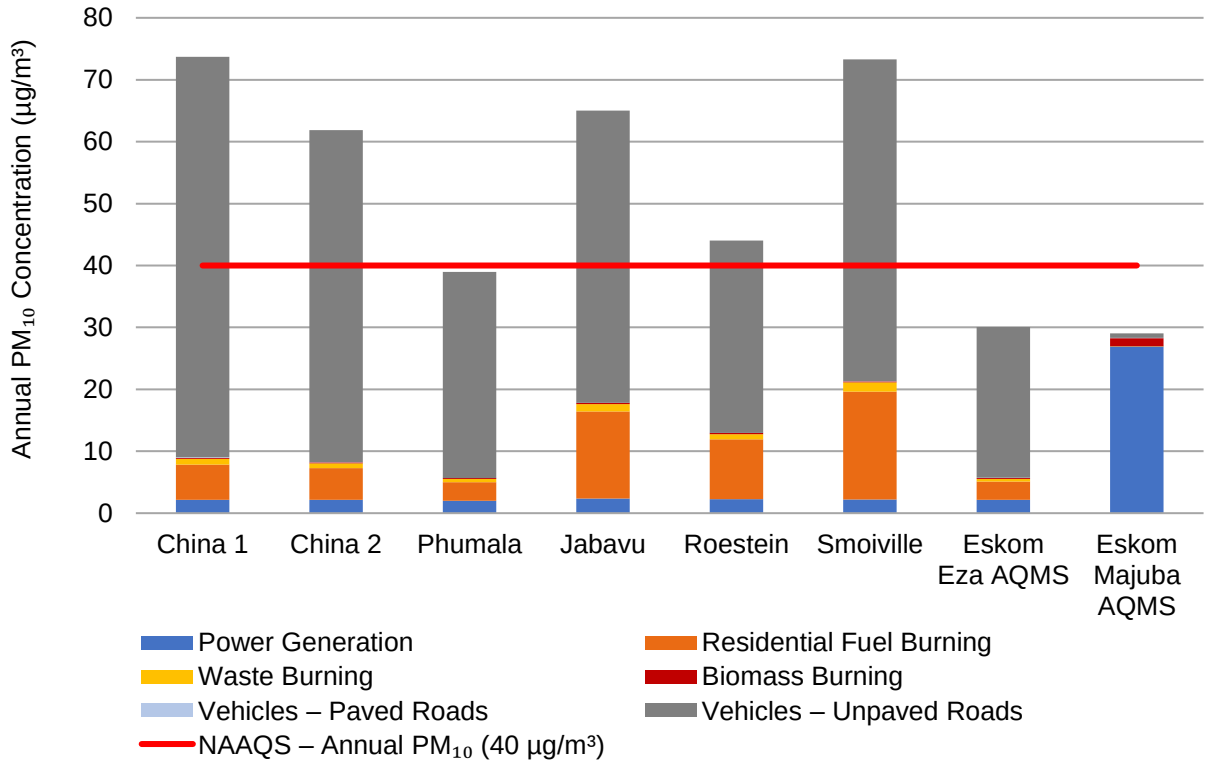

Figure 5-110: Stacked bar graph representing model predicted annual PM_{10} ambient concentrations in µg/m³ at discrete receptors for the six emission source categories

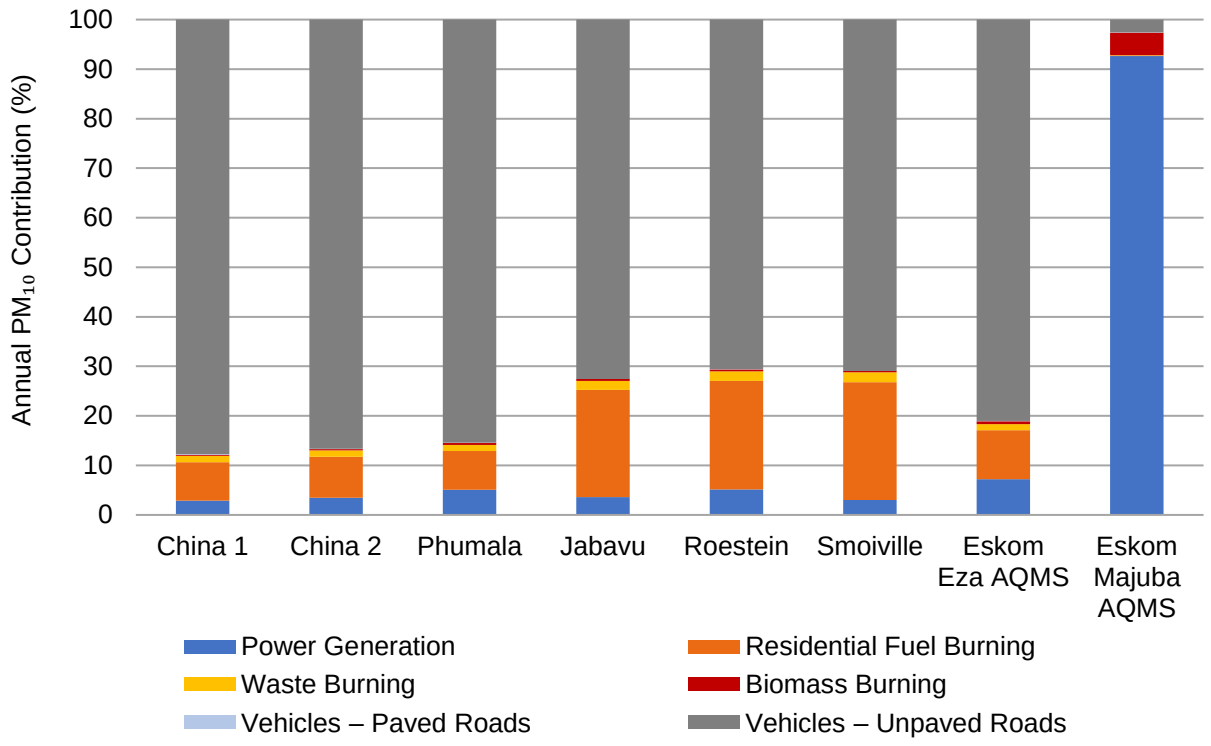

Figure 5-111: Stacked bar graph representing the percent contribution of PM_{10} ambient concentrations at discrete receptors as a function of source category

5.4 PREDICTED $PM_{2.5}$ AMBIENT CONCENTRATIONS

5.4.1 24-HOUR $PM_{2.5}$

Model predicted 24-hour $PM_{2.5}$ ambient concentrations at discrete receptors and at the point of maximum for the seven emission source categories are presented in Table 5-11. If applicable, exceedances of the NAAQS are highlighted in red.

Bar graphs for model predicted 24-hour $PM_{2.5}$ ambient concentrations at discrete receptors are presented in the following order:

- Figure 5-112 for the Power Generation emission source category
- Figure 5-114 for the Residential Fuel Burning emission source category
- Figure 5-116 for the Waste Burning emission source category
- Figure 5-118 for the Biomass Burning emission source category
- Figure 5-120 for the Vehicles – Paved Roads emission source category
- Figure 5-122 for the Vehicles – Unpaved Roads emission source category
- Figure 5-124 for the All Sources emission source category

Contour plots for model predicted 24-hour $PM_{2.5}$ ambient concentrations for the Greater Ezamokuhle Airshed are presented in the following order:

- Figure 5-113 for the Power Generation emission source category
- Figure 5-115 for the Residential Fuel Burning emission source category
- Figure 5-117 for the Waste Burning emission source category
- Figure 5-119 for the Biomass Burning emission source category
- Figure 5-121 for the Vehicles – Paved Roads emission source category
- Figure 5-123 for the Vehicles – Unpaved Roads emission source category
- Figure 5-125 for the All Sources emission source category

Contour plots for model predicted 24-hour $PM_{2.5}$ ambient concentrations for the Ezamokuhle airshed is presented in Figure 5-126 for the All Sources emission source category.

With respect to contour plots for the primary and Ezamokuhle airshed, areas of exceedance of the NAAQS is coloured in red.

Table 5-11: Model predicted 24-hour $PM_{2.5}$ ambient concentrations (99th percentile) in µg/m^3 at discrete receptors and at the point of maximum for the seven emission source categories

Discrete Receptors	Power Generation	Residential Fuel Burning	Waste Burning	Biomass Burning	Vehicles – Paved Roads	Vehicles – Unpaved Roads	All Sources
China 1	15.21	13.36	2.09	0.62	0.24	16.18	40.56
China 2	13.85	12.56	1.82	0.57	0.15	13.74	37.46
Phumala	13.84	7.55	1.17	0.58	0.11	8.60	24.32
Jabavu	15.67	32.76	2.64	0.71	0.09	11.72	56.31
Roestein	14.00	23.80	2.06	0.57	0.10	8.47	45.66
Smoiville	14.38	34.55	2.85	0.60	0.09	11.77	54.39
Eskom Eza AQMS	14.14	7.40	0.93	0.58	0.11	6.74	25.34
Eskom Majuba AQMS	89.42	0.24	0.02	4.17	0.03	0.56	90.46
Maximum	286.92	72.45	6.10	17.42	1.50	33.24	291.70
	NAAQS – 24-hour $PM_{2.5}$ (40 µg/m^3)						

According to Table 5-11, model predicted 24-hour $PM_{2.5}$ ambient concentrations exceed the 24-hour $PM_{2.5}$ NAAQS of 40 µg/m^3 at the point of maximum for the Power Generation, Residential Fuel Burning and All Sources emission source category. The NAAQS is also exceeded at the Eskom Majuba AQMS for the Power Generation emission source category; and at China 1, Jabavu, Roestein, Smoiville and the Eskom Majuba AQMS for the All Sources emission source category.

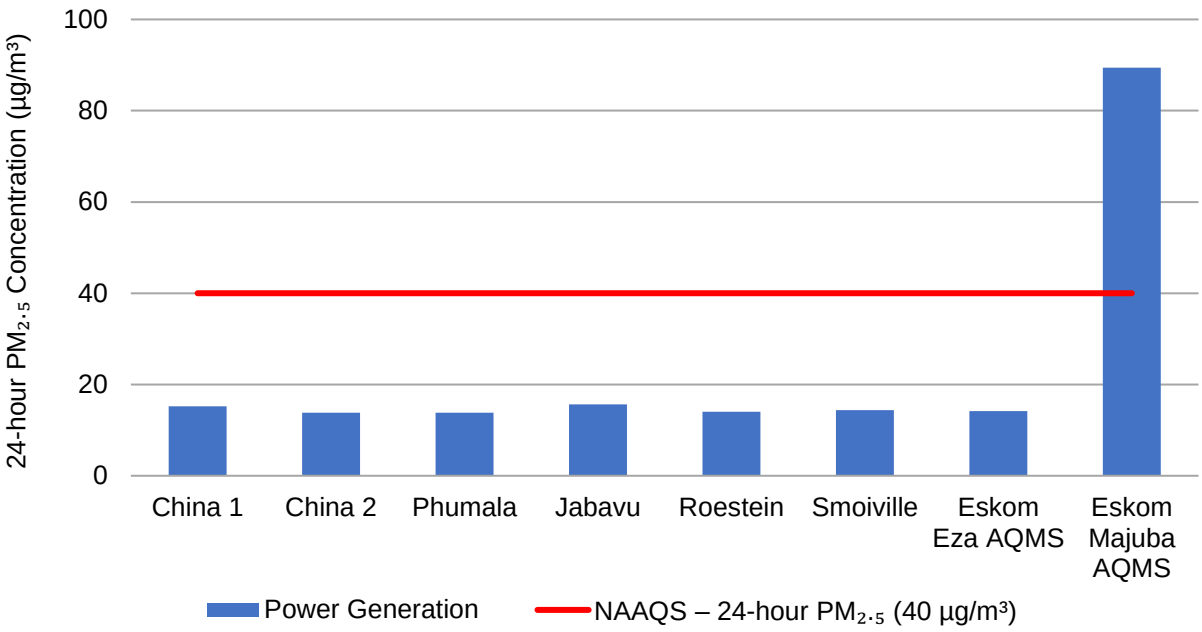

Figure 5-112: Model predicted 24-hour $PM_{2.5}$ ambient concentrations (99th percentile) in µg/m³ at discrete receptors for the Power Generation emission source category

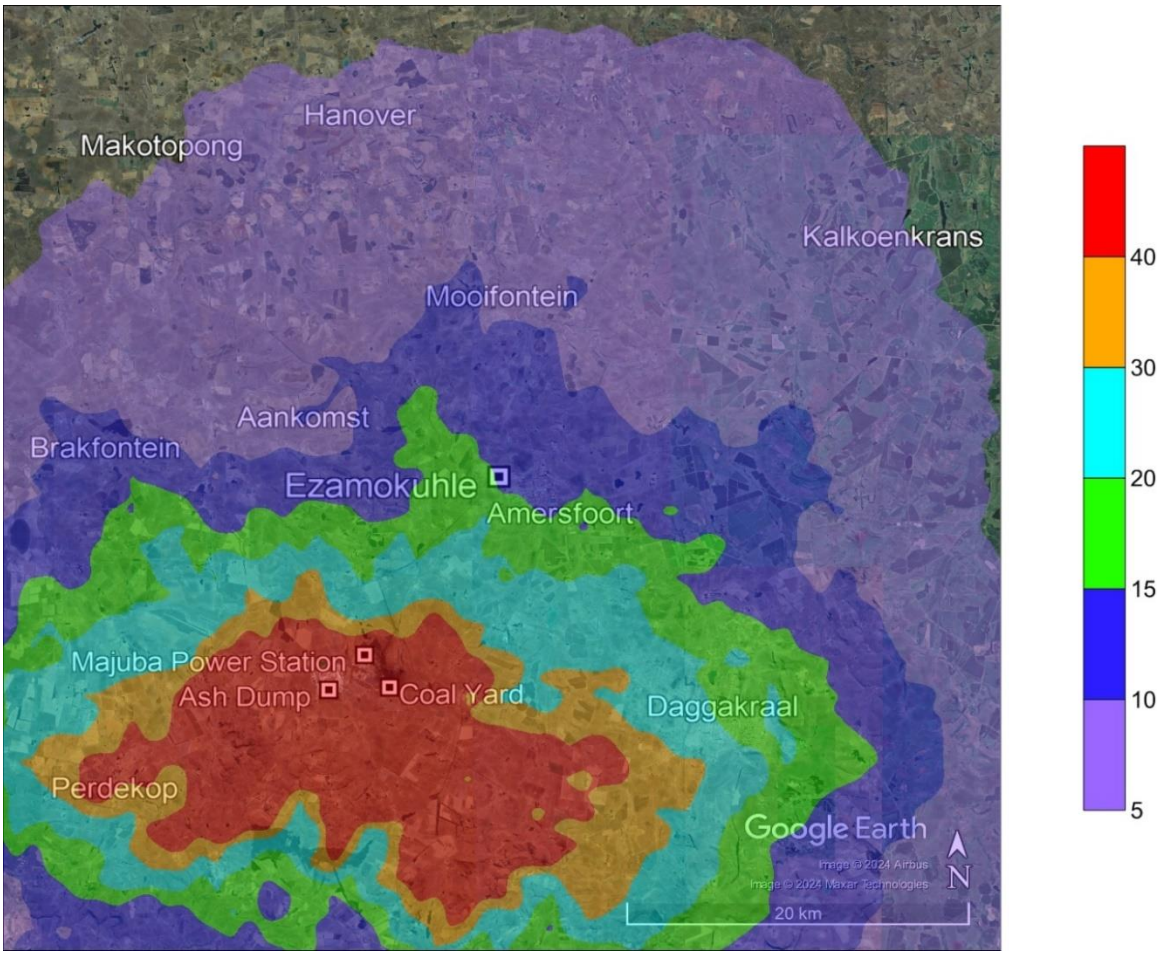

Figure 5-113: Model predicted 24-hour $PM_{2.5}$ ambient concentrations (99th percentile) in µg/m³ for the Power Generation emission source category within the Greater Ezamokuhle Airshed

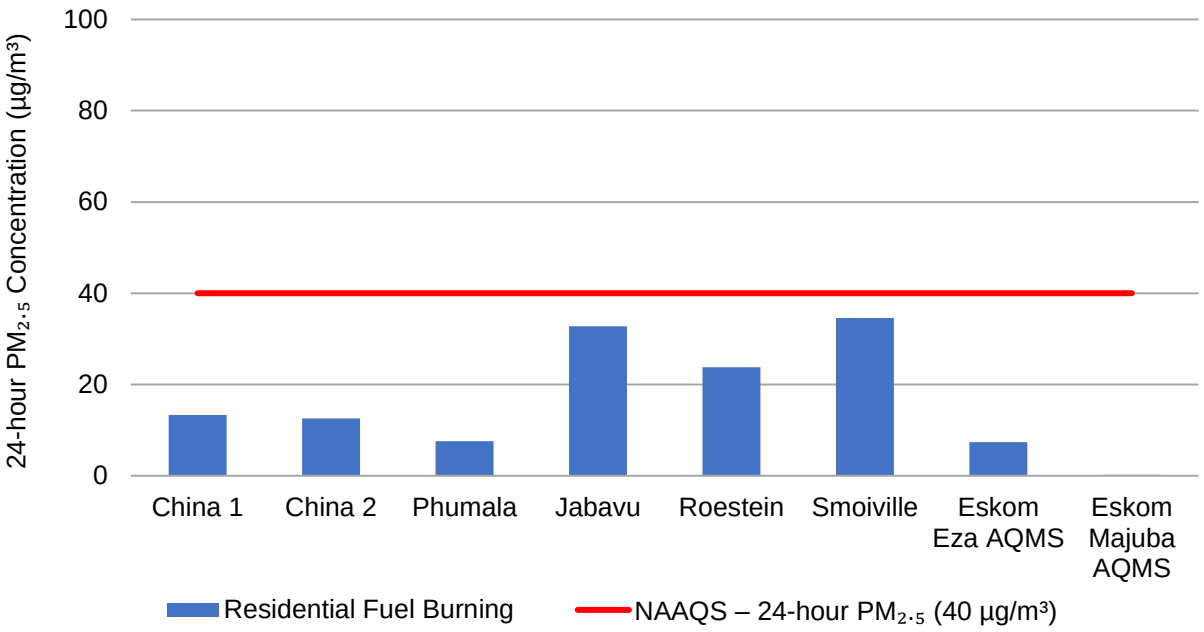

Figure 5-114: Model predicted 24-hour $PM_{2.5}$ ambient concentrations (99th percentile) in µg/m³ at discrete receptors for the Residential Fuel Burning emission source category

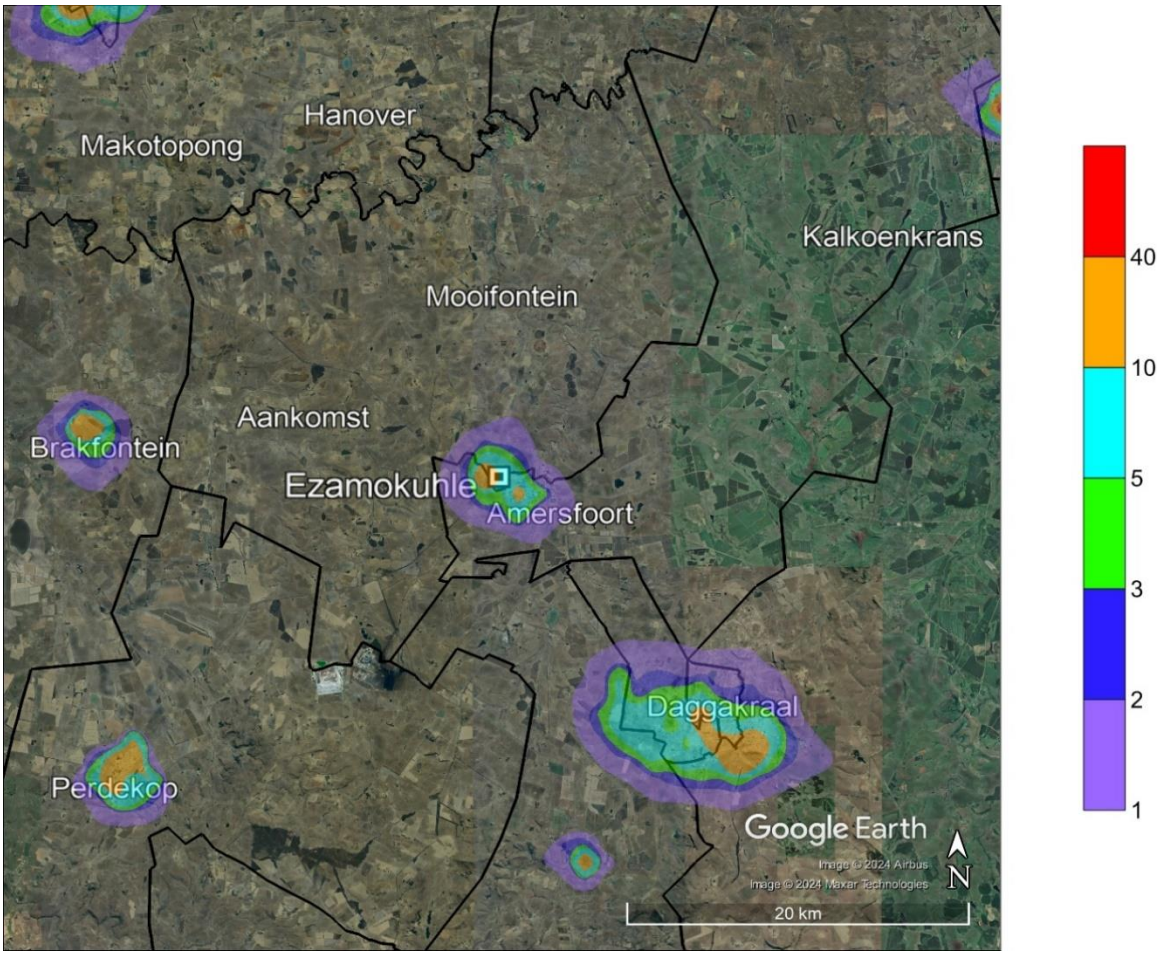

Figure 5-115: Model predicted 24-hour $PM_{2.5}$ ambient concentrations (99th percentile) in µg/m³ for the Residential Fuel Burning emission source category within the Greater Ezamokuhle Airshed

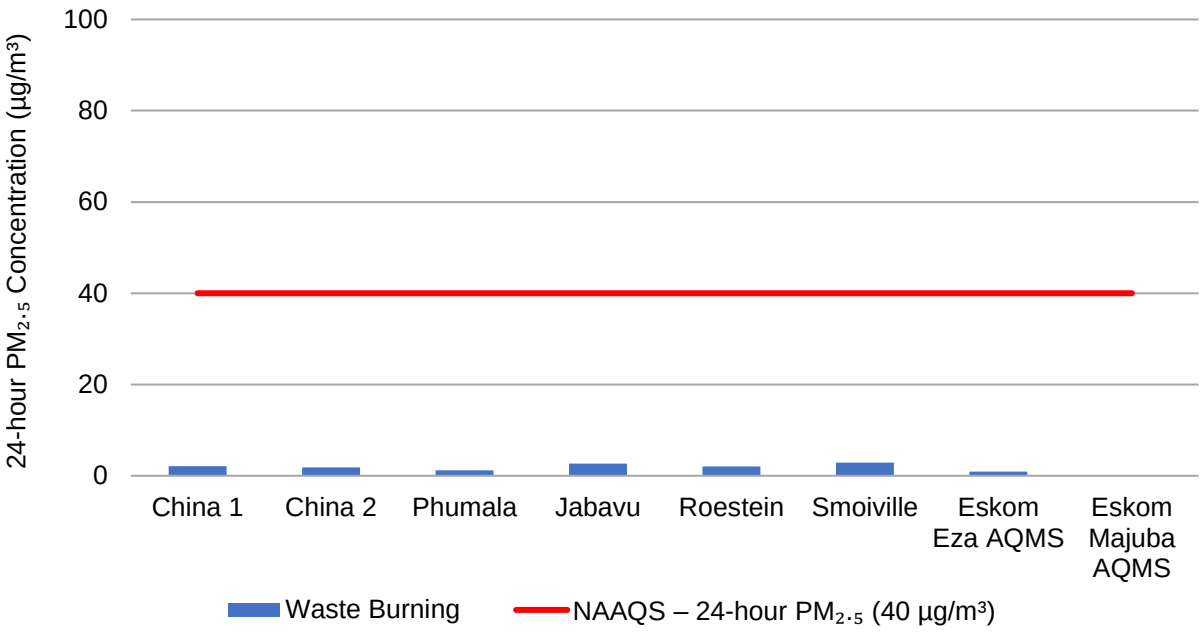

Figure 5-116: Model predicted 24-hour $PM_{2.5}$ ambient concentrations (99th percentile) in µg/m³ at discrete receptors for the Waste Burning emission source category

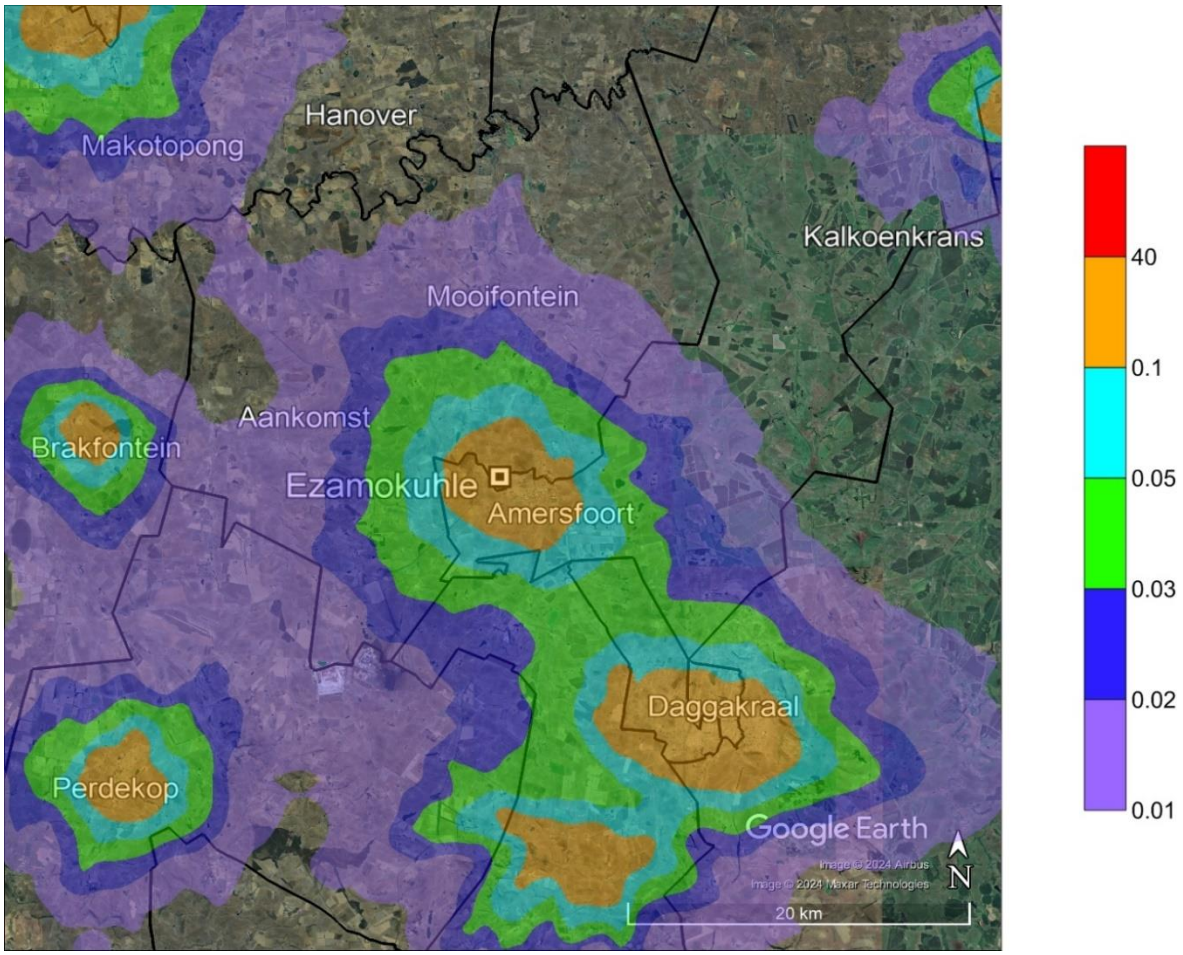

Figure 5-117: Model predicted 24-hour $PM_{2.5}$ ambient concentrations (99th percentile) in µg/m³ for the Waste Burning emission source category within the Greater Ezamokuhle Airshed

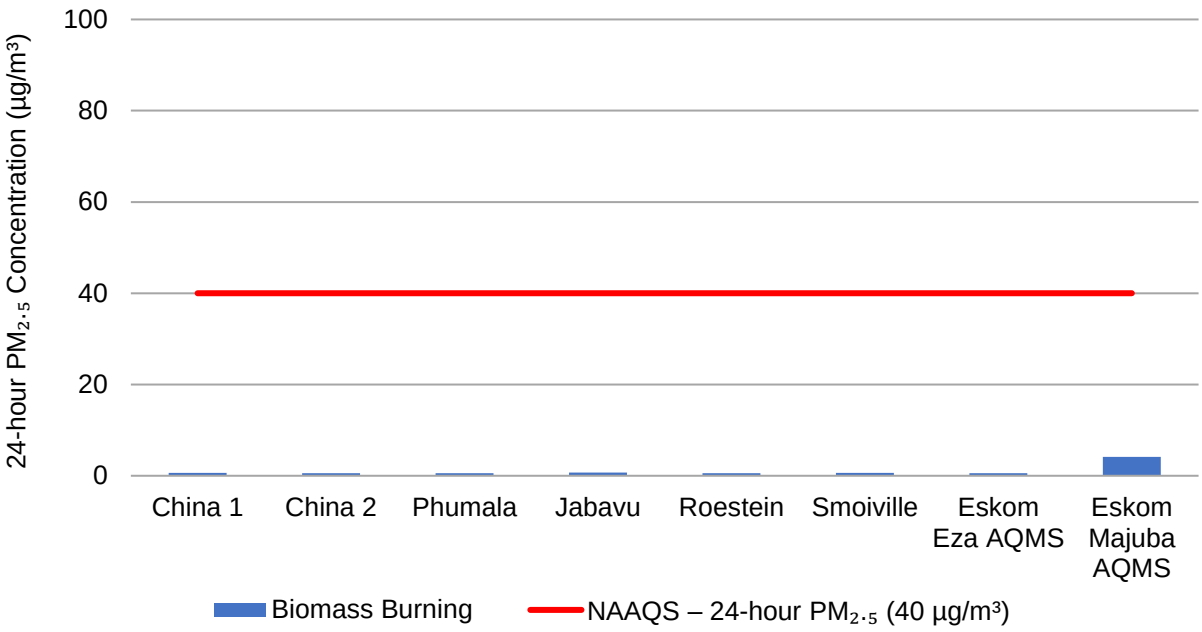

Figure 5-118: Model predicted 24-hour $PM_{2.5}$ ambient concentrations (99th percentile) in µg/m³ at discrete receptors for the Biomass Burning emission source category

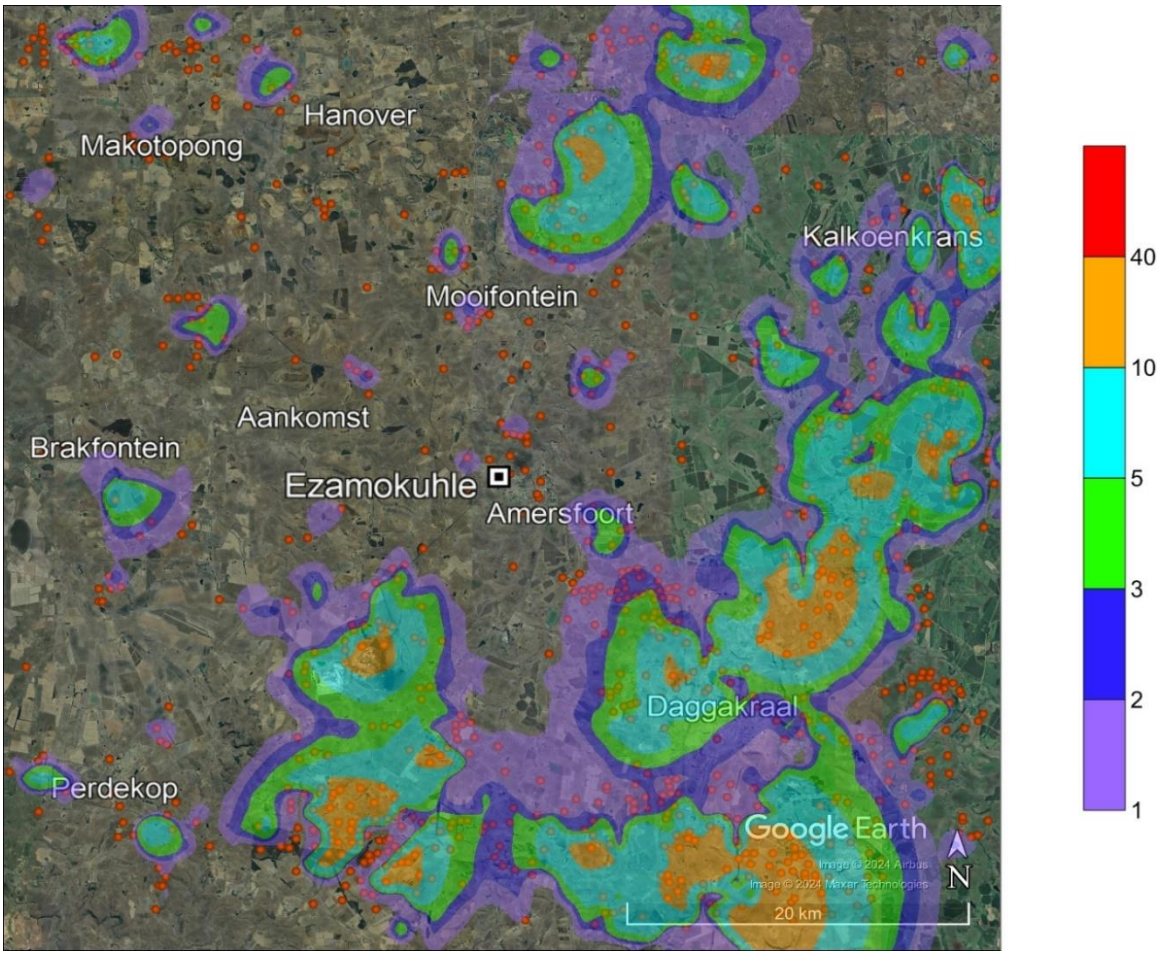

Figure 5-119: Model predicted 24-hour $PM_{2.5}$ ambient concentrations (99th percentile) in µg/m³ for the Biomass Burning emission source category within the Greater Ezamokuhle Airshed

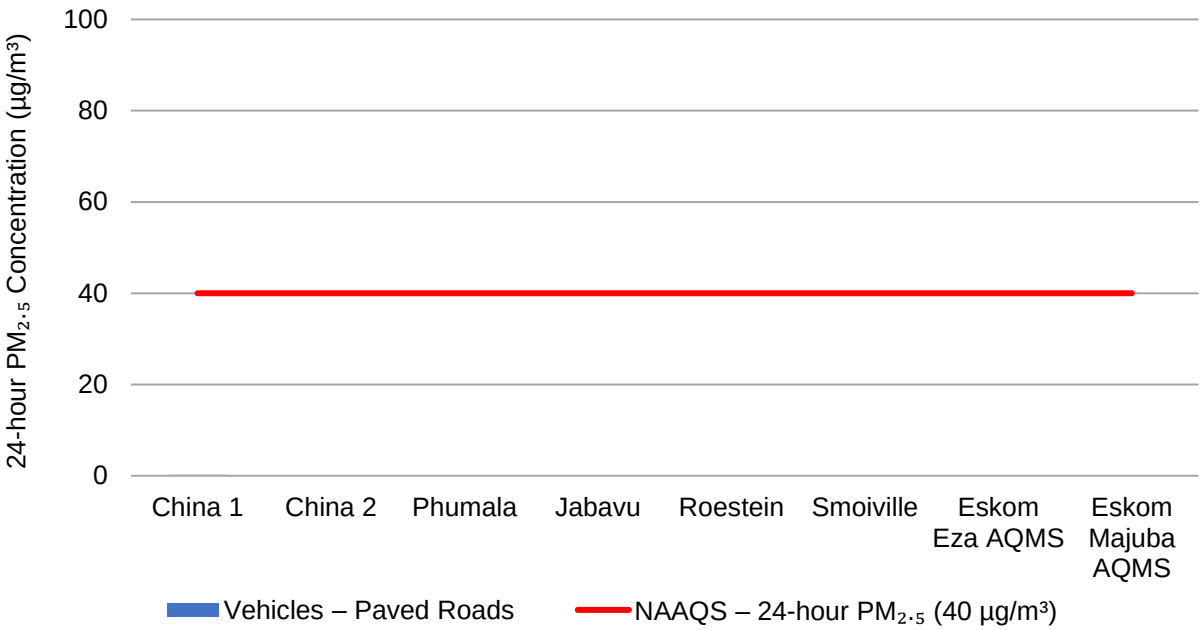

Figure 5-120: Model predicted 24-hour $PM_{2.5}$ ambient concentrations (99th percentile) in µg/m³ at discrete receptors for the Vehicles – Paved Roads emission source category

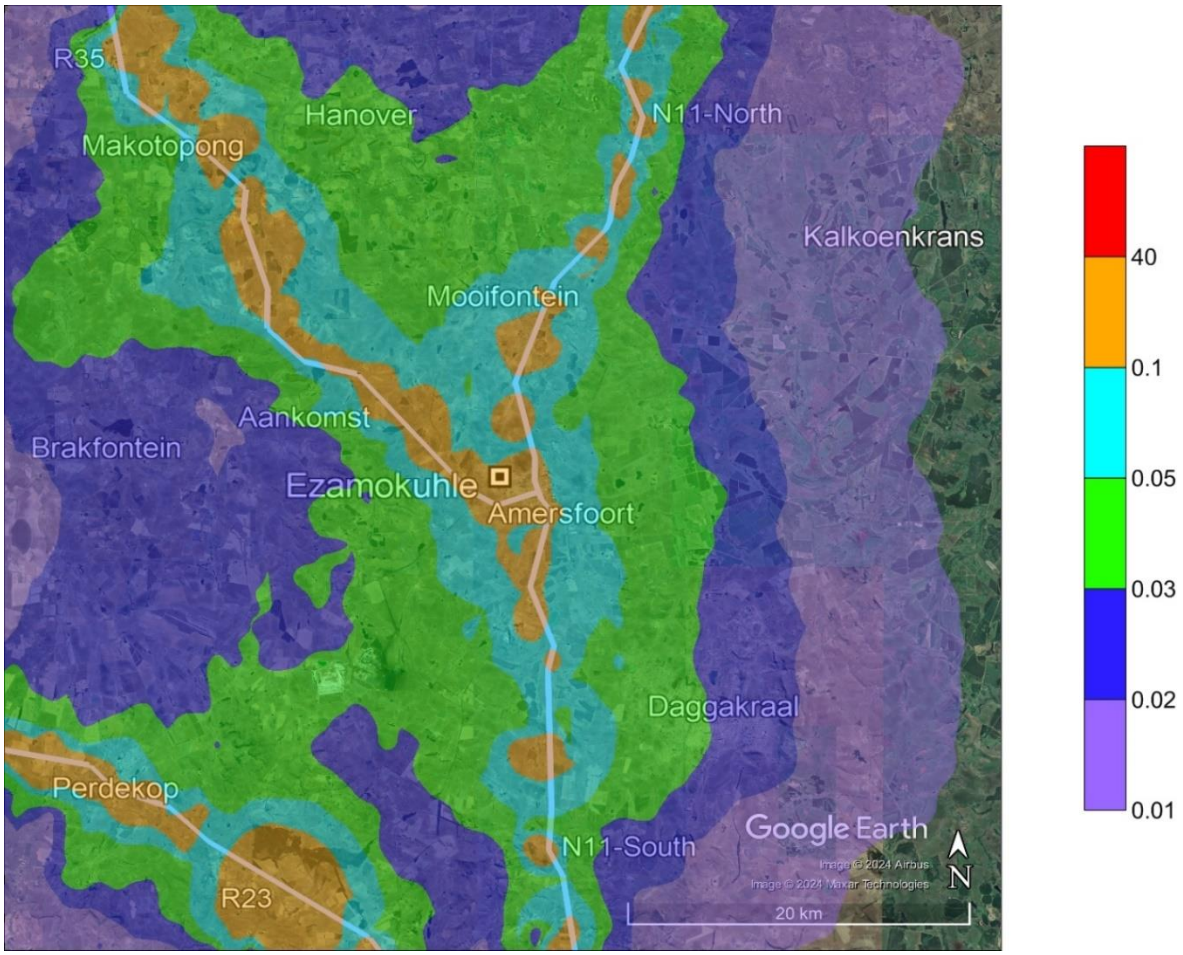

Figure 5-121: Model predicted 24-hour $PM_{2.5}$ ambient concentrations (99th percentile) in µg/m³ for the Vehicles – Paved Roads emission source category within the Greater Ezamokuhle Airshed

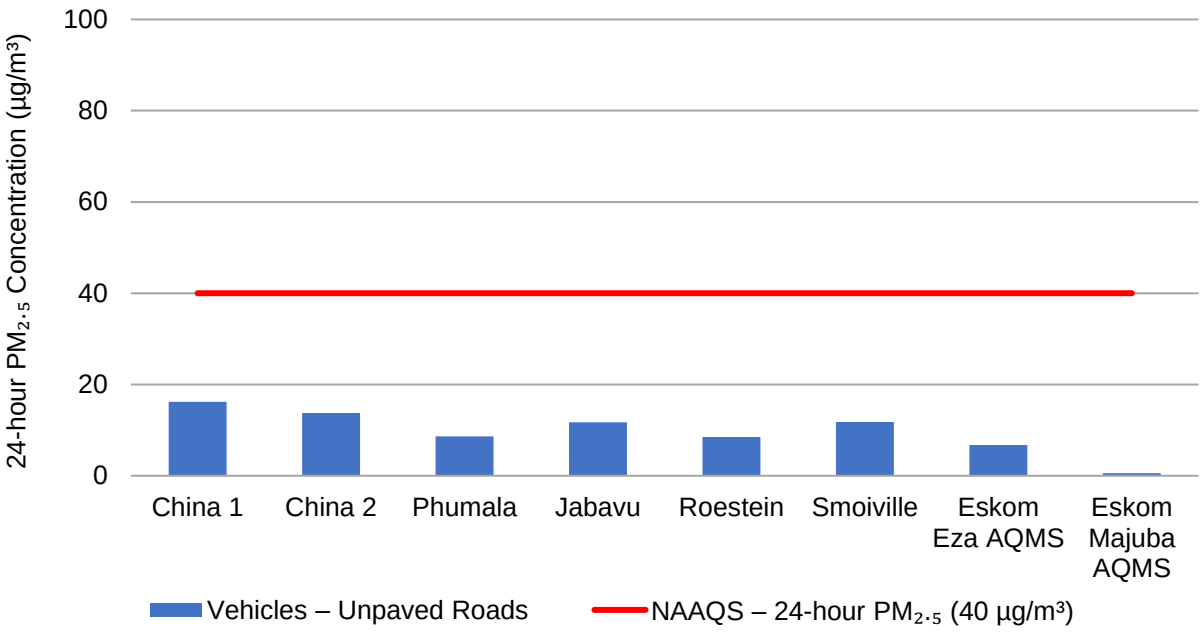

Figure 5-122: Model predicted 24-hour $PM_{2.5}$ ambient concentrations (99th percentile) in µg/m³ at discrete receptors for the Vehicles – Unpaved Roads emission source category

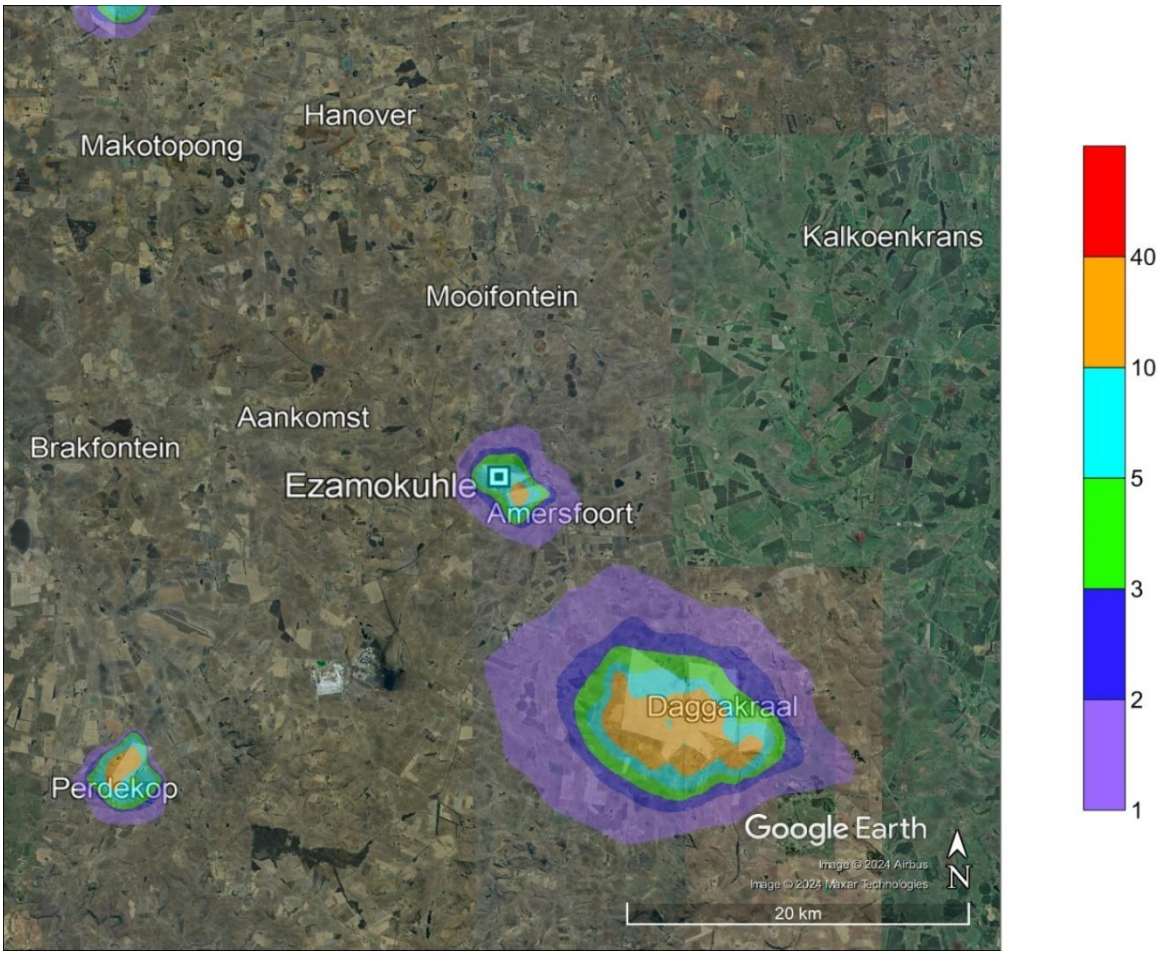

Figure 5-123: Model predicted 24-hour $PM_{2.5}$ ambient concentrations (99th percentile) in µg/m³ for the Vehicles – Unpaved Roads emission source category within the Greater Ezamokuhle Airshed

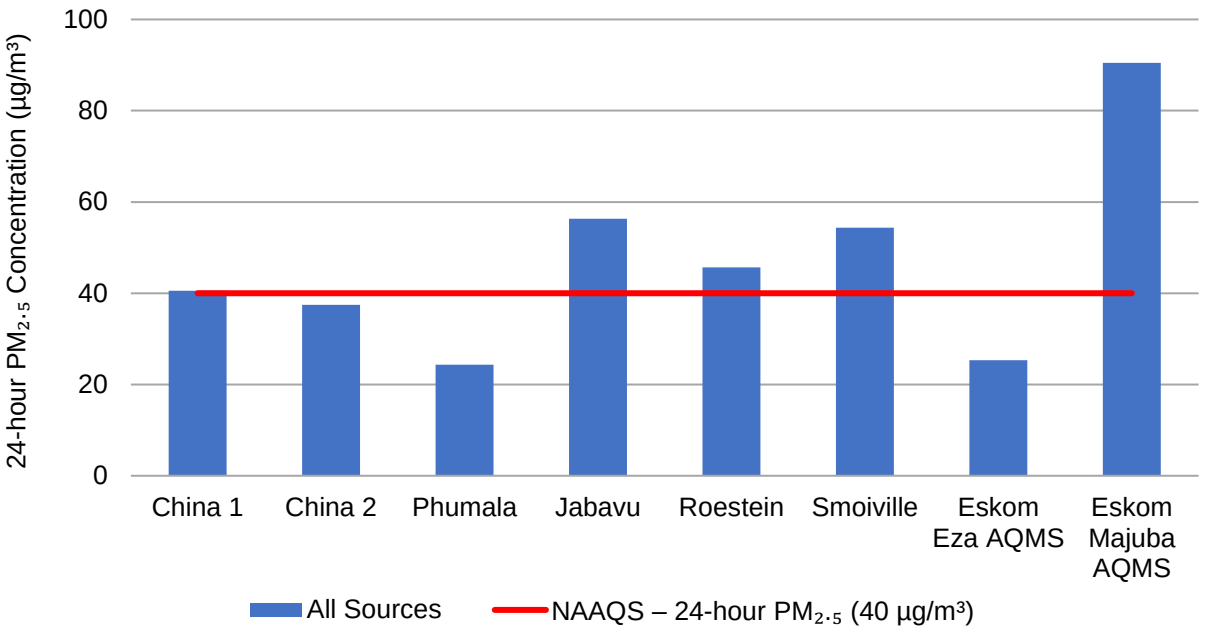

Figure 5-124: Model predicted 24-hour $PM_{2.5}$ ambient concentrations (99th percentile) in µg/m³ at discrete receptors for the All Sources emission source category

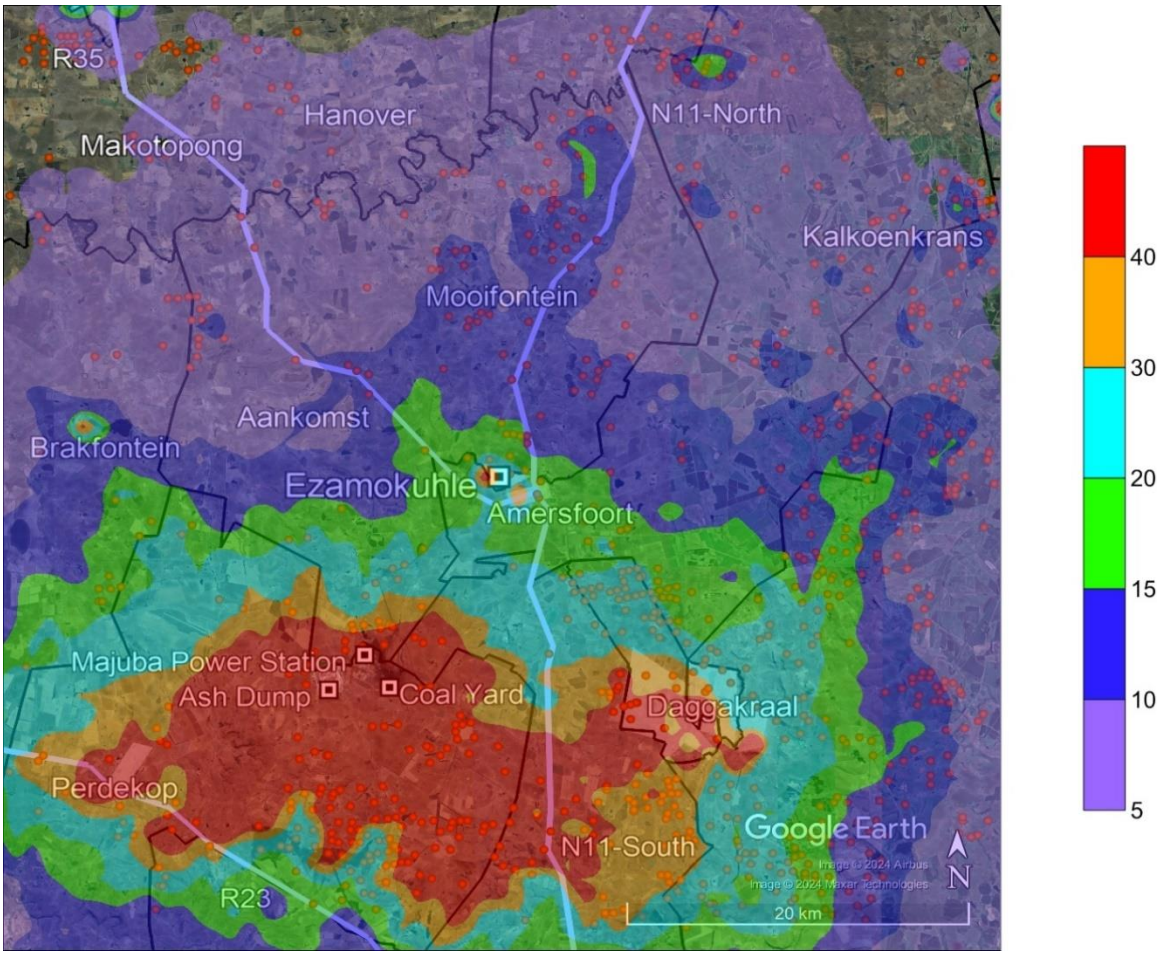

Figure 5-125: Model predicted 24-hour $PM_{2.5}$ ambient concentrations (99th percentile) in µg/m³ for the All Sources emission source category within the Greater Ezamokuhle Airshed

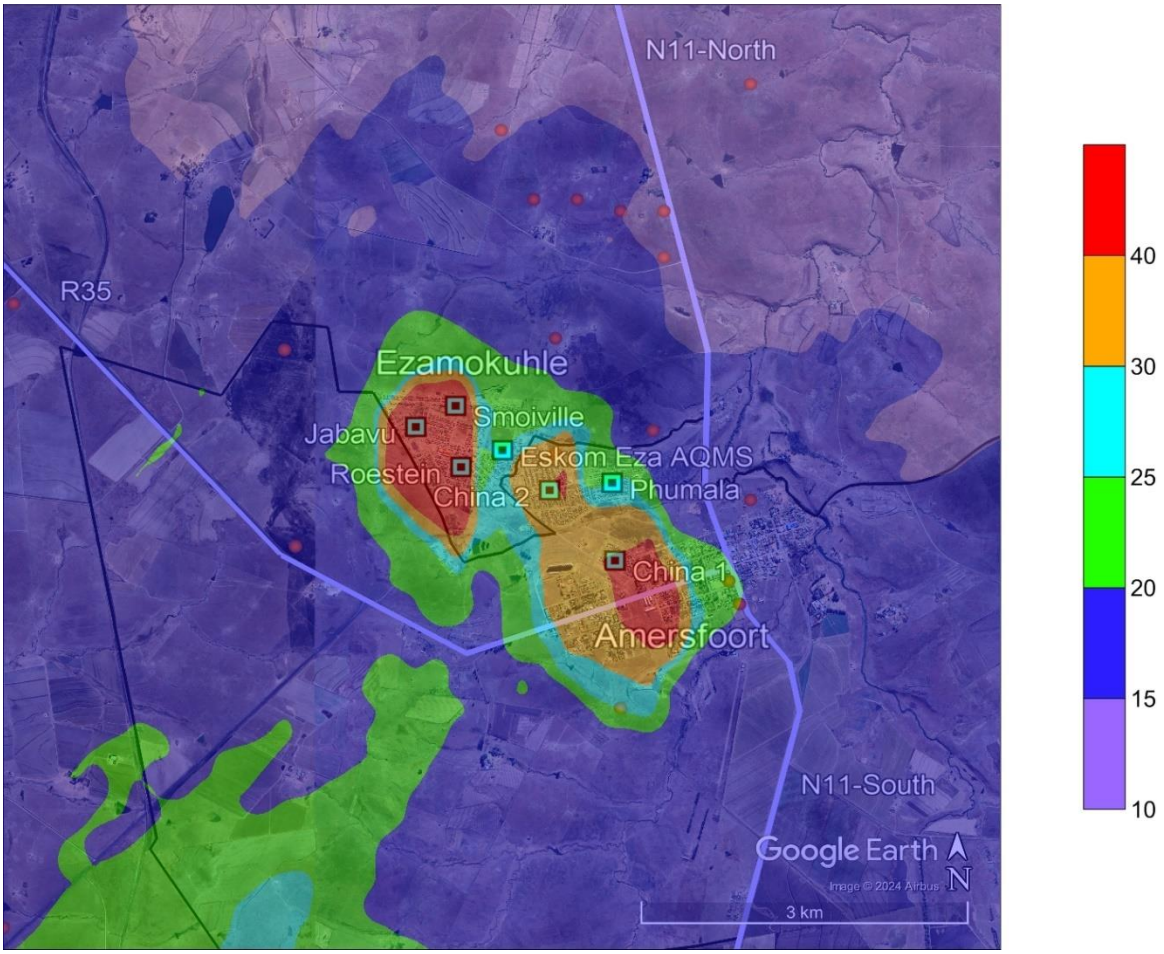

Figure 5-126: Model predicted 24-hour $PM_{2.5}$ ambient concentrations (99th percentile) in µg/m^3 for the All Sources emission source category within Ezamokuhle airshed

5.4.2 ANNUAL $PM_{2.5}$

Model predicted annual $PM_{2.5}$ ambient concentrations at discrete receptors and at the point of maximum for the seven emission source categories are presented in Table 5-12. If applicable, exceedances of the NAAQS are highlighted in red.

Bar graphs for model predicted annual $PM_{2.5}$ ambient concentrations at discrete receptors are presented in the following order:

- Figure 5-127 for the Power Generation emission source category
- Figure 5-129 for the Residential Fuel Burning emission source category
- Figure 5-131 for the Waste Burning emission source category
- Figure 5-133 for the Biomass Burning emission source category
- Figure 5-135 for the Vehicles – Paved Roads emission source category
- Figure 5-137 for the Vehicles – Unpaved Roads emission source category
- Figure 5-139 for the All Sources emission source category

Contour plots for model predicted annual $PM_{2.5}$ ambient concentrations for the Greater Ezamokuhle Airshed are presented in the following order:

- Figure 5-128 for the Power Generation emission source category
- Figure 5-130 for the Residential Fuel Burning emission source category
- Figure 5-132 for the Waste Burning emission source category
- Figure 5-134 for the Biomass Burning emission source category
- Figure 5-136 for the Vehicles – Paved Roads emission source category
- Figure 5-138 for the Vehicles – Unpaved Roads emission source category
- Figure 5-140 for the All Sources emission source category

Contour plots for model predicted annual $PM_{2.5}$ ambient concentrations for the Ezamokuhle airshed is presented in Figure 5-141 for the All Sources emission source category.

With respect to contour plots for the primary and Ezamokuhle airshed, areas of exceedance of the NAAQS is coloured in red.

Table 5-12: Model predicted annual $PM_{2.5}$ ambient concentrations in µg/m³ at discrete receptors and at the point of maximum for the seven emission source categories

Discrete Receptors	Power Generation	Residential Fuel Burning	Waste Burning	Biomass Burning	Vehicles – Paved Roads	Vehicles – Unpaved Roads	All Sources
China 1	1.03	5.71	0.88	0.16	0.07	6.49	14.34
China 2	1.04	5.13	0.75	0.16	0.03	5.38	12.49
Phumala	0.98	3.03	0.46	0.15	0.02	3.34	7.98
Jabavu	1.12	14.05	1.13	0.22	0.02	4.73	21.28
Roestein	1.09	9.66	0.79	0.17	0.02	3.12	14.86
Smoiville	1.07	17.41	1.41	0.19	0.02	5.21	25.30
Eskom Eza AQMS	1.05	2.96	0.36	0.17	0.02	2.44	7.00
Eskom Majuba AQMS	10.93	0.05	0.00	1.32	0.01	0.08	12.38
Maximum	41.19	21.53	2.28	6.34	0.35	13.55	42.93
	NAAQS – annual $PM_{2.5}$ (20 µg/m³)						

According to Table 5-12, model predicted annual $PM_{2.5}$ ambient concentrations exceed the annual $PM_{2.5}$ NAAQS of 20 µg/m³ at the point of maximum for the Power Generation, Residential Fuel Burning and All Sources emission source category. The NAAQS is also exceeded at Jabavu and Smoiville for the All Sources emission source category.

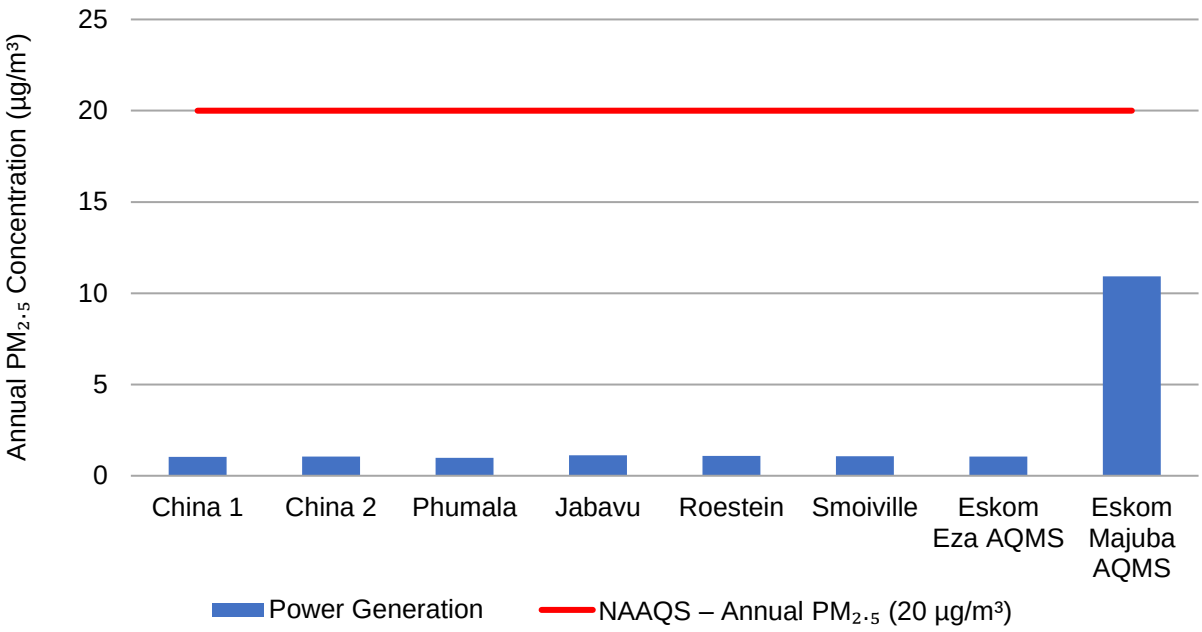

Figure 5-127: Model predicted annual $PM_{2.5}$ ambient concentrations in µg/m³ at discrete receptors for the Power Generation emission source category

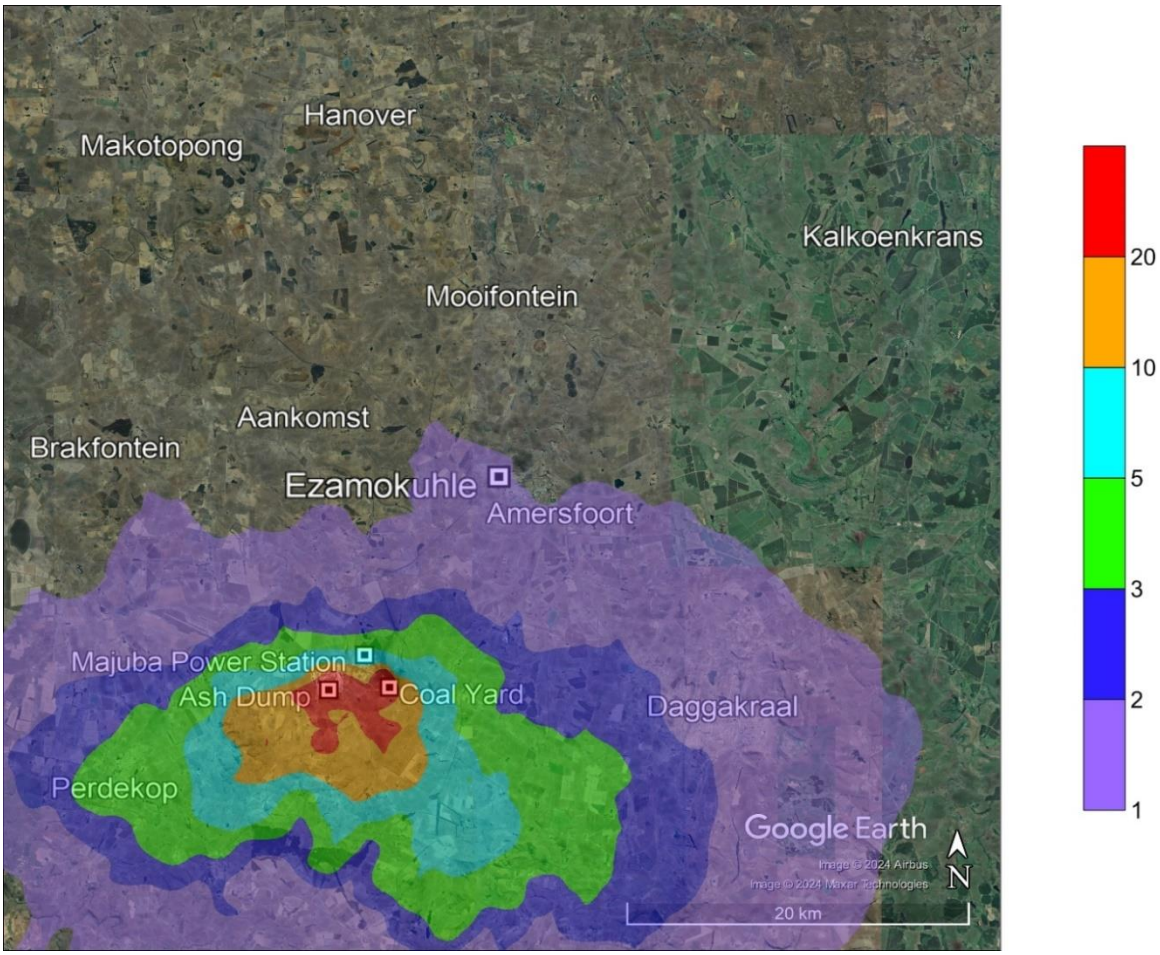

Figure 5-128: Model predicted annual $PM_{2.5}$ ambient concentrations in µg/m³ for the Power Generation emission source category within the Greater Ezamokuhle Airshed

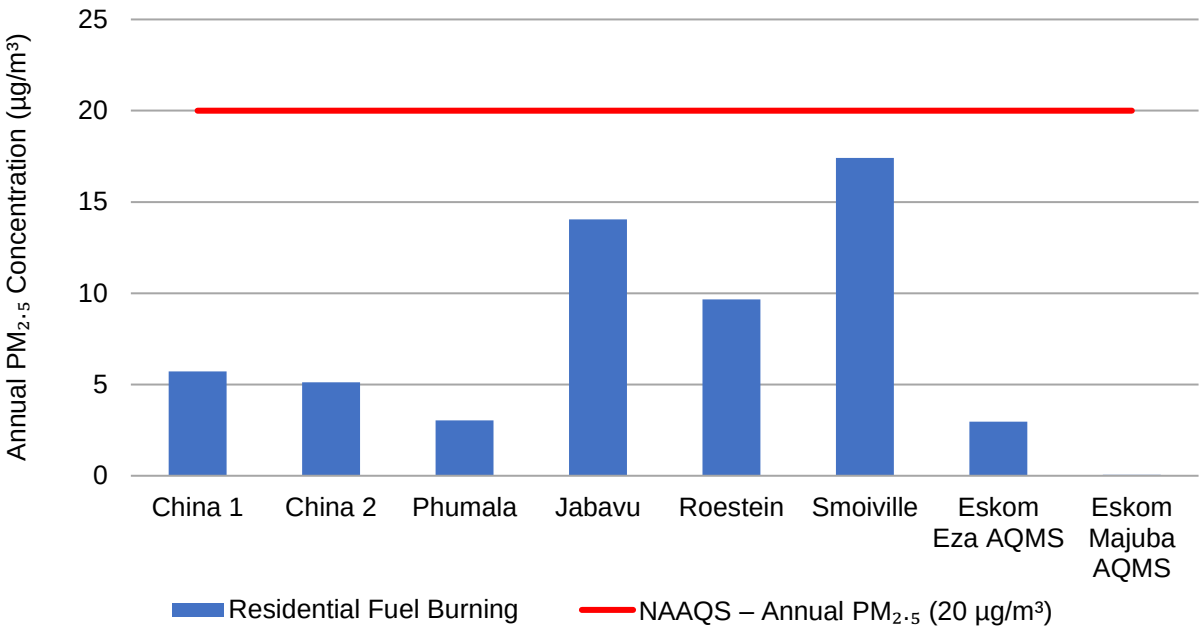

Figure 5-129: Model predicted annual $PM_{2.5}$ ambient concentrations in µg/m³ at discrete receptors for the Residential Fuel Burning emission source category

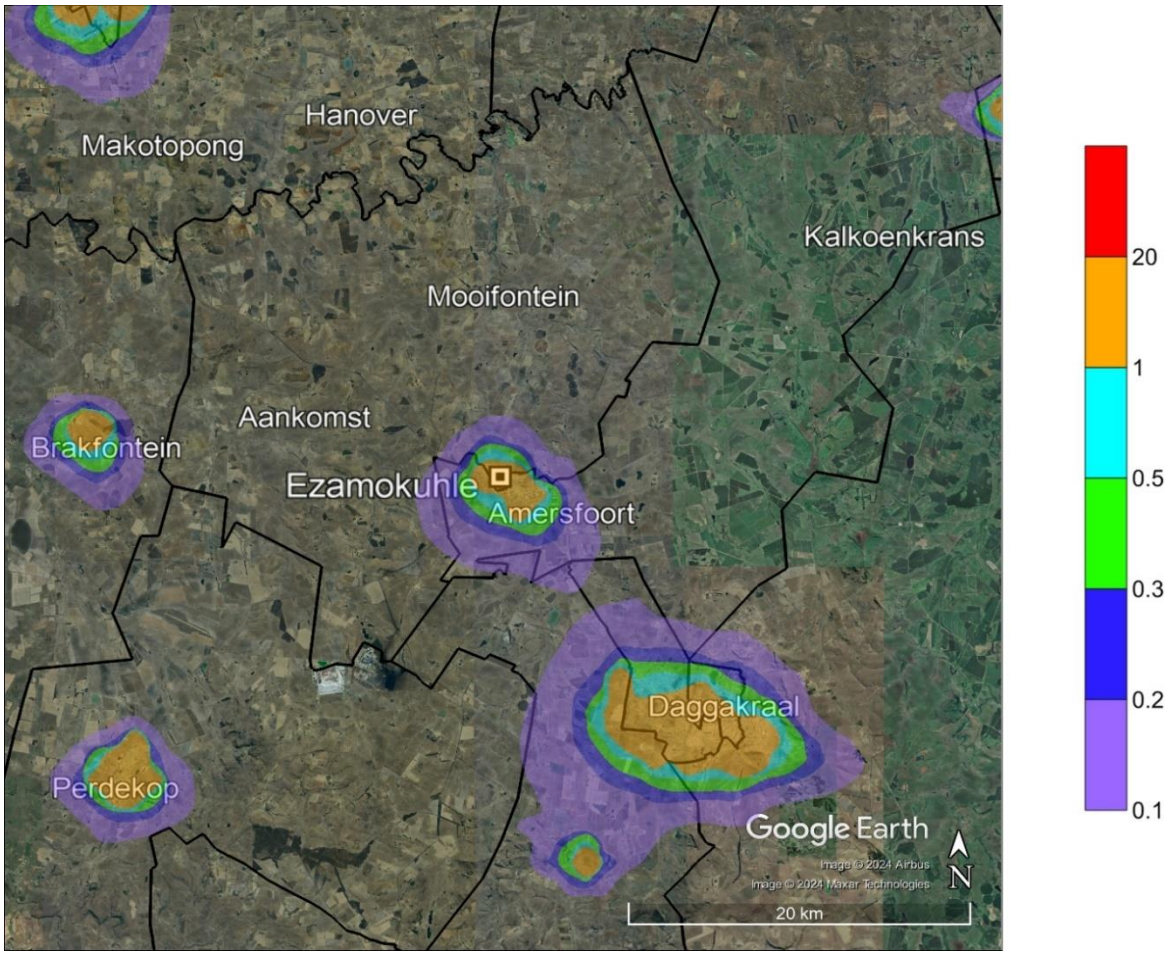

Figure 5-130: Model predicted annual $PM_{2.5}$ ambient concentrations in µg/m³ for the Residential Fuel Burning emission source category within the Greater Ezamokuhle Airshed

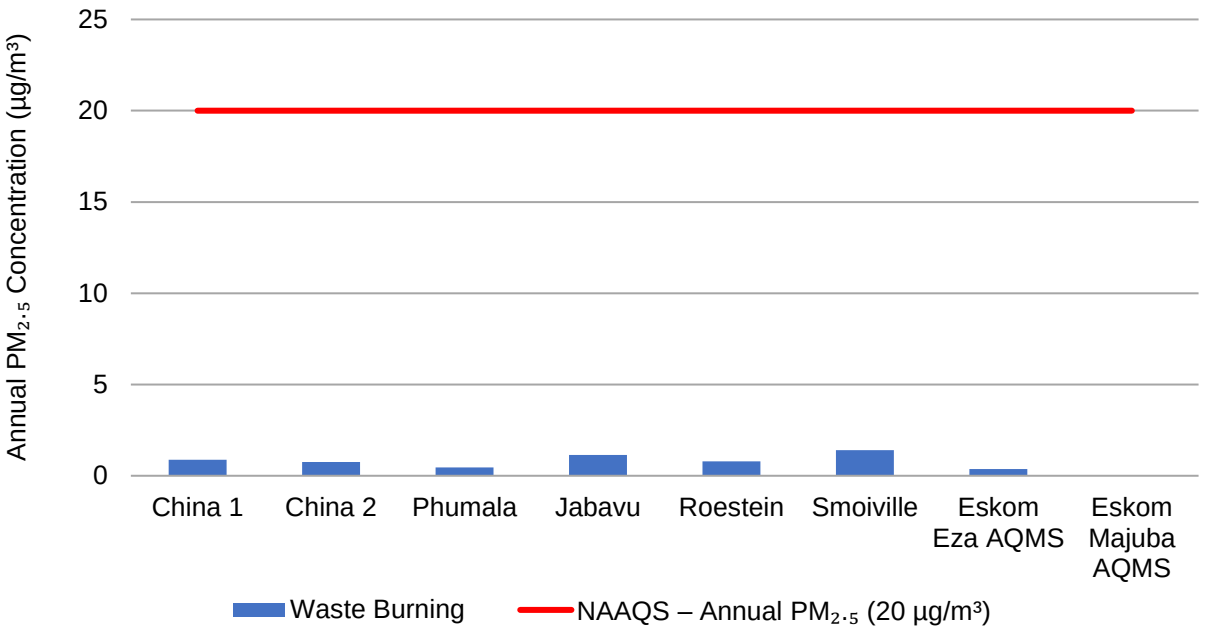

Figure 5-131: Model predicted annual $PM_{2.5}$ ambient concentrations in µg/m³ at discrete receptors for the Waste Burning emission source category

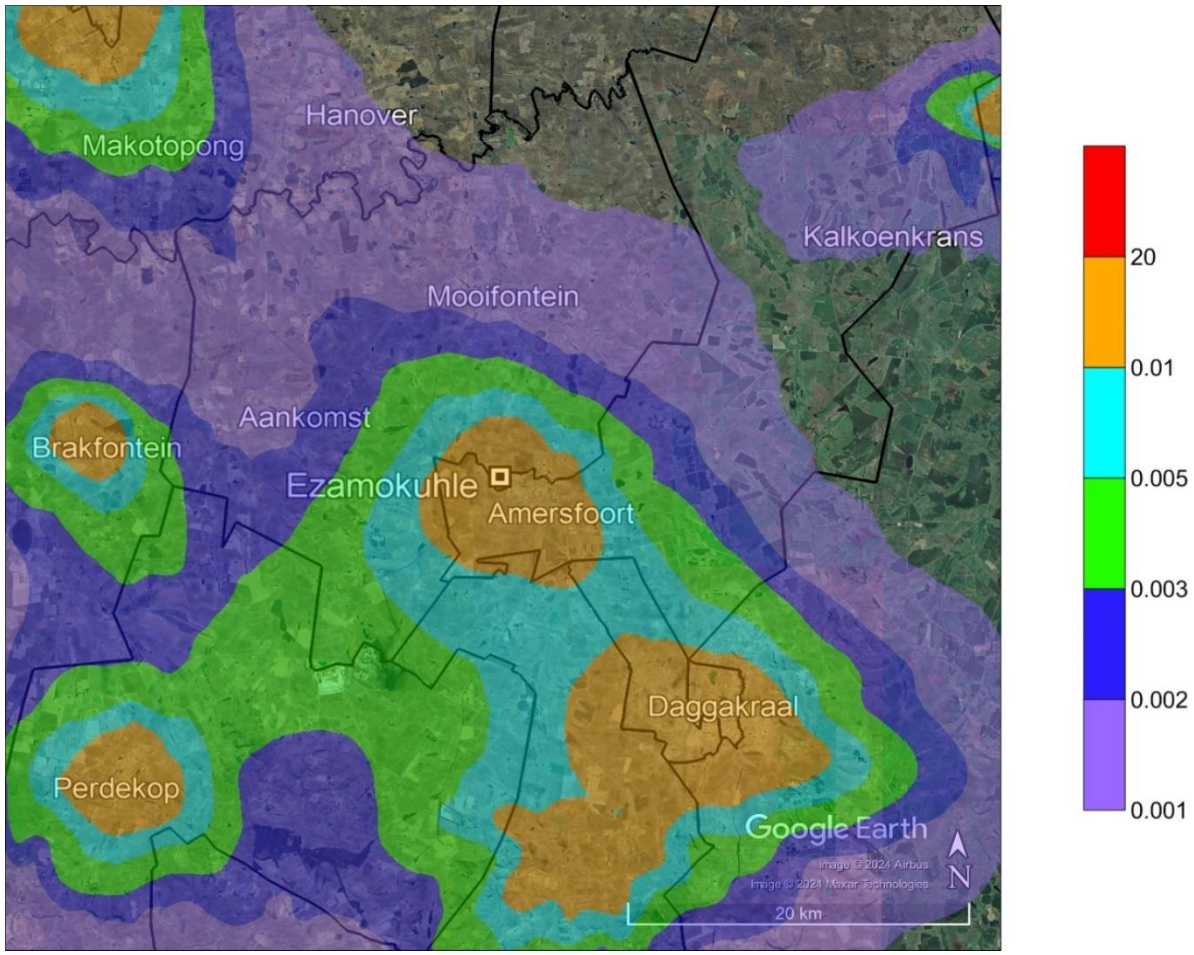

Figure 5-132: Model predicted annual $PM_{2.5}$ ambient concentrations in µg/m³ for the Waste Burning emission source category within the Greater Ezamokuhle Airshed

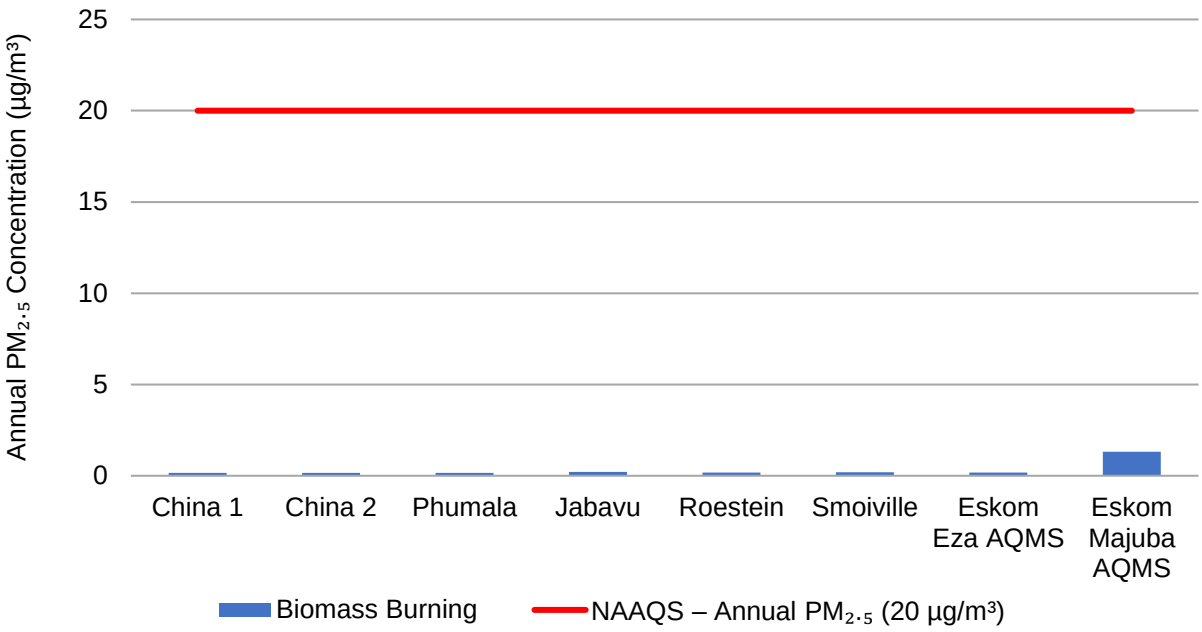

Figure 5-133: Model predicted annual $PM_{2.5}$ ambient concentrations in µg/m³ at discrete receptors for the Biomass Burning emission source category

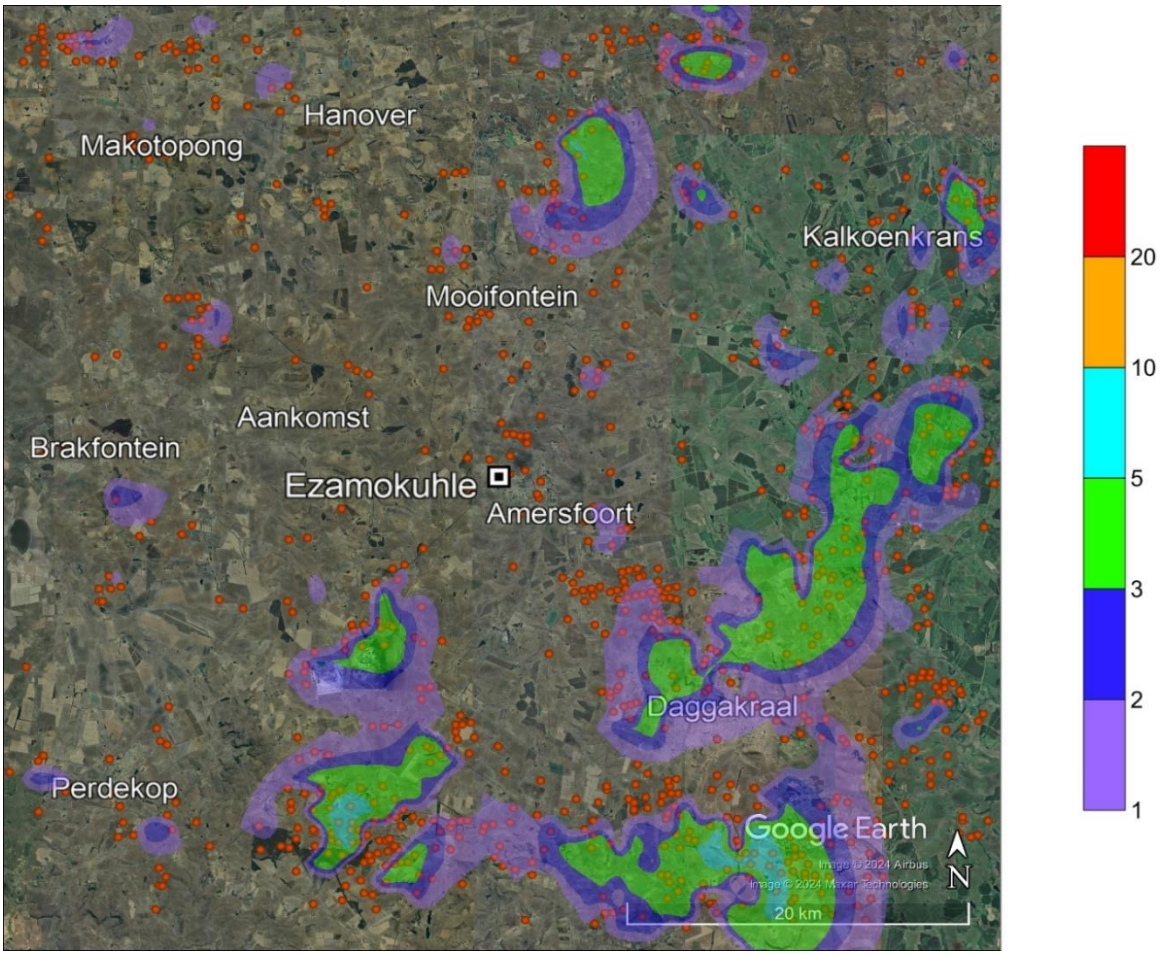

Figure 5-134: Model predicted annual $PM_{2.5}$ ambient concentrations in µg/m³ for the Biomass Burning emission source category within the Greater Ezamokuhle Airshed

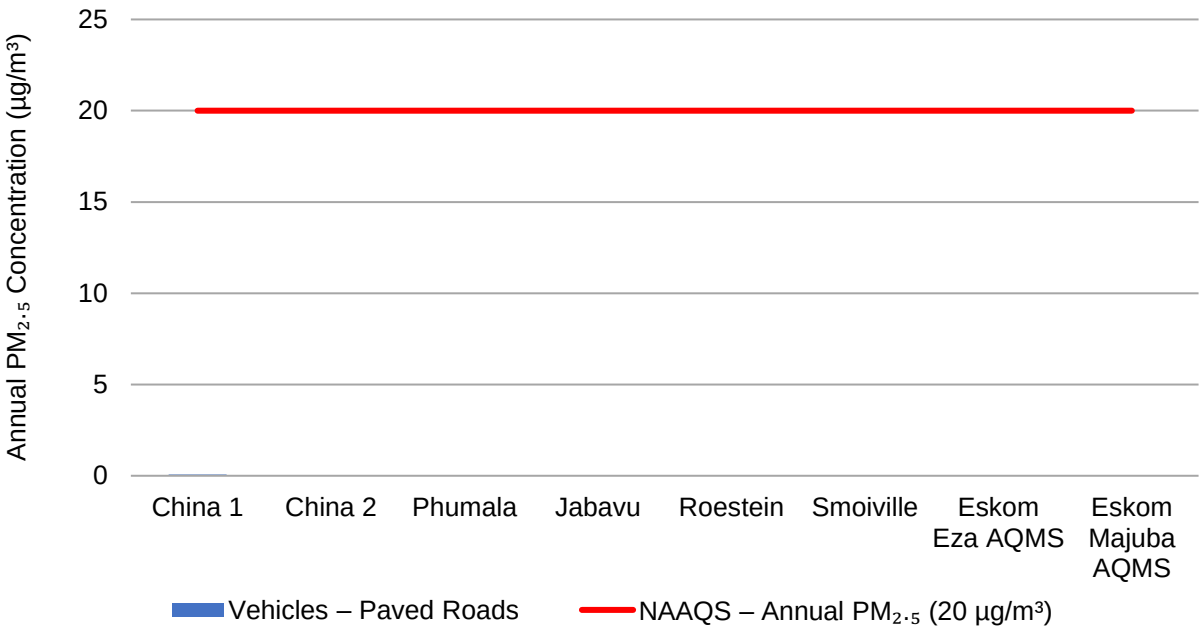

Figure 5-135: Model predicted annual $PM_{2.5}$ ambient concentrations in µg/m³ at discrete receptors for the Vehicles – Paved Roads emission source category

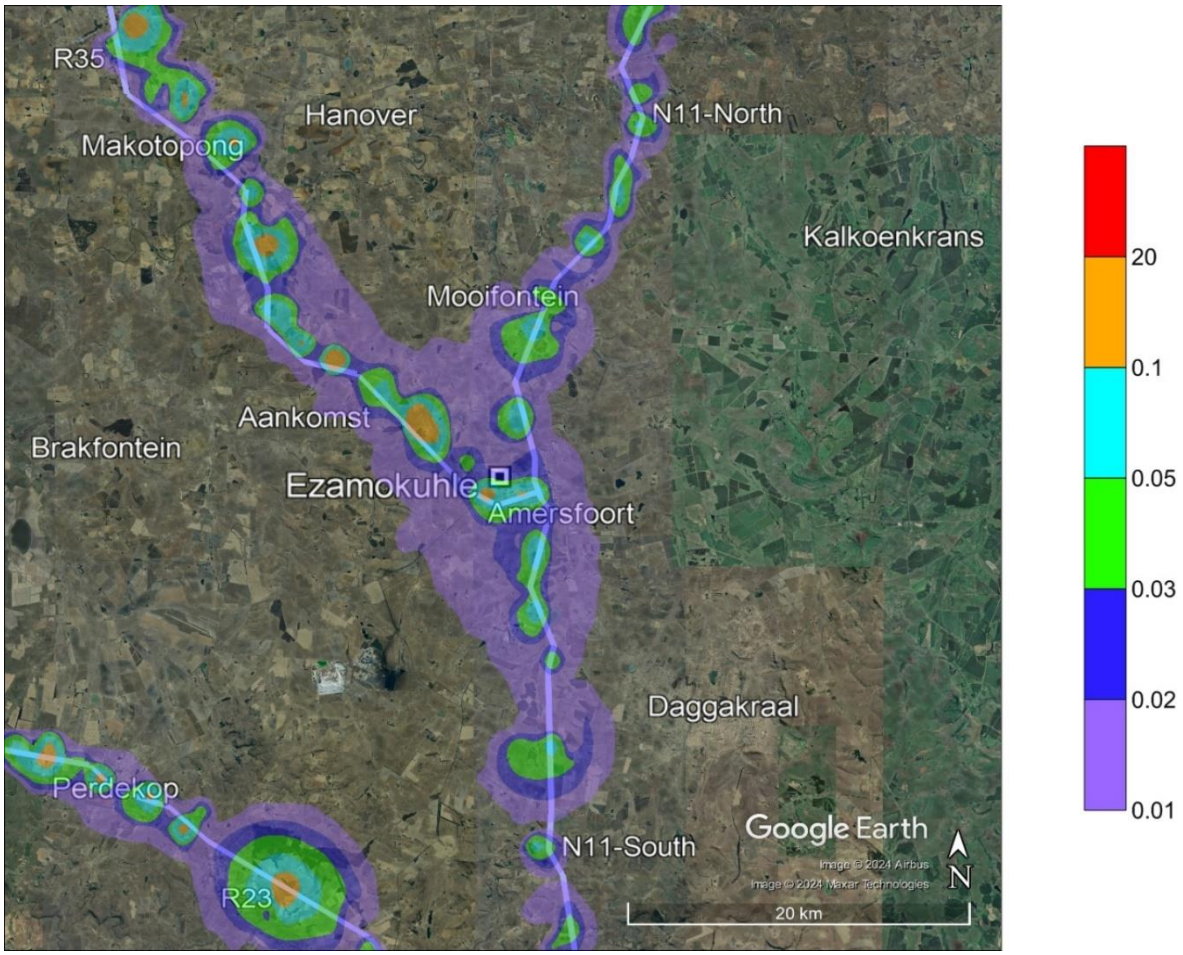

Figure 5-136: Model predicted annual $PM_{2.5}$ ambient concentrations in µg/m³ for the Vehicles – Paved Roads emission source category within the Greater Ezamokuhle Airshed

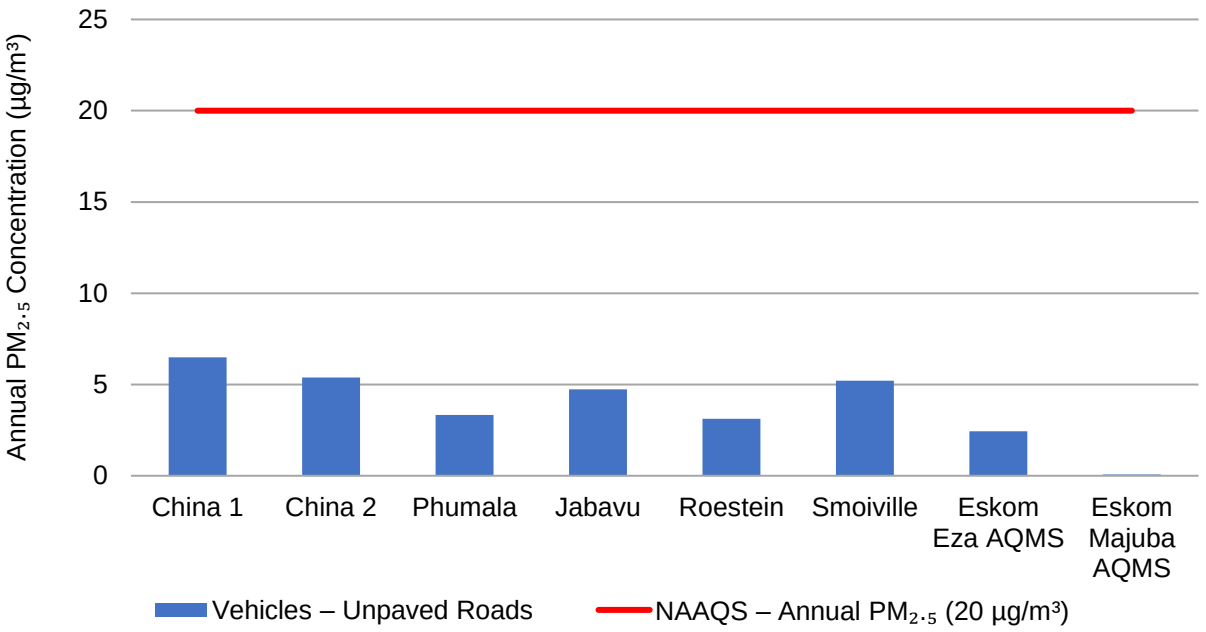

Figure 5-137: Model predicted annual $PM_{2.5}$ ambient concentrations in µg/m³ at discrete receptors for the Vehicles – Unpaved Roads emission source category

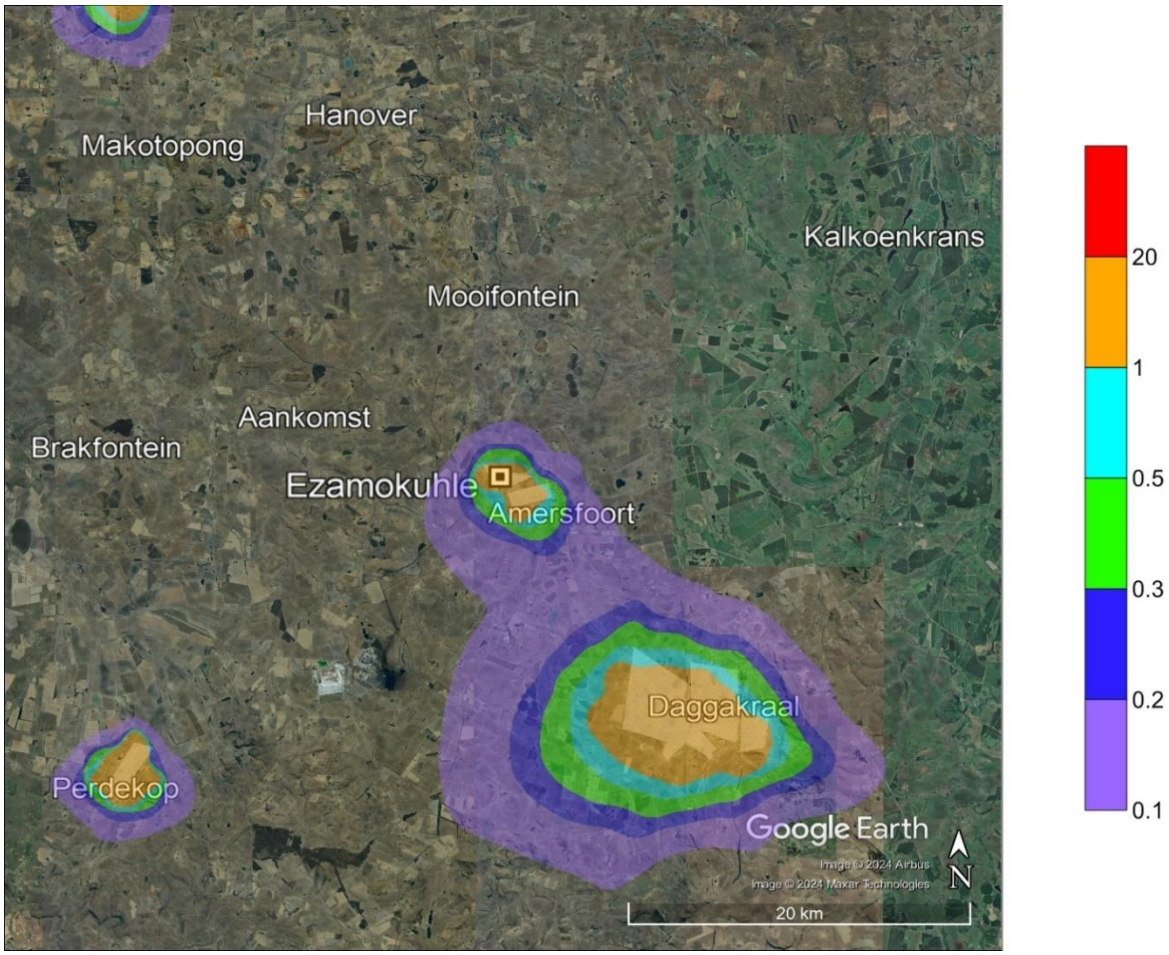

Figure 5-138: Model predicted annual $PM_{2.5}$ ambient concentrations in µg/m³ for the Vehicles – Unpaved Roads emission source category within the Greater Ezamokuhle Airshed

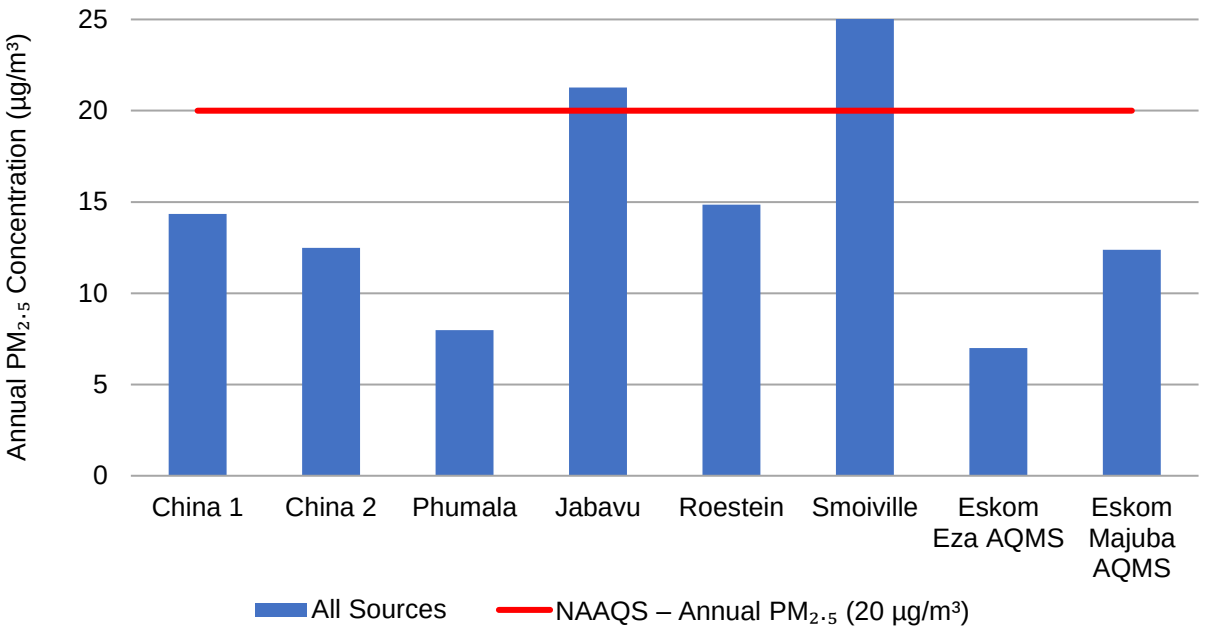

Figure 5-139: Model predicted annual $PM_{2.5}$ ambient concentrations in µg/m³ at discrete receptors for the All Sources emission source category

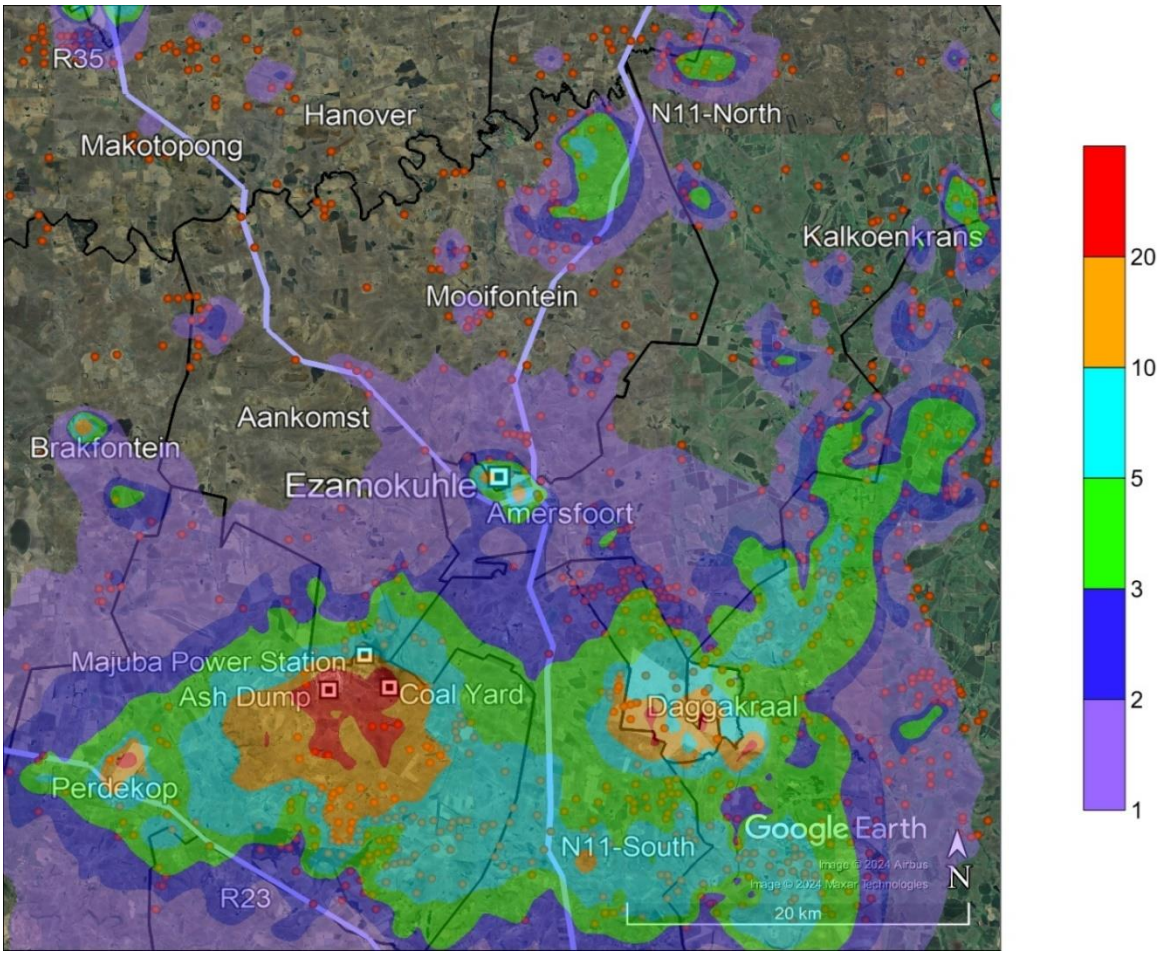

Figure 5-140: Model predicted annual $PM_{2.5}$ ambient concentrations in µg/m³ for the All Sources emission source category within the Greater Ezamokuhle Airshed

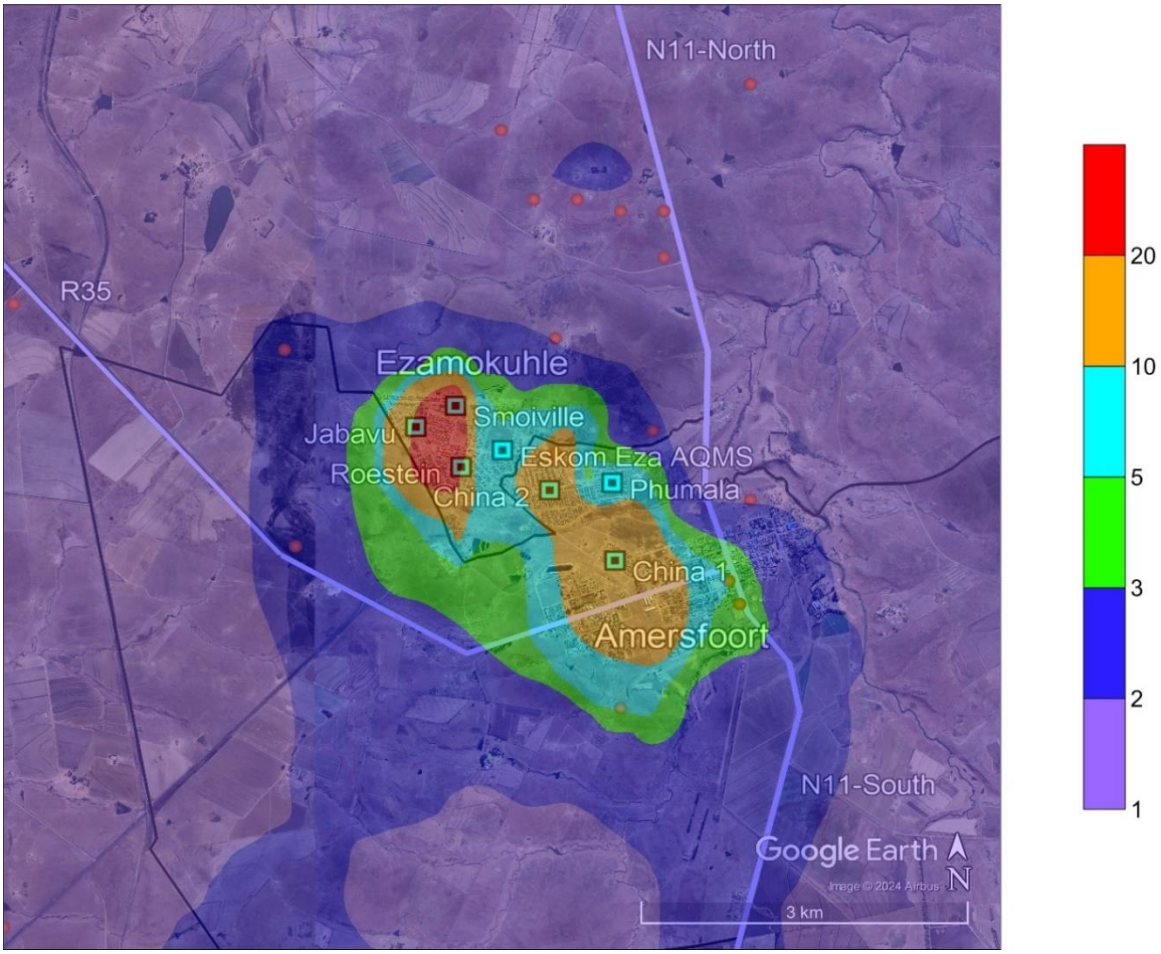

Figure 5-141: Model predicted annual $PM_{2.5}$ ambient concentrations in µg/m³ for the All Sources emission source category within Ezamokuhle airshed

5.4.3 $PM_{2.5}$ SOURCE CONTRIBUTION ANALYSIS

In this study, the $PM_{2.5}$ source contribution analysis is based on model predicted annual $PM_{2.5}$ ambient concentrations at the discrete receptors for the six emission source categories which include power generation, residential fuel burning, waste burning, biomass burning, vehicles – paved roads and vehicles – unpaved roads (Table 5-12). Table 5-12 is used to calculate the percent contribution of $PM_{2.5}$ at each discrete receptor as a function of the six source categories, and is presented in Table 5-13.

Table 5-13: $PM_{2.5}$ source contribution (%) at discrete receptors for the six emission source categories based on model predicted annual $PM_{2.5}$ ambient concentrations

Discrete Receptors	Power Generation	Residential Fuel Burning	Waste Burning	Biomass Burning	Vehicles – Paved Roads	Vehicles – Unpaved Roads	All Sources
China 1	7.21	39.84	6.15	1.11	0.47	45.22	100.00
China 2	8.36	41.05	5.97	1.29	0.26	43.05	100.00
Phumala	12.28	37.95	5.72	1.94	0.28	41.84	100.00
Jabavu	5.28	66.04	5.33	1.03	0.09	22.24	100.00
Roestein	7.36	65.01	5.35	1.15	0.13	20.99	100.00
Smoiville	4.22	68.79	5.56	0.75	0.07	20.60	100.00
Eskom Eza AQMS	15.04	42.26	5.15	2.40	0.29	34.87	100.00
Eskom Majuba AQMS	88.25	0.41	0.03	10.63	0.06	0.62	100.00

$PM_{2.5}$ ambient concentrations (in terms of µg/m^3) for each emission source category at each discrete receptor is presented in the form of a stacked bar graph in Figure 5-142. The total $PM_{2.5}$ ambient concentrations at each discrete receptor (which is made up of individual contributions representing each of the six emission source categories) represents the All Sources emission source category. The $PM_{2.5}$ source contribution in terms of percentages is presented in the form of a stacked bar graph in Figure 5-143. The sum of individual contributions resulting from each emission source category makes up 100%.

The source contribution analysis indicates that residential fuel burning and vehicles travelling on unpaved road surfaces are the main contributors to ambient $PM_{2.5}$ levels in the region. It also indicates that power generation is a relatively large contributor to the ambient $PM_{2.5}$ levels. Ambient contributions from waste burning, biomass burning and vehicles travelling on paved roads are much smaller in comparison.

Power generation sources account for approximately 88% of the total $PM_{2.5}$ ambient concentrations at the Eskom Majuba AQMS but are much lower at the Eskom Ezamokuhle AQMS and ward centroid discrete receptors (4-15%). This is expected as the Eskom Majuba Power Station ash dump and coal stockpile are located close to the Eskom Majuba AQMS in comparison with the Eskom Ezamokuhle AQMS and ward centroid discrete receptors.

Residential fuel burning sources account for approximately 0.4% of the total $PM_{2.5}$ ambient concentrations at the Eskom Majuba AQMS but are much higher at the Eskom Ezamokuhle AQMS and ward centroid discrete receptors (37-69%). This is expected as residential areas are located further away from the Eskom Majuba AQMS in comparison with the Eskom Ezamokuhle AQMS and ward centroid discrete receptors.

Vehicle emission sources from unpaved roads account for approximately 0.6% of the total $PM_{2.5}$ ambient concentrations at the Eskom Majuba AQMS but are much higher at the Eskom Ezamokuhle AQMS and ward centroid discrete receptors (20-45%). This is expected as residential areas and the

dense network of unpaved roads is located further away from the Eskom Majuba AQMS in comparison with the Eskom Ezamokuhle AQMS and ward centroid discrete receptors.

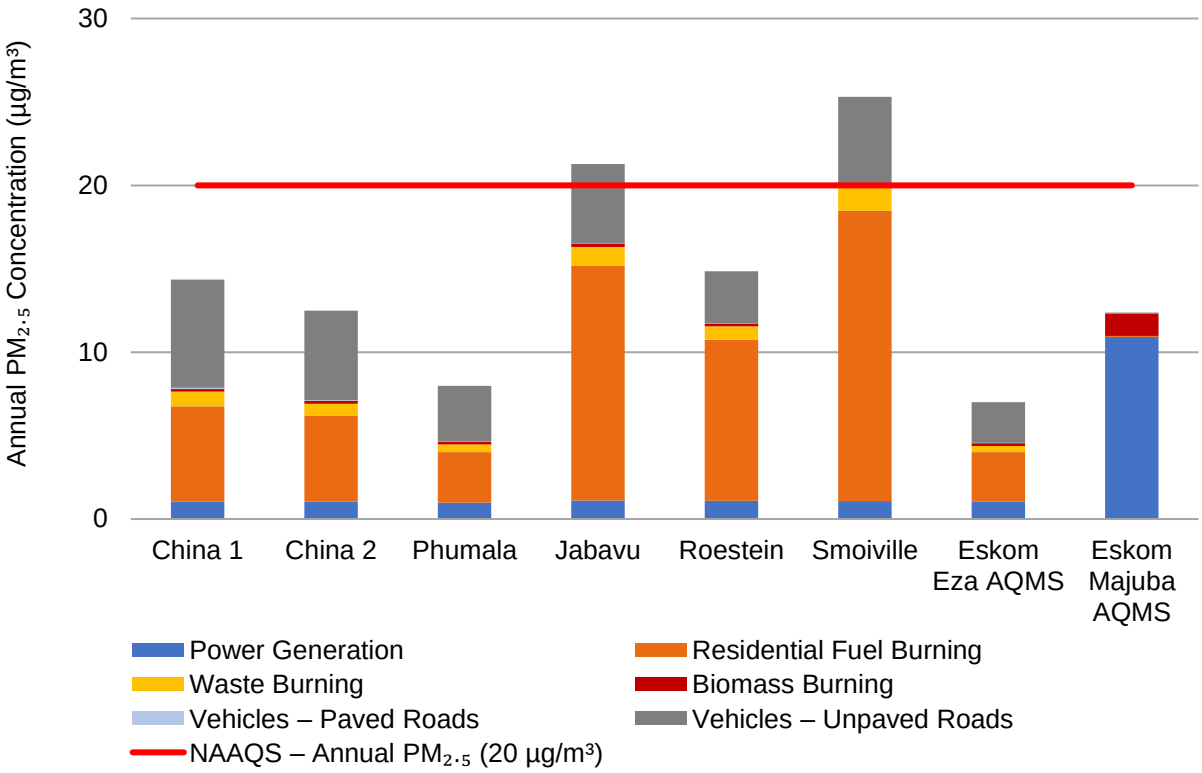

Figure 5-142: Stacked bar graph representing model predicted annual $PM_{2.5}$ ambient concentrations in µg/m³ at discrete receptors for the six emission source categories

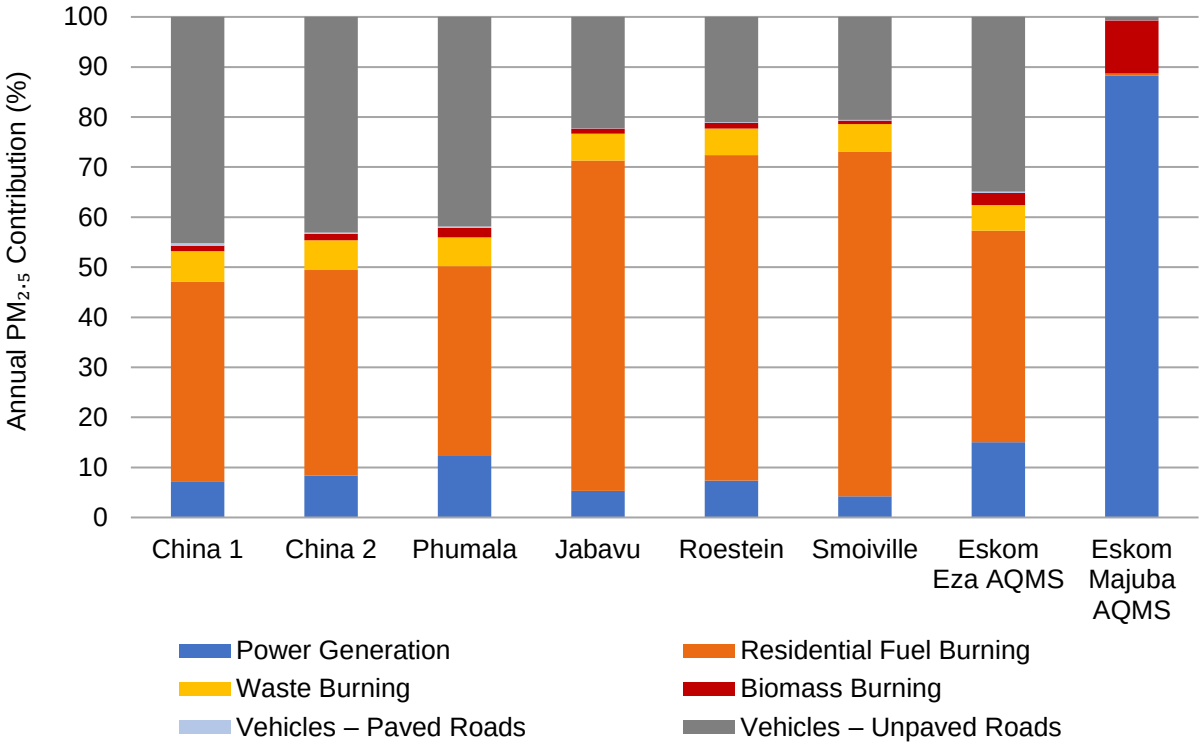

Figure 5-143: Stacked bar graph representing the percent contribution of $PM_{2.5}$ ambient concentrations at discrete receptors as a function of source category

5.5 PREDICTED DUSTFALL RATES

5.5.1 24-HOUR DUSTFALL RATES

Model predicted 24-hour dustfall rates at discrete receptors and at the point of maximum for the Vehicles – Unpaved Roads emission source category is presented in Table 5-14 (as indicated at the beginning of this section, TPM was only considered for this emission source category). If applicable, exceedances of the National Dustfall Standard is highlighted in red.

Bar graphs for model predicted 24-hour dustfall rates at discrete receptors is presented in Figure 5-144 for the Vehicles – Unpaved Roads emission source category.

Contour plots for model predicted 24-hour dustfall rates for the Vehicles – Unpaved Roads emission source category is presented in Figure 5-145 for the Greater Ezamokuhle Airshed and in Figure 5-146 for the Ezamokuhle airshed. With respect to contour plots for the Greater Ezamokuhle and Ezamokuhle airshed, areas of exceedance of the Dustfall Standard is coloured in red.

Table 5-14: Model predicted 24-hour dustfall rates in mg/m^2/day at discrete receptors and at the point of maximum for the Vehicles – Unpaved Roads emission source category

Discrete Receptors	Vehicles – Unpaved Roads
China 1	699.32
China 2	643.47
Phumala	389.48
Jabavu	529.16
Roestein	423.05
Smoiville	572.44
Eskom Eza AQMS	342.71
Eskom Majuba AQMS	35.24
Maximum	1496.50
	National Dustfall Standard for residential area (600 mg/m²/day)
	National Dustfall Standard for non-residential area (1 200 mg/m²/day)

According to Table 5-14, model predicted 24-hour dustfall rates exceed the National Dustfall Standard for residential areas of 600 mg/m^2/day at China 1 and China 2. The National Dustfall Standard for non-residential areas of 1 200 mg/m^2/day is exceeded at the point of maximum. Dustfall rates are lowest at the Eskom Majuba AQMS and substantially higher at the Eskom Ezamokuhle AQMS and ward centroid discrete receptors. This is expected as the unpaved road networks within townships are located further away from the Eskom Majuba AQMS in comparison with the Eskom Ezamokuhle AQMS and ward centroid discrete receptors.

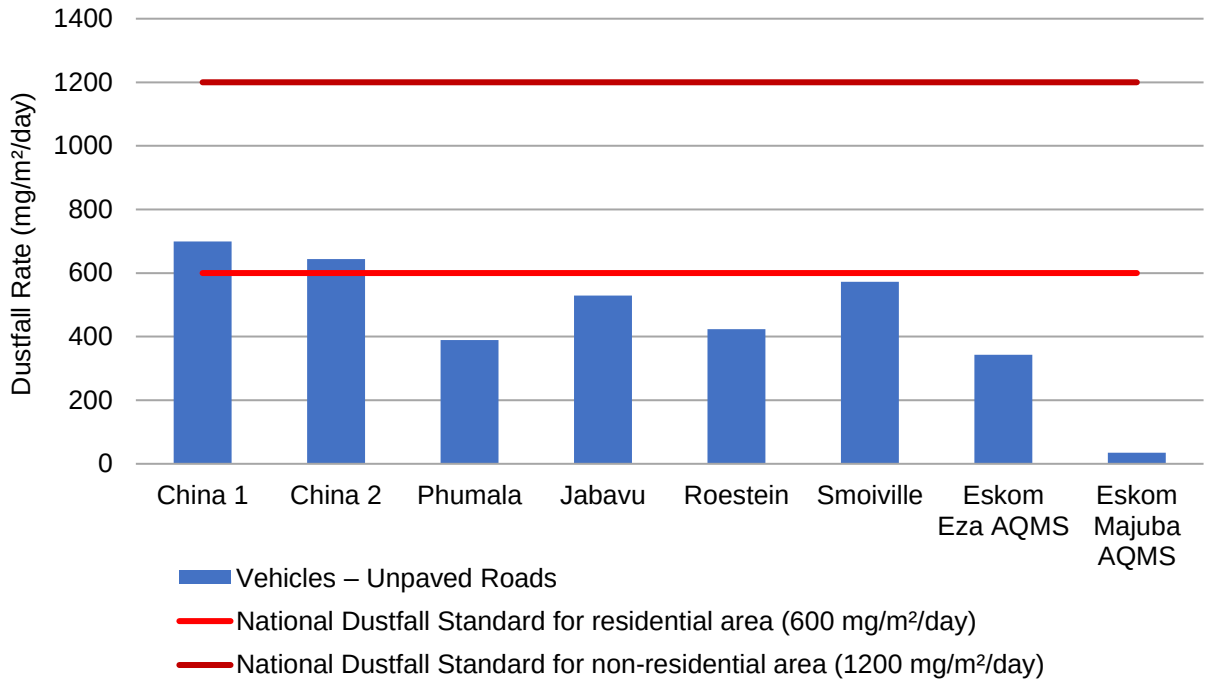

Figure 5-144: Model predicted 24-hour dustfall rates in mg/m²/day at discrete receptors for the Vehicles – Unpaved Roads emission source category

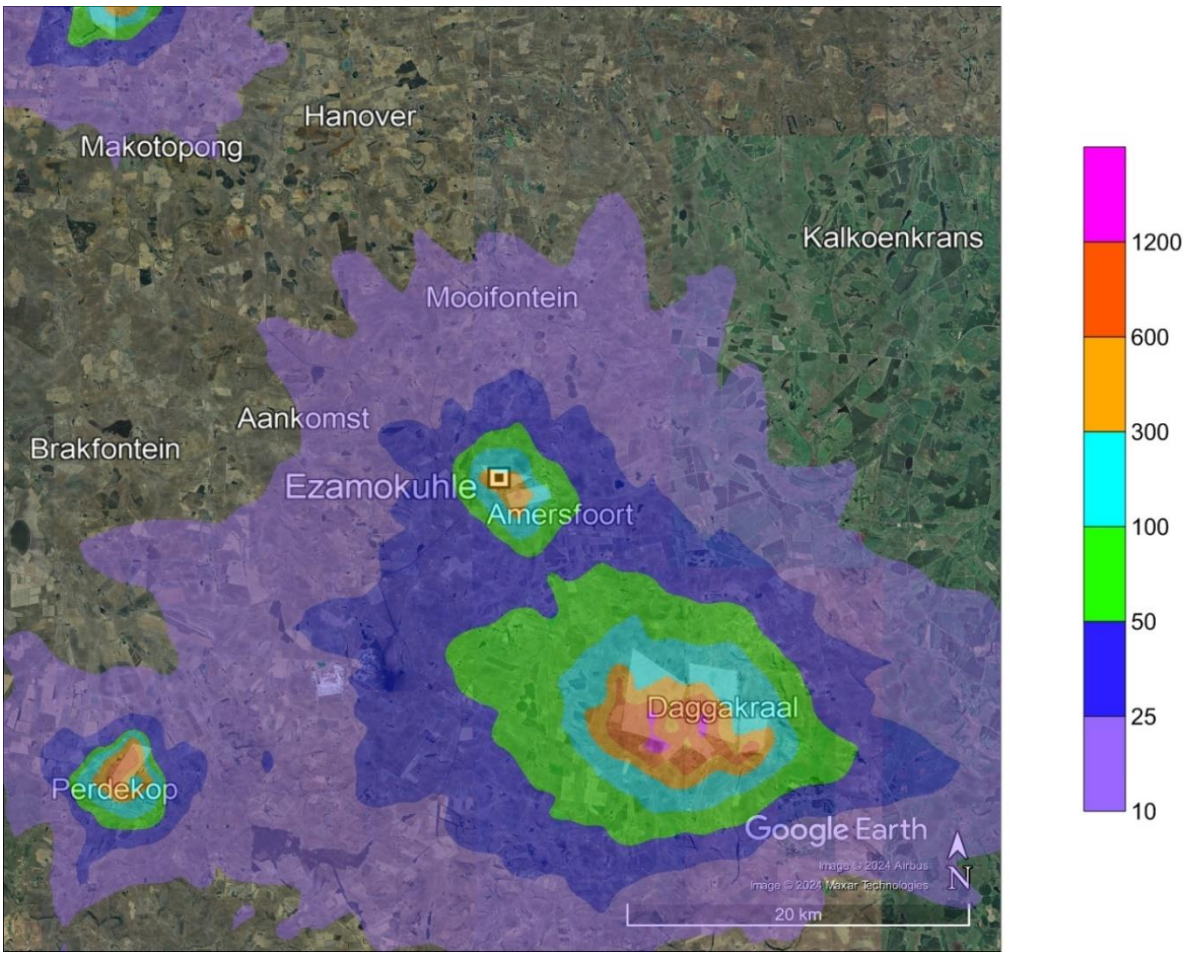

Figure 5-145: Model predicted 24-hour dustfall rates in mg/m²/day for the Vehicles – Unpaved Roads emission source category within the Greater Ezamokuhle Airshed

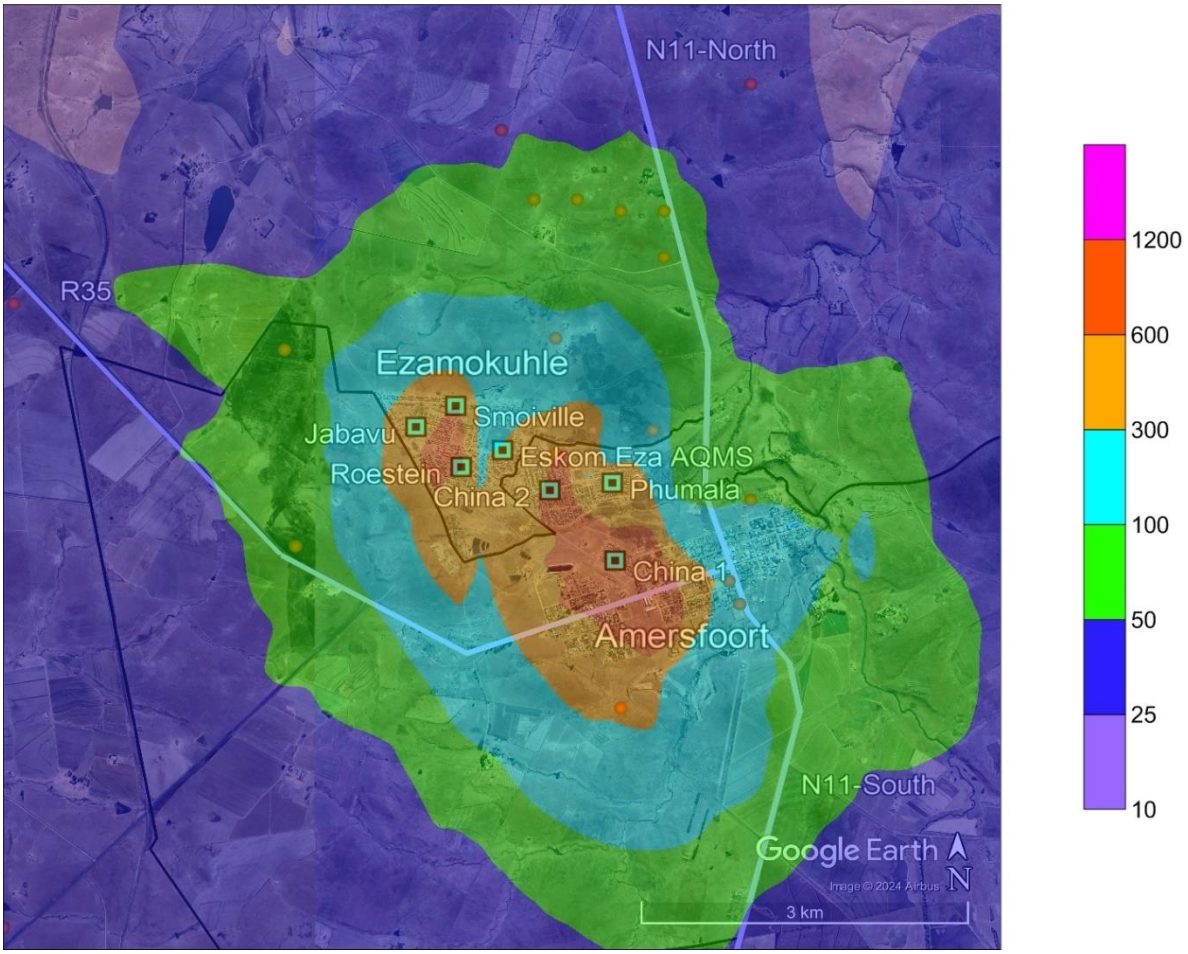

Figure 5-146: Model predicted 24-hour dustfall rates in mg/m^2/day for the Vehicles – Unpaved Roads emission source category within Ezamokuhle airshed

5.6 COMPARISON OF THE EZAMOKUHLE STUDY WITH THE SECOND-GENERATION AQMPS FOR THE VAAL TRIANGLE AIRSHED PRIORITY AREA (VTAPA STUDY) AND THE HIGHVELD PRIORITY AREA (HPA STUDY)

The emission source categories common to the Eskom Ezamokuhle Study and both of the Second Generation Air Quality Management Plans (AQMPs) for the Vaal Triangle Airshed Priority Area (VTAPA Study) (DEA, 2020) and the Highveld Priority Area (HPA Study) (DEA, 2022) are industrial sources, residential fuel burning, waste burning, biomass burning and vehicle emissions. The only industrial source considered for the Eskom Ezamokuhle Study was the Eskom Power Station while the VTAPA and HPA Studies considered a large database of the main industrial sources. The emission estimation methodology used for residential fuel burning, waste burning, vehicle exhaust emissions and biomass burning are very similar across all three studies. Particulate emissions for unpaved road sources in the VTAPA and HPA Studies were limited to haul roads, while emissions for the Eskom Ezamokuhle Study were calculated for unpaved roads in all residential areas, where applicable.

In the VTAPA and HPA Studies, the Weather research and forecasting (WRF) model (Advanced Research WRF (ARW) was used to generate meteorological data for input into the CAMx model, which is a photochemical model. In the Eskom Ezamokuhle Study, TAPM was used to generate meteorological data for input into the CALPUFF model, which does not take photochemistry into account.

In terms of predicted ambient concentrations for the VTAPA and HPA Studies, several areas were impacted by high levels of SO_2, NO_2, PM_{10} and $PM_{2.5}$ and exceedances of these pollutants. In the Eskom Ezamokuhle Study, high levels of PM_{10} and $PM_{2.5}$ were predicted mainly around residential areas, with a number of exceedances for both PM_{10} and $PM_{2.5}$ for some of the emission scenarios. SO_2 and NO_2 were below the NAAQS throughout the study area.

An important difference between the studies is that a source contribution analysis for discrete receptors was only undertaken for the Eskom Ezamokuhle Study. This analysis has provided in-depth insight in terms of ranking of sources that have a significant contribution to ambient concentrations in the study area.

5.7 Comparison of the Ezamokuhle Modelling Study with the Ezamokuhle Source Apportionment Study

In accordance with the scope of work, for Activity 10.8 Source apportionment (baseline) for Ezamokuhle, ARM undertook a scientifically credible source apportionment to identify the potential sources of the particulate matter during the 2023 winter baseline for Ezamokuhle (ARM, 2024). This study identified outdoor dust as the largest contributing source. This was primarily from exposed surfaces like unpaved roads. Mechanical disturbance of these unpaved road surfaces by vehicular and pedestrian traffic results in agitation and entrainment of the dust particles. (ARM, 2024). This is aligned with findings of this study which also identified dust particles from unpaved road surfaces as the largest contributing source in Ezamokuhle. Furthermore, the source apportionment study identified the: burning of municipal solid waste; coal-based thermal power plant emissions and residential fuel burning as significant contributors to ambient PM concentration measured at Ezamokuhle.

Furthermore, the source apportionment study identified the: burning of municipal solid waste; coal-based thermal power plant emissions and residential fuel burning as significant contributors to ambient PM concentration measured at Ezamokuhle. The results of this study corroborate with this earlier research, which highlights solid waste burning, coal-based thermal power plant emissions, and residential fuel burning as major sources of ambient PM concentrations in the Ezamokuhle airshed. The consistency of these directional results across multiple studies suggests a reliable framework for understanding the emissions contribution for the Ezamokuhle airshed.

6. MODEL VALIDATION

The importance of model validation is crucial for ensuring the accuracy and reliability of models. A model validation exercise can help to identify any potential errors or limitations that may impact their accuracy, reliability and performance. Although atmospheric dispersion models are indispensable in air quality assessment studies, their limitations should always be taken into account. In this study, the model predicted concentrations for the All-Sources emission source category (cumulative baseline emissions from all specified sources within the modelling domain) were compared with measured ambient data recorded at the Eskom Majuba AQMS. The time-series data for both datasets were statistically analysed using the index of agreement (IOA).

INDEX OF AGREEMENT (IOA)

The parameter IOA is a measure of correlation between the predicted and observed time series of concentrations. IOA = 1[(P-O)2/(P-O) + (O-O)2] where the Predicted (P) values by the model are compared against Observed (O) data (Reza et al., 2005). The IOA varies from 0.0 (theoretical minimum) to 1.0 (perfect agreement between the observed and predicted values). An IOA with a value greater than about 0.5 is considered to be good (Hurley, 2000). The IOA for the Eskom Majuba AQMS is presented in Table 6-1 and Figure 6-1.

Table 6-1: Comparative IOA statistics between monitored data and model predictions

Pollutant	Eskom Majuba AQMS
1-hour SO_2	0.29
1-hour NO_2	0.29
24-hour PM_{10}	0.58
24-hour $PM_{2.5}$	0.5

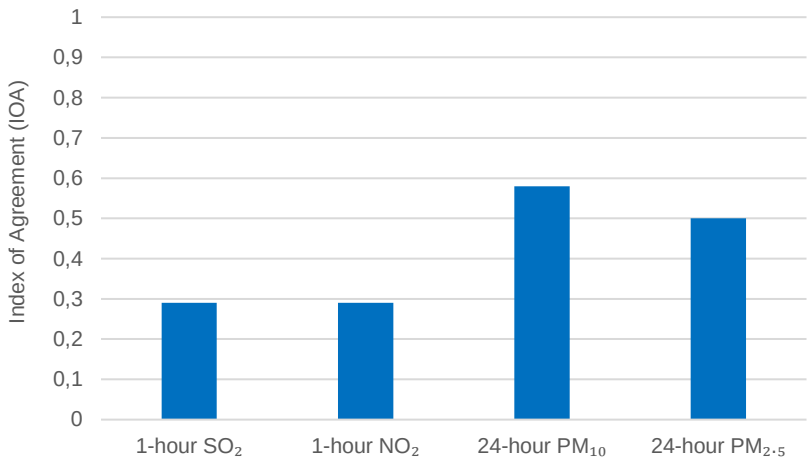

Figure 6-1: Comparative IOA statistics between monitored data and model predictions

The IOA value of 0.58 for the predicted and measured time series of 24-hour PM_{10} and of 0.5 for the predicted 24-hour $PM_{2.5}$ shows a very good correlation of PM. The model under-predicted both SO_2 and NO_2. The extent to which a user has reliable information on emissions data, meteorological data and the correct model physics set-up will influence the accuracy of the model predicted concentrations. Section 7 outlines the underlying limitations of this study which results in the under-predicting of the simulated results.

7. LIMITATIONS, POTENTIAL BIASES, UNCERTAINTIES & DATA GAPS

7.1 LIMITATIONS OF STUDY

For this baseline modelling assessment study, the following limitations must be noted:

i. Atmospheric Emission License (AEL) data serve as the principle information source for activity data in order to estimate emissions from industrial sources. Although ARM submitted a request to the Department of Environment, Forestry and Fisheries (DEFF) requesting the AEL data for industrial sources within the modelling domain, DEFF was unable to provide the data. DEFF responded stating that they will not be able to disclose the data due to data policy privacy issues. Thus the cumulative impact of other industrial sources are not included in the model simulation which will result in an under-prediction of pollutant ambient concentrations for this emission source category.

ii. The South African National Atmospheric Emission Inventory System (NAEIS) contains emissions information for mines, controlled emitters and facilities identified in accordance with the local by-laws. DEFF was not able to provide ARM with the NAEIS emissions data due to data policy privacy issues. Thus cumulative impact of mines, controlled emitters and facilities identified in accordance with the local by-laws have therefore been excluded from this study, which results in an under-prediction of the simulated pollutants.

iii. The data required to model “local unpaved roads” dust emissions are currently not available for Ezamokuhle and other parts of the modelling domain. The information required to model these local roads include the location of unpaved roads, silt content of each road, number of vehicles, vehicle types, empty and full weight of cars, buses, heavy-duty vehicles and taxis using these roads. In order to develop an emission inventory for this emissions source category (Vehicles – Unpaved Roads), a number of assumptions had to be made based on best judgement. These are discussed under assumptions in Section 4. Thus the model predicted results may be under-predicted.

iv. Residential fuel burning for the modelling was estimated based on energy use data at the sub-place level for Ezamokuhle using Stats SA Census data. There is currently no finer resolution residential fuel burning data for Ezamokuhle. The model simulated results are therefore constrained by the granularity of this data. Thus the model predicted results may be under-predicted.

7.2 LIMITATIONS AND POTENTIAL BIASES OF THE CALPUFF MODEL

Although the CALPUFF dispersion modelling system is very sophisticated and supports a wide range of modelling scenarios, it does have some limitations. One limitation of the system is that there is a finite number of sources that can be specified in the model input parameters. For example, CALPUFF

can only accommodate a finite number of sources for each source type in a single model run. Each executable (e.g., CALMET, CALPUFF, CALPOST) has a corresponding parameterization file which defines these limits. If a project has one of these parameters which exceeds the model limit, the model executables need be recompiled in FORTRAN to accept higher limits; or multiple model runs can be built, and then CALSUM can be used to combine model runs together. Another limitation of the CALPUFF air dispersion model is that it can only be executed on a single processor (i.e., serially). Again, CALPUFF can be run with a single source to run faster, and then CALSUM can be used to combine single runs to assess the cumulative impacts.

The CALPUFF model is an objective dispersion modelling tool that uses mathematical formulations to characterize the atmospheric processes that disperse a pollutant emitted by a source and thereby predict ambient concentrations, based on emissions and meteorological inputs. The model does not favour and is not biased by any source or source type, and relies on the input parameters provided.

7.3 UNCERTAINTIES IN THE CALPUFF MODEL

Dispersion models are used to predict ambient concentrations based on certain measured parameters, such as wind speed, wind direction, temperature, relative humidity, pressure, solar radiation; and emission rates. Variations in model parameters that are not measured and which are inherent in the model (including complex atmospheric processes that are, by their nature, highly variable), can have an influence on the predicted concentrations. Uncertainties can also result from inadequate model physics and model formulations which are used to predict the ambient concentrations, as well as inaccuracies in model algorithms and input values. These include meteorological data and emission data which is unrepresentative, poor source characterisation in the model and errors in the concentrations measured at AQMS that are used for comparison with model predictions.

The primary areas of uncertainty relevant to this modelling study include uncertainties in the TAPM modelled meteorological data fields (i.e. how accurately the actual wind fields and other meteorological parameters are represented in the modelling), source emissions data and ambient air quality monitoring data. These data elements represent the most important sources of uncertainty in the model inputs. There may be some differences between the TAPM predicted wind speeds and temperature fields and values recorded at available observational stations, and in the modelling domain. These differences would be expected to increase the levels of uncertainty in the modelling results. In terms of the uncertainty in measured ambient concentrations, it is assumed that Eskom has minimized the associated uncertainty by conducting regular assessments and calibration of the ambient monitoring stations used in the analysis. The uncertainty of model predicted concentrations will scale directly with uncertainty in the emission estimates. Emission rates for the power generation emission source category in this study are based on actual emissions provided by Eskom, and are

considered to be accurate. Emission rates in this study for all other emission source categories are based on robust methodologies and are also considered to be accurate.

Uncertainties can be minimised by using accurate input data, preparing the input files correctly, double checking for errors, correcting for odd model behaviour, ensuring that the errors in the measured data are minimised and applying appropriate model physics. The accuracy of model predictions in this assessment was done by ensuring that all uncertainties in the input data and model parameterisation were kept to a minimum.

7.4 DATA GAPS

The exclusion of a source category can have a significant or insignificant impact on the results of a study depending on the magnitude and importance of the source category.

When compared with the VTAPA and HPA Study, the emission source categories common across all three studies include:

- Industrial Sources
- Residential Fuel Burning
- Waste Burning
- Biomass Burning
- Vehicle Emissions

When compared with the VTAPA Study and HPA Study, emissions source categories not included in the Ezamokuhle Study are:

- Mining Sources
- Wind Blown Dust from Exposed Topsoil Areas
- Biogenic VOC's
- Agricultural Ammonia
- Spontaneous Combustion

As mentioned in Section 7.1, although ARM submitted a request to the DEFF requesting the AEL data for industrial sources and NAEIS data containing emissions information for mines, controlled emitters and facilities identified in accordance with the local by-laws within the modelling domain, DEFF was unable to provide the data due to data policy privacy issues. Thus, cumulative impact of other industrial sources, mines, controlled emitters and facilities have therefore been excluded from this study, which results in an under-prediction of pollutant ambient concentrations.

Regardless of this, the emission source categories for the Ezamokuhle Study are considered to be adequate, as all important sources have been included in the study. For industrial emissions, there

are very few industrial sources in the modelling domain. The Eskom Majuba Power Station Stacks and fugitive emissions, which are included in the modelling, are one of the main industrial sources in the modelling domain.

Although mining sources and wind-blown dust from exposed topsoil areas are not included in this study, it must be remembered that the effect of these emissions in the ambient environment is localised and limited to the immediate surroundings of the areas where they are located. Emissions from spontaneous combustion (burning and smouldering of coal dumps) are relatively small in comparison to the total emissions calculated for both the VTAPA and HPA studies; and impacts in the ambient environment is also considered to be localised. The inclusion of these source categories in the model will not have a significant impact on the results.

Biogenic VOC’s and agricultural ammonia are not relevant to the Ezamokuhle Study.

8. CONCLUSION AND RECOMMENDATIONS

In this study, the CALPUFF suite of models was used to predict the dispersion of the following pollutants: SO_2, SO_4, NO_X, HNO_3, NO_3, PM_{10}, $PM_{2.5}$ and TPM (to calculate particulate/dust deposition rates) using the MESOPUFF II Scheme chemical transformation method. This baseline modelling study has taken a conservative approach (Scire, 2014) whereby the total concentrations of particulate matter (PM_{10} or $PM_{2.5}$) was computed as the sum of primary particulate matter concentrations (PM_{10} or $PM_{2.5}$) plus the contribution of concentrations from secondary particulate matter, including ammonium nitrate and ammonium sulphate. Results of the modelling were evaluated against the applicable NAAQS and dustfall rates.

The model simulated results indicate that there are only exceedances of the NAAQS for particulate matter (PM_{10} or $PM_{2.5}$) in the Ezamokuhle airshed. An analysis of the modelled source contribution analysis indicates that the emission sources that have the most significant particulate matter air quality impact in Ezamokuhle include inter alia unpaved roads, residential fuel burning, coal fired power stations and waste burnings. These outcomes align closely with the past source apportionment studies, reinforcing the validity of the modelled patterns. These preliminary results, directionally indicate there may be opportunities to possibly consider alternate emission source categories for Ezamokuhle. However, it is noted that the viability and feasibility of these possible alternatives may need to be investigated & unpacked further. As a first step, it is recommended that ARM together with ESKOM resubmit a request to the DFFE requesting the AEL data for industrial sources and NAEIS data containing emissions information for mines, controlled emitters and facilities identified in accordance with the local by-laws within the modelling domain. This will enhance the completeness of the emission inventory and is expected to improve future modelling results.

9. ACKNOWLEDGEMENTS

Air Resource Management would like to thank the following individuals for their assistance in this study:

- Mr. Gavaza Mhlarhi for providing the Eskom Lethabo Power Station emission inventory.
- Ms. Bontle Moiloa for providing the Lethabo AQMS data to ARM.
- Mr. Motshewa Matimolane, Mr. Abel Moatshe and Mr. Bryan McCourt for their technical comments on the Modelling Plan of Study.
- Dr. Gerhard Fourie for his in-depth technical peer review herein.

REFERENCES

Afrane-Okese, Y.1998. Domestic energy-use database for integrated energy planning. Unpublished MSc Thesis, Energy and Development Research Centre (EDRC), University of Cape Town.

Ainslie, B., and Jackson, P.L., 2009. The use of an atmospheric dispersion model to determine influence regions in the prince george, B.C. airshed from the burning of open wood waste piles, Journal of Environmental Management, 10, 1-9.

Akagi, S. K., Yokelson, R. J., Wiedinmyer, C., Alvarado, M. J., Reid, J. S., Karl, T., Crounse, J. D., and Wennberg, P. O.: Emission factors for open and domestic biomass burning for use in atmospheric models, Atmos. Chem. Phys., 11, 4039–4072, https://doi.org/10.5194/acp-11-4039-2011, 2011.

Alapaty, K., 1995. Sensitivity of regional oxidant model predictions to prognostic and diagnostic meteorological fields, Journal of Applied Meteorology, 34, 1787-1801.

Andreae, M. O. and Merlet, P.: Emission of trace gases and aerosols from biomass burning, Global Biogeochem. Cycles, 15, 955–966, https://doi.org/10.1029/2000GB001382, 2001.

Andreae, M. O. and Rosenfeld, D.: Aerosol–cloud–precipitation interactions. Part 1. The nature and sources of cloud-active aerosols, Earth-Sci. Rev., 89, 13–41, https://doi.org/10.1016/j.earscirev.2008.03.001, 2008.

Beychok, M. R., 2005. Fundamentals of Stack Gas Dispersion, Ch 8, 88 - 102, Irvine, California.

Buonicore and Davis (1992: Fugitive Emissions. Air Pollution Engineering Manual, Chapter 4, First Edition, 1992, , AWMA, New York, USA

Busillo, G., Calastrin, G., Carpentieri, F., Matteo, A and Giovanni, G., 2005. Meteorological input for atmospheric dispersion models: an inter-comparison between new generation models, Atmospheric Environment, 8, 1212-1221.

Carroll, M., Townshend, J. R. G., Hansen, M. C., Dimiceli, C., Sohlberg, R. A., and Wurster, K.: Vegetative Cover Conversion and Vegetation Continuous Fields, in: Land Remote Sensing and Global Environmental Change: NASA's Earth Observing System and the Science of Aster and MODIS, vol. 11, Springer-Verlag, 725–746, 2011.

Carslaw D.C., Ropkins K. 2012. “Openair – an r package for air quality data analysis”. Environmental Modelling and Software, pp27–28: pp52–61

Carslaw, D."The Openair Manual Open-Source Tools for Analysing Air Pollution Data", King's College, London, 2015.

Carslaw, D.C.,and Carslaw, N., 2007. "Detecting and characterising small changes in ur-ban nitrogen dioxide concentrations". Atmospheric Environment Vol 41(22): pp 4723-4733.View at: http://dx.doi.org/10.1016/j.atmosenv.2007.03.034

Davakis, E., Andronopoulos, I., Bartzisd, J.G and Nychasa, S.G., 2007. Data assimilation in meteorological pre-processors: Effects on atmospheric dispersion simulations. Atmospheric Environment, 41, 2917–2932

Davies, D. K., Ilavajhala, S., Wong, M. M., and Justice, C. O.: Fire Information for Resource Management System: Archiving and Distributing MODIS Active Fire Data, IEEE T. Geosci. Remote, 47, 72–79, https://doi.org/10.1109/TGRS.2008.2002076, 2009.

DEA (2014). Code Of Practice For Air Dispersion Modelling In Air Quality Management In South Africa, Gazette No 37804; published 11 July 2014.

DEA, (2009). National Ambient Air Quality Standards, Government Gazette, 32861, Vol. 1210, 24 December 2009.

DEA, 2011: The Highveld Priority Area Air Quality Management Plan, October 2014.

DEA, 2014: The Waterberg-Bojanala Priority Area Air Quality Management Plan: Baseline Characterisation, October 2014.

DEA, 2020: The Draft Second Generation Air Quality Management Plan for Vaal Triangle Airshed Priority Area, June, 2020.

DEA, 2022: Development of the Second-Generation Air Quality Management Plan for the Highveld Priority Area: Baseline Air Quality Assessment Report, July, 2022.

DEFF (2007): The Vaal Triangle Priority Area Air Quality Management Plan – Baseline Characterisation.

DEFF (2013): Integrated Strategy for the control of Motor Vehicle Emissions: Motor Vehicle Emission Inventory.

DEFF (2019): The Second Generation Vaal triangle Airshed Priority Area Air Quality Management Plan- (URL: https://saaqis.environment.gov.za/NewsPage/CorrentNew/21)

Fang, Z., Deng, W., Zhang, Y., Ding, X., Tang, M., Liu, T., Hu, Q., Zhu, M., Wang, Z., Yang, W., Huang, Z., Song, W., Bi, X., Chen, J., Sun, Y., George, C., and Wang, X.: Open burning of rice, corn and wheat straws: primary emissions, photochemical aging, and secondary organic aerosol formation, Atmos. Chem. Phys., 17, 14821–14839, https://doi.org/10.5194/acp-17-14821-2017, 2017.

Friedl, M. A., Sulla-Menashe, D., Tan, B., Schneider, A., Ramankutty, N., Sibley, A., and Huang, X.: MODIS Collection 5 global land cover: Algorithm refinements and characterization of new datasets, Remote Sens. Environ., 114, 168–182, https://doi.org/10.1016/j.rse.2009.08.016, 2010.

Garstang, M., Tyson, P.D., Swap, R., Edwards, M., Kållberg, P. and Lindesay, J.A. (1996). Horizontal and vertical transport of air over Southern Africa. Journal of Geophysical Research, 101 (D19), 23721-23736.

Grundstrom, M., Tang, L., Hallquist, M., Nguyen, H., Chen, D., and Pleijel,H. "Influence of atmospheric circulation patterns on urban air quality during the winter" Atmospheric Pollution Research,Vol 6(2), pp 278-285. View at: https://doi.org/10.5094/APR.2015.032.

Hoelzemann, J. J.: Global Wildland Fire Emission Model (GWEM): Evaluating the use of global area burnt satellite data, J. Geophys. Res., 109, D14S04, https://doi.org/10.1029/2003JD003666, 2004.

Holmes, N.S. and Morawska, L., 2006. A review of dispersion modelling and its application to the dispersion of particles: An overview of different dispersion models available, Atmospheric Environment, 40, 5902–5928.

Hurley, P., Manins, P., Lee, S., Boyle, R., Leung, Y. and Dewundege, P., 2003. Year-long, high-resolution, urban airshed modelling: verification of TAPM predictions of smog and particles in Melbourne, Australia, Atmospheric Environment, 37, 1899–1910

Hurley, P., Physick, W., Luhar, A. and Edwards, M., 2005b. The Air Pollution Model (TAPM) Version 3. Part 2: Summary of some verification studies. CSIRO Atmospheric Research, 72, 20-36.

Hurley, P.J., 2005c: The Air Pollution Model (TAPM) Version 3 Part 1: Technical Description. www.dar.csiro.au/tapm

Hurley, P.J., Edwards, M., Physick, W.L. and Luhar, A.K., 2005. TAPM V3 – Model Description and Verification , Clean Air and Environmental Quality, 39, 7-15.

Hurley, P.J., Physick, W.L. and Luhar, A.K., 2005a. TAPM: a practical approach to prognostic meteorological and air pollution modelling. Environmental Modelling and Software, 20, 737-752.

Hurley, P.J., Edwards, M. and Luhar, AK., 2008. TAPM V4. Part 2: Summary of Some Verification Studies.. CSIRO Marine and Atmospheric Research Paper No. 26. October 2008. ISBN: 978-1-921424-72-4 ISSN: 1835-1476

International Trade Administration (ITA) 2024), U.S. Department of Commerce, South Africa - Country Commercial Guide, Energy (https://www.trade.gov/country-commercial-guides/south-africa-energy)

Jones, A.M., Harrison, R.M., Baker, J., 2010. "The wind speed dependence of the concentrations of airborne particulate matter and NO_X". Atmospheric Environment Vol 44(13), pp 1682-1690. View at:http://www.sciencedirect.com/science/article/B6VH3-4Y7P72C-2/2/f6c65e5f49ac3e9862d4c1803d4735c0.

Köppen, W. 1884. "Die Wärmezonen der Erde, nach der Dauer der heissen, gemässigten und kalten Zeit und nach der Wirkung der Wärme auf die organische Welt betrachtet" [The thermal zones of the earth according to the duration of hot, moderate and cold periods and to the impact of heat on the organic world)]. Meteorologische Zeitschrift. 20 (3). Translated by Volken, E.; Brönnimann, S (published 2011): 351–360. Bibcode:2011MetZe..20..351K. doi:10.1127/0941-2948/2011/105. S2CID 209855204. Archived from the original on 8 September 2016. Retrieved 2 September 2016.

Liebenberg, H., 1999. "Air pollution population exposure evaluation in the Vaal triangle using GIS" (Doctoral dissertation, University of Johannesburg).

Liu, X., Huey, L. G., Yokelson, R. J., Selimovic, V., Simpson, I. J., Müller, M., Jimenez, J. L., Campuzano-Jost, P., Beyersdorf, A. J., Blake, D. R., Butterfield, Z., Choi, Y., Crounse, J. D., Day, D. A., Diskin, G. S., Dubey, M. K., Fortner, E., Hanisco, T. F., Hu, W., King, L. E., Kleinman, L., Meinardi, S., Mikoviny, T., Onasch, T. B., Palm, B. B., Peischl, J., Pollack, I. B., Ryerson, T. B., Sachse, G. W., Sedlacek, A. J., Shilling, J. E., Springston, S., St. Clair, J. M., Tanner, D. J., Teng, A. P., Wennberg, P. O., Wisthaler, A., and Wolfe, G. M.: Airborne measurements of western U.S. wildfire emissions: Comparison with prescribed burning and air quality implications, J. Geophys. Res.-Atmos., 122, 6108–6129, https://doi.org/10.1002/2016JD026315, 2017.

Liu, Z., Ballantyne, A. P., and Cooper, L. A.: Biophysical feedback of global forest fires on surface temperature, Nat. Commun., 10, 214, https://doi.org/10.1038/s41467-018-08237-z, 2019.

McMeeking, G. R.: The optical, chemical, and physical properties of aerosols and gases emitted by the laboratory combustion of wildland fuels, Ph.D. Dissertation, Department of Atmospheric Sciences, Colorado State University, Ft. Collins, CO, 109–113, 2008.

Paton-Walsh, C., Smith, T. E. L., Young, E. L., Griffith, D. W. T., and Guérette, É.-A.: New emission factors for Australian vegetation fires measured using open-path Fourier transform infrared spectroscopy – Part 1: Methods and Australian temperate forest fires, Atmos. Chem. Phys., 14, 11313–11333, https://doi.org/10.5194/acp-14-11313-2014, 2014.

Pielke, R.A., Uliasz, M., 1998. Use of meteorological models as input to regional and mesoscale air quality models limitations and strengths, Atmospheric Environment 32, 1455–1466

Pouliot, G., Rao, V., McCarty, J. L., and Soja, A.: Development of the crop residue and rangeland burning in the 2014 National Emissions Inventory using information from multiple sources, J. Air Waste Manag. A., 67, 613–622, https://doi.org/10.1080/10962247.2016.1268982, 2017.

Raghunandan, A., Scott, G. Zunckel, M. and Carter, W., 2008. TAPM verification in South Africa: modelling surface meteorology at Alexander Bay and Richards Bay. In prep. To be submitted to South African Journal of Science or Atmospheric Environment.

Richard Reiss, Elizabeth L. Anderson, Carroll E. Cross, George Hidy, David Hoel, Roger McClellan and Suresh Moolgavkar (2007) Evidence of Health Impacts of Sulfate-and Nitrate-Containing Particles in Ambient Air, Inhalation Toxicology, 19:5, 419-449, DOI: 10.1080/08958370601174941

Sandberg , D.A. Levaggi , R.E. DeMandel and W. Siu (1976) Sulfate and Nitrate Particulates as Related to SO_2 and NO_X Gases and Emissions, Journal of the Air Pollution Control Association, 26:6, 559-564, DOI: 10.1080/00022470.1976.10470283

Schroeder, W., Oliva, P., Giglio, L., and Csiszar, I. A.: The New VIIRS 375 m active fire detection data product: Algorithm description and initial assessment, Remote Sens. Environ., 143, 85–96, https://doi.org/10.1016/j.rse.2013.12.008, 2014.

Scire J (2014). Peer Review Report on the approach to the Atmospheric Impact Report https://docs.srk.co.za/sites/default/files/File/South-Africa/publicDocuments/SASOL_Postponements/ANNEXURE_B_SYNFUELS_AIR_Peer_Review.pdf

Scire, J.S., and Robe, F., 2004. Evaluating performance of meteorological models in regulatory application studies, oral presentation at the 8th International Conference on Harmonisation within Atmospheric Dispersion Modelling for Regulatory Purposes.

Scire, J.S., Robe, F., Yamartino, R.J., 1999a. A User's Guide for the CALMET Meteorological Model (Version 5). Earth Tech, Concord.

Scott, G.M., Diab, R.D., 2000. Forecasting Air Pollution Potential: A synoptic climatological approach, Journal of Air and Waste Management Association, 50, 1831-1842.

South African National Biodiversity Institute (2004): National Spatial Biodiversity Assessment

Swap, R., Garstang, M., Macko, S.A., Tyson, P.D., Maenhaut, W., Artaxo, P., Kallberg, P. and Talbot, R. (1999). The long-range transport of southern African aerosols to the tropical south Atlantic. Journal of Geophysical Research, 101 (D19), 23777-23791.

US Environmental Protection Agency., 2005. 40 CFR Part 51 Revision to the Guideline on Air Quality Models: Adoption of a Preferred General Purpose (Flat and Complex Terrain) Dispersion Model and Other Revisions; Final Rule Appendix W (PDF), Extracts from the Guideline on Air Quality Models.

Urbanski, S.: Wildland fire emissions, carbon, and climate: Emission factors, Forest Ecol. Manage., 317, 51–60, https://doi.org/10.1016/j.foreco.2013.05.045, 2014.

USEPA AP-42 (2003): Appendix C.1: Procedures for sampling surface/Bulk dust loading, Compilation of Air Pollutant Emission Factors, Volume 1, Stationary Point and Area Sources, USEPA, USA

USEPA AP-42 (2006): Unpaved Roads-Chapter 13.2.2, Compilation of Air Pollutant Emission Factors, Volume 1, Stationary Point and Area Sources, USA

van Leeuwen, T. T., van der Werf, G. R., Hoffmann, A. A., Detmers, R. G., Rücker, G., French, N. H. F., Archibald, S., Carvalho Jr., J. A., Cook, G. D., de Groot, W. J., Hély, C., Kasischke, E. S., Kloster, S., McCarty, J. L., Pettinari, M. L., Savadogo, P., Alvarado, E. C., Boschetti, L., Manuri, S., Meyer, C. P., Siegert, F., Trollope, L. A., and Trollope, W. S. W.: Biomass burning fuel consumption rates: a field measurement database, Biogeosciences, 11, 7305–7329, https://doi.org/10.5194/bg-11-7305-2014, 2014.

Wiedinmyer, C. and Emmons, L.: Fire INventory from NCAR (FINN) v2.5(MODIS), MOZART VOC speciation (v2.5), Zenodo [code], https://doi.org/10.5281/zenodo.7868652 (last access: 7 July 2023), 2023.

Wiedinmyer, C., Akagi, S. K., Yokelson, R. J., Emmons, L. K., Al-Saadi, J. A., Orlando, J. J., and Soja, A. J.: The Fire INventory from NCAR (FINN): a high resolution global model to estimate the emissions from open burning, Geosci. Model Dev., 4, 625–641, https://doi.org/10.5194/gmd-4-625-2011, 2011.

Zawar, P., Reza, T., Kingham, S. and Pearce, J., 2005. Evaluation of a year- long dispersion modelling of PM_{10} using the mesoscale model TAPM for Christchurch, New Zealand, Science of the Total Environment, 349, 249– 259.

Zunckel, M.,2007c. Air quality modelling activities in Southern Africa and the feasibility of a regional modelling centre, Report done on behalf of APINA.

ANNEXURE 1

REPORT DISCLAIMER

Air Resource Management (Pty) Ltd has prepared this report based on an agreed scope of work and acts in all professional matters as an advisor to the Client and exercises all reasonable skill and care in the provision of its professional services in a manner consistent with the level of care and expertise exercised by air quality management professionals.

Reports are commissioned by and prepared for the exclusive use of the Client. They are subject to and issued in accordance with the agreement between the Client and Air Resource Management (Pty) Ltd. Air Resource Management (Pty) Ltd is not responsible and will not be liable to any other person or organisation for or in relation to any matter dealt within this Report, or for any loss or damage suffered by any other person or organisation arising from matters dealt with or conclusions expressed in this report (including without limitation matters arising from any negligent act or omission of Air Resource Management (Pty) Ltd or for any loss or damage suffered by any other party relying upon the matters dealt with or conclusions expressed in this Report). Other parties should not rely upon the report or the accuracy or completeness of any conclusions and should make their own inquiries and obtain independent advice in relation to such matters.

Except where expressly stated, Air Resource Management (Pty) Ltd has not verified the validity, accuracy or comprehensiveness of any information supplied to Air Resource Management (Pty) Ltd for its reports.

Reports prepared by Air Resource Management (Pty) Ltd cannot be copied or reproduced in whole or part for any purpose without the prior written agreement of Air Resource Management (Pty) Ltd.

Where site inspections, testing or fieldwork have taken place, the report is based on the information made available by the client or their nominees during the visit, visual observations and any subsequent discussions with regulatory authorities. The validity and comprehensiveness of supplied information has not been independently verified and, for the purposes of this report, it is assumed that the information provided to Air Resource Management (Pty) Ltd is both complete and accurate. It is further assumed that normal activities were being undertaken at the site on the day of the site visit(s), unless explicitly stated otherwise.

COPYRIGHT